



**HAL**  
open science

# Role of the most abundant plant sphingolipids, Glycosyl Inositol Phosphoryl Ceramides GIPCs, in membrane structure and host/pathogen interactions

Adiilah Mamode Cassim

► **To cite this version:**

Adiilah Mamode Cassim. Role of the most abundant plant sphingolipids, Glycosyl Inositol Phosphoryl Ceramides GIPCs, in membrane structure and host/pathogen interactions. Human health and pathology. Université de Bordeaux, 2019. English. NNT : 2019BORD0413 . tel-03506261

**HAL Id: tel-03506261**

**<https://theses.hal.science/tel-03506261v1>**

Submitted on 2 Jan 2022

**HAL** is a multi-disciplinary open access archive for the deposit and dissemination of scientific research documents, whether they are published or not. The documents may come from teaching and research institutions in France or abroad, or from public or private research centers.

L'archive ouverte pluridisciplinaire **HAL**, est destinée au dépôt et à la diffusion de documents scientifiques de niveau recherche, publiés ou non, émanant des établissements d'enseignement et de recherche français ou étrangers, des laboratoires publics ou privés.

THÈSE PRÉSENTÉE  
POUR OBTENIR LE GRADE DE  
**DOCTEUR DE**  
**L'UNIVERSITÉ DE BORDEAUX**

ÉCOLE DOCTORALE des Sciences de la Vie et de la Santé

SPÉCIALITÉ : Biologie Végétale

**Par Adiilah MAMODE CASSIM**

**Role of the most abundant plant sphingolipids, Glycosyl  
Inositol Phosphoryl Ceramides GIPCs, in membrane  
structure and host/pathogen interactions**

Sous la direction de : Dr. Sébastien MONGRAND  
Directrice de thèse : Prof. Lilly MANETA-PEYRET

Soutenance le 18 décembre 2019

Membres du jury :

M. HERNOULD Michel  
Mme. JOUHET Juliette  
Mme. SARAZIN Catherine  
Mme. SIMON-PLAS Françoise  
M. DUFOURC Erick  
M. MONGRAND Sébastien

Professeur de l'Université de Bordeaux  
Directrice de Recherche CNRS  
Professeur de l'Université de Picardie  
Directrice de Recherche INRA  
Directeur de Recherche CNRS  
Directeur de Recherche CNRS

Président  
Rapporteur  
Rapporteur  
Rapporteur  
Invité  
Invité



## Résumé :

Les Glycosyl-Inositol Phosphoryl Céramides (GIPCs) sont les sphingolipides majeurs de la biosphère. Ils représentent jusqu'à 40%mol des membranes plasmiques (MP) des plantes et des champignons. Les GIPCs sont cependant restés presque totalement ignorés depuis leur découverte il y a plus de 50 ans. Aucune donnée n'est disponible sur leurs rôles dans la structuration des membranes biologiques, leur organisation en nanodomains membranaires et leurs interactions avec les autres lipides et les protéines. De nombreuses questions à propos des GIPCs de plantes restent encore sans réponse, telles que la structure chimique exacte de la tête polaire dont le nombre de sucres ; l'influence de ces molécules sur l'épaisseur de la membrane ou encore sur la structuration des nanodomains ; et enfin l'implication des GIPC dans les relations hôte-pathogène chez les plantes. Le but de ce projet est de purifier et caractériser les différentes classes de GIPCs de plantes, afin d'étudier leurs rôles structurants avec les phytostérols et les phospholipides par des méthodes de biophysique et de biochimie structurale. Ce projet multidisciplinaire permettra l'émergence d'une nouvelle thématique et procurera une base de données indispensable pour comprendre la structure des MP végétales et entre autres, leurs rôles dans la réponse contre les pathogènes.

## Summary :

Glycosyl Inositol Phosphoryl Ceramides (GIPCs) are the major sphingolipids of the biosphere. They account for up to 40 mol% of the plasma membranes (PM) of plants and fungi. Since their discovery over 50 years ago, GIPCs remained however almost completely ignored. No data are available on their roles in the structure of biological membranes, on their organization in membrane nanodomains and their interactions with other lipids and proteins. Many questions about plant GIPCs remain unanswered, such as the exact chemical structure of the polar as well as the number sugars grafted; their influence on the thickness of the membrane or on the structure of nanodomains; and also their involvement in host-pathogen interactions in plants. The purpose of this project is to purify and characterize the different classes of plant GIPCs to study their structural roles with phytosterols and phospholipids by biophysical and structural biochemistry methods. This multidisciplinary project will enable the emergence of a new theme and will provide an essential database for understanding the structure of plant PM and among others, their roles in the response against pathogens.

# Remerciements

Je souhaite remercier en premier lieu, les membres du jury d'avoir acceptés d'évaluer mon travail.

Je remercie mon directeur de thèse, Sébastien Mongrand pour ses conseils, directives, encouragements, bonne humeur et optimisme en toute circonstance, tout au long de ma thèse. Merci à Lilly Maneta-Peyret de m'avoir accepté comme ton étudiante en thèse, pour ton soutien. Sans toi, je n'aurais pas pu participer à tous ces congrès.

Un grand merci à tous les collaborateurs de ce projet : Minoru N. du Japon, Jenny M. des USA, Laurence L. et Magali D. de la Belgique, Isabel A. et Thornsten N. d'Allemagne, Laurent H. et Yotam N. de Grenoble, Eric L. et Françoise S-P. de Dijon, Axelle G. et Marion D. de l'IECB et CBMN à Bordeaux.

Mes remerciements à toute l'équipe d'enseignement de la biologie végétale, que j'ai côtoyée de près ou de loin, pendant les 96h de TP réalisés pendant ces deux dernières années. Merci Vero G., d'avoir été ma tutrice pendant cette expérience enrichissante, pour les petites formations 'correction des copies'.

Je remercie Jean-Jacques B., le directeur du LBM la journée (et 'Uber' l'aprem), ainsi que tout le LBM de m'avoir accueillie au sein des vôtres. Merci aux membres de la plateforme lipidomique, Laetitia F. et Pierre VD. pour m'aider à mieux maîtriser la GC-MS (surtout en période de canicule !). Merci Pierre pour le réapprovisionnement de mon stock perso de bouteilles de solvants. A mes voisins de paillasse (team Joubes et team PD), qui ont dû subir mon monopole constant des hottes, ainsi que le doux parfum de soupe de GIPC de poireau/chou-fleur/riz. Merci pour votre compréhension. Merci beaucoup à Jennifer H. pour l'entretien de notre laverie et de tout gérer comme une pro !

A mes amis de bureau, Amazigh H. et Rodrigo G. pour toutes nos conversations très intéressantes, non-scientifiques. Au bureau de Yohann B., pour les goûters (chocolats et rires) qui nous ont ressuscité en fin de journée pendant la rédaction de cette thèse. Merci Yohann pour tes conseils et les discussions qui m'ont redonnés espoir en mon projet. Je te promets de m'investir dans la maîtrise et l'utilisation d'AI ! Thank you Yoko I. for your friendship, it means a lot to me. A Anne-Flore, la seule et unique, merci d'avoir été ma binôme pendant ma thèse, et ma binôme pendant toutes ces soirées bien dépensées !

A la famille Jeannel, ma famille d'adoption, pour le soutien pendant ces longues années loin des miens. A mes copines pour leur support psychologique.

A toute ma famille, *mo lacaz*, cette thèse vous est dédiée ...

# Table of Content

<b>List of Abbreviations</b> .....	1
<b>Introduction</b> .....	5
A Biophysics overview of the Plasma Membrane as a lipid bilayer.....	6
Biophysical tools for PM lipid characterisation and study.....	8
PM lipid homeoviscosity and thermal adaptation.....	12
GIPC, plant major sphingolipid, as a mediator in PM signalling in salt stress.....	14
GIPC metabolites in biotic stresses.....	16
The plant plasma membrane in a biological point of view.....	17
<i><b>Plant lipids: Key players of plasma membrane organization and function</b></i> .....	19
<b>Thesis Objectives</b> .....	46
<b>Chapter 1: Multipolar approaches into deciphering GIPC structure and its role in membrane organisation</b> .....	50
Draft Paper : Multiple approaches to study the role of plant sphingolipids GIPC in plasma membrane organization.....	55
<b>Additional data</b> .....	86
A survey to analyse the structure of tobacco GIPC polar head by liquid-state 1H-NMR.....	86
Phase transition of GIPC containing-vesicles analysed by liquid state 2H-NMR and 31P-NMR.....	100
<b>Chapter 2: Role of VLCFA and hydroxylation in PM marker mobility</b> .....	103
<b>Results</b> .....	111

Metazachlor treatment modifies sphingolipid pool in purified PM.....	111
PM membrane markers are visible after Mz treatment of wild type and in At fah mutants.....	112
The recovery of PM marker GPI-GFP is significantly higher in metazachlor-treated plants.....	113
Anionic lipid sensors and metazachlor treatment.....	114
PM outer-leaflet order decreases with Metazachlor treatment.....	115
<b>Discussion and Perspectives</b> .....	117
Metazachlor treatment and PM lipids.....	117
FRAP analysis and GPI-GFP lateral mobility affected by metazachlor treatment.....	121
Order of the phases in the PM leaflets.....	122
Material and Methods.....	125
<b>Chapter 3: GIPC, receptor to microbial NLP, determine host sensitivity</b> .....	128
<i>Eudicot plant-specific sphingolipids determine host selectivity of microbial NLP cytolysins, Science 2017</i> .....	131
Discussion and Perspectives.....	164
<b>Chapter 4 : Miscellaneous</b> .....	170
<i>Lipids light up in plant membranes, Nat. Plants 2019</i> .....	172
<b>General Conclusions and Perspectives</b> .....	174
<b>Annexes</b> .....	184
<b>References</b> .....	187

# List of Abbreviations

ADS2, Acyl- CoA Desaturase

AFM, Atomic Force Microscopy

AGs, Arabinogalactans

Ap, Allium porrum

Ara, Arabinose

ASG, Acylated Steryl Glycosides

At, Arabidopsis thaliana

At-BI1, Arabidopsis thaliana-BAX inhibitor 1

Bo, Brassica oleracea

BY-2, Bright-Yellow 2

CAZyme, CArbohydrate-active enzymes data base

CER or Cer, Ceramides

CNC, cellulose nanocrystals

Cryo-EM, Cryogenic Electronic Microscopy

CT-B Cholera toxin B

Ctrl, control

d18:0, sphinganine

d18:1, sphingosine

DIM, Detergent Insoluble Membrane

DLS, Dynamic Light Scattering

DMPC, 1,2-dimyristoyl-sn-glycero-3-phosphocholine

DOPC, 1,2-dioleoyl-sn-glycero-3-phosphocholine

d-POPC, deutereuted palmitoyl oleoyl phosphatidyl choline

DPPC, 1,2-diPalmitoyl-sn-glycero-3-phosphocholine

DRM, detergent-resistant membrane

DRP1A, Dynamin-Related Protein1A

DSC, Differential scanning calorimetrie

ECR, Enoyl-CoA Reductase (ECR)

EM, electron microscopy

ER, Endoplasmic Reticulum

EVs, Extracellular Vesicles

FA, fatty acid

FAH, fatty acid hydroxylase

FRAP, Fluorescence Recovery After Photobleaching

G proteins, Guanine nucleotide-binding proteins;

Gal, Galactose

GC-MS, Gas Chromatography – Mass Spectrometry

GFP, Green Fluorescent Protein

GINT1, Glucosamine Inositol Phosphorylceramide Transferase 1

GIPC, Glycosyl Inositol Phosphoryl Ceramides

Glc, Glucose

GlcN, Glucosamine

GlcNAc, N-Acetyl Glucosamine

GlucA, Glucuronic Acid

GluCer, glucosylCeramide

GM<sub>1</sub> or GM1, mono-sialo-tetrahexosyl ganglioside

GMT1, GIPC Mannosyl-Transferase 1

GONST, Golgi Localized Nucleotide Sugar Transporter

GPI, glycosylphosphatidylinositol

GPI-APs, GPI anchor proteins

GPMV, Giant Plasma Membrane Vesicle

GT, GlycosylTransferases

GUV, Giant Unilamellar Vesicle

HCD,  $\beta$ -hydroxyacyl-CoA dehydratase (HCD) and

Hex, Hexose

hFA, hydroxylated fatty acid

HM, HyperMatrix

HPTLC, high-performance thin layer chromatography

HVA, homeoviscous adaptation

hVLCFA, 2-hydroxylated Very Long Chain Fatty Acid

Ins, Inositol

IPC, Inositol Phosphoryl Ceramide

IPCS, Inositol Phosphoryl Ceramide Synthase

IPUT1, Inositol Phosphorylceramide Glucuronosyl Transferase 1

IR, InfraRed

ISO, Inside Out vesicles

KCR,  $\beta$ -ketoacyl-CoA reductase

KCS,  $\beta$ -ketoacyl-CoA synthase

LCB, Long Chain Base

LC-MS, Liquid Chromatography – Mass Spectrometry

ld, liquid-disordered

lo, liquid-ordered

LOH, LAG One Homolog

LUV, large unilamellar vesicle

Man, Mannose

MAP, Myristoylated and Palmitoylated

MD, Molecular Dynamics

MOCA1, monocation-induced  $\text{Ca}^{2+}$  increase 1

MSC, Membrane Surface Charge;

Mz, metazachlor

Nep1, necrosis and ethylene-inducing peptide 1

NLP, necrosis and ethylene-inducing peptide 1 (Nep 1)-like proteins

NMR, Nuclear Magnetic Resonance

Nt, Nicotiana tabacum

Os, Oryza sativa

P, Phosphate

PA, phosphatidic acid

PALM, Photo-Activated Localization Microscopy

PaNIE, Novel Protein Elicitor from Pythium aphanidermatum

PAP, Prenylated and Prenylated

PC, PhosphatidylCholine

PCD, Programmed Cell Death

PdBG2, Plasmodesmata Beta-1,3-Glucanase 2

PDCB1, Plasmodesmata Callose Binding 1

PD, Plasmodesmata

PE, PhosphatidylEthanolamine

Pen, Pentose

PI, phosphatidylinositol

PI3,4,5P<sub>3</sub>, phosphatidylinositol- 3,4,5-triphosphate

PI3,5P<sub>2</sub>, phosphatidylinositol-3,5-bisphosphate

PI3P, phosphatidylinositol-3-phosphate

PI4,5P<sub>2</sub>, phosphatidylinositol-4,5-bisphosphate

PI4P, phosphatidylinositol-4-phosphate

PIPs, Polyphosphoinositides or phosphatidylinositol-phosphates

PLPC, Palmitoyl Linoleoyl  
Phosphatidyl Choline

POPC, Palmitoyl Oleoyl Phosphatidyl  
Choline

PS, PhosphatidylSerine

ROP6, Rho of Plants 6

RSO, Right Side Out vesicles

SA, salicylic acid

SBL, supported bilayer

SG, Steryl Glycosides

SL, Sphingolipid

SLD, LCB  $\Delta 8$  desaturase

SLD, Scattering length density

SM, Sphingomyelin

So, Solid-ordered

SOS, Salt Overly Sensitive

SPT, Serine palmitoyltransferase

SPT-PALM, Single particle tracking-  
photoactivated localization microscopy

ssNMR, Solid state-NMR

STED, Stimulated Emission Depletion  
Microscopy

STORM, Stochastic Optical  
Reconstruction Microscopy

t18:0, phytosphingosine

PS, Phosphatidylserine

REM, Remorin

RGII, Rhamnogalacturonan II

Rha, Rhamnose

t18:1, 4-hydroxy-8-sphinganine

T<sub>m</sub>, phase transition temperature

VLCFA, Very Long Chain Fatty Acid

WB, Western Blot

WT, wild type

# General Introduction

## **A Biophysics overview of the Plasma Membrane as a lipid bilayer**

The plasma membrane (PM) forms a selective biological barrier between the cell and the extracellular medium. This membrane is essential for the protection, survival and integrity of living cells from prokaryotes to eukaryotes. It is not only a simple structural delimitation but also constitutes a sensor for any modification of the cellular environment and a platform for the orchestration of signal transduction allowing the translation of external signals into finely tuned appropriate adaptive responses. Danielli-Davidson model first described in 1935 the cell membrane as a lipid bilayer with proteins bound to the bilayer outer regions. The fluid mosaic model of Singer and Nicolson represented the structure and random organization of lipids in a relative symmetrical bilayer with a highly asymmetrical distribution of proteins in biological membranes (Singer & Nicolson, 1972). In this model, both lipids and protein are in constant motion through translational diffusion, taking into consideration thermodynamic limitation. Membrane proteins can also be intrinsic, that is, integrated in the lipid bilayer, or peripheral, that is associated with the lipid bilayer polar headgroups. However, this basic model of cell membrane was updated to incorporate new aspects (Goñi, 2014). One of those aspects is the temporary docking of proteins to the membrane. These non-permanent membrane proteins interact with the membrane through 'interfacial hydrophobicity' (White, 2007). The strength of interaction varies. They can interact strongly with the membrane through hydrophobic forces (but not exclusively), such as, in the case of bacterial toxins binding with membrane lipid of the outer leaflet to form macromolecular pores.

"Membranes are more mosaic than fluid." wrote Engelman in his updated version of the general model of membrane structure (Engelman, 2005). Membrane proteins have varying shapes and with lipids tend to group together to form lipid-lipid and lipid-protein interactions. Lipid-protein interactions can be selective causing the distortion of the membrane thickness, hence patches in the membrane. The lipid region varies in thickness and composition (Engelman, 2005). The mean thickness of the plasma membrane of the abdominal sympathetic ganglion of a bullfrog is 53 Ångström, or 5.3 nm (YAMAMOTO, 1963).

The spatial organization due to preferential interactions creates regionalization of the membrane and lateral segregation into 'patches', 'rafts' or 'domains', heterogeneous in size but less than 100nm, characterized by a specific composition and defined function (Goñi, 2014). These domains are the result of lipid-protein interactions, protein-protein interactions, protein crowding and lipid packing. They are transient structures enriched in sphingolipid and sterols, important for the membrane trafficking of lipid and cell signaling cascades (Gronnier et al., 2019; Simons & Ikonen, 1997).

Lipids can also move between the bilayer. This phenomenon is known as flip-flop. This is the case for phosphatidylserine localized in the inner leaflet of cell membrane, is exposed to the outside, thus signaling the apoptotic cell removal by macrophages. Ceramides can even cause flip-flop of lipids with a bulky polar headgroup, such as a ganglioside (Contreras, Villar, Alonso, Kolesnick, & Goñi, 2003). Not all lipids are miscible with each other hence they are present in different phases. The difference in the structure of the lipid gives way to shape and phase polymorphism. A phase is defined as a region of space throughout which all physical properties of a material are uniform. "Phase" is synonym of "state of matter". Phases are thermodynamic concepts, ideal entities to which real objects resemble more or less. The condition of uniformity in the context of membrane lipids is at the macroscopic level. The main phases formed by membrane lipids in excess water are: lamellar phase, micellar phase, inverted hexagonal phase (HII) and inverted cubic phase (Goñi, 2014).

Lamellar phases are well documented as they are relevant to cell membrane bilayer organization. We will focus more on lamellar phases than non-lamellar phases. Most saturated membrane lipids can give rise to a gel (or solid ordered phases (so))  $L\beta$  lamellar phase at a given temperature, and to a fluid (or liquid crystalline or liquid disordered (ld))  $L\alpha$  phase observed at a higher temperature. In the  $L\alpha$ , the lipids exhibit high translational and rotational diffusion due to high alkyl chain disorder.  $L\alpha$  phases contain mainly lipid with unsaturated acyl chains.  $L\beta$  phases are promoted by low temperature and long saturated fatty acid such as phospholipids. A study by Mason JT in 1998, shows the gel packing and phase transition of mixed-chain-length PC and PE being affected by their fatty acid chain (Mason, 1998). Gel phase regions tend to exclude proteins and have low lateral diffusion (Florine & Feigenson, 1987; Rubenstein, Smith, & McConnell, 1979).

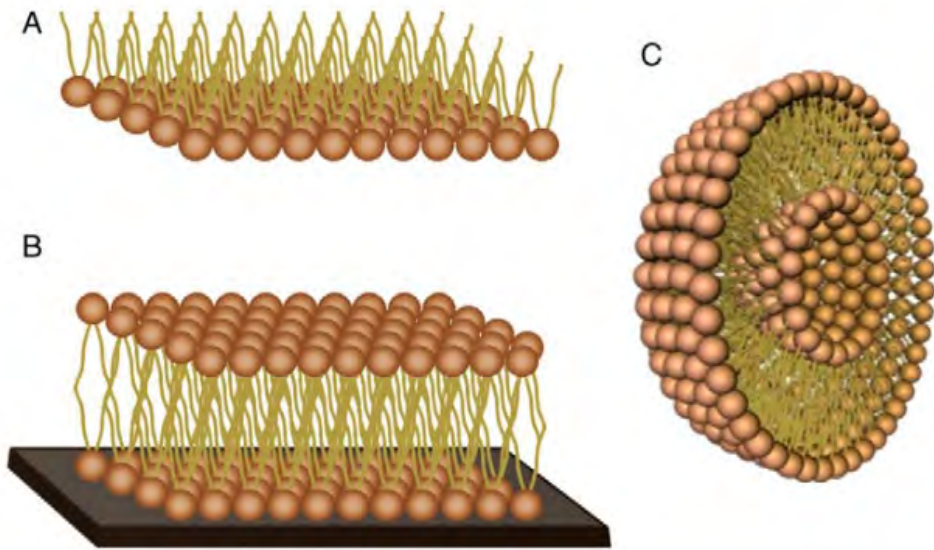
However, saturated phospholipid bilayer is an unrealistic biological model. In nature, lipids are mainly unsaturated and organisms have developed adaptive mechanism to modify the saturation of their lipids to avoid the formation of gel phases in low environmental temperature (discussed further below). Exception to the rule, the only membranes with gel phase domains are in the brain specifically in regions enriched in cholesterol and glycosylceramide (Ruocco & Shipley, 1984). Liquid-ordered (lo) phases are tightly packed and referred as the phase of the 'raft' domain, highly enriched sphingolipids, sterols and lipids with saturated acyl chains. They are essential features for signal perception and transduction, it is important to study the elements involved in the lipid rafts. The concept of rafts will be further discussed in the PLR Review "Plant lipids: Key players of plasma membrane organization and function" (see Review below).

### **Biophysical tools for PM lipid characterisation and study**

The PM is a biological barrier that allows trafficking and signal transduction in and out of the cell. It is fundamental to understand the interacting mechanism of bioactive molecules with the PM at the molecular level. With the advent of new technologies, new approaches have been set up to study this complex entity of the cell. Biophysical tools provide a vast array of techniques to investigate the PM (for review, (Deleu, Crowet, Nasir, & Lins, 2014)). It is important to know the type of model and technique that yield the desired information. In this subchapter, I will focus on the concept of some of the biophysical tools used during my PhD project.

#### *Model membrane*

Membranes are complex in their composition and interaction. It is very difficult to study the biophysical interactions between a given membrane with bioactive molecules or to investigate the interactions between molecules within the membranes *in vivo*. A simplified version of membrane mimicking the natural bilayer lipid membrane has been developed to enable investigating molecular interactions (Deleu et al., 2014). There are three model membrane systems mimicking lipid arrangement of natural membrane that are widely: lipid monolayers, supported bilayers (SLB) and liposomes (Eeman & Deleu, 2010). The simplest models are lipid monolayers representing half



Schematic representation of membrane models described (A) lipid monolayer, (B) supported lipid bilayer, (C) liposome. Adapted from the review by Deleu et al. 2014

the bilayer of biological membranes. They are formed at the air–water interface when lipids are spread onto the subphase of a Langmuir trough (Deleu et al., 2014). To be closer to the representation of a bilayer membrane, supported lipid bilayers (SLBs) are the models to be used. They consist of a flat lipid bilayer supported onto a solid surface such as mica, glass or silicon oxide wafers. These biomimetic models are often used to investigate lipid head group interactions, lateral lipid membrane organisation and phase behaviour (Eeman & Deleu, 2010). However, while monolayers and SLBs lack membrane curvature, liposomes are versatile biomimetic membrane model, fit to study a wide range of parameters: phase behaviours, membrane fusion and trafficking, cell adhesion and recognition. There are several techniques to make liposomes depending on the generated size (small unilamellar vesicles, large unilamellar vesicles, giant unilamellar vesicles and multilamellar vesicles). They are formed from aqueous dispersion of lipids and enclose the aqueous medium in which they are formed. Due to osmotic pressure, giant unilamellar vesicles are quite fragile and maybe stable only over a short period of time (Marques, 2000) .

### *Langmuir trough*

The Langmuir trough technique has been devised in the beginning of the 20<sup>th</sup> century and is applied on insoluble monolayer model at the air-water interface (Daen, 1966). This technique has long been used to characterize lipid-lipid, lipid-protein, lipid-bioactive molecules interaction at molecular level (Deleu et al., 2014). It is an easy way to screen and learn about the molecular interactions occurring at the cell surface combined with complementary techniques (Giner-Casares, Brezesinski, & Möhwald, 2014; Stefaniu, Brezesinski, & Möhwald, 2014). For instance, compression isotherm assays are basic experiments to record surface pressure changes when the occupied area by insoluble molecules at the air-liquid interface is reduced at equilibrium. This leads to information on the molecular area, monolayer stability and phases, the compressibility parameters of the monolayer, and the interaction of molecular species in the subphase with the molecules of the monolayer (Dynarowicz-Łątka, Dhanabalan, & Oliveira, 2001). The behaviour of the molecules upon compression of the monolayer mix can be evaluated by thermodynamic analysis (excess free energy of mixing can be calculated). Therefore, it is possible to assess molecular interaction between

different species spread at the air-liquid interface (Eeman & Deleu, 2010; Maget-Dana, 1999).

### *Atomic Force Microscopy*

Atomic Force Microscopy, invented in 1986, is applied to a broad field of bio-imaging of molecules such as DNA, DNA-protein interaction, proteins, lipid membranes, cells (Engel, Gaub, & Müller, 1999)(Alessandrini & Facci, 2005). We can also study the lateral organization of supported lipid model with nanometer resolution and obtain information on the surface topography of membrane segregation (Giocondi et al., 2010). Physical parameters of the model membrane are recorded such as the adhesion, deformation, indentation, dissipation and elasticity. Single-molecule inter- and intra-molecular interactions can be assessed by the use of force curves (Alessandrini & Facci, 2005). The atomic force microscopy belongs to the local probe microscopy methods. The local probe scans directly the sample surface. The tip interacts with the surface *via* the electronic charges of the atoms such that the interacting forces between the tip and the sample surface is converted into measurements (Müller & Dufrêne, 2009). AFM can operate in different modes depending on the interaction between the tip and the sample. Contact or tapping modes are used to visualize surface structures and lateral organisation while force spectroscopy is applied to investigate intra- and intermolecular forces (Deleu et al., 2014).

### *Nuclear Magnetic Resonance (NMR)*

NMR is undeniably one of the most powerful tools to study PM lipid and protein structures and dynamics (Grelard, Couvreur, Loudet, & Dufourc, 2009). Both liquid-state and solid-state NMR rely on the presence of active atomic nuclei in the system to be studied:  $^1\text{H}$ ,  $^{31}\text{P}$ ,  $^{15}\text{N}$ . Lipids can be deuterated ( $^2\text{H}$ ) or fluorinated ( $^{19}\text{F}$ ). Phospholipids are organized in bilayers, which analysed in a  $^{31}\text{P}$  spectrum have a typical asymmetric profile with a peak at high and a shoulder at low fields. The chemical shift anisotropy,  $\Delta\sigma$  corresponds to the difference between the peaks. It is used to determine specific interactions between candidate molecules at molecular level (Deleu et al., 2014; Grelard et al., 2009). Phase transitions caused by varying temperature affects the chemical shift. The structural modifications of molecules, specially peptides,

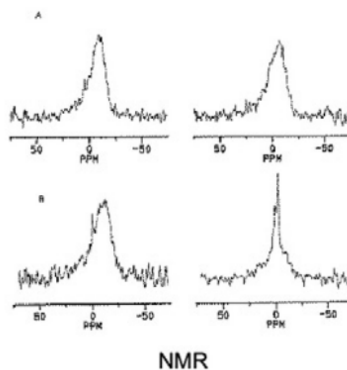
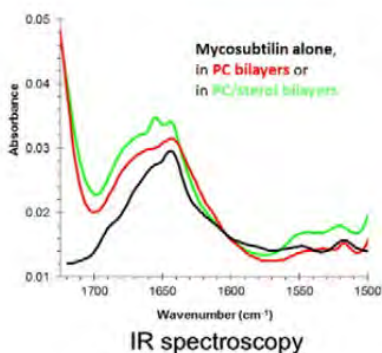
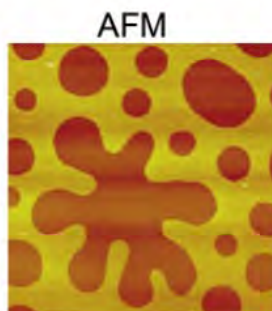
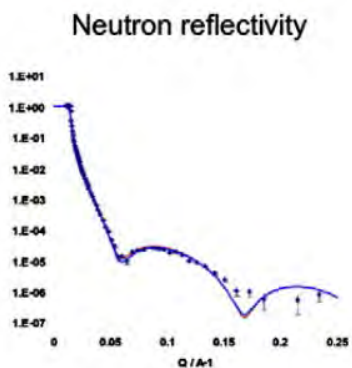
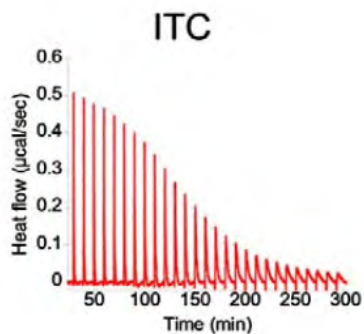
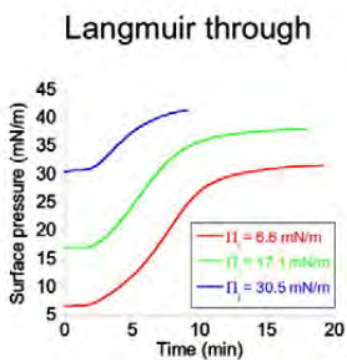
upon anchoring or binding to lipid membrane can also be analysed by NMR (Gronnier et al., 2017). The physical states of lipid membrane model can also be determined (lamellar, hexagonal or cylindrical, lo, ld...). The dynamics of deuterated lipid molecules in lamellar phase membrane can give information on the thickness, organisation and order of the lipid organisation in the membrane (Deleu et al., 2014; Eeman & Deleu, 2010; Grelard et al., 2009).

### *Isothermal Titration Calorimetry*

Isothermal titration calorimetry (ITC) measures the heat released or adsorbed when two interacting components are brought together in the same environment to initiate a reaction. One molecular partner is titrated in buffer containing the other partner at regular interval at a constant temperature (Heerklotz & Seelig, 2000; Jelesarov & Bosshard, 1999). The heat energy variations are recorded over time. By evaluating the enthalpy changes due to the interaction of the molecular partners, a complete thermodynamic profile of the interaction and molecular binding can be set up. It is a very sensitive method allowing the thermodynamic characterization of interactions at equilibrium conditions, such as the interaction between receptor–ligand, enzyme–substrate, without requiring a specific labelling(Seelig, 2004).

### *Neutron Reflectivity*

Specular neutron reflectivity (NR) is a tool to characterize the average structure and composition of ultra-thin film to a nanometric scale (~2 nm) (F. Ott, Cousin, & Menelle, 2004). Neutron scattering occurred from materials upon interaction with the nucleus of the atoms (F. Ott et al., 2004). The sensitivity of the neutron reflection to the film structure depends on the contrast in neutron refractive indexes of the layer components and the surrounding media. The structural parameters measured include thickness, surface coverage and refractive index of the film layers. This information is derived from variation in reflected intensity as a function of the wave vector related to the angle of incidence and the neutron beam wavelength (Vacklin, Tiberg, Fragneto, & Thomas, 2005). Neutron reflectivity has been successfully used in life science studies to characterize biomimetic membranes and investigate membrane/ candidate molecule interactions (Deleu et al., 2014).



Schematic representation of recordings of most of the different biophysical tools described and used to study specific interaction of PM lipids. Adapted from the review by Deleu et al. 2014

## **PM lipid homeoviscosity and thermal adaptation**

Plants, as bacteria, fungi, reptiles and fish, are poikilothermic organisms, that they do not control their body temperature. Their survival depends on their ability to acclimate themselves to thermal changes. They maintain their membrane fluidity by adapting their membrane lipids. This adaptive response was termed homeoviscous adaptation (HVA). This response is thoroughly studied in the animal kingdom with a particular focus on the acyl chain composition of membrane lipids (Los & Murata, 2004; Martin, Oh, & Jiang, 2007; Saita, Albanesi, & De Mendoza, 2016; Tiku, Gracey, Macartney, Beynon, & Cossins, 1996). The paper of (Malekar et al., 2018) is a study investigating the evolutionary HVA in Antarctic and non-Antarctic fishes to determine the membrane lipid composition of the four Perciformes fish: three Antarctic species and one non-Antarctic species. They also investigated acclimatory HVA (that is short period adaptive responses) to determine whether Antarctic fish that have evolved in stable cold conditions for generations, still have the acclimatory capacity to modulate their membrane saturation states. They established that the lipid profile is consistent for all three Antarctic species, and that membrane lipid composition varies between Antarctic species and the non-Antarctic. High levels of unsaturated fatty acids (predominantly cis-vaccenic acid and EPA) and modulation of membrane cholesterol level was recorded in Antarctic fish membranes as a mechanism for cold adaptation.

Plants being sessile, it is necessary for their survival to activate efficiently rapid responses to thermal stress. They have to adapt to varying temperatures during night and day cycles and from 40°C in summer to negative temperatures in winter. This includes rapid biochemical and physiological adjustments. Several recent studies have shown that the tolerance mechanisms in plants when undergoing thermal treatment are diverse targeting different aspects of the plant metabolism: photosynthesis, maintenance of the cell membrane integrity, production of heat shock proteins, antioxidants among others (Nievola, Carvalho, Carvalho, & Rodrigues, 2017). The work of (Martinière et al., 2011) emphasized the direct effect of temperature on plant PM viscosity. They investigated the effect of temperature fluctuations on *Arabidopsis* PM viscosity by using dispersion tracking of photoactivated green fluorescent protein<sup>12</sup>

(GFP) and fluorescence recovery after photobleaching in wild-type and desaturase mutant. The lipid profile was monitored to analyse the effect of temperature and membrane lipid composition in PM viscosity. They showed that the PM viscosity in *A. thaliana* reflects ambient temperature only in constant-temperature conditions. In a varying temperature environment, the plant is actively modulating its PM viscosity by altering the proportion of desaturated fatty acids in the membrane. Plasma membrane viscosity is regulated by altering the proportion of desaturated fatty acids. In cold conditions, cell membranes accumulate desaturated fatty acids (C18:2 and C18:3), which decreases membrane viscosity and vice versa. Fatty acid desaturase 2 (FAD2)-dependent lipid desaturation is important for PM homeoviscosity. *fad2.2* plants are impaired in their PM 'homeoviscosity' and show aberrant temperature responses (Martinière et al., 2011).

Mass spectrometry-based lipidomics can provide new insights in the complex of lipid remodeling triggered during adaptive responses to thermal stress. The team of (Lynch & Steponkus, 1987) was the first to show the putative role of sphingolipids of PM in cold responses. Four classes of sphingolipids are present in plants: Long Chain base (LCB, free or phosphorylated), Ceramide (Cer, consisting of an LCB amidified by a fatty acid), Glucosylceramide (gluCer with a glucose head group graft to a ceramide) and GIPC, Glycosyl Inositol Phospho Ceramide. PM fractions of rye leaves were isolated from non-acclimated and acclimated seedlings for lipid analysis. They found that gluCer decreased from 16 to 7 mole % of the total lipid following cold acclimation. In addition, the relative proportions of associated hydroxy fatty acids, including h22:0, h24:0, h22:1, and h24:1 were altered (Lynch & Steponkus, 1987). (Yoshida, Washio, et al., 1988) used differential scanning calorimetry (DSC) to investigate the thermotropic properties of lipids extracted from plasma membrane and tonoplast isolated from the chilling-sensitive mung bean. DSC measurements on the separated classes of lipids revealed that gluCer and a highly saturated phospholipid of the membranes are involved in the phase transitions of the total lipid fractions, hence the possible role of gluCer in chilling responses.

The reduction of PM gluCer from 7.3 to 4.3 mol % after cold acclimation of *Arabidopsis* genotypes was characterized by (Uemura, Joseph, & Steponkus, 1995). When comparing grapevine species having different tolerance levels to freezing

temperatures, (Kawaguchi, Imai, Naoe, Yasui, & Ohnishi, 2000) demonstrated that high levels of t18:1(8Z) in gluCer were correlated with freezing-tolerant species.

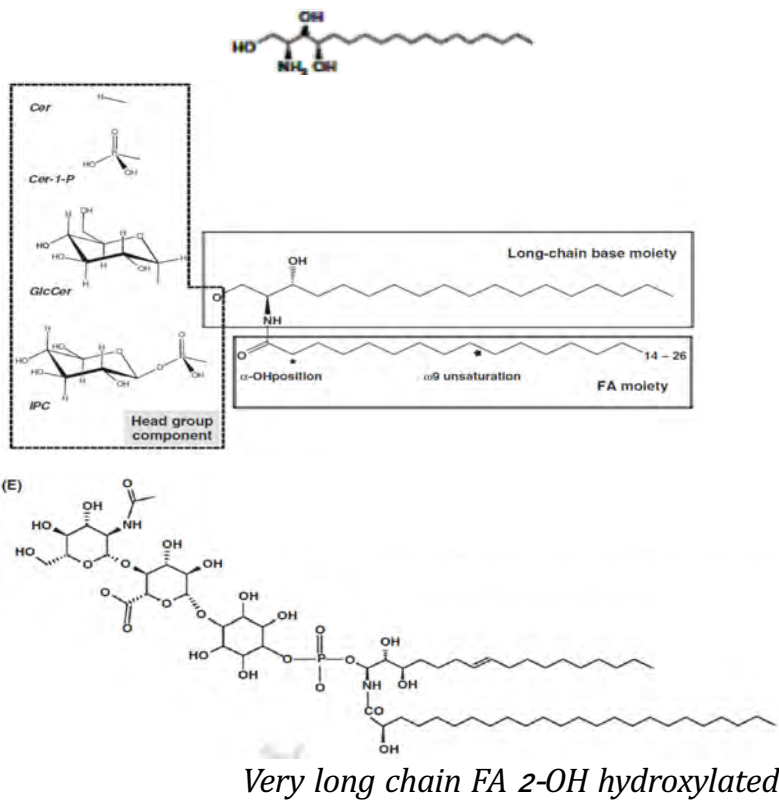
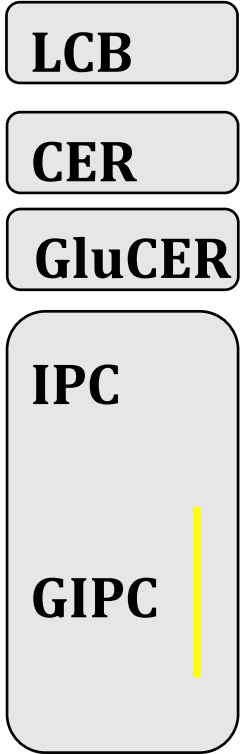
More recently, delta 8 desaturases in Arabidopsis (AtSLD1 and AtSLD2) were characterized by (Ming Chen, Markham, & Cahoon, 2012). These enzymes are involved in low temperature responses. Double *sld1 sld2* mutants lacked apparent growth phenotypes under optimal conditions, but displayed altered responses when exposed to low temperatures. The mutants displayed reduced levels of gluCer and when complemented with wild-type AtSLD1, an increase in GIPC was observed (see below for details of GIPC structure metabolism and function, PLR review, chapter 6.1.2). Hence, there might be specific channeling of ceramides for the synthesis of gluCer or GIPC in response to chilling stress (M. Chen, Han, Dietrich, Dunn, & Cahoon, 2006). This paves the way into understanding more about the role of sphingolipid, especially GIPC, in structuring the PM under cold stress.

### **GIPC, plant major sphingolipid, as a mediator in PM signalling in salt stress**

A tight equilibrium of different sphingolipid species is important for the survival and growth of plants during both biotic and abiotic stresses. Various cellular and environmental responses are conducted by sphingolipid metabolites and sphingolipids (Hou, Ufer, & Bartels, 2016).

Recently, the involvement of GIPC was shown in response to salt stress. Salt stress is caused by high concentration of sodium and chloride ions in the soil, it severely impairs plant growth as it imposes osmotic and ionic stresses (Ismail, Takeda, & Nick, 2014; Sewelam, Oshima, Mitsuda, & Ohme-Takagi, 2014). Excess soluble salt is damaging for plant development and growth. It has wide agricultural and economic impact. Salt stress triggers short-term responses, perceived and transmitted signals then activates long-term responses at the transcriptional level regulating the plant development and growth. One of the main mysteries of the perception of salt stress in plant is salt sensors. Sensing salt stress triggers different and complex stress-response pathways such abscisic acid (ABA) pathway, osmotic stress signalling, salt overly sensitive

P  
O  
L  
A  
R  
I  
T  
Y



**Four classes of sphingolipids found in plants ; .** Four classes of sphingolipids are present in plants: Long Chain base (LCB, free or phosphorylated), Ceramide (Cer, consisting of an LCB amidified by a fatty acid), Glucosylceramide (gluCer with a glucose head group graft to a ceramide) and GIPC, Glycosyl Inositol Phospho Ceramide.

(SOS) pathway and even plant cell through plasma membrane-located Arabidopsis leucine-rich repeat receptor kinases (LRR-RKs) (Yang & Guo, 2018).

Salt is responsible to exert osmotic and ionic stress as high salinity increases both osmotic pressure and ionic strength (Munns & Tester, 2008; Yang & Guo, 2018). To isolate Arabidopsis mutants defective in osmotic stress-induced  $\text{Ca}^{2+}$  increases,  $\text{Ca}^{2+}$ -imaging is used combined with genetic screens. As a result, osmosensing OSCA1  $\text{Ca}^{2+}$  channel was discovered (Yuan et al., 2014). In a similar approach, a recent work by (Jiang et al., 2019), optimized a similar  $\text{Ca}^{2+}$ -imaging-based genetic screens and isolated Arabidopsis mutants defective specifically in ionic stress-induced increases in calcium ions. One of the mutants is called *monocation-induced  $\text{Ca}^{2+}$  increase 1* (*moca1*). MOCA1 protein is a glucuronosyltransferase (GT) for glycosyl inositol phosphorylceramide (GIPC) in the plant PM. In *moca1* plants, monovalent cations are reduced and an increase in calcium ions in response is observed. In the mutant, GIPC level decreases while inositol phosphoryl ceramide (IPC) is increased. MOCA1 encodes a glucuronosyltransferase for GIPCs. Hydrophobicity analyses showed that MOCA1 is an integral membrane protein with six trans- membrane (TM)  $\alpha$ -helices and the *moca1* mutant has a four-amino-acid-residue deletion in TM6.

It is suggested that in *moca1*, GIPC levels are above the threshold level required for normal growth and development but being low enough to compromise salt sensing (Jiang et al., 2019). The negatively charged GIPCs are structural homologues of animal gangliosides, which regulate receptors and ion channels as well as  $\text{Ca}^{2+}$  homeostasis (Gronnier, Germain, Gouguet, Cacas, & Mongrand, 2016) (Ledeen & Wu, 2015). It was hypothesized that the highly negatively charged GIPCs could provide  $\text{Na}^+$ -binding sites on the cell surface. Just like its homologous in animal involved in the regulation of channels, GIPC could gate  $\text{Ca}^{2+}$  influx channels in plants (Green, 1991). They measured the cell surface charges in response to sodium ion treatment, and found that in wild-type protoplasts, an increase in NaCl concentration leads to increasing the  $\zeta$ -potential corresponding to cell-surface potentials. In *moca1* however, the  $\zeta$ -potential was lower than in wild-type protoplasts. The  $\zeta$ -potentials of the mutant did not respond to NaCl treatment. This demonstrates the importance of GIPC in maintaining the electric charges on the surface of the plant plasma membrane.

## **GIPC metabolites in biotic stresses**

In this subchapter, we shall discuss briefly the importance of sphingolipids in maintaining plant integrity when faced by biotic stresses (bacteria, fungi ...). We shall focus on the importance of sphingolipid metabolites and some enzymes involved in the biosynthesis of GIPC.

One of the main enzymes involved in the biosynthesis of GIPC polar head group is InositolPhosphorylCeramide Synthase (IPCS) (see Annexe for biosynthetic pathway of GIPC). A mutation in the inositol phosphoryl ceramide synthase (IPCS) gene was shown to result in an increased level of ceramides leading to cell death. In its functional form, IPCS gene is associated with plant defence by suppressing RPW8-mediated resistance to powdery mildew (Wang et al., 2008).

Mycotoxins, such as fumonisin B1 (FB1) are able to inhibit the key ceramide synthase enzymes, inducing programmed cell death (PCD) (Michaelson, Napier, Molino, & Faure, 2016). The accumulation of long chain bases (LCBs) is a signal for PCD even when other ceramides are depleted. These symptoms can be avoided by treatment with the drug myriocin. Myriocin inhibits the serine palmitoyltransferase (SPT) activity resulting in the reduced accumulation of LCB (Spassieva, Markham, & Hille, 2002). Hence, the plant remains viable during pathogen invasion and proliferation. During pathogen invasion, the non-phosphorylated forms of sphingolipids are produced, which trigger PCD, this is a defense reaction activated by plants at the site of infection.

(Luttgeharm, Chen, et al., 2015) showed that the overexpression of ceramide synthase genes in *Arabidopsis* triggered PCD. The ceramide synthase genes, LOH1 (At3g25540), LOH2 (At3g19260) and LOH3 (At1g13580) are key enzymes of sphingolipid synthesis. LOH1 and LOH3 produce ceramides characterized by very long-chain fatty acids (VLCFA) linked to trihydroxy LCBs, this is the biosynthetic route of ceramides enriched in GIPC (see Annexe for biosynthesis scheme). LOH2 produces ceramide enriched in GlcCer, which have dihydroxy-LCBs and C-16 fatty acids acyl chain (Luttgeharm, Chen, et al., 2015). The overexpression of LOH2 causes dwarf growth, enhanced salicylic acid (SA) production and the constitutive expression of

hypersensitive genes leading to PCD. The study also shows that LOH2 and LOH3 overexpression in *Arabidopsis* increases resistance to FB1, while FB1 strongly inhibits LOH1. The constitutive induction of PCD may have been caused by increased accumulation of C16 fatty acids containing dihydroxy ceramides, which are the product of LOH2, and that C16-ceramide may have enhanced the production of SA.

Another example of the important role of sphingolipid in plant/pathogen interaction is described in (Siebers et al., 2016). Fungi, just as plants, synthesize gluCer and GIPC. *Fusarium graminearum* is a common pathogenic fungus of cereal grains. The mutant deficient in GlcCer has reduced virulence on wheat but is able to retain its virulence on *Arabidopsis* leaves and flowers. This implies that the sphingolipid plays an important role in inducing host dependent virulence. For fungi such as *Fusarium graminearum*, the methylation of gluCer at the C-9 position is important for pathogenicity. This is helpful in agriculture as a strategy to reduce fungal pathogen infection. Crop performance can be improved during fungal attack by introducing structure specific demethylation mechanism in plant system integrating the sensing of C-9 methylated GlcCer and regulating the ultimate response (Ali, Li, Wang, & Guo, 2018). The importance of GIPC as receptors to pathogen-secreted toxins will be discussed in the PLR review, chapter 6.1.2 (see below).

### **The plant plasma membrane in a biological point of view**

The review ***Plant lipids: Key players of plasma membrane organization and function*** thoroughly describes the plant plasma membrane in its organization (lipid composition, protein, bilayer structure...) and physiological roles. I am co-first author of this review with Paul Gouguet, published during the third year of my thesis. Contributing to the edition of this paper has been a rich experiment. I was responsible of writing chapter 2.2. on plant Sphingolipids, chapter 4.1. on the Asymmetric composition of inner and outer leaflet, as well as correcting and proof-reading the entire document.

Here is a summary of the important aspects of the PM focusing on GIPCs followed by the review ***Plant lipids: Key players of plasma membrane organization and function:***

The PM of eukaryotic cells is made up of protein and lipids. We shall focus on lipids. There are three main classes of lipids: glycerolipids, sterols and sphingolipids, for which several thousand different molecular species exist (Yetukuri et al., 2008; Shevchenko et al., 2010). In plants, sphingolipids are highly complex with a large structural diversity, and are of four main groups: LCB, ceramides (CER), glucosylCERamide (gluCER) and Glycosyl Inositol Phosphoryl Ceramides (GIPCs) representing ca. 0.2 %, 2%, 34% and 64% of total sphingolipids, respectively, in *Arabidopsis thaliana* (Markham et al., 2006). GIPCs represent up to 45 mol% of the total plant PM lipids, they are absent in animal and structurally homologous to gangliosides.

GIPCs interact preferentially with themselves or with sterols to form segregated highly-ordered domains or nanodomains (Cacas et al., 2016). By undergoing phase separation into liquid-disordered (Ld) and liquid-ordered (Lo) phases, lipids regulate and mediate protein clustering in the membrane, sub-organizing the PM into nanodomains. GIPCs enhance the sterol-induced ordering effect by increasing the formation and size of sterol-dependent ordered membrane domains in model membranes (Grosjean et al., 2015). In addition, there is also an important trans-leaflet lipid asymmetrical distribution in the PM (Takeda & Kasamo, 2001; Tjellstrom, Hellgren, Wieslander, & Sandelius, 2010). Unsaturated phosphoglycerolipids and galactolipids (DGDG) are mostly in the cytosolic PM leaflet, while sterols and gluCER are likely located in the outer leaflet (Cacas et al., 2016a; Tjellstrom et al., 2010). The exact location of GIPCs, between the two leaflets, still remains to be experimentally determined although it is proposed that they are entirely located in the outer leaflet(Cacas et al., 2016a).



## Review

## Plant lipids: Key players of plasma membrane organization and function

Adiilah Mamode Cassim<sup>a,1</sup>, Paul Gouguet<sup>a,1</sup>, Julien Gronnier<sup>a,2</sup>, Nelson Laurent<sup>b</sup>,  
Véronique Germain<sup>a</sup>, Magali Grison<sup>a</sup>, Yohann Boutté<sup>a</sup>, Patricia Gerbeau-Pissot<sup>b</sup>,  
Françoise Simon-Plas<sup>b,3</sup>, Sébastien Mongrand<sup>a,\*,3</sup>

<sup>a</sup> Laboratoire de Biogenèse Membranaire (LBM), CNRS, University of Bordeaux, UMR 5200, F-33882 Villenave d'Ornon, France

<sup>b</sup> Agroécologie, AgroSup Dijon, INRA, University of Bourgogne Franche-Comté, F-21000 Dijon, ERL 6003 CNRS, Dijon, France



## ARTICLE INFO

## Keywords:

Plant  
Plasma membrane  
Sphingolipids  
Sterols  
Phospholipids  
Signaling  
Nanodomain  
Microdomain  
Raft  
Plasmodesmata  
Liposome  
Model membrane  
Detergent  
Biophysics  
Interleaflet registration  
Interdigitation  
Pinning

## ABSTRACT

The plasma membrane (PM) is the biological membrane that separates the interior of all cells from the outside. The PM is constituted of a huge diversity of proteins and lipids. In this review, we will update the diversity of molecular species of lipids found in plant PM. We will further discuss how lipids govern global properties of the plant PM, explaining that plant lipids are unevenly distributed and are able to organize PM in domains. From that observation, it emerges a complex picture showing a spatial and multiscale segregation of PM components. Finally, we will discuss how lipids are key players in the function of PM in plants, with a particular focus on plant-microbe interaction, transport and hormone signaling, abiotic stress responses, plasmodesmata function. The last chapter is dedicated to the methods that the plant membrane biology community needs to develop to get a comprehensive understanding of membrane organization in plants.

## 1. Introduction

The Plasma Membrane (PM) is a key structure protecting the cell, regulating nutrient exchanges and acting as a control tower allowing

the cell to perceive signals. Plasma comes from the greek *πλάσμα* meaning “which molds”, meaning that the PM takes the shape of the cell by delimitating it. The PM harbors the appropriate signaling cascades allowing adaptive responses ensuring proper cell functions in a

**Abbreviations:** ASG, Acylated Steryl Glycosides; BY-2 cell, tobacco Bright-Yellow 2 cell culture; CAZyme, CARbohydrate-active enZymes data base; CER, CERamides; DOPC, 1,2-DiOleoyl-sn-glycero-3-PhosphoCholine; DPPC, 1,2-DiPalmitoyl-sn-glycero-3- PhosphoCholine; DRM, Detergent-Resistant Membrane fraction; DRP1A, Dynamain-Related Protein1A; ER, Endoplasmic Reticulum; EVs, Extracellular Vesicles; FRET, Fluorescence Resonance Energy Transfer; G proteins, Guanine nucleotide-binding proteins; GIPC, Glycosyl Inositol Phosphoryl Ceramides; gluCer, glucosylCeramide; GT, GlycosylTransferases; GUV, Giant Unilamellar Vesicles; hVLCFA, 2-hydroxylated Very Long Chain Fatty Acid; ISO, Inside Out Vesicles; K-Ras, Kirsten RAT Sarcoma virus; Ld, liquid-disordered; Lo, liquid-ordered; MCS, Membrane Contact Site; MSC, Membrane Surface Charge; PALM, Photo-Activated Localization Microscopy; PAMPs, Pathogen-Associated Molecular Patterns; PC, Phosphatidylcholine; PdBG2, Plasmodesmata Beta-1,3-Glucanase 2; PDCB1, Plasmodesmata Callose Binding 1; PDs, plasmodesmata; PIN, PINformed; POPC, palmitoyl-oleoyl-PC; PRR, Pattern Recognition Receptor; REM, REMorin; RGS1, Regulator of G-protein signaling; RSO, Right Side Out vesicles; SG, Steryl Glycosides; SIM, Structured Illumination Microscopy; SMLM, Single-Molecule Localization Microscopy; So, solid-ordered; STED, Stimulated Emission Depletion Microscopy; STORM, Stochastic Optical Reconstruction Microscopy; VLCFA, Very Long Chain Fatty Acid

\* Corresponding author at: Laboratoire de Biogenèse Membranaire (LBM), Unité Mixte de Recherche UMR 5200, CNRS, University of Bordeaux, F-33882 Villenave d'Ornon, France.

E-mail addresses: [francoise.simon-plas@inra.fr](mailto:francoise.simon-plas@inra.fr) (F. Simon-Plas), [sebastien.mongrand@u-bordeaux.fr](mailto:sebastien.mongrand@u-bordeaux.fr) (S. Mongrand).

<sup>1</sup> AMC and PG must be considered as co-first authors.

<sup>2</sup> Present address: Cyril Zipfel's laboratory. Institute of Plant Biology, University of Zurich, Zollikerstrasse 107. 8008 Zurich Switzerland.

<sup>3</sup> FSP and SM must be considered as co-corresponding and last authors.

<https://doi.org/10.1016/j.plipres.2018.11.002>

Received 31 July 2018; Received in revised form 7 November 2018; Accepted 9 November 2018

Available online 19 November 2018

0163-7827/ © 2018 Elsevier Ltd. All rights reserved.

continuously fluctuating environment, crucial for cell survival. To address this challenge, the PM needs to be both stable and robust yet incredibly fluid and adaptable. This amazing combination of long-term stability and short-term dynamics in order to adapt to signals relies on its fascinating molecular organization. PMs are extremely complex systems, harboring many different molecular species of lipids in which heterogeneity is more likely to occur than homogeneity. In plants as in animals, the recent development of proteomics, lipidomics and methods to visualize lipids and proteins *in vivo* has greatly increased our knowledge of the PM.

The combination of biophysical, biochemical, and cell biology approaches, recently including super-resolution imaging both of the PM's physical state and of the nanometric distribution of its constituents has significantly broadened our vision of PM organization. In this update review, we will present the current state of knowledge of the plant-PM lipid composition, then we will examine how lipids govern the nano- and micro-scopic properties and organization of the plant PM. We will illustrate how the available data show that lipids are not distributed homogeneously within and between each leaflet of the PM. The role of interdigitation and registration between these two leaflets will be also discussed. Finally, we will show how lipids contribute to the organization of the PM, and how this organization plays a decisive role in a certain number of essential processes of plant cell physiology including immunity, abiotic stress and cell-to-cell communication through plasmodesmata. The involvement of lipids as signaling second messenger molecules are not reviewed in details here, except for plant microbe interactions, and we prompted the readers to refer to reviews [1].

## 2. Update on the lipid content of plant PM: how to visualize them?

The PM is an asymmetric proteo-lipidic matrix. The lipid-to-protein ratio (mass/mass) was experimentally determined to be close to 1.3 in tobacco PM [2]. Therefore, one can estimate a molar ratio of 1 protein for 50–100 molecules of lipids. Proteomic data on purified plant PM identified *ca.* 500–1000 proteins in the PM, and the lipidome is theoretically made up of thousands molecular species of glycerophospholipids, sphingolipids and sterol-based structures [3]. A conserved feature of cellular organelles is the distinct lipid composition of their membranes, essential to specify their identity and function.

Highly purified RSO (right side out) PM vesicles are easily obtained using a two-phase aqueous polymer partition system from various plant material [4]. Enzymatic reactions or western blotting are generally used to address the purity of the PM fractions and the absence of contaminants. In parallel, development of high-throughput lipidomic methods by LC-MS allow the complete characterization of the main class of lipids present in the plant PM [5,6]: phospholipids [7], phosphoinositides [8], sphingolipids [9,10] and sterols [11,12]. Such procedures allow the characterization of the molecular species of each lipid class at a level of detail including the fatty acid position for glycerolipids, the nature of long-chain bases for sphingolipids and the many classes of phytosterols [13]. Besides these biochemical tools, strategies have been developed to visualize lipids *in vivo* using biosensors showing affinity for lipids. Imaging lipidomics have also been developed, particularly in seeds [14,15] but the resolution is not yet high enough to allow the characterization of lipids inside a given membrane. Recently, “Imaging lipidomics: automated MS imaging of tissue with lipid structure identification” by Ellis et al. (Nature Methods) reported a method that enables the acquisition of lipid tandem mass spectrometry data in parallel with a high-resolution mass spectrometry imaging experiment. Authors developed a lipidome-per-pixel approach able to identify in rat cerebellar tissue hundreds of lipid molecule species and their spatial locations [16,17]. Nano-SIMS (Secondary-ion mass spectrometry) has also been developed with labeled lipids allowing the deciphering of lipid segregation in the plane of the PM in animal cell culture with a lateral resolution of 90 nm [18]. This high-resolution method is yet to be introduced in plants as the cell wall could strongly

impair access to the PM.

### 2.1. Glycerolipids: galactolipids, phospholipids and phosphoinositides

Phospholipids represent *ca.* 30% of tobacco PM lipids [2]. As can be expected, Phosphatidylcholine (PC) and Phosphatidylethanolamine (PE) are the major phospholipids of plant PM with palmitic and linoleic acids as main acyl chains [7,19–24]. Phosphatidylglycerol (PG), phosphatidylinositol (PI), phosphatidic acid (PA) and phosphatidylserine (PS) are minor phospholipids. Among these phospholipids, only PS is associated with a high proportion of very long chain fatty acids *e.g.*, behenic C22 and lignoceric C24 acid.

Polyphosphoinositides or phosphatidylinositol-phosphates (PIPs) represent a minor fraction of total phospholipids; they are composed of a PI backbone with up to 3 phosphorylations on the inositol moiety. PIPs are involved in many regulatory processes, such as cell signaling and intracellular trafficking. Membrane compartments are enriched or depleted in specific PIPs, providing a unique signature for these compartments. The precise subcellular localizations and dynamics of PIPs were revealed in plants thanks to the design of genetically encoded biosensors with distinct relative affinities [25,26]. Recently, a full set of phosphoinositide biosensors was generated in *Arabidopsis thaliana* called “PIP-lines” [27]. This library extended the range of available PIP biosensors and allowed rapid progress in the understanding of PIP dynamics in plants as well as its monitoring *in vivo*, see below. Hence, not only phosphatidylinositol-4-phosphate (PI4P), phosphatidylinositol-3-phosphate (PI3P), phosphatidylinositol-4,5-bisphosphate (PI4,5P<sub>2</sub>), phosphatidylinositol-3,5-bisphosphate (PI3,5P<sub>2</sub>), phosphatidylinositol-3,4,5-triphosphate (PI3,4,5P<sub>3</sub>), but also PS and PA can be visualized via these biosensors [27–30]. Quantitative imaging analysis revealed that there is a gradient of PI4P throughout the cell, with the highest concentration at the PM, intermediate concentration in post-Golgi/endosomal compartments, and the lowest concentration in the Golgi apparatus. A similar gradient of PI3P was observed from high concentrations in late endosomes to low concentrations in the tonoplast. Inside the PM, polyphosphoinositides (PI4P and PI4,5P<sub>2</sub>) were enriched in detergent resistant membranes (DRMs, see below) compared with the whole PM, suggesting that PIPs could be present inside domains at the PM [31]. This hypothesis was further supported by the visualization of nanodomain-like clustering by immunogold labeling [31]. Importantly, PIPs and PS influence membrane biophysical properties, which emerge as important features in specifying cellular territories; this is discussed in the chapter 2.

Note that Digalactosyldiacylglycerol (DGDG), present in plastids, is also found in the plant PM particularly in response to phosphate deprivation [32,33]. Neutral lipids like diacylglycerol (DAG) were also visualized *in vivo* [34] and showed to be present at the PM of root epidermal cells in the transition zone, at the trans-Golgi network, the cell plate during cytokinesis, and the apex of growing root hairs.

### 2.2. Sphingolipids

Sphingolipids are ubiquitous in eukaryotes with a sphingoid backbone called the long-chain amino-alcohol base (LCB). They are abundant and essential components of biological membranes and they can represent up to 10% of total lipids in plants [35] Detected for the first time in 1870 in brain samples, their name comes from the greek Σφιγξ “to squeeze, to strangle” related to the strong amide bond that composes the link between their two lipophilic moieties and with an allusion to the Sphinx for the cryptic nature of these lipids at the time of their discovery. In animal PMs, the main sphingolipid class is sphingomyelin, which is not present in plants. Minor sphingolipids called gangliosides are a class of acidic glycolipids that play an important role in immunity and modulate cellular signal transduction events [36].

Plant sphingolipids are of four major classes: ceramides (CER), glucosylceramide (gluCer), Glycosyl Inositol Phosphoryl Ceramides

(GIPC) and free Long Chain Bases (LCBs), representing ca., 2%, 34%, 64% and 0.5% of total sphingolipids, respectively in *Arabidopsis thaliana* [10]. In addition to the PM, sphingolipids are enriched in endosomes and tonoplasts, representing around 10 to 20% of total membrane lipids [37]. The complex structural diversity of plant sphingolipids arises from the possible occurrence of three very diverse building blocks: the polar head, the fatty acyl chain linked by an amide bond (forming a ceramide) to the LCB [38].

In this review, we will mostly focus on GIPC because recent discoveries on the role of these lipids in the organization of the PM [39] and as toxin receptors [40] swung them into the spotlight. GIPC are representatives of a class of acidic glycolipids from plants, possibly analogous to the acidic gangliosides found in animal cell membranes. They have been discovered during the late 1950's by Edward Carter [41], studied during 20 years and later forgotten until the beginning of the 2000's, see below. GIPC are composed of a ceramide and a glycan polar head group. The diversity of GIPC resides in: 1/the length, the number and position of hydroxylations and unsaturations in the FA chain; 2/the hydroxylation degree, saturation and position of double bond(s) in the LCB; 3/the nature and the number of glycans, and the type of glycosidic links between the glycans that compose the polar head group [38,42]. In general, the ceramide moiety of plant GIPC consists mainly of a t18:0 (trihydroxylated saturated LCB of 18 carbon atoms) or a t18:1 (trihydroxylated and monounsaturated LCB of 18 carbon atoms) as LCB, amidified to a Very Long Chain Fatty Acid (VLCFA) or 2-hydroxylated VLCFA (hVLCFA). Hence, 95 mol% of PM VLCFA and hVLCFA are amidified in GIPC [39]. The polar head of GIPC is made up of a phosphate linked to an inositol to which glycan moieties are bound. The degree of glycosylation of the GIPC polar head groups defines the different GIPC series.

The basic structure of the GIPC polar head is an inositol phosphoryl ceramide (IPC) backbone linked to a glucuronic acid (GlcA). A sugar unit bound to GlcA-IPC forms the series A GIPC. Only a few structures have been fully resolved with the exact sugars and the nature of the sugar bond: tobacco series A GIPC has the most basic known structure: GlcNAc( $\alpha$ 1- > 4)GlcA( $\alpha$ 1- > 2)inositol-1-O phosphorylceramide [43]. Additional sugar moieties such as glucosamine (GlcN), *N*-acetylglucosamine (GlcNAc), arabinose (Ara), galactose (Gal) and mannose (Man) may lead to glycan patterns of three to seven sugars, so-called series B to F GIPC, see Fig. 1. GIPC found in corn seeds display branched polar heads, see for review [44]. These series are species- and tissue-specific [10,45–48]. In *Arabidopsis*, series A Man-GlcA-IPC is predominant in leaves [45,49], and GlcN(Ac)-GlcA-IPC is mainly in seeds and leaves [50], seeds [51], as well as in cultured tissues of rice [52] and tobacco [45]. The core structure of series B, predominant in monocots is yet to be deciphered. A broad study of the GIPC polar head of 23 plant species from algae to monocots [46] further showed that polar head structures are largely unknown and versatile for the different biological taxa. Kaul and Lester calculated the ratio between carbohydrate/LCB/Inositol in purified polyglycosylated GIPCs and showed that GIPCs may contain up to 19–20 sugars [53].

The polar head also accounts for the high polarity of the GIPC and its subsequent insolubility in traditional lipid extraction solvents, such as chloroform/methanol (2/1, v/v). Hence, even 50 years after their discovery, the structure and character of GIPC remain elusive. GIPC are not commercially available but different purification procedures have been published [45,49,53–55]. With the emergence of more comprehensive extraction techniques and technological advances in the field of sphingolipidomics over that past decade, more accurate quantification of sphingolipids and the discovery of novel structures are underway.

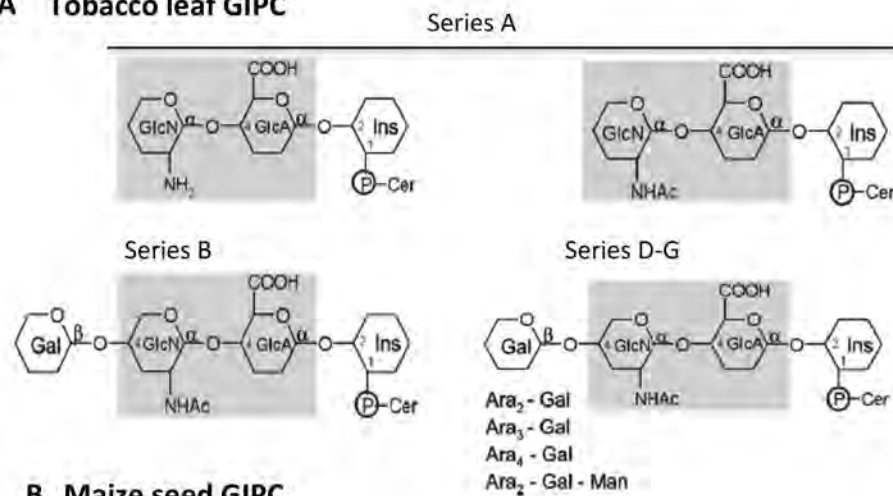
While the synthesis pathway of gangliosides, their animal counterparts, are well studied, that of plant GIPC remain uncharacterized. The biosynthesis of sphingolipids starts with the condensation of serine and palmitoyl-CoA in the Endoplasmic Reticulum (ER), catalyzed by serine palmitoyl transferase (SPT) forming the 3-ketosphinganine [38]. The second step is the reduction of 3-ketosphinganine by the enzyme 3-

ketosphinganine reductase (KSR) generating sphinganine (d18:0), the most basic LCB. The condensation of an LCB with a fatty acyl chain (in the case of GIPC a VLCFA) by ceramide synthases also known as Lag 1 Homolog or LOH 1,2 and 3 produce a ceramide. The specificity of these enzymes relies on the length of the acyl chain and the hydroxylation degree (di- or tri-hydroxylation) of the LCB [56]. The next steps are the modifications of LCBs by the LCB C-4 hydroxylase,  $\Delta$ 4 desaturase, and  $\Delta$ 8 desaturase arising up to nine different LCB structures [9]. LCB unsaturation steps are estimated to occur after condensation into ceramide (discussed in [57]). Although this is not fully evidenced in plants, but free LCB composition in plants supports this statement (much lower unsaturation rate than complex ceramides) and animal delta-4 desaturase does catalyze unsaturation of [58].

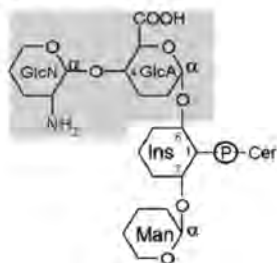
Ceramides can also be phosphorylated in the ER by ceramide kinases CERK or ACD5 [59]. There can also be a hydroxylation of the alpha-carbon of the fatty acyl chain [35,45] yielding hydroxyl-ceramide. The hydroxylation of sphingolipids likely plays a role in the interaction of the hydroxyl group between GIPC and with sterols in the PM [60,39]. The enzymes responsible for the hydroxylation have been identified in *Arabidopsis*, named FAH 1 and FAH2. As biosynthetic intermediates, ceramides are used in the synthesis of the two major PM sphingolipids: GluCer and GIPC accounting for 5–10% and 40 mol% of PM lipids, respectively [2]. The synthesis of GluCer is located in the ER and is catalyzed by plant a glucosylceramide synthase (GCS) with sterol glucoside (SG) acting as a glucosyl donor [61]. The ceramides are converted to GIPC by several glycosylation steps in the Golgi apparatus. The first enzyme involved in the synthesis of GIPC is the inositol phosphorylceramide synthase (IPCS) converting ceramide into inositol phosphorylceramide (IPC). In plants and fungi, PI is the donor of the phosphorylinositol moiety [62]. This enzyme first identified as ERH1 (enhance RPW8-mediated Hypersensitive response-like cell death) in plant holds a key role in modulating plant programmed cell death associated with defense [62]. The pool of ceramide for GluCer or GIPC synthesis is determined by the hydroxylation state of the LCB and acyl chain length. In *Arabidopsis* seedlings, trihydroxy-LCBs (mostly t18:1) are predominant in both GIPC and GluCer. GIPC are characterized by the presence of t18:0 largely associated with VLCFAs while GluCer are composed of dihydroxy-LCBs (d18:1  $\Delta$ 8) in association with 16–18 carbon atom fatty acids (C16) [9]. In both cases, the KO mutation of GCS or IPCS leads to dramatic functional and developmental impairments.

The second enzyme of the GIPC synthesis pathway is the inositol phosphoceramide glucuronosyltransferase (IPUT1). IPUT1 encodes an IPC glucuronosyltransferase, transferring an alpha-glucuronic acid (GlcA) residue onto the IPC backbone. It was the first GIPC glycosylation enzyme to be characterized. The silencing of IPUT1 triggers the accumulation of IPC in *Nicotiana benthamiana*, as well as ceramides and GluCer. Its overexpression increases GIPC content. In *Arabidopsis*, IPUT1 is essential for pollen tube viability. The major defect of the *iput1* mutant pollen is a dysfunction in tube guidance and ovule fertilization [63]. Further glycosylation patterns of GIPC and glycosyltransferases involved are still not well documented. So far only three more proteins involved in the glycosylation process have been characterized. Understanding the diversity of sugar moieties of the polar head and all the biosynthetic pathways involved remain a challenge. Golgi-localized nucleotide sugar transporter (GONST1) was shown to be indirectly involved in GIPC synthesis by specifically supplying GDP-mannose to the Golgi lumen for GIPC glycosylation. Interestingly, in *gonst1* mutants, only mannosylation of GIPC is defective, while that of the cell wall polysaccharides remain unchanged [47]. The mutants also have a dwarfed phenotype and display spontaneous Hypersensitive Response highlighting the importance of GIPC sugar head groups in different plant functions such as defense signaling. Alongside GONST1, GIPC mannosyl-transferase (GMT1) of the GlycosylTransferases (GTs) found in the Carbohydrate-Active Enzymes data base (CAZyme, <http://www.cazy.org>), located in the Golgi and specifically targeting GIPC has

## A Tobacco leaf GIPC



## B Maize seed GIPC



recently been reported to transfer a mannose (Man) onto the GIPC head group by Mortimer team [49]. The phenotype of *gmt1* mutant is fairly similar to that of *gont1* affecting GIPC mannosylation level, displaying a constitutive plant immune response and reducing cellulose content. In plants, GIPC are highly glycosylated with the most common pattern being a GlcA-IPC to which additional glycan moieties such as Man but also glucosamine (GlcN), *N*-acetyl glucosamine (GlcNac) and arabinose (Ara) can be attached [42,45]. The most recent GT identified is glucosamine inositolphosphorylceramide transferase1 (GINT1). It is involved in GIPC glycosylation in seeds and pollen yielding GIPC containing GlcNac and/or GlcN. The study also showed the importance of GlcN(Ac) GIPC in rice seedling survival suggesting once again the importance of GIPC glycan patterns in essential and specific plant functions [64].

Beside biochemical methods (*i.e.* purification of PM coupled with lipidomic analyses), the location of sphingolipids is hardly known *in vivo* due to the lack of appropriate biosensors and fluorescently-labeled lipid-probes. Only one publication reported lipid staining protocols and the use of several fluorescent lipid analogues in *Arabidopsis* leaf tissue and protoplasts [65]. As stated earlier, tobacco PM contains GIPC representing up to 40 mol% of total tobacco lipids, enriched in the outer-leaflet and interacting with sterols in the formation of microdomains of *ca.* 35 nm. GIPC are further enriched in the DRMs. GIPC in DRMs are in their polyglycosylated forms [39]. Modeling approaches of the organization of lipids in the plant PM proposed that acyl terminal ends (six to seven carbon atoms) of the apoplasmic leaflet (h)VLCFA of GIPC penetrate within the inner-leaflet and interdigitate with carbon chains of the inner-leaflet phospholipids [39]. This remains to be fully determined *in vivo*. Interdigititation is an interesting phenomenon which could explain the limited diffusion of proteins in the PM and thermal adaptation [66]. All these aspects of GIPC function will be further discussed in this review.

**Fig. 1.** Determined structures of GIPC glycosidic polar head from tobacco and maize.

A, tobacco GIPC of series A are major in tobacco leaves (top) with glucuronic acid (GlcA) and either glucosamine (GlcN) or *N*-acetyl glucosamine (GlcNac). Other minor polar head of series B and higher glycosylated GIPC with arabinose (Ara), galactose (Gal) and Manose (Man) have been identified, but the precise structure remains to be determined. Grey part is the conserved glycan moiety of glucuronic-Hex. Cer indicates the ceramide moiety, in tobacco, with t18:0 and t18:1 for LCB, and VLCFA mostly alpha 2-hydroxylated; B, GIPC found in corn seeds with branched polar head.

### 2.3. Free and esterified phytosterols

The amount of sterols is relatively stable among plant species *i.e.* 2–3 mg of total sterols per dry gram plant. Synthesized in the ER, sterols accumulate in the PM and reach up to 30 mol% of PM lipids [2]. Higher-plant cells contain a vast array of sterols: *e.g.* 61 sterols and pentacyclic triterpenes have been identified in maize seedlings [67]. Sterols are characterized by a planar sterol backbone made up of four condensed aliphatic rings. Phytosterols are mainly C28 and C29 desmethylsterols with nine or ten carbons side chains. In most cases, the second ring has a double bond between carbon C5 and C6. Phytosterols mainly differ from mammalian cholesterol on the side chain by an extra alkyl group in the C24 position (Fig. 2A, B). For example, campesterol is the phytosterol whose chemical structure is the most similar to that of cholesterol, with only an additional methyl group. In contrast, the  $\Delta^5$ -sterols, with an ethyl group, are represented by  $\beta$ -sitosterol and stigmasterol which contain an additional double bond in the C22 position. The most abundant plant sterol is sitosterol in most species reported including the plant model *Arabidopsis*, except for a few cases such as stigmasterol in tobacco, spinasterol in *Medicago* and isofucosterol ( $\Delta^5$ avenasterol) in many plants [68]. Proportions of other pathway end-products are genetically defined in higher plants [69]. In comparison with cholesterol, the interesting fucosterol that is the major sterol in green algae exhibits modifications at the hydrocarbon tail with a branched chain and a double bond at position C24. Biosynthesis of phytosterols is described in recent reviews [68].

Steryl glycosides (SGs) and acylated steryl glycosides (ASGs) are derivatives of a typical membrane-bound sterol molecule (Fig. 2C). The composition of sterols in SG reflects usually the free sterol composition of the plant. The sugar moiety, the number of sugar and the configuration of its linkage to the sterol may vary. The sugar moiety, most common being the pyranose form of D-glucose, is attached to the 3-hydroxy group at the C3-atom of a sterol and a hydrocarbon side chain at C17. SGs generally carry one or more sugar residues, the steryl D-monoglucopyranoside being the most abundant SG in plants. Finally, an

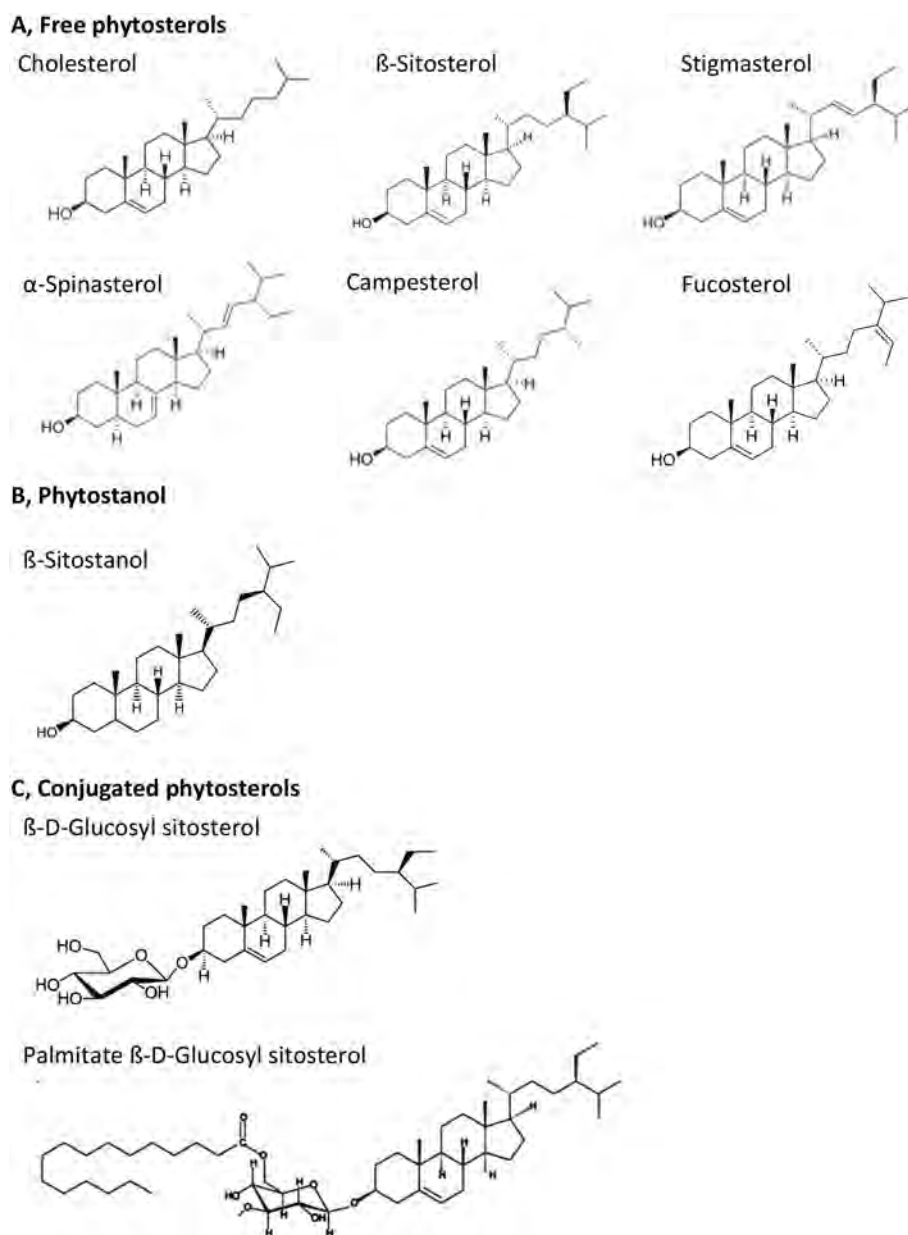


Fig. 2. Structures of specific plasma membrane phytosterols compared with animal cholesterol. A, free phytosterols; B, phytostanol; C, conjugated phytosterols.

acylation of the sugar moiety could increase SG diversity producing ASG forms. Indeed, SGs may be acylated, usually at the C6-atom of the sugar moiety with palmitic, oleic and less frequently with stearic, linoleic, and linolenic acid. Interestingly, the proportions of SG and ASG in PM differ extremely depending on the plant species and the growth conditions [22,70]. The biological role of conjugated sterols has been discussed recently in [68,71].

Elucidation of sterol function benefit from the development of tools for *in situ* visualization, together with forward and reverse genetic approaches are reviewed in. Several methods to visualize sterols have been developed, for review [72]. Filipin has been extensively used as a specific probe for detection of fluorescent filipin-sterol complexes, including on fixed samples. It is the only established tool for sterol visualization in plants [73–76]. Although powerful to visualize domains enriched or deprived in sterol, filipin has also been used to measure the asymmetrical distribution of sterol using purified Right Side Out (RSO) vs. Inside Out (ISO) PM oat vesicles [77]. Recently, imaging method using tunable orthogonal cholesterol sensors allowed simultaneous *in*

*situ* quantification of cholesterol in two leaflets of various mammalian cell PM [78]. This study revealed a marked transbilayer asymmetry of PM cholesterol, with the concentration in the inner leaflet being 12-fold lower than that in the outer leaflet. The asymmetry was maintained by active transport of cholesterol and its chemical retention in the outer leaflet [78]. Development of such sensors for phytosterols (free and conjugated) is of great importance in order to address the role of these lipids in plant biology.

### 3. Lipids govern global properties of the plant PM

#### 3.1. Fluidity of PM

Confined in a restricted two-dimensional space, PM constituents are mobile and animated with membrane fluidity reflecting the dynamic organization of biological membranes [79]. Hydrocarbon chains perform balance and bending movements, giving elasticity to the PM. These undulations are sources of fluidity and can be measured by

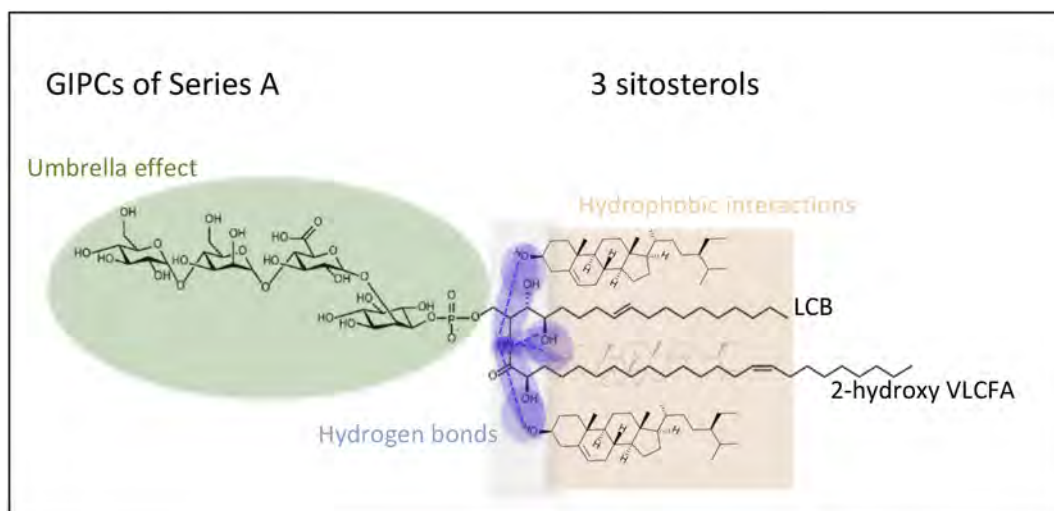


**Fig. 3.** Biophysical features involved between a GIPC of series A and three molecules of sitosterols. These interactions are important for nanodomain formations in the PM. LCB, Long Chain Base; VLCFA, Very Long Chain Fatty Acid.

atomic force microscopy that regrettably shows its real limits of use in plants due to the presence of the cell wall. Lipids and proteins by rotating around their axis or moving in the plane of the PM, lead to increase fluidity. Notably, lateral diffusion within plant PM was firstly evaluated around the order of  $0.02 \mu\text{m}^2 \cdot \text{sec}^{-1}$  for the agglutinin receptor of the PM of wheat grain cells [80], whereas more recent data gives a more than ten-fold higher value of  $0.34 \mu\text{m}^2 \cdot \text{sec}^{-1}$  for the flagellin receptor FLS2 in Arabidopsis protoplast [81]. Indeed, PM proteins exhibit distinct relatively low short-distance lateral mobility within plant PM [82,83]. Depending on the lipid environment, the diffusion of labeled tracer molecule also varies from 0.1 to  $6 \mu\text{m}^2 \cdot \text{sec}^{-1}$  in model membranes [84] highlighting the effect on lipid dynamics of unsaturated and saturated PC and cholesterol. Thus, several factors affect PM fluidity, notably the steric hindrance and the interactions of its constituents. The huge diversity of plant lipids, many of which deviate from the canonical cylindrical form, would thus imply that the PM is bound to be very heterogeneous in its geometrical arrangement [85]. For example, PC occupies similar volumes at both its extremities *i.e.* its polar head and its two acyl chains, corresponding to a cylinder, this geometry generates a spontaneous organization in lamellar phase [86]. Furthermore, the level of unsaturation results in a larger steric hindrance of the carbon chain, and therefore a greater disorder in the arrangement of the lipids.

Alterations in lipid composition during cold acclimation have been known to be associated with increase in tolerance of plants to cold stress *e.g.* [87]. In particular, accumulation of *N*-acylphosphatidylethanolamines (NAPEs) that is related to high lipid unsaturation degree is critical to maintain membrane fluidity. Indeed, changes in lipid composition regulate cryobehavior of the PM [88] by contributing to maintain the membrane phase transition temperature below the chilling temperature [89]. In cold conditions, plant cell PMs accumulate unsaturated fatty acids to decrease membrane viscosity [90]. A similar positive effect on membrane stability is achieved by a decrease in the unsaturation level of individual phospholipids and total lipids during water deprivation [23].

### 3.2. Phytosterols are crucial regulators of membrane order

Sterols are known to favor the packing effect in the membrane bilayer as firstly described for cholesterol in animal membranes [91]. Phytosterols are the major component contributing to plant PM rigidity [92–94]. Interestingly, major free phytosterols differentially modulate the level of membrane order [95,96]. Indeed, campesterol shows a high potency to organize lipid bilayers [97,98] which could be attributed to

its short hydrocarbon tail. Stigmasterol exhibits a much weaker ordering effect than other sterols [99], even if it is a somewhat controversial question [100]. This phytosterol carries an extra carbon-carbon double-bond on the side chain in the C22 position, similarly with  $\alpha$ -spinasterol [101] and brassicasterol [95] that both also display a feeble ordering capacity. Ultrasound velocimetry studies [102] and thermodynamic analysis [103,104] propose a better condensing efficiency for  $\beta$ -sitosterol than for stigmasterol. Such variable ability to pack lipid bilayer has been explained by differential interactions between plant sterols and unsaturated or saturated lipids [105,106]. It is worth noting that phytosterols exist as a mixture within plant PM, and as such allows to finely control the level of membrane order in artificial membrane [99], in model PM of soybean [106] and in native PM of Arabidopsis mutants [107].

Conjugated forms of phytosterols, SG and ASG present in plant PM (Fig. 2) have also been shown to have a strong ability to order membranes [108,109]. Furthermore, free and conjugated phytosterols work in synergy to order the membrane [99]. Regardless of the distribution of SG and ASG between different phases of the PM, it seems very likely that the proportion of these lipids in certain membrane domains clearly exceeds those of phospholipids and thus could locally participate in the control of the biophysical properties of membrane domains. Regarding the scarcely documented properties of phytosterols *i.e.* the saturated analogues of sterols reduced in the double bond in a ring skeleton, Langmuir monolayer studies have evidenced that  $\beta$ -sitostanol (Fig. 2B) exhibited a similar ability to  $\beta$ -sitosterol in strongly interacting with saturated phospholipids [110]. Accordingly, incorporation of  $\beta$ -sitostanol into artificial membranes is able to modify their packing level as well as their behavior [111]. Overall, the multiple phytosterols are essential regulators of membrane order.

### 3.3. Involvement of sphingolipids in PM membrane order

Plant sphingolipids also interact with phytosterols to increase the level of plant PM order, with the notable exception of stigmasterol-GluCer association [92–94,112]. In mammalian models, cholesterol appears to interact preferentially with sphingolipids over phospholipids [113]. Several parameters have been proposed to explain such affinity: 1/sterols emphasize a better shielding from water by the bulky sphingolipid head group; 2/a pairing between the two lipids *i.e.* hydrogen bonding between these lipid species, with the low amount of water at the PM interface increasing the stability of these bonds (Fig. 3). The interface within the region of the membrane of the amide bond of the sphingolipid LCB can both donate and accept a hydrogen bond as well

as the hydroxyl groups of the LCB and Fatty acids; 3/the saturation of sphingolipid hydrophobic tails which increases the order level [114].

In plants, GIPC also show an ability to increase, in a sterol-dependent manner, the lipid packing of the PM [99] and both mechanisms could be similarly proposed (Fig. 3). First, the major GIPC polar head is composed of Hexose–glucuronic acid–inositol–phosphate, and up to seven sugar moieties can be added [45]. Thus, the volume occupied by the head group of GIPC is far much bulkier than phospholipid head groups, and, as a general trend the volume occupied by the phospho-inositol-sugar head group increases with the complexity of the oligo-saccharide chain. Predictions based on the geometrical properties of glycosphingolipid molecules indicated accordingly that local enrichment of such bulkier head group strongly favors phase separation and is concomitantly accompanied by spontaneous acquisition of a positive membrane curvature (for review [36]). Moreover, GIPC LCB profiles are abundant in tri-hydroxylated LCB species in widely varying proportions (for review, see [38]), and one hydroxyl residue is very often present at the 2 position of the fatty acid. One may hypothesize that the presence of these three hydroxyl and the amide groups at the interface between the polar phase and hydrophobic phase of the bilayer may be of importance for sphingolipid/phytosterol interactions, see Fig. 3, but also sphingolipid/sphingolipid interactions [60]. Similar mechanisms have been experimentally confirmed, showing strong interactions between phytoceramides and POPC (palmitoyl-oleoyl-PC) into a highly packed gel phase ( $32.1 \text{ \AA}^2/\text{molecule}$ ) [115], and between GIPC and sitosterols [2].

### 3.4. Electrostatic charge and pH domains of the PM

In all eukaryotes, the PM cytosolic-leaflet is the most electro-negative compartment of the cell [116]. Electrostatic territories are controlled by a combination of negatively charged lipids that are organized as a gradient along the endocytic pathway. Membrane surface charge (MSC) is critical for the specific recruitment to membranes of proteins with polybasic regions. Thus, PM electrostatics is fundamental parameter in signaling, intracellular trafficking and polarity. For example, MSC controls the PM localization and function of the polar auxin transport regulator PINOID as well as proteins from the BRI1 kinase inhibitor 1 (BKI1)/Membrane-associated kinase regulator (MAKR) family, which are involved in brassinosteroid and receptor-like kinase signaling [117]. MSC can be probed by biosensors constituted of a fluorescent protein fused to an unstructured peptide of varying net positive charges [117]. Negatively charged lipids regulate the MSC in plant PM. By contrast to yeast and animals, PI4P strongly accumulates at the PM establishing a negative inner surface potential of this membrane [117]. In addition, it was recently shown that PM surface potential varies according to other negatively charged PM lipids such as PA and PS which are separately required to generate the electrostatic signature of the plant PM [118]. Therefore, the combinatorial lipid composition of the cytosolic leaflet of PM not only defines electrostatic territory but also distinguishes different compartments within this territory by specifying their MSC. How the spatiotemporal pattern of PIPs is established and maintained within plant cell is one of the many future challenges to tackle.

A recent study showed that the pH on both sides of the plant PM is different *in vivo*. Genetically encoded fluorescent pH sensors enable access to membrane-associated pH and transmembrane differential pH values from the surface of the root to the deepest cell layers beyond the Casparian strip barrier [119]. This study demonstrated that the apoplastic pH close to the PM was maintained at values ranging from 6.0 to 6.4 in mature root cells despite direct contact with the soil. By contrast, the overall pH in the apoplastic space is far more acidic [119]. The role of lipids in this observation remains to be determined.

## 4. Plant lipids are unevenly distributed within the PM and able to organize into domains

### 4.1. Asymmetric composition of inner and outer leaflets

During the 1970's, alongside the fluid mosaic model proposed by Singer and Nicholson (1972), experimental evidences showed that proteins and specially lipids could segregate forming a heterogeneous membrane with both lateral and transversal asymmetry. It is also well established in animal cells that there is a compositional heterogeneity of PM lipids between the two leaflets of the PM. In human erythrocyte membranes, the prototype of animal cell PMs, the outer-leaflet is composed of mostly PC and sphingolipids, while the inner-leaflet of PS, PE, and PI as described in [120]. Minor lipids such as PIPs and PA are located in the inner-leaflet, whereas glycosphingolipids face the outer surface. This out-of-equilibrium is maintained by the activity of lipid translocases (namely flippases, floppases and scramblases), which compensate for the slow spontaneous diffusion of lipids. Because of the heterogeneity of lipids, the two monolayers display different physical properties: the inner-leaflet has a lower average viscosity than the outer-leaflet. The importance of membrane asymmetry is well studied in animals, see for recent reviews [121,122].

In plants, only two publications experimentally address the asymmetry of lipids in the PM: by using a phospholipase A2 treatment, filipin labeling and immuno-labeling with antibodies against DGDG and gluCer on purified oat PM, it was shown that DGDG was exclusively located in the inner-leaflet together with 60% of phospholipids, and the GluCer and sterols were enriched in the outer-leaflet [77]. Unfortunately, GIPC and the exact phospholipid content were not addressed in this study. GIPC are synthesized inside the Golgi apparatus, with their polar heads inside the lumen, see Fig. 4, therefore it is very likely that these lipids are located in the outer-leaflet of the PM after fusion of the secretory vesicles. Moreover, the large size of the GIPC' polar heads likely prevents spontaneous flip between the two leaflets. Immunogold labeling on tobacco PM vesicles showed that polyglycosylated GIPC mostly locate in the outer-leaflet of the PM [39].

By taking together these scarce experimental evidences, we recently proposed a model for the distribution of lipids in the plant PM: 1/GIPC and GluCer are exclusively located in the outer-leaflet; 2/sterols (free and conjugated) are enriched in the outer leaflet; 3/phospholipids are enriched in the inner-leaflet with PIPs, 4/PS, PA exclusively in the inner leaflet [39]. Future work should be dedicated to the in depth analysis of the lipid composition of each PM leaflet with special focus on deciphering the diversity of the various molecular species *i.e.* fatty acid content (unsaturation and length) of each class of lipids will be done and the different forms of sterols will be characterized. Numerous methods are available on RSO vs. ISO purified PM vesicles or on live protoplasts cells to address this delicate question [123].

### 4.2. Membrane phases in model and biological membranes

#### 4.2.1. Membrane phases, dyes and modeling approaches

Assembly of lipids can adopt different physical states, the so-called phases. Following the nomenclature introduced by Ipsen [124], lipid organization of lamellar bilayer structures can be divided in three main phases: the solid-ordered (So), liquid-ordered (Lo) and liquid-disordered (Ld) phases depending on the lipid species, acyl chain unsaturation, temperature, pressure and several additional parameters. In So phases, lipids are tightly packed and lateral diffusion is very slow. In Ld phases, lipids are much less condensed, acyl chains are mobile and loosely packed, and lateral diffusion coefficients are high, especially at high temperatures [125]. In Lo phases, like in So phases, a high degree of acyl chain order is observed, but lateral diffusion coefficients are comparable to those of Ld phases. Phase formation in lipid mixtures has been extensively studied *in vitro* with liposomes and giant unilamellar vesicles (GUV) as models. In most reports, GUV membranes exhibit

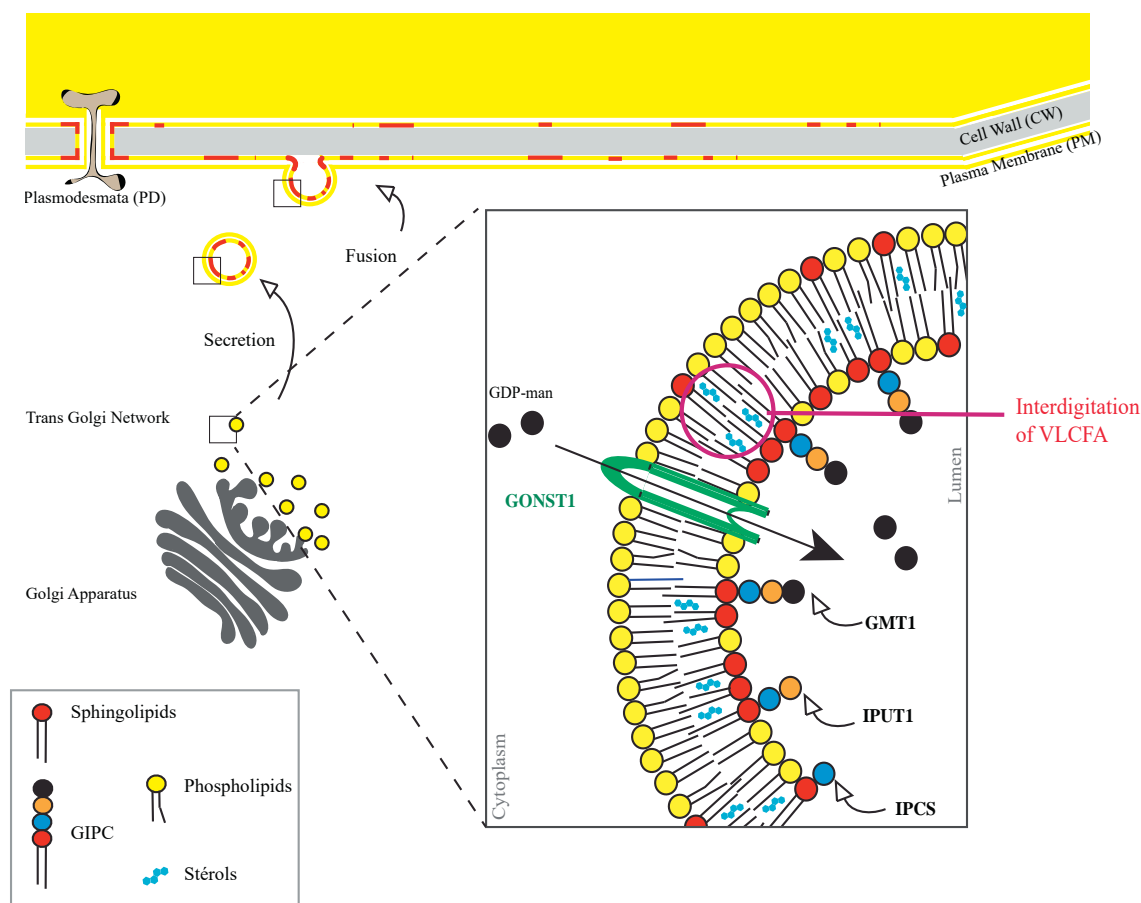


Fig. 4. Formation of GIPC- and sterol-enriched domains along the secretory pathway.

GIPC are synthesized in the lumen of the trans Golgi network (TGN) by grafting on the ceramide sequentially inositol-phosphate (IPCS, inositolphosphorylceramide synthase), glucuronic acid (IPUT1, inositol phosphorylceramide glucuronosyltransferase) and mannose (GMT1, GIPC mannosyl-transferase1). Golgi-localized nucleotide sugar transporter (GONST1) is responsible for the import of GDP-mannose to fuel GIPC synthesis. After vesicular fusion to the PM, GIPC polar heads face the apoplasm. Polyglycosylated GIPC form nanodomains in the PM (in red) [99].

micrometer-size liquid immiscibility over a wide range of temperatures. GUVs with such properties contained a minimum of three components: high-melting temperature lipids (e.g. saturated VLCFA-containing sphingolipids), low melting temperature lipids (e.g. not necessarily but often unsaturated phospholipids), and sterols, for more details see review [126]. Lo phases are also referred to as cholesterol-dependent phases because cholesterol was used in most studies on the subject, [127,128] for reviews. In the mammalian model, lateral partitioning of Lo and Ld phases is thus explained by a preferential interaction of sphingolipids with cholesterol over phospholipids, likely due to better shielding from water by the sphingolipid headgroup [99].

Lo phases are also observed in the presence of various free- and conjugated-phytosterols such as SG and ASG [109,129,130]. Use of environmental fluorescent probes sensitive to membrane order such as di-4-ANEPPDHQ and Laurdan [131] allow the analysis of phase separation on GUVs made of various mixtures of plant lipids. This reveals contrasted abilities of free-phytosterols to control phase separation on model membranes. Although stigmasterol added to 1,2-dioleoyl-sn-glycero-3-phosphocholine (DOPC)/1,2-dipalmitoyl-sn-glycero-3-phosphocholine (DPPC) vesicles fail to induce the lateral segregation of lipids into domains of different order levels, GUVs containing sitosterol and campesterol promote the formation of Lo domains at the surface of model membranes [99]. Noteworthy, SG and ASG added separately exhibit the same ability as the corresponding free sterols, increasing the amount of Lo phase. This effect is reinforced when used in combination and increases strikingly when free and conjugated sterols are present in the mixture [99]. The same study indicates that GIPC, the major plant

sphingolipids [2] are not able alone to promote the formation of a liquid-ordered phase within a phospholipid bilayer revealing no extensive phase separation in the binary sphingolipid/phospholipid system. By contrast, this study shows the ability of GIPC to increase the amount of Lo phase of the membrane in presence of phytosterol and interestingly this remains still the case even in the absence of saturated phospholipids such as DPPC. These *in vitro* studies expose the complex association of different classes of lipids necessary to form distinct phases that are *in vivo* linked to various membrane functions such as cell signaling or development. Yet there is a real benefit to be able to observe this partitioning *in vivo* via fluorescent probes and dyes.

The partitioning of lipid fluorophores between coexisting Lo and Ld phases for different ternary lipid mixtures has been extensively performed by comparing fluorescence intensities in coexisting domains. These labeled lipids have a fluorophore (e.g. NBD, Texas Red, Bodipy, etc...) attached either to the head group or to the hydrocarbon chain. Studies using fluorescently labeled lipid analogues in different mixtures must be analyzed cautiously for several reasons: 1/the fluorophore might alter the distribution of the lipids on which it is grafted *i.e.* a large fluorophore attached to an acyl chain might hamper the incorporation of the labeled lipids into the Lo domains, as found in the case of fluorescent ganglioside probes [132]; 2/It has been shown that the same fluorescent probe might have different partitioning preferences depending on the chosen lipid mixture [133]. Nevertheless, an important finding from this body of research is that partitioning in ordered-phases is increased for fluorophores with saturated chains that approximately match the thickness of one leaflet of the host membrane

[134]. Fluorescent lipid probes with unsaturated chains are found to partition into the Ld phase. These studies indicate the ability of different molecular species of lipids to partition selectively in the different phases of a complex model membrane, according to their structure [135,136].

There is a current lack of such fluorescent probes designed from typical structures of plant PM lipids. This prevents unambiguous assessing of specific lipid behaviors in different complex mixtures. Non-perturbing specific-labeling of PM nanodomains in plant cells has been, and remains, one of the foremost challenges in the field.

Modeling approaches based on simulation can also bring grist to the mill of such experimental evidence. For example, very recent work by Ingolfsson et al., in a pioneering *in silico* study of PM-lipid assembly mimicking the complexity of the animal PM, confirmed the non-ideal lateral mixing of the different lipid species [137]. Based on large-scale molecular dynamics simulation, this study provided a high-resolution view of the lipid organization of the PM at an unprecedented level of complexity since the model consists of 63 different lipid species, 14 types of head groups and 11 types of aliphatic moieties asymmetrically distributed across the two leaflets. This closely mimics an idealized mammalian PM. A general non-ideal lateral mixing of the different lipid species was observed together with the formation and disappearance on the microsecond time scale of transient domains with liquid-ordered characteristics: in the outer leaflet, distinct nanodomains consisting of gangliosides were observed, and PIPs showed preferential clustering in the inner leaflet of PM. Nonetheless, the lack of biophysical parameters for plant lipids necessary for the calculation of molecular dynamics impairs the use of these approaches to modelize plant PM (see section “Conclusions”).

#### 4.2.2. Solubilization by detergents: evidences from model membranes

Detergents are amphiphilic molecules, most of them consisting of a polar head and a hydrophobic chain. These molecules have a conical shape and spontaneously form micellar structures displaying a positive curvature in aqueous solution. Detergents have thus the ability of incorporating themselves into membranes and of solubilizing proteins by replacing their lipid environment. Pioneering work evidencing correlations between resistance to detergent solubilization of a fraction of the PM and its peculiar lipid and protein composition suggested the possible existence of lipid domains in the PM of mammalian cells [138].

Detergent-resistant membrane fractions (DRMs) could be isolated from a variety of eukaryotic cells and gave birth to the hypothesis that such fractions are present within native PM as a distinct phase within the bilayer. DRMs are rich in saturated phospholipids, sphingolipids and sterols, and display the properties of the Lo phase previously described in model membranes. Such a hypothesis received strong support from parallel studies on lipid vesicles constructed to mimic the lipid composition of these membranes [139]. In particular, [140] demonstrated that when mixtures of sphingolipids, unsaturated phospholipids and cholesterol were treated in the cold with nonionic detergents such as Triton X-100, the lower-melting phospholipids were readily solubilized while the higher-melting sphingolipid species, and to a lesser extent cholesterol, were largely recovered in an insolubilized and sedimentable fraction. Similar results were obtained using analogous lipid mixtures without cholesterol, or in which long-chain saturated phospholipids replaced the sphingolipid component. Measurements of diphenylhexatriene fluorescence polarization have suggested that the existence of a DRM fraction was correlated with the presence of Lo phases in the original bilayers. Since that, numerous studies have addressed the differential sensitivity of Lo and Ld domains to detergent solubilization. Nevertheless, only a few reports, like that of [141] compared the effect of distinct detergents on Ld and Lo domain solubilization within model bilayers. Most works indeed focused solely on the impact of Triton X-100. Atomic Force Microscopy (AFM) observations on vesicles containing dioleoyl-PC/sphingomyelin/cholesterol provided evidence for both Triton X-100-insoluble domains composed

of sphingomyelin and cholesterol, and Triton X-100-soluble areas surrounding them [142]. Similarly, using real-time AFM imaging of dioleoyl-PC/sphingomyelin/cholesterol mixtures, [143] found that detergent did not affect sphingomyelin/cholesterol Lo phases, while dioleoyl-PC Ld phases were completely solubilized. Developing the same experimental approach on dioleoyl-PC/dipalmitoyl-PC vesicles, authors showed that Triton X-100 concentrations right above the critical micellar concentration (CMC) enabled the solubilization of the dioleoyl-PC matrix, but prevented dipalmitoyl-PC domains from solubilization [144]. [145] proposed a model based on equilibrium thermodynamics showing that resistance to solubilization only depends on the target lipid affinity with the micellar phase. The effects of cholesterol on the resistance of lipid mixtures to solubilization have also been investigated. Ahyayauch et al. demonstrated that cholesterol facilitates PC solubilization better than sphingomyelin [146]. Furthermore, cholesterol was found to induce higher resistance to solubilization of dipalmitoyl-PC vesicles, with a notable exception at 4 °C. Interestingly, cholesterol also induced higher resistance of palmitoyl-oleoyl-PC bilayers to detergent solubilization on a broader range of temperatures (from 4 to 15 °C) [147]. In addition, sterols are not the only lipid family determining detergent insolubility. For example, it was shown that addition of 5–30 mol% ceramides prevented Triton X-100 from completely solubilizing sphingomyelin-containing bilayers [148]. It is noteworthy that microscopic observations carried out by Staneva et al. [147] revealed neither domain formation, nor domain coalescence in response to Triton X-100 treatment in heterogeneous GUV systems. Such observation supports the idea that isolation of DRM from biological membranes by detergent-induced extraction is not an artifact and moves the question of DRM controversy back to the central importance played by the used methodology.

Cholesterol is not the only sterol to induce resistance to detergent solubilization. Plant sterols, had similar capacity even if a weaker effect than cholesterol, when incorporated in phospholipid bilayers [100], with the lowest efficiency being observed with stigmasteryl, see below. All these results, based on biophysical analysis performed on model membranes indicate: 1/that animal and plant PM-mimicking lipid mixtures undergo a segregation between different phases corresponding to different physical states; 2/that the different lipids present within the bilayer partition differentially in these phases according to their chemical structure; 3/that there is a close correlation between the composition and physical characteristics of the DRM fraction isolated from model membranes and the ones displayed by the Lo phase.

#### 4.2.3. Isolation of detergent resistant membranes from PM, biochemical fractions with a specific lipid composition

Based on the conceptual framework exposed in the previous sections, a tremendously high number of publications (about 2000 in the last 40 years) reported the isolation and characterization of DRMs from biological membranes from a wide variety of animals, plants and microorganisms [149]. Virtually all protocols rely on a similar experimental procedure: treatment of either intact cells or purified membranes with a nonionic detergent (most frequently Triton X-100, but Triton X-114, Brij or Lubrol have also been used), generally at low temperature (4 °C) followed by ultra-centrifugation on a sucrose (or Ficoll) gradient to recover the insoluble fraction [150]. Parameters which have been proven to be crucial and were carefully adapted to each material concern mainly the concentration of detergent and the detergent-to-membrane ratio used. The protein yield recovered in the insoluble fraction may vary between 5 and 20% of the initial amount of membrane proteins, depending on the biological material and the experimental conditions. In animal cells, extensive characterizations of lipids associated to DRMs consistently revealed a 3- to 5-fold enrichment in lipids associated to the Lo phase of model membrane, in particular cholesterol, saturated phospholipids, gangliosides and sphingomyelin [151,152]. Analyses of the phospholipids content of DRMs classically exhibit a decrease in anionic phospholipids compared to the

whole membrane [153], an increase of the proportion of saturated fatty acids [154], and a typical enrichment in GM1 gangliosides [155]. The biochemical analysis of such DRMs extracted from animal cell membranes have been extensively performed using proteomics approaches (see for review [156]). It emerged from this huge amount of data that some typical proteins, such as caveolin, or protein families, such as kinases of the Src family or small G proteins (Guanine nucleotide-binding proteins), are in a systematically enriched in such fractions, together with some proteins harboring particular post-translational modifications such as GPI-anchored proteins. We can note here that some detergent-free methods to isolate sub-fraction of the PM have also been developed. [157–159].

In plants, DRMs were first purified in tobacco, with the first isolation reported by [160] and the characterization of DRM-associated proteins and lipids provided by [19]. Similar studies revealing by mass spectrometry the catalogue of proteins were then performed on different species such as *Arabidopsis thaliana* [161–165], *Medicago truncatula* [166,167], *Oryza sativa* [168], *Avena sativa* and *Secale cereale* [169] or more recently *Beta vulgaris* [170]. According to the methodology used, the amount of proteins may differ between the studies but the continuous improvement of performance and sensitivity of the mass spectrometry approaches, led to an increase of the number of proteins identified which reached > 300 proteins in the more recent studies [163,164,171]. The latest extensive analysis published on plant PM proteome, performed in rice, allowed the identification of > 3900 proteins, which is quite consistent with the yield of PM-derived DRM proteins which is typically around 10% of total proteins in most studies [19,172]. The family of proteins identified in the different studies is also quite consistent, with a high proportion of proteins involved in signal transduction, responses to different stress, and plant-micro-organism interactions. Accordingly, a few studies implementing quantitative proteomics approaches based on different methodologies, clearly revealed a qualitative and/or quantitative modification of the proteins associated to DRMs upon environmental modifications, for instance in the early steps of plant defense signaling [171,164,168], or following abiotic stress [173,170]. Note that by contrast with proteins where genetically encoded fluorescent tags or specific antibodies are available, generating DRMs is the most used technique in order to study the potential segregation of lipids. In the next chapters, we will discuss the lipids found in DRMs purified from plant PMs.

**4.2.3.1. Glycerolipids in plant DRMs.** As expected from biophysical work, major structural phospholipids, *i.e.* PC, PE, PS, PA are markedly depleted in plant DRMs when compared to the total PM [19,162]. The case of phosphoinositides (PIPs) deserves a particular attention. Despite the real challenge related to the detection of such a minor class of lipids in very reduced biological sample such as DRMs, the combined use of Thin-Layer Chromatography to separate the different classes of phosphoinositides prior to quantitative Gas Chromatography-Mass Spectrometry analysis [174] allows to quantify PI4P and PI(4,5)P<sub>2</sub> in DRMs isolated from tobacco leaves and tobacco Bright-Yellow 2 cell culture (BY-2 cells) [31]. It was shown that both PIPs isomers represent < 5 mol% of the total lipids of tobacco PM. However, their relative amount is 11-fold higher in DRMs compared to PM from which they originate. Hence, it is estimated that 50 mol% of PM phosphoinositides likely segregate in BY-2 cell PM-domains. A lower increase in PI4P and PI(4,5)P<sub>2</sub> was also observed in tobacco leaf DRMs: 43 and 31 mol% of the isomers were found to concentrate in this fraction respectively. Moreover, PIPs display highly saturated fatty acids in both DRMs and PM, with 16:0, 18:0 and 18:1 being the major fatty acids, which is all the more consistent with the packed lipid environment or liquid-ordered phase characteristic of this fraction. This work has demonstrated that PIPs are the only glycerolipids enriched in plant DRMs, which is in agreement with biochemical studies performed on animal cells. In good agreement with this result, the nanodomain-protein marker from the potato REM group 1 isoform 3 (STREM1.3 or

REM) was shown to cluster in the PM inner-leaflet nanodomain by specific binding to PI4P [175]. The question arises whether PI4P is clustered in PM-nanodomains before the anchoring of REMORIN, or whether REM's C-terminal anchor promotes PI4P clustering. In line with the results obtained for PIPs, striking evidence related to the characteristics of the fatty acyl chains associated to DRM glycerolipids have been obtained. Indeed, the comparative analysis of polar lipids from tobacco leaves or BY-2 cells revealed a very significant enrichment in saturated fatty acids (C16:0 and C18:0), in agreement with a DRM phospholipids double-bond index lower than that of the overall PM [19]. This was consistently observed in maize embryos and bean leaves with the total amount of saturated long-chain fatty acids being higher in the PM than in DRMs. Similarly, the saturated/unsaturated ratio PM/DRM also rised in the DRMs compare with PM [176]. These characteristics perfectly fit with the direct relationship classically observed in model membranes between the proportion of lipids with saturated fatty acyl chains and the global order of the bilayer which has been confirmed using lipids from plant PMs [99].

**4.2.3.2. Sterols in plant DRMs.** In all plant tissues tested, free sterols are major components of isolated DRMs. Quantitative analyses showed a clear increase in the sterol-to-protein ratio to around 1.7-fold in DRMs prepared from both tobacco leaves and *Medicago truncatula* roots [19,166] or even 2.7- and 4-fold enrichment in DRM fractions from bean leaves and *Arabidopsis* cell cultures [161,177]. On the other hand, maize embryo [177] and *Arabidopsis* seedlings [173] exhibited a smaller free-sterol accumulation with only an 1.3-fold enrichment in DRM fractions indicating a range of plant sterol enrichment factors as broad as that observed in animal cells. In general, relative abundances of individual free-sterol species such as stigmasterol, spinasterol and sitosterol fractions are similar in DRM and PM [19,161,162], with the noticeable exception of maize embryo membranes [177]. For the first two sterols that showed very low even not clear ability to order membrane, such observation is surprising. However, their differential ability to order membrane had been measured in artificial membranes, a context in which i) they are the only one sterol among the lipid mixture (a crucial difference with PM sterol mixture, where an additive effect of ordering-capacity of each sterol was furthermore demonstrated [99]) and ii) their specific capacity to segregate into a DRM fraction was not assessed to date, to the best of our knowledge.

Moreover, additional results reinforced the possible role of phytosterol in the structuration of plant PM domains suggested by their enrichment in DRMs. They were essentially provided by the use of the pharmacological compound methyl- $\beta$ -cyclodextrin. This cyclic oligosaccharide able to trap sterols from artificial and biological membranes has been widely used to lower the content of membrane cholesterol in various types of animal cells and to assess sterol-associated membrane structuring, see for review [178] to read about the specific and non-specific effects of cyclodextrins. This molecule has been proven to remove from isolated plant PM, with a comparable efficiency to that associated with cholesterol, the free phytosterols (campesterol, stigmasterol, sitosterol and isofucosterol) [93]. Such a treatment resulted in a decrease by about 50% of BY-2 cell PM sterols, without affecting PM-content in conjugated sterols, phospholipids, sphingolipids and proteins. Importantly, methyl- $\beta$ -cyclodextrin treatment totally abolished the recovery of any DRM fraction after PM solubilization at 4 °C with Triton X-100 [93]. Moreover, the use of environment sensitive fluorescent probes allowed to associate this depletion in free-sterols with a decrease in liquid phase heterogeneities, and particularly in Lo phases [93]. This work on isolated PM has been further corroborated by similar results obtained on living BY-2 cells showing a clear decrease of the proportion of ordered PM-domains by cyclodextrin treatment that reduced by *ca.* 20% the amount of PM sterols [92]. Finally, the combination of cyclodextrin and extensive quantitative proteomic characterization of DRMs isolated from *Arabidopsis* PM identified a subset of proteins, whose association to DRMs is sterol-dependent [163,165].

As exposed in Section 1.3, phytosterols can be conjugated with sugars, which in turn can be acylated to form SG and ASG (for a review see [71]). Lipidomic analyses have shown varying amounts of SG and ASG in plant DRMs. In *M. truncatula* roots, the same enrichments in SG, ASG and free-sterols were observed in DRMs compared to PM fractions [166]. Conversely, while free-sterols did not show any significant enrichments in DRMs from *Arabidopsis thaliana* seedlings and plants, SG and ASG were found considerably enriched (> 4-fold) in these fractions [162,173]. In oat roots, conjugated-sterols were observed in similar proportions in PM and DRMs whereas a clear enrichment of free-sterols was reported [77]. Furthermore, total sterol amounts were markedly increased in tobacco leaf DRMs, mainly because of the high-enrichments in free-sterols and ASG [31]. As exposed in section 2.1, conjugated-sterols in combination with free-phytosterols are potent modulators of the order level of model membranes, suggesting again a close relationship between the composition of the DRM fraction and the presence of a Lo phase in plant PM.

**4.2.3.3. Sphingolipids in plant DRMs.** By contrast with DRMs extracted from animal cells, plant DRM sphingolipid content has only been investigated in very few studies. A first line of evidence of the enrichment of sphingolipids in DRMs relies on the characterization of their VLCFA content. By analyzing highly-purified PM from bean leaves and germinating maize embryos, a 3- to 4-fold increase of VLCFA relative amount in DRMs compared to PM was evidenced [176]. Moreover in the two plant species considered, VLCFAs harboring 20- to 32-carbon chains were present in DRMs. A significant enrichment of VLCFAs (from C20:0 to C26:0) in DRMs compared to PM was also observed in tobacco leaves and BY-2 cells [2]. Among the hundreds of sphingolipid species that exist in plants many possess 2-hydroxy fatty acids, containing a hydroxylated C-2 position [9] may contribute to the rigid binding of sphingolipids between themselves and other lipids through hydrogen-bonding between hydroxyl groups, as evidenced in artificial membranes [179,180]. It is thus likely that 2-hydroxy sphingolipids contribute to the ordered structure of PM domains. Using mutant rice lines in which the levels of sphingolipids containing 2-hydroxy fatty acids were decreased by knocking-down two genes encoding fatty acid 2-hydroxylases (FAH1 and FAH2), [52] demonstrated that the DRM/PM ratio was altered in these lines. This result suggested a role for such lipids in structuring Lo phases within the PM, which was further confirmed by the observation using the environmental probe ANEPPDHQ that the PM in OsFAH1/2-KD1 was significantly more disordered than in the wild type.

GluCer belongs to the monosaccharidic cerebroside family, and many GluCer species have been reported in plants, and lipidomics approaches showed that GluCer can exhibit a wide range of LCB and fatty acid composition [38]. Their relative abundance in plant PMs has not been unequivocally determined, varying significantly from one species to another and also according to the photosynthetic activity of the tissue considered [181]. In line with those observations, various quantitative data have been reported concerning the enrichment of GluCer in DRMs. In DRMs isolated from tobacco leaves and BY-2 cells [19] or *Medicago truncatula* roots [166], GluCer was only slightly enriched. On the other hand, GluCer was found significantly enriched in *Arabidopsis* and leek DRMs prepared from PM and microsomal membranes [161,173]. DRMs isolated from leek Golgi membranes displayed a 4-5-fold in GluCer compared to the PM [162]. Similarly, DRMs isolated from tobacco pollen tubes harbored a percentage of GluCer which increased up to two fold with the detergent/protein ratio [182]. Taking into account these data, it is difficult to conclude whether or not GluCer enrichment can be considered as an essential component of plant DRMs, even if its relative proportion increased in this fraction compared to the PM, in most studies performed.

The first indication of an enrichment of GIPC in plant DRMs was reported by [161], showing an approximately 5-fold higher LCB-to-protein ratio in DRMs extracted from *Arabidopsis* microsomal fractions.

The relative decrease of (8Z)-4-hydroxy-8-sphingenine (abbreviated t18:1c) in the DRMs compared with microsomes and the increase of the ratio of this LCB compared with its stereoisomer (8E)-4-hydroxy-8-sphingenine (t18:1t) in the DRMs suggested that DRMs might contain a high proportion of GIPC, which have a greater 8Z:8E ratio than cerebroside [161]. However, although GIPC belong to one of the earliest classes of plant sphingolipids that were identified [41], their study has for long been impaired by their limited solubility in typical lipid extraction solvents, and very recent progress concerning their structural characterization and role in membrane organization relies on the development of efficient protocols of purification [42,54]. By taking advantage of such methodological developments, [39] showed that the hVLCFA and VLCFA contents were highly comparable between DRMs and purified GIPC, with an even higher proportion of hVLCFAs in DRMs purified from BY-2 cells, suggesting that hVLCFA-containing GIPC are most likely present in this fraction. Moreover, levels of the two LCBs t18:0 and t18:1, which are mostly present in GIPC [45], strongly increase in DRMs when compared with PM, reaching 80% of total LCBs in DRMs. A further characterization indicated that series A GIPC were found in both PM and DRM fractions of tobacco leaves, whereas for BY-2 cell series B GIPC were 3-fold enriched in DRMs when compared with the PM, reaching 17% of total GIPC in BY-2 DRMs [39]. When the global lipid composition of the PM and DRM fractions was recalculated taking into account these data, it appeared that GIPC represent 45 and 30 mol% of total PM lipids isolated from leaves and BY-2 cell suspensions, respectively, and up to 60 mol% of the DRM fraction, suggesting that the contribution to sphingolipid-enrichment in PM Lo phases is mainly due to GIPC [39].

#### 4.2.4. The use of DRMs to study the segregation of lipids in plant PM; some limits but significant contributions

The “raft hypothesis” states that specific PM-lipids, mainly sterols and saturated sphingolipids, interact together to form dynamic nanoscale clusters by recruiting lipids and proteins that are present in signaling and trafficking platforms in the PM [114]. Experimentally, the nonionic detergent Triton X-100 is used to separate Lo phases from the rest of membrane preparation by isolation of DRMs isolated in the upper-phases of a sucrose density gradient after ultracentrifugation. DRMs are considered by many as *in vitro* counterparts of membrane rafts [150]. The characterization of lipids found in DRMs isolated from PM fractions of various plant species gave rise to an overall feature such as a global decrease of glycerolipids content, with the noticeable exception of phosphoinositides; a strong enrichment in lipids containing saturated fatty acyl chains; an increase in free- and conjugated-sterols; and a strong enrichment in sphingolipids, and in particular in GIPC. These characteristics are consistent with the canonical description of DRMs isolated from a plethora of animal PMs whilst taking into account the specificities of plant PM lipids [183]. Moreover, it appears that such a composition is typical of the Lo phase in model membranes, as detailed in Section 3.2.1. Yet, as stated in several publications (e.g. [184–187]) the use of DRMs to evidence PM-associated dynamics should be accompanied with great precaution as DRM fractions should not be considered as direct equivalents to PM-domains. However, the numerous convergent correlations obtained on many different biological materials and model membranes have indicated for instance that 1/a consistency between the composition of the Lo phase *in situ* and the DRM lipid content; 2/a relationship between the presence and abundance of DRMs and the order of biological membranes; 3/the association of particular proteins to DRMs and their clustered distribution within the PM make them valuable tools to progress towards a better understanding of plant PM organization. An example of this last point is the PM-associated NADPH-oxidase RbohD, which was demonstrated to be responsible for the oxidative burst observed in the very early steps of the plant immune signaling cascade, was proved to be exclusively associated to DRMs in tobacco [19]. This characteristic could be related to the immunoelectron microscopy observation that this protein is

**Table 1**

Examples of inhibitors used to modify *in vivo* the pools of lipids, and some recent related references.

The used concentration of the inhibitors is indicative, and must be tested for each plant species or tissues. To address the modification of the PM lipid pool, a phase partition to purify PM vesicles must be conducted coupled with a dedicated lipidomic approach. PLD, Phospholipase D; PLC, Phospholipase C, DAG, Diacylglycerol; VLCFAs, Very Long Chain Fatty Acids; HMG-CoA reductase, 3-hydroxy-3-methyl-glutaryl-coenzyme A reductase.

	Inhibitors of:	Name	References
Phosphoinositides	PI3-Kinase (50–100 $\mu$ M)	LY-294002	[398]
	PI3P 5-Kinase (1 $\mu$ M)	YM-201636	[399]
	PI4-Kinase (30–60 $\mu$ M)	Phenylarsine oxide (PAO)	[117,398]
	PI3-Kinase (1 $\mu$ M)	Wortmannin	[283,31]
	PI3-Kinase + PI4-Kinase (30 $\mu$ M)	Wortmannin	
Sphingolipids	Ceramide synthase (1 $\mu$ M)	Fumonisin B1 (1 mg)	[400,401]
	Glucosylceramide synthase (50 $\mu$ M)	DL-THREO-PDMP	[402]
	VLCFAs/sphingolipid (50–100 nM)	Metazachlor	[235]
	Serine palmitoyltransferase (SPT)	Myriocin	[56,403]
	Inositol phosphorylceramide synthase (fungi)	Aureobasidin A	[404]
Diacylglycerol/phosphatidic acid	Lyso PA Acyl transferase	CI-976	[405–407]
	PLD-derived PA formation (50 $\mu$ M)	(R)-(+)-Propranolol hydrochloride	[408]
	PLD-derived PA formation (0.2–0.4%)	1- butanol	[409,410]
	PLC-derived DAG formation (5 $\mu$ M)	U73122 (active analog)	[31,411]
	PLC-derived DAG formation (5 $\mu$ M)	U73343 (inactive analog)	[411]
	PLC-derived DAG formation (50 $\mu$ M)	Edelfosine	[283]
	DAG-Kinase (50 $\mu$ M)	R59022	[283]
Sterols	Cyclopropylsterol isomerase 1, CPI1	Fenpropimorph	[7,175,162]
	HMG-CoA reductase	Lovastatin	[7]

organized within the PM in clusters of about 20 nm in diameter [188]. Upon activation, NADPH-oxidase products (the Reactive Oxygen Species) were also present as discrete nanometer sized patches along the PM [189]. Similarly, the enrichment of the flagellin receptor FLS2 in DRMs observed a few minutes after treatment of Arabidopsis cells with the bacterial elicitor flagellin flg22 is fully consistent with recent results observed using super-resolution microscopy indicating its clustered distribution in the PM. Noteworthy, a significant modification of its dynamics within PM, namely an increased population of long-lived receptor clusters and a reduction of its lateral displacement was observed a few minutes after flg22 treatment [190]. Moreover, group 1 Remorin proteins were the first biochemical markers of plant DRMs and observed as forming PM-associated clusters of about 75 to 100 nm in diameter [191,192]. Such nanodomain-organization was shown to be sterol-dependent as it was strongly impaired by the use of sterol-chelator methyl- $\beta$ -cyclodextrin [191] or by inhibitors of sterol biosynthesis, see Table 1 [175]. More recent data have confirmed the confinement of group 1 Remorin in PM-nanodomains to be sterol- and PI4P-dependent and by using *in vivo* single-particle tracking microscopy that the size of group 1 Remorin-associated domains were of ca. 80 nm in diameter [175].

One must note that the colocalization studies of Remorins of different phylogenetic groups, namely groups 1, 3, 4 and 6 have shown the coexistence of highly-distinct membrane domains in the plane of the PM [193]. These results have demonstrated that the use of biochemical approaches such as DRMs cannot be sensitive enough to accurately represent the biological complexity of membrane-compartmentalization *in vivo*. A decisive milestone will be the ability to describe, in an extensive and comprehensive manner, the distribution of the various lipids together with proteins within PM, and to identify key causal mechanisms underlying such an organization. To do so, super-resolution microscopy with one or more fluorophores can be used for proteins to visualize *in vivo* whether the protein of interest is enriched in nanodomains; this kind of method is currently at its infancy for lipids due to the few fluorescently-labeled lipids available and because it is hard to insure a proper intake of such dyes in plant cells (see below). The use of chelator of lipids, fluorescent lipid probes or lipid-biosynthesis inhibitors (Table 1) are the next steps to address the role of lipids in PM-nanodomain formation and maintenance.

## 5. Spatial and multiscale segregation of lipids and proteins: a complex picture emerging from the combined use of various imaging techniques

Since the publication of the fluid mosaic model for biological membranes in 1972, a lot of experimental evidences revealed the outstanding complexity of the PM. Rafts characterized by tight lipid-packing are involved in a wide variety of cellular processes: regulation of *endo*- and *exocytosis*, hormone signaling, membrane trafficking in polarized epithelial cells, T-cell activation, cell migration, life cycle of influenza and HIV viruses [194]. As expected for biology as an experimental science, understanding the organization of the PM strongly relies on the evolution of microscopic methods. Thanks to the development of new efficient methodologies, among them imaging lipids and super-resolution microscopy [114], very important results have been published refining this organization but at the same time raising new questions. Currently, we can clearly state that the PM is organized in domains that differ in the nature of their components, their stability and their size from the nanometer to the micrometer scale. This complex remodeling is highly-dynamic and respond to various abiotic and biotic stresses. Particular interest of the scientific community for cell surface signaling processes in the past decade has led to an improved vision of the PM's membrane organization: a complex multi-component and multi-scale heterogeneity with a high degree of subcompartmentalization into micro- to nano-domains have been evidenced *in vivo* and deserve to be clearly qualified. Domains were originally referred as to "lipid-rafts" but the designation has very much evolved since. It is now known that lipid-rafts do not cover a single type of domain but rather include a collection of domains differing in their protein and lipid composition and their resident time (aggregation/disaggregation).

### 5.1. Micro- and nano-domains coexist in the plant PM

#### 5.1.1. Microdomains in plant cells

Cell polarization-induced PM-microdomains (above 1  $\mu$ m) are easily observed by classical confocal fluorescence microscopy in leaf, root and pollen tube cells [185,195]. The accumulation of proteins and lipids into microdomains is involved in defining cells' fate, functional specialization for cell polarity and specialization of host membranes for defense [196,197]. These include the polar distribution of PINFORMED (PIN), AUX1–Auxin transporter protein 1, ABCB (ATP-binding cassette

protein subfamily B)/P-glycoprotein, Auxin binding protein 1 (ABP1) or RAC/Rho of plants GTPases (ROP) that localize to the apical or basal pole of a cell [198] and the lateral and equatorial domains in plant endodermal cells populated by DYNAMIN-RELATED PROTEIN1A (DRP1A) or CASPARIAN STRIP MEMBRANE DOMAIN PROTEINS (CASPs) [185,199]. Similarly, tip-growing cells like pollen tubes and root hairs are also of particular interest for the study of membrane microdomains. For instance, the pollen-specific H<sup>+</sup>-ATPase is located in the shank whereas Phospholipase C, G proteins and phosphoinositide kinases are located at the apex of the pollen tube (for review see [200]). Lipids are also segregated into microdomains *i.e.* sterol-, phosphoinositide-, PI4,5P<sub>2</sub> and diacylglycerol-rich microdomains are shown to be especially concentrated in the apex of the pollen tube [182]. The presence of microdomains enriched in phosphoinositides (PIPs) plays an important role in polar tip growth by regulating the machinery maintaining polarity and by controlling cytoskeletal dynamics and the remodeling of vesicle trafficking [201]. In root endodermal cells, EXO70A1 exocyst subunits colocalize with PI4,5P<sub>2</sub> [202]. Finally, in plants, plasmodesmata (PDs), which are channels characterized by the apposition of the ER and the PM possess a specific lipid composition [203]. These PM-lined PD (PD-PM) have been shown to contain definite microdomains where not only proteins such as Plasmodesmata-located protein 1 (PDLP1) and PD callose binding proteins (PDCBs), but also lipids such as sterols and sphingolipids are enriched [204,205,7].

Importantly, besides local enrichment of specific lipids and proteins within microdomains, the characterization of the biophysical state of pollen tube microdomains has shown that they are highly-segregated in the cell, *i.e.* they are especially concentrated at the PM of the cellular apex but also present as a ring-like distribution around the tube [74,182]. Similarly, the cell plate of Arabidopsis contains highly-ordered membrane microdomains which rely on sterols and DRP1A-dependent endocytosis [206]. Yet, how the localization of proteins and lipids in microdomains relies on the cooperativity of multiple mechanisms is not yet understood [207,208,200].

### 5.1.2. Nanodomains in plant PM

The development of new methods of high- and super-resolution imaging has provided the ability to observe membrane domains at the nanoscale level, termed nanodomains and defined by a size below 1 μm [209,210]. These methods include mainly stimulated emission depletion microscopy (STED), structured illumination microscopy (SIM) and single-molecule localization microscopy (SMLM), including methods such as Photo-Activated Localization Microscopy (PALM) and Stochastic Optical Reconstruction Microscopy (STORM)). These techniques have been routinely used in animal cells but have only recently emerged in plant studies. Super-resolution microscopy techniques allow the acquisition of high-density super-resolved nanoscale maps of individual fusion-protein localizations and trajectories in the PM [211]. Single-molecule tracking combined with photoactivated localization microscopy (spt-PALM) allows not only the description of the supramolecular organization of proteins at the PM level far below the resolution limit of confocal microscopy but also allows the determination of the mobility dynamics of single molecules or particles in the PM.

Super-resolution microscopy methods have shown that PM-associated proteins are sub-compartmentalized within nanodomains, to only name a few: Hypersensitive Induced Response HIR1 [212] PIN2 [207], Borate efflux transporter (BOR1) [213], Dynamamin-related protein 1a (DRP1A), Cellulose synthase A6 CESA6 [214], IDQ family of calmodulin-binding proteins [207,213,215] S-type anion efflux channel/Calcium protein kinase SLAH3/CPK21 and REM1.3 [192,175], flagellin receptor FLS2 [190], Brassinosteroid insensitive 1/Somatic embryogenesis receptor kinase 1- BRI1-associated receptor kinase 1 BRI1/SERK1-BAK1 [216], Flotilin [217] and the NADPH oxidase [218]. Notably, the study of group 1 REM mutants has revealed that the protein mobility rate (measured by the Mean Square Displacement) and protein supramolecular organization are not necessarily coupled. These results

have shown that proteins displaying the same mobility rate can however assemble into clusters of different sizes [175]. Differential combinations of multiscale organizations have been evidenced as for instance PIN2, which is preferentially targeted in a polar fashion to PM-microdomains in Arabidopsis roots, locates at a lower scale into PM-nanodomains as shown by STED microscopy [207]. By contrast, REMORIN StREM1.3 localizes in nanodomains of *ca.* 80 nm observed by SPT-PLAM [175], but without a particular polar localization in *N. benthamiana* leaf epidermal cells.

Lipids are also found in nanodomains both in the inner-leaflet and in the outer-leaflet. Immunogold-electron microscopy has shown that PI (4,5)P<sub>2</sub> is found clustered in the inner-leaflet of the PM [31]. Interestingly this cluster formation was not significantly sensitive to sterol depletion [31]. More recently, immunogold-electron microscopy strategy has revealed that the distribution of polyglycosylated GIPC, likely in interaction with phytosterols, form nanodomains of *ca.* 40 nm in the outer-leaflet of tobacco PM [39]. These two results strengthen the idea that lateral nano-segregation of lipids also takes place at the PM in plants. Yet, tools dedicated to the study of the dynamic of plant lipids at the nanoscale level are still lacking, impairing progress in understanding their molecular distribution, behavior and dynamics of PM lipids.

Therefore, the plant PM must be acknowledged as a fluid yet highly-compartmentalized mosaic wherein numerous membrane domains with different compositions and biophysical properties co-exist at different scales [195,219]. The challenging questions now reside in clearly defining the essential mechanisms governing specific interactions between the different molecular species of PM intrinsic components. Currently microscopy methods are able to localize and track single molecules with a resolution of 1 nm achieving an ultimate resolution limit in fluorescence microscopy: MINFLUX [220,221], subdiffusive motion at the single trajectory level [222] or motion transition state [223]. Such methods must be adapted to plant cells to address the specific question of plant PM biology and will pave the way to a better understanding of the PM's dynamic organization.

### 5.2. PM lipids are critical regulators of plant PM organization at the nanometer scale

Lipid-lipid interactions and protein-lipid interactions are believed to be key regulation parameters governing plant PM organization. In pollen tubes, various isoforms of the exocyst complex colocalize with either PI4,5P<sub>2</sub> or PA, resulting in the formation of PM domains [224]. The localization of EXO70A1 not only coincides with, but is also required for the accumulation of PI4,5P<sub>2</sub> [202]. The targeting of REMs to inner-leaflet PM nanodomains is independent of the secretory pathway, although it is still mediated by direct interactions with PI4P in a sterol-dependent manner [175]. This understanding of the anchoring mechanisms of REMs confirms the impairment of clustered distribution of REMs by phytosterol depletion [191,225]. The use of raster image correlation spectroscopy (RICS) has shown that the lateral mobility of auxin transporters PIN is dependent on the amount of sterols in tobacco cell PM, arguing in favor of a sterol-dependent protein organization within the plant PM [82].

In PD, modulations of the sterol composition alter callose-mediated PD permeability and reversibly impaired the PD localization of the glycosylphosphatidylinositol-anchored proteins Plasmodesmata Callose Binding 1 (PDCB1) and the Plasmodesmata beta-1,3-glucanase (PdBG2). This study emphasizes the importance of lipids in defining PD membrane microdomains and is in line with the lipid-raft model postulating the existence of nanoscopic assemblies of sphingolipids and sterols in the outer-leaflet of the PM. Finally, it is important to acknowledge that nanodomains exist in both leaflets and the lipid content of each of them regulates the clustering of proteins and lipids. The possible interaction between nanodomains across the two leaflets (a process called pinning or registration) will be discussed in the following

section.

### 5.3. PM heterogeneity might originate from a tight control along the secretory pathway

The neo-synthesis of lipids found at the PM results from intricate pathways that originate at the ER, which is certainly the most ancient eukaryotic endomembrane compartment. From the ER, lipids are transported to the Golgi apparatus where they are further assembled and modified before reaching the PM, see Fig. 4. At the PM, it is thought that the auto-association of glycerolipids, sphingolipids and sterols drives membranes close to a demixing point (phase separation) and induces sorting of lipids to either Lo phases or Ld phases of the membrane [226]. The Lo phase is enriched in sphingolipids and sterols. A higher proportion of free-hydroxyl groups in the long-chain-bases and acyl-chains of sphingolipids as compared to glycerophospholipids, allows more interactions with sterols and thereby ensuring the stabilization of sphingolipid-enriched membrane domains (see Section 3). The characteristic length of sphingolipid acyl-chains is a particularity among lipids that confer special physical properties to biological membranes. This particularity increases the melting-point of sphingolipids as compared to other lipids and causes strong hydrophobic mismatches between sphingolipid acyl-chains and the polar heads of other lipids with smaller acyl-chains. Hence, sphingolipids are segregated and more physically-ordered microdomains are created within the membrane [227]. Acyl-chain length also induces the formation of interdigitated phases (interdigitated lipid-leaflets) and plays a role in membrane stiffness and thickness [227,66].

Considering that these different phases are observed at the PM, one might ask how this complexity is implemented. Does this PM-lipid heterogeneity already occur within secretory pathways that lead to the PM and does it have a role in the secretion of proteins? In mammalian cells, a protein secretion model called the rapid-partitioning model, proposes a *cis-to-trans* gradient of the sphingolipid/glycerophospholipid ratio that would account for a partitioning of transmembrane cargos and enzymes into distinct domains of the Golgi: domains enriched in Golgi resident enzymes (low sphingolipid/glycerophospholipid ratio) and domains where transmembrane cargos are progressively enriched (high sphingolipid/glycerophospholipid ratio) at the *trans*-most cisterna of the Golgi until their loading into post-Golgi vesicles [228]. This model is in agreement with the observation that newly arrived cargos exit the Golgi with mono-exponential export kinetics. Moreover, alteration of sphingolipid homeostasis by treating mammalian cells with short acyl-chain ceramides (for further incorporation in sphingolipids at the Golgi) impacts the export of protein cargos from the Golgi, reduces the lipid order in Golgi membranes, and alters the ultrastructure of Golgi cisternae from flat to highly-curved membrane sacs, further supporting the role of very-long-chain sphingolipids in Golgi morphodynamics and sorting [229,230].

In plants, inhibition of the condensation of glucose with ceramides (produces GluCer) results in the disaggregation of Golgi cisternae into vesicular structures and in the inhibition of secretion [231]. In animal and plant cells, the *trans*-most cisterna of the Golgi apparatus is continuous with a tubular, branching and reticulated Golgi structure called the *trans*-Golgi Network (TGN). In yeast, it has been observed that secretory vesicles budding-off of the TGN are enriched in sterols and sphingolipids and possess a high proportion of Lo phases [232]. In mammalian cells, a genetically encoded probe that labels sphingomyelin has revealed that sphingomyelin synthesis at the Golgi promotes sphingomyelin enrichment in a subset of TGN-derived secretory vesicles, where the sorting of a glycosylphosphatidylinositol-anchored protein is in turn also promoted [233]. In plants, extraction of DRMs has revealed that both PM and Golgi yield DRMs suggesting that they can be enriched in sterols and sphingolipids [162]. However, as stated before, this method can generate artificial segregations of lipids within membranes. Therefore, a combination of subcellular remodeling of

sterols using the fluorescent probe filipin, and a novel extraction approach to specifically immuno-purify TGN sub-domains and Golgi apparatus without any detergents coupled with quantitative mass spectrometry, has opened new perspectives in defining which lipids are present in these compartments [234,235]. The *in situ* subcellular remodeling of sterols by filipin has revealed that sterols are the most present at the PM and in sub-populations of TGN vesicles [234]. Further on, purification fractions of TGN sub-domains and Golgi have identified an enrichment of sterols and  $\alpha$ -hydroxylated VLCFAs, a specific signature of plant sphingolipids. Moreover, this signature was specifically stronger in a sub-domain of TGN: Secretory Vesicles [235]. Not only an enrichment of sphingolipids is observed in TGN-derived vesicles, but the length of the sphingolipid acyl-chains is found to be a critical factor for the correct polarized secretory sorting of the auxin-carrier protein PIN2 in root epidermal cells [235]. Altogether, the enrichment of sterols and sphingolipids at TGN-derived secretory vesicles seems to be a conserved feature in eukaryotic cells, and appears to be required for sorting and vesicle budding. This enrichment is favorable to Lo phase lipid-segregation at TGN and suggests that a gradient of lipids along the secretory pathway is established from the ER where no enrichment of sterols and sphingolipids is observed through the TGN to the PM. This membrane heterogeneity is not only a structuration of pre-PM lipids but it has as well an important role to play in many intracellular trafficking pathways, see Fig. 4.

The lipid heterogeneity within the secretory pathway also exists for lipids other than sterols and sphingolipids. In plants, the TGN-localized choline transporter like1 (CTL1) is involved in PM-recycling of the ion transporter NRAMP1 and the auxin efflux carrier PIN1 [236]. An interesting observation is that free-choline, but not PC, can inhibit phospholipase D (PLD) activity [236]. PLD hydrolyses PC and PE to produce PA, a phospholipid that favors the fission of vesicles [237]. Hence, one hypothesis is that CTL1 transports choline inside the TGN lumen to maintain a low choline concentration on the cytoplasmic side of TGN in order to conserve high PLD activity converting PC and PE into PA. This mechanism would require further characterization, but it could be a possible way to establish membrane heterogeneity between the luminal and cytoplasmic leaflets of TGN membranes. Another example of phospholipid membrane heterogeneity is with PS in yeast where it has been suggested that PS resides primarily in the luminal leaflet of the Golgi and is flipped to the cytosolic leaflet in the TGN [238]. This leaflet translocation of PS is operated by PS flippases at the TGN and is thought to control oxysterol-binding proteins (OSBP), which exchange ER-associated sterols with TGN-associated PI4P in unidirectional fashion [238]. The exchange of lipids participates in creating sterol enrichment and membrane lipid order at the TGN [239]. An elegant model has proposed that this exchange of sterols for PI4P occurs at ER-TGN membrane contact sites, where PI4P is generated at the TGN by PI4 kinases (PI4KII $\alpha$ ) which are themselves regulated in an oscillatory (waves of PI4P consumption by OSBPs) fashion by sterols [239]. These studies have revealed a crucial characteristic of membrane heterogeneity at the TGN: its highly-dynamic and oscillatory nature.

In plants, PIPs are localized in a gradient throughout the endomembrane system, PI4P being mainly located at the PM with a secondary pool at the TGN while PI3P is mainly located in late endosomal compartments, see Section 1 [27]. The function of PI4P at the TGN and its relationship with other lipids have not yet been addressed in plants and will definitely be an exciting field to explore in respect to plant trafficking specificity. In plants, unlike animal TGNs, at least two populations of TGNs are observed, one is associated to the Golgi apparatus and one is independent from it, as TGNs detach from the Golgi apparatus to form a highly-dynamic Golgi-independent structure [200], [240–243]. This highly-dynamic TGN can undergo homotypic fusion and can associate transiently with the Golgi apparatus similarly to what is found for early endosomes and TGN in mammalian cells. In addition, it has been observed that the plant TGN can integrate the endocytic tracer FM4-64 relatively fast (a couple of minutes) during endocytosis

before reaching Late endosomes/MVBs [244,242]. Hence, plants have no early endosomes as described in animals, and endocytic vesicles converge directly to the TGN, where endocytic cargoes are sorted for recycling and/or degradation [242,240,200]. As such, plant TGNs can be viewed as a functional equivalent of mammalian early endosomes. Hence, it will be interesting in the future to see how the two systems evolve in respect to lipid heterogeneity regulation at the plant TGN.

#### 5.4. A model for plant PM organization, interdigitation, pinning and registration

##### 5.4.1. A model for plant PM organization: mechanisms at work

All these observations led to a model of plant PM organization that supposes both lipid-driven phase segregation and protein-dependent protein localization. This model is based on experiments on artificial membranes, composed of lipids mimicking plant PMs (lipids and/or proteins), indicating that lipid-lipid interactions strongly order plant membranes [99], whereas protein-lipid interactions could untighten plant PM organization [245]. Several models could explain lipid-lipid interactions. The “condensed lipid complex” model has been stated following the visualization of low-energy free stoichiometric cholesterol-lipid complexes occupying smaller molecular lateral zones than those occupied by each lipid alone [246]. Sphingolipids, originally proposed as preferred partners of cholesterol, cannot form this type of complex. The existence of cholesterol superlattice in lipid bilayers highlights a parallel model proposing long-distance repulsion forces between cholesterol molecules as the source for sterol-lipid interactions [247]. The “umbrella” model states that the shift between the small polar head of cholesterol and its large apolar body determines its preferential association with some adjacent molecules of the membrane [248]. In this model, cholesterol is covered by the polar heads of neighboring phospholipids to limit the unfavorable free energy due to the exposure of the apolar portion of cholesterol to water molecules. Such interactions between cholesterol and “large-headed” lipids provide increased protection. In addition, the free energy needed to cover a cholesterol cluster is larger than the energy required to cover a single cholesterol. An essential property thus emerges from these models, namely the strong tendency of cholesterol molecules not to regroup, which has been accordingly demonstrated by Monte Carlo simulations [249]. By sailing between lipid molecules, proteins increase membrane line tension and modify the mean size of the ordered domains as reported in Lung Surfactant Monolayers [250]. In agreement, it has been demonstrated that short hydrophobic transmembrane peptides decrease the affinity of sterols for neighboring phospholipids.

In animal, all these data led to a model that incorporates the importance of hydrophobic matching between integral membrane proteins and the lipid bilayer thickness considered in the so-called “mattress” model [251]. This thermodynamic model includes the elastic properties of lipids and proteins, as well as indirect and direct lipid-protein interactions expressed in terms of the geometrical variables. The notion of hydrophobic mismatch regions between lipids and proteins is also an important component of the model. This proposal remains speculative in plants and calls for further investigations.

##### 5.4.2. PM asymmetry, interdigitation, pinning and registration

As stated before, the animal cell PM has a highly asymmetric distribution of lipids with PIPs, PE and PS mostly confined to the inner-leaflet, and sterols and sphingolipids to the outer-leaflet [252]. The same observations seem to be true in plant PM [77,2]. In addition, the PM contains dynamic nanodomains involved in a continuous repartitioning of components between different domains. Recent experimental data in the animal field have shown that transient links between lipids and proteins involving both the extracellular matrix and cytoplasmic components may temporarily pin membrane domains, see below. It is becoming increasingly clear that asymmetry and pinning processes, also called registration, play important roles in PM

nanodomain formation and coupling between the 2 PM leaflets [253].

For example, a direct interaction between outer-leaflet sphingolipids Lactosylceramides containing VLCFAs, and inner-leaflet nanodomain acylated-protein kinase has been shown. This interleaflet pinning has been shown to specifically modulate neutrophil activity [254]. Similarly, transbilayer pinning between outer-leaflet long-acyl-chain-GPI-anchored proteins and inner-leaflet PS are demonstrated to be pivotal in generating actin-dependent nanoclusters of PM lipid-anchored proteins [255]. These interactions may provide clues to the underlying mechanisms for the registration of functional lipid domains between both leaflets of the PM. Yet, cross leaflet lipid-lipid interactions seem to be the main driving force behind the formation of ordered membrane domains *in vivo* [256].

How asymmetry, pinning, and interdigitation contribute to PM organization is only beginning to be unraveled in animals. Currently, very little is known in plants but this area of research will surely be developed in the next few years of membrane biology. The pending questions are of a fundamentally compelling nature. One may ask whether VLCFA-containing GIPC in PD could register with acylated-proteins across the plant PM, or whether phytosterols in one leaflet influence the fluidity of the other leaflet. This makes PM domains exceptionally challenging to study and even then, much of what is known about membrane domains has been deduced from studies on model membranes at equilibrium. However, living cells are by definition not at equilibrium, PM-lipids are still distributed asymmetrically *in vivo* so model membranes may not be as biased as can be expected. Moreover, each phospholipid group encompasses a wealth of species that vary according to their different acyl-chain combinations, and consequently their lateral distribution is heterogeneous and modulated *in vivo*. It is therefore with a combination of *in vivo* and *in vitro* analyses that these questions clearly need to be tackled in plant membrane biology.

## 6. Lipids are key players in plant PM function

Proteins and lipids located in PM nanodomains serve as modulators of host–pathogen interactions such as the binding of the cholera toxin to animal PM-located outer-leaflet gangliosides GM1 to form a pore through the PM [257]. The discovery of a high level of saturated sphingolipids and cholesterol in the viral envelope of HIV also proposed that enveloped virus budding is nanodomain-mediated [258,259]. Besides, a large number of proteins and lipids that are associated with cancer, atherosclerosis and immune responses have been found in nanodomains, see the recent review [114]. The example of the K-Ras protein is of particular interest as the molecular mechanisms to understand its precise PM localization have been detailed in recent reviews [260–262]. In the next chapter, we will focus on the role of plant PM lipids in different physiological functions.

### 6.1. Plant-microbe interactions

#### 6.1.1. Membrane lipids in plant-microbe interactions

Plants counteract pathogenic microbes by sensing non-self and modified-self molecules by cell-surface and intracellular localized immune receptors [263]. PM lipids and lipid-derived metabolites have been shown to operate in plant immune signaling [264,265]. As a result of the sensing of a pathogen, enzymes hydrolyzing the polar heads of phospholipids are mobilized to trigger signaling cascades essential for cellular responses. Phospholipases generate crucial messenger molecules such as oxylipins, jasmonates and notably PA which can regulate the activity of defense-associated proteins [266,267]. For example, the activation of phosphoinositide-specific phospholipase C (PI-PLC) is one of the earliest responses triggered by the recognition of several microbe-associated molecular patterns (MAMPs), such as xylanase, flg22, and chitosan or of pathogen effector proteins [268–270]. PI-PLC catalyzes the hydrolysis of phosphatidylinositol 4-phosphate and phosphatidylinositol 4,5-bisphosphate (PIP2) to generate water-soluble inositol

bisphosphate (IP<sub>2</sub>) or inositol triphosphate (IP<sub>3</sub>), and diacylglycerol (DAG), which remain in the membrane. In plants, DAG produced by PI-PLC activity is phosphorylated by DAG kinase (DGK) to produce PA [271,272]. PA has been implicated specifically in the modulation of immune signaling components, such as MAPKs and PHOSPHOINOSITIDE-DEPENDENT PROTEIN KINASE 1, PDK1; [273,274]). Binding of PA to proteins/enzymes has been shown to affect their activity, localization, and binding to other signaling components [275,276,267]. For example, PA binds to the NADPH oxidase isoforms RBOHD and RBOHF to induce ROS formation during abscisic acid (ABA)-mediated stomatal closure [277]. PM-localized PI-PLC2 [278], is rapidly phosphorylated upon flg22 recognition [279] and plays an important role in stomatal pre-invasion immunity and non-host resistance as it associates with RBOHD [280]. This suggests a potentially central regulation of the Arabidopsis NADPH oxidase and, consequently, of ROS-dependent processes induced by PLC2.

In addition, it has been shown that PLC activity is required for ROS production during effector triggered immunity (ETI) responses [281], that NPC2 is involved in the response of Arabidopsis to *Pseudomonas syringae* attack, by regulating elicitor-induced ROS production [282]. Furthermore, it has been demonstrated that DGK-produced PA is required for optimal ROS production in response to cryptogin [283]. Nonetheless, direct regulation of Rboh isoforms by PA binding during immune responses remains to be investigated. In addition, PA binding inhibits regulator of G-protein signaling (RGS1) activity to affect specific immune signaling pathways in Arabidopsis. Interestingly, the central immune receptor cytoplasmic-like kinase BIK1 directly linked nanodomain-localized pattern recognition receptor (PRR) [190] and RBOHD [284]. BIK1 regulates RGS1 activity by direct phosphorylation [285] and by inhibiting PLC activity. FLS2 has been shown to be no longer endocytosed after binding to flg22 [286], pointing PA as a core regulatory component of plant receptor kinase-based immunity. Interestingly, remodeling of cortical actin network in response to elicitors is mediated by the negative regulation of CAPPING PROTEIN by PLD-produced PA [287].

The production of PA by Phospholipase D enzymes (PLD) is involved in ROS production in response to elicitation [288]. This production of PA has been also shown to be essential for phytoalexin biosynthesis [289] yet considering the various subcellular localizations of PLDs this may not be specific to PM-associated PA [290]. PLD $\delta$  has been also found to be involved in non-host resistance of *A. thaliana* epidermis against the barley powdery mildew fungus *Blumeria graminis* f. sp. *Hordei* and the pea powdery mildew fungus *Erysiphe pisi*. PM-localized PLD $\delta$  is enriched at the penetration sites and PA is supposedly produced and necessary for resistance considering the observed increase in susceptibility after treatment with n-butanol, a PLD inhibiting drug [291]. PLD-produced PA is also involved in plant-virus interactions by promoting the RNA replication of the Red clover necrotic mosaic virus. A viral auxiliary replication protein binds PA *in vitro* and the exogenous addition of PA increase replication rates. This is consistent with the observed increase of PA levels in infected cells [292]. PA could therefore play a central role in viral replication by tethering protein complexes to each other and to the membrane, thereby putatively modulating catalytic activities [293] and membrane curvature [294]. As PA negatively favors curved membranes [295], a local increase in PA levels is likely to impact membrane structure and charge. Nonetheless, stimuli-dependent impact of PA production on membrane organization and the dynamics of plant immune component remain to be studied. What are the molecular function(s) of PA in immunity is still to be further studied.

In addition to PA, both phosphoinositides and lysophospholipids have been shown to play a role in plant defense. Lysophospholipids are derived from glycerophospholipids by the action of PLAs. Examples of lysophospholipids include L-PA, lysophosphatidylcholine, sphingosylphosphorylcholine, and sphingosine-1-phosphate [296]. The signaling activity or specificity of these compounds is dependent on the length

and position of the acyl chain, the degree of saturation, and the presence of the phosphate head group. Acyl chain length and degree of saturation have been shown to influence plant-pathogen interactions. The accumulation of C16:1 and C16:2 fatty acids in tomato and eggplant, due to the overexpression of a yeast delta-9-desaturase, resulted in a heightened resistance to powdery mildew *Erysiphe polygoni* DC and *Verticillium dahliae*, respectively. An increase in C18:2 and C18:3 has also been shown to increase resistance to *Colletotrichum gloeosporioides* and *Pseudomonas syringae* in avocado and tomato respectively [297,298]. Moreover, bean resistance to *Botrytis cinerea* induced by a non-pathogenic strain of *Pseudomonas* has been correlated with an increase of C18:2 and C18:3 [299].

As stated in chapter 1, plant sterols are core components of membrane and accumulate in the PM. Conversely, PM sterols are conserved regulators of membrane organization. Mutants altered in sterol biosynthesis and the use of sterol-biosynthesis inhibiting drugs, affect cell wall composition and induce abnormal callose and lignin deposits (cell wall compounds involved in biotic stress) [300]. Cryptogin is able to induce an increase in PM-fluidity *via* sterol-binding [112]. Highly-hydroxylated sphingolipids increase membrane stability and decrease membrane permeability which are both associated to increased defense against phytopathogenic fungi [35,301]. Rice *fah1/2* knock-down mutants, displaying the lack of an  $\alpha$ -hydroxyl group on the fatty-acid moiety of sphingolipids, exhibit a decrease in PM order level [52]. These mutants show reduced resistance to the rice blast fungus *Magnaporthe oryzae*, with the delocalization of major actors of innate immunity such as NB-LRRs, NADPH oxidases, Small GTPases and Calcium-dependent kinases [52]. On the contrary, Arabidopsis *fah1/2* knock-out mutants display an increased resistance to obligate biotrophic fungi *Golovinomyces cichoracearum* potentially due to a consequential increase in intracellular ceramides and salicylate [302]. Interestingly, a sphingosine analogue produced by the fungal pathogen *Alternaria alternata* f. sp. *Lycopersici* (AAL), serves as a virulence factor that induces PCD in plants and animals [303].

#### 6.1.2. Sphingolipids as receptors of necrotrophic toxins and plant-pathogen elicitors

Glycosylated lipids are often receptors in insect host binding to microbial toxins [304]. One very important glycosylated lipids of the animal kingdom are gangliosides. Their polar heads act as surface recognition markers and surface receptors for bacterial toxins such as cholera and Bt toxins [257]. They are recognized and used by virus to enter and infect cells [305]. Plant GIPC bear structural similarities with gangliosides because they contain negatively charged glycan polar heads located in the outer-leaflet of the PM [306].

A recent study has shown that GIPC were located in the outer-leaflet of plant PM are receptors to Necrosis and ethylene-inducing peptide 1-like (NLP) proteins [40]. In the study of Lenarčić et al. 2017, microbial NLP proteins are used for the identification and characterization of NLP receptors. NLPs are part of a superfamily of cytotoxins produced by plant pathogens such as bacteria, fungi and oomycetes [307]. They can be cytotoxins, inducing symptoms on eudicot plants but not monocot plants where no necrotic and cytolytic effects are observed [308]. The secretion of NLPs occurs in the extracellular environment of host plants with the toxins targeting the PM outer-leaflet [307,309]. *In vitro*, NLPs were shown to specifically bind to purified GIPC from tobacco and Arabidopsis but not to phospholipids, GluCer or sphingomyelin. Moreover, NLPs also bind to all GIPC, irrespective of the plant clade, with similar affinities [40]. Upon binding to the sugar moieties of the GIPC polar heads, NLPs undergo structural changes triggering the conformational modification of their L3 loop and the incorporation of a Mg<sup>2+</sup> ion responsible for its cytotoxicity. This results in the interaction of the W155 residue of the L3 loop with the membrane, crucial for cytotoxicity [40]. The study has also showed that sugar residues exposed on the plant outer membrane surface are important for NLP toxicity, such that Glucosamine, Man/Glucose being GIPC terminal sugars of

tobacco and Arabidopsis respectively, induces membrane damage upon binding to NLPs. Plant mutants impaired in the GIPC biosynthetic pathway, are less sensitive to NLPs, implying the importance of intact GIPC for NLP cytotoxicity [40]. The sensitivity to NLP toxicity occurs only for eudicots but not monocots with the exception of a monocot *Phalaenopsis* species (an orchid). This intriguing fact could be explained by the presence of different GIPC series in these two plant clades. While both have similar terminal sugars with similar affinity to NLPs; eudicots GIPC contain two sugars linked to IPC (series A GIPC) whereas monocot GIPC contain three sugars (series A GIPC), with the exception of *Phalaenopsis* containing both series A and B. Biophysical characterization of GIPC series in monolayer artificial membranes suggests a perpendicular arrangement of the polar head of both series A and B GIPC, such that the terminal hexose in series B GIPC, is located further away from the membrane surface compared to series A GIPC. Hence, NLPs binding to series B GIPC terminal sugars have their L3 loop positioned farther from the plant membrane, preventing NLP contact with the membrane and thereby, cytolysis. Both, the length of GIPC head groups and the structural design of the NLP sugar-binding sites explain the differential sensitivity of host plants to NLP toxins.

### 6.1.3. Lipid domain-associated proteins in plant-microbe interaction

Remorins (REM) are plant-specific nanodomain-organized proteins notably involved in plant-microbe interactions. REMs are anchored by their C-terminal domain to the cytosolic leaflet of the PM. The anchoring and lateral segregation in the PM is PI4P- and sterol-mediated [175]. REM1.3 was shown to be delocalized after sterol disrupting treatments, such as methyl- $\beta$ -D-cyclodextrin [192,225,163,191,175] or fenpropimorph [175]. Both their presence at the PM and their correct partitioning within their cognate nanodomains, are essential for their cellular function, e.g. StREM1.3's role in hindering Potato Virus X cell-to-cell movement [175,310]. Other REM-group proteins have been evidenced as key players in biotic interactions such as SYMREM1 (MtREM2.2) involved in the nodulation process of *M. truncatula* with *Sinorhizobium meliloti* [311] Its role was also shown to be essential in the dynamic stabilization of the LYK3-FLOT4-SYMREM1 PM-nanodomains, important for root bacterial symbiosis [312]. Remorins are found in DRM, the closest biochemical counterpart to PM-nanodomains known today, in virtually all clades of land plants: Poplar [313], Oat and Rye [169], Tobacco [172], Arabidopsis [165]. The role of REMs as actors involved in a wide range of biotic interactions has been established throughout the years: ranging from susceptibility factors to viral infections [314], to oomycetes [315] or on the contrary as resistance factors to Potato Virus X [191]. Their capacity to impact PD permeability [175,316] also demonstrates their implication in innate immunity. Super-resolution microscopy has been used to understand the role of nanodomain dynamics in the context of viral infection, revealing that an optimal partition (*i.e.* size of nanodomains, number of molecules in and out domains, and mobility) of REM-associated nanodomains was necessary for the function of REMs [175].

PM receptors involved in the oxidative-burst response to the perception of Pathogen-Associated Molecular Patterns (PAMPs) are key players in plant innate immunity [317]. Their PM localization gives them the role of gatekeepers capable of dynamically associating to co-receptors complexes and triggering signaling pathways to prepare the cell for immediate and short-to-mid-term defense responses [317]. The best example is FLS2, an LRR receptor-like kinase involved in the perception of the bacterial elicitor flagellin (flg22) in Arabidopsis [318]. PM-subcompartmentalization *via* raft-like domains is an essential phenomenon in the PAMP perception and response processes. Upon cryptogeiin treatment on tobacco cells, a quantitative proteomics approach has evidenced the delocalization of various Dynamin and 14-3-3 proteins into the DRM fraction, both involved in PM-based signaling [171]. The reorganization of the PM in response to elicitors is not only observed *via* its protein composition but also *via* the biophysical properties conferred by lipids: upon elicitation with flg22 or cryptogeiin, PM order

and fluidity are altered [92]. As regards to flg22's cognate receptor FLS2, it was shown to relocate to DRM fractions upon flg22 treatment as well as many other key proteins involved in immunity-associated signaling [164], revealing that PM-remodeling, at both the lipid and protein level, is important for a functional immune response.

In good agreement, perception of flg22 in BY-2 cells induces global increase of the order level of the PM. While this modification of the PM properties correlates with signal initiation [319], the potential functional implication and molecular basis of such membrane modification remains to be elucidated. Cryptogeiin is shown to be able to induce an increase in PM-fluidity *via* sterol-binding [112]. Sterols and their associated micro-environments appear to be crucial for immune responses at the cellular level to the extent that both mutants for sterol biosynthesis and sterol-biosynthesis inhibiting drugs affect cell wall composition and induce abnormal callose and lignin deposits *i.e.* cell wall compounds involved in biotic stress [300].

### 6.1.4. GPI-anchored proteins & outer-leaflet PM domains

The importance of outer-leaflet PM-nanodomains enriched in sphingolipids and sterols is also underscored by the presence of GPI-anchored proteins in these domains, many of which are implicated in host responses to invading microbes. GPI-anchored  $\beta$ -1,3-glucanases (BGs), responsible for callose degradation, are found in DRM fractions alongside callose synthases [313]. Their presence in microdomains around PD enable a turnover of callose deposits when proper signaling occurs. The localization of BGs at PD is regulated by the presence of sterol-enriched domains at the PM, which share a virtually identical lipid composition with the PD-PM interface to the extent that sterol-biosynthesis inhibitors abolish this targeting [7]. The PD-enriched GPI-anchored protein LYM2 has been found to impact PD conductance in response to chitin treatments [320]. Several GPI-anchored BGs have been shown to associate to PD thanks to their GPI-anchoring motif [321] in a salicylic acid-dependent fashion [322] consolidating the idea that addressing proteins to PM-PD microdomains *via* GPI-anchoring plays a significant role in host responses to pathogens.

### 6.1.5. Extracellular vesicles & host-induced gene silencing

Extracellular vesicles (EVs) are PM-derived vesicles secreted in the extracellular matrix involved in inter-cellular communication and in response to stress, notably biotic stimuli. The existence of these vesicles has been first observed in plants in the 1960's [323] yet EVs have only recently been better characterized [324] regarding their function during plant-pathogen interactions. They are observed upon xylanase treatment [325] and in response to hormone treatments [326]. EVs are believed to be derived from multi-vesicular bodies (MVB) which accumulate around appressoria and haustoria during defense against fungal pathogens [327,328]. They have recently been shown to contain a number of biotic stress-related compounds such as phytoalexins like glucosinolates [326], small-interfering RNAs that can effectively silence pathogen-associated virulence and/or housekeeping genes [329–331] and signaling-associated enzymes, such as PLD and PLC [332]. The presence of these phospholipases hints to the possibility of EVs being involved in lipid signaling pathways.

Plant EVs contain phospholipids such as PI4P [325,333], PI and PA [326]. The lipid composition may vary upon which organ they are secreted, and upon different stimuli applied to the secreting cells. For example, upon jasmonic acid treatment, sunflower seed-derived EVs will be enriched in PI4P and depleted in PI [326]. The lipidome of plant EVs, in different conditions, has yet to be published and it will surely reveal crucial information on their biogenesis and activity.

## 6.2. Hormone signaling and transport

Lipid-mediated protein sorting mechanisms at TGN have strong impact on plant development since they are involved in directing the secretion and endosomal recycling pathways of a set of proteins that

includes hormone transporters. Higher plants are multi-cellular organisms able to respond and quickly adapt to their environment. In particular, the plant hormone auxin plays a fundamental role in the regulation of a variety of developmental processes enabling plants to adapt to their environment, including directional growth as gravitropism [334–340]. Auxin mediated control of plant development relies on establishment of concentration gradient of auxin that are generated by the activity of plasma membrane localized auxin carriers [338–342]. Therefore, the mechanisms that control the remodeling of auxin carriers represent a key control point for signals that control plant development and response to abiotic stress. Several studies have shown that the TGN is involved in auxin-carrier trafficking but the sorting mechanisms are poorly understood [343–345]. Several elements related to G proteins are known to be involved in TGN-mediated auxin-carriers' trafficking. Our goal in this review is not to create an exhaustive list of all these elements but we can name a few: the small GTPase protein RAB-A1b, the ECHIDNA protein which interacts with YPT/RAB GTPase interacting protein 4a (YIP4a) and YIP4b, the ADP ribosylation factor (ARF) ARF1 as well as the ARF-guanine exchange factors (ARF-GEFs) GNOM and BIG1-5, and finally the ARF-GTPase activating proteins (ARF-GAPs) SCARFACE/VAN3 [345–350]. On the lipid side, sphingolipids represent a class of lipids particularly interesting since VLCFAs, an imprint of sphingolipids, are enriched at TGN [235]. Shortening of the acyl-chain using pharmacological and genetic tools reveal that the length of sphingolipid acyl-chains is involved in the secretory sorting of the efflux auxin carrier PIN2 (but not in PIN1 or AUX1 trafficking), auxin redistribution during root response to gravity (root gravitropism) and root gravitropism *per se* [235]. Interestingly, it had been shown before that VLCFA-containing sphingolipids are involved in PIN1 and AUX1 trafficking (but not PIN2 trafficking) and lateral root formation [56]. These results are not necessarily contradictory. Indeed, the structural diversity of sphingolipids is wide and has been described in chapter 1 and in several reviews [35,301]. LCBs are not always found included in a ceramide molecule but can also be freely found at non-negligible proportion inside the cell as sphinganine and phytosphingosines. Finally, aside from sphingolipids, VLCFAs can also be included in some phospholipids. On this topic, it has been shown that the *pas2* mutant displays a reduced level of VLCFA-containing PE and show endocytic trafficking defects [351]. Decrease of VLCFA-containing PE in the *pas2* mutant targets the RAB-A2a compartment and the plasma membrane endocytic recycling of the auxin efflux-carrier PIN1 but has no effect on PIN2 localization [351,352].

Coming back on sphingolipids, it has been shown that the *loh1/loh2* double mutant, which is defective in ceramide synthases LOH1 and LOH2, are involved in endocytosis and plasma membrane recycling of the auxin carriers PIN1 and AUX1, but not PIN2, potentially through RAB-A2a compartments [56]. Hence, it is possible that VLCFA-containing sphingolipids are important for endocytic/recycling of certain subset of proteins from plasma membrane through a RAB-A2a-positive subdomain of TGN that would host the recycling pathway. In contrast, the herbicide metazachlor, that drastically modifies both GluCer and GIPC fatty acids composition by replacing VLCFAs in GluCer and GIPC pools by 16–18 carbon atom fatty acids without modifying the global quantity of either GluCer or GIPC, alters PIN2 polarity at plasma membrane while it neither affects PIN1 polarity nor AUX1 localization [235]. Importantly, metazachlor blocks PIN2 predominantly at SYP61/secretory vesicles (SVs) compartments as compared to RAB-A2a/CCVs [235]. Concomitantly, metazachlor treatment neither alters endocytosis nor plasma membrane recycling of PIN2 but rather blocks the secretion of *de novo* synthesized PIN2 at SYP61/SVs compartments. From these studies, it can be postulated that TGN-associated RAB-A2a/Clathrin-coated vesicles (CCVs) compartments could host the ceramide-dependent PM recycling of auxin carriers PIN1 and AUX1 while TGN-associated SYP61/SVs compartments could host VLCFA-containing GluCer and GIPC-dependent secretory sorting of PIN2. However, future challenges on this topic need to address TGN sub-domains' dynamics,

interactions and maturation, which could involve a tight regulation of lipid homeostasis and crosstalk to define the identity of each sub-domain.

The VLCFAs of sphingolipids determine a specific physical property of sphingolipids, which is the ability to insert their acyl-chain within the opposing leaflet of the membrane, a phenomenon known as interdigitation, see Fig. 4. Interestingly, it has been shown in animal cells that the coupling of membrane leaflets is cholesterol-dependent [66]. In yeast and in plants, it has been shown by immuno-purification of intact compartments coupled with lipid mass spectrometry analyses, that TGN-derived secretory vesicles are enriched in both sphingolipids and sterols [232,235]. Currently, it is not clear whether the pool of sterols at the TGN would play a role in the trafficking of auxin carriers. Previously, it has been shown that sterols are involved in endocytosis and recycling at plasma membrane of the PINs auxin carriers [353–355]. Sterol-mediated endocytosis is involved in PIN2 polarity establishment after cytokinesis by removing PIN2 from the new basal membrane of daughter cells, while PIN2 at the new apical membrane remains [354]. Sterol-mediated auxin carriers' sub-cellular localization impacts auxin distribution at the tissue-level, which has repercussions on plant development such as the graviresponse of the root [354]. Interestingly, not only are the major sterols: sitosterol, stigmasterol and campesterol involved in plant development, but also some very rare intermediate-sterol compounds such as derivatives of cycloartanol (4-carboxy-4-methyl-24-methylenecycloartanol) and 4 $\alpha$ -methyl sterols (24-ethyllophenol and 24-ethylidenlophenol) [356,357]. Future studies will reveal how sterols interplay with other lipids such as sphingolipids and anionic phospholipids to regulate hormone transport.

### 6.3. Abiotic stress

Lipids have been involved as second messengers in many responses to abiotic stress, see for review [265,358–360,361]. PLD and PLC/DGK-mediated PA formation and its subsequent phosphorylation to form Diacylglycerol Pyrophosphate (DGPP) are key players in this response [362]. Other lipids participate to the response: oxylipins, PIPs, sphingolipids, fatty acids, lysophospholipids, N-acyl ethanolamines and galactolipids, see for reviews [1,363]. Studies have started deciphering the different isoforms of enzymes involved in these transduction pathways as well as their tight regulations, for recent reviews see [364]. For example, PA displays different modes of action, including direct target protein binding and biophysical effects on cell membranes. It is puzzling that PA production can be triggered by opposite stressors, such as cold and heat. How PA regulates this diversity of response is discussed in this recent review [267].

PLD-derived PA was shown to recruit the ABA-regulated ABI1 phosphatase 2C (PP2C) to the PM [365]. The identification of ABI1 as a direct target of the PA provides a functional link between the two families of important signaling enzymes, PLD and PP2C. Recently, a study on the regulation of ion transport in plants showed that C2-domain ABA-related (CAR) family of small proteins is involved in the Ca<sup>2+</sup>-dependent recruitment of the pyrabactin resistance 1/PYR1-like (PYR/PYL) ABA receptors to the PM. CARs are peripheral membrane proteins that cluster at the PM and generate strong positive membrane curvature. These features represent a mechanism for the generation, stabilization, and/or specific recognition of PM discontinuities involved in the recruitment of PYR/PYL receptors and other signaling components in cell responses to salt stress [366].

### 6.4. Plasmodesmata function

Plasmodesmata (PD) are specialized nano-sized membrane-lined channels, which cross the walls of plants and of some algal cells. PDs enable direct, regulated, symplastic transport of small RNAs and molecules between cells. They are also hijacked by phytoviruses to allow their propagation from cell-to-cell. Ultrastructure of PD has been

deciphered. They are lined by the PM forming what is termed the PD-PM subcompartment (PD-PM) and contain a strand of tubular modified ER called desmotubule, and the space between these two membranes is thought to control PD permeability [203]. A recent study has reconstructed PD three-dimensional ultrastructure with an unprecedented resolution using electron tomography, showing that ER-PM contact sites undergo substantial remodeling events during cell differentiation [367]. Post-cytokinesis PD, called type I PD, present an intimate ER-PM contact along the entire length of the pores whereas during cell expansion, the PD pore widens and the two membranes separate, leaving a cytosolic sleeve spanned by tethers whose presence correlates with the appearance of the intermembrane gaps, called type II PD. Surprisingly, the type II PD allow diffusion of macromolecules despite the apparent lack of an open cytoplasmic sleeve, forcing the reassessment of the mechanisms that control plant cell-to-cell communication [367].

The membrane organization of PDs is therefore characterized by the close apposition of the ER-derived desmotubule and the PM with spoke-like structures linking the two membranes likely defining microdomains of the PM, PD-PM and desmotubules has been recently proposed to be membrane contact sites (MCS). MCS control close appositions between two membranes that form microdomains involved in the control of lipid exchanges or in coupling events (review in [368]). MCS-subdomains are likely to display specific biophysical properties and may cluster proteins and negatively-charged lipids like phosphoinositides, promoting specific physicochemical membrane properties taking part in shaping local membrane electronegativity gradients [368].

Firmly anchored within the cell wall, PDs are difficult to purify. A two-step simple purification procedure (consisting in isolating cell wall fragments containing intact PD and an enzymatic degradation of the wall matrix to release of PD) has been successfully design to obtain highly-purified PD preparations [369]. Hence, analyses of PD fractions have provided valuable information on the functional and structural elements that define PD, particularly for lipids. PD membranes display enrichment in sterols and sphingolipids with saturated VLCFAs (likely GIPC) when compared with the bulk of the PM. This profile is reminiscent of DRMs although the isolation procedure is detergent-free and suggest that lipids are laterally segregated at the PD-PM cell-to-cell junction in *Arabidopsis thaliana* [7]. This study identifies a role for sterols in modulating cell-to-cell connectivity, possibly by establishing and maintaining the positional specificity of callose-modifying GPI-anchored proteins at PD and emphasizes the importance of lipids in defining PD-associated nanodomains. The role played by the other major lipid constituents, such as GIPC and glycerolipids in defining specialized membrane domains in PD, remains to be further studied. This change of paradigm regarding the membrane organization of PD will likely pave the way to a deep understanding of cell-to-cell communication in plants.

## 7. Conclusions and perspectives: how to get a comprehensive membrane organization in plants?

The deep-seated understanding of how the plant PM is organized in terms of the involvement of lipids and proteins clearly necessitates multiple approaches. Our community needs to develop new dedicated methodologies and dare multidisciplinary even further that what we have been accustomed to. For example, the extensive use of biophysical approaches to study lipid/protein interactions as reviewed in [370], among them: 1/surface plasmon resonance [40], isothermal titration calorimetry (ITC), Langmuir monolayer tensiometry, liposomes binding and lipid strips and arrays [117] to study the interaction of proteins with lipids; 2/liposome leakage and lipid-mixing assays [310] to investigate how proteins can destabilize membrane bilayers; 3/Circular dichroism [310], Fourier-transform infrared spectroscopy [175], solid-state NMR with labeled lipids or proteins [371] to obtain 3D structures of the membrane-bound interaction-complexes; 4/Atomic force microscopy (AFM) to scan the surface of bilayers and access the topology of

different membrane organizations. A deep understanding of the structural aspects of protein/lipid interactions will allow the targeted-mutagenesis of key residues, the biological role of which could be further addressed by reverse genetics approaches.

In all the methods described above, there is an urgent need for biochemistry to obtain purified proteins and lipids, in order to reconstitute proteoliposomes. Concerning proteins, the problem of insolubility of highly hydrophobic proteins could be solved by using different expression systems [372]. As for lipids, most of plant lipids are commercially available with the notable exception of GIPC. The lack of commercially-available GIPC strongly impairs any serious *in vitro* reconstitutions of true plant PM-like vesicles. One must undertake hardcore preparative biochemistry as described during the 1970's to obtain milligrams of purified GIPC from living material [53,55]. Purification of mg amount of GIPC will also pave the way to the development of fluorescently labeled sphingolipid analogs by conjugating a hydrophilic fluorophore to the headgroup or a hydrophobic fluorophore to the amidified fatty acids e.g. [373]. Unfortunately, very few plant lipids labeled with a fluorochrome or deuterated are available. Similarly, none of the great diversity of free- and conjugated-phytosterols are commercialized in a labeled form, which strongly impairs NMR studies that would enable to further enquire about the role of each molecular species individually. From purified lipids, the preparation of asymmetrical liposomes will also be very challenging. To have access to the properties of asymmetric vesicles that mimic the plant PM would provide means to understand lipid raft formation or transmembrane helix orientation [374],

Molecular dynamics (MD) is a method that computes the physical movements of atoms and molecules in order to give a view of the dynamic evolution of a virtual chemical system. It can therefore study the interaction dynamics of lipids and proteins, or the conformational changes of molecules, for a fixed period of time. MD computes lipid-lipid and lipid-protein interactions and provides a comprehensive atomistic model of a typical lipid bilayer and gather information on membrane domain formations [375,376]. MD has been used in plant membrane biology to decipher the structural basis of the unconventional lipid-binding motif of REM that confers nanodomain organization [175]. Such approach of “computational microscopy” captures the molecular interactions within a complex system at a spatiotemporal resolution, unmatched by any other conventional experimental methods e.g. [137,377]. MD can be of particular interest in grasping the intricacies of plant PM dynamics because the control of the thermodynamic parameters permitted by MD can be used to mimic the constantly varying environmental conditions sustained by plants in their natural habitats, and thereby to understand the biophysical implications of these variations on the PM. Unfortunately, neither plant sphingolipids (GluCer, GIPC), nor phytosterols (free or conjugated) have been, to this day, modeled in the force field, preventing all MD studies with plant PM lipids. The force field refers to the functional form and parameter sets used to calculate the potential energy of a system of atoms or coarse-grained particles; it is the necessary step for MD simulations. The parameters of the energy functions may be derived from experiments in physics (solid-state NMR, Langmuir monolayer, calorimetry...) or chemistry (chemical structure, liquid-state NMR...) [378]. All-atom force fields provide parameters for every type of atom in a system. Coarse-grained potentials, which are often used in long-time simulations of macromolecules and multi-component complexes, provide even cruder representations for higher computing efficiency. Such modelization must be carried for plant sphingolipids and phytosterols as it was described for animal gangliosides in [379].

Other aspects still missing in the plant membrane biology field, are the methods to image lipids *in vivo* necessary to follow their segregation at the nanoscale level, their dynamics and interactions with proteins. Two reasons can be given: firstly, as stated before, very few fluorescently-labeled lipids are available, and secondly, the cell wall strongly impairs the intake of fluorescently labeled molecules. Nevertheless, the

use of *in vivo* bioorthogonal click chemistry could be an elegant approach to circumvent this problem in plants [380,381]. Although genetically encoded biosensors for PIPs, PA, DAG and PS have already been developed [27,117,118], biosensors of plant sphingolipids and phytosterols are crucially missing and will surely be developed using lipid-binding domains found in plant proteins. Inhibitors of lipid synthesis (Table 1), and genetically-modified lipid-using enzymes (phosphoinositides kinase, lipid phosphatase, lipase) able to target the PM and specifically modify *in vivo* pools of lipids, are used to address the question of the role of lipids in nanodomain formation and dynamics [118,175,382]. Similarly, membrane surface charge or pH biosensors must be improved as described in animal literature with intramolecular fluorescence resonance energy transfer (FRET) sensors [383,384]. The development of environmentally-sensitive probes to label the outer- or inner-leaflet and measure independently the fluidity of plant PM leaflets, must also be engaged (see examples of available probes in [385]). Furthermore, super-resolution microscopy will continue to allow a deep understanding of segregation and dynamics of proteins and lipids at the nanometer scale. The development of fluorescent bimolecular tracking in the live-cell PM will reveal whether proteins and lipids may directly or indirectly interact with each other [211].

Finally, state of the art lipidomics [386] and proteomics approaches must be further developed including phosphoproteomics and lipid-modification of proteins (myristoylation, palmitoylation, isoprenylation and GPI-anchoring, review in [387]).

The study of K-RAS protein which controls cell proliferation in animal cells should be exemplified for the combinations of approaches mobilized by Hancock's group to tackle its function in relation to its organization within PM [260–262,388–390]. K-Ras controls cell proliferation, and when mutated, cells continuously proliferate and often develop into cancer. This group tackled the role of K-Ras in PM nanodomains by using in parallel biochemistry, biophysics, modeling, high-resolution imagery, mutagenesis, structural biology, model membranes, transcriptomics, cancerology and genetics techniques. This form of multidisciplinary approach has led to a deep understanding of the anchoring, the clustering of K-Ras with PM lipids, as well as the integration of these molecular mechanisms into higher levels of cell biology, hence determining their consequences on the fate of the cell. For example, a recent paper of this group has shown that K-Ras anchoring sequences can create lipid nanodomains with a remarkable specificity [261], and that lipid nanodomains are not preexisting. A matter of the chicken or the egg causality dilemma! Similarly the works of Katharina Gaus' [383,384,391–394] or Akihiro Kusumi's labs [132,395–397] are exemplary to understand, by developing single-molecule imaging methods, how T-cells initiate an immune response and to better fathom the intricate complexity between cytoskeleton and protein/lipid segregation. These two research groups have been remarkable by developing, in collaboration with biophysicists, state of the art technology to follow single-molecules in the PM.

Taken together, tools and methods must be developed by the plant membrane biology community in the near future to pave the way towards the better understanding of the intimate molecular relationships between lipids and proteins at the basis of domain segregation, dynamics, signaling and function.

## Acknowledgements

We apologize to researchers whose work could not be cited here because of space limitations. AMC and PG are supported by the Ministère de l'Enseignement Supérieur et de la Recherche, France (MERS, doctoral grants). This work was supported by the Bordeaux Metabolome Facility-MetaboHUB (grant no. ANR-11-INBS-0010). We acknowledge the platform Metabolome-Fluxome-Lipidome of Bordeaux (<http://www.biomemb.cnrs.fr/INDEX.html>) for contribution to lipid analysis.

## Conflict of interest

No conflict of interest declared.

## References

- [1] H.W. Xue, X. Chen, Y. Mei, Function and regulation of phospholipid signalling in plants, *Biochem J* 421 (2009) 145–156.
- [2] J.L. Cacas, C. Bure, K. Grosjean, P. Gerbeau-Pissot, J. Lherminier, Y. Rombouts, et al., Re-visiting plant plasma membrane lipids in tobacco: a focus on sphingolipids, *Plant Physiol* 170 (2015) 367–384.
- [3] L. Yetukuri, K. Ekroos, A. Vidal-Puig, M. Oresic, Informatics and computational strategies for the study of lipids, *Mol Biosyst* 4 (2008) 121–127.
- [4] C. Larsson, M. Sommarin, S. Widell, Isolation of highly purified plant plasma membranes and separation of inside-out and right-side-out vesicles, *Methods Enzymol* 228 (1994) 451–469.
- [5] T. Samarakoon, S. Shiva, K. Lowe, P. Tamura, M.R. Roth, R. Welti, Arabidopsis thaliana membrane lipid molecular species and their mass spectral analysis, *Methods Mol Biol* 918 (2012) 179–268.
- [6] D. Yu, T.W.T. Rupasinghe, B.A. Boughton, S.H.A. Natera, C.B. Hill, P. Tarazona, et al., A high-resolution HPLC-QqTOF platform using parallel reaction monitoring for in-depth lipid discovery and rapid profiling, *Anal Chim Acta* 1026 (2018) 87–100.
- [7] M.S. Grison, L. Brocard, L. Fouillen, W. Nicolas, V. Wewer, P. Dormann, et al., Specific membrane lipid composition is important for plasmodesmata function in Arabidopsis, *Plant Cell* 27 (2015) 1228–1250.
- [8] F. Doignon, P. Laquel, E. Testet, K. Tuphile, L. Fouillen, J.J. Bessoule, Requirement of phosphoinositides containing stearic acid to control cell polarity, *Mol Cell Biol* 36 (2015) 765–780.
- [9] J.E. Markham, J.G. Jaworski, Rapid measurement of sphingolipids from Arabidopsis thaliana by reversed-phase high-performance liquid chromatography coupled to electrospray ionization tandem mass spectrometry, *Rapid Commun Mass Spectrom* 21 (2007) 1304–1314.
- [10] J.E. Markham, J. Li, E.B. Cahoon, J.G. Jaworski, Separation and identification of major plant sphingolipid classes from leaves, *J Biol Chem* 281 (2006) 22684–22694.
- [11] K. Schrick, S. Shiva, J.C. Arpin, N. Delimont, G. Isaac, P. Tamura, et al., Steryl glucoside and acyl steryl glucoside analysis of Arabidopsis seeds by electrospray ionization tandem mass spectrometry, *Lipids* 47 (2012) 185–193.
- [12] V. Wewer, I. Dombink, K. Vom Dorp, P. Dormann, Quantification of sterol lipids in plants by quadrupole time-of-flight mass spectrometry, *J Lipid Res* 52 (2011) 1039–1054.
- [13] M.R. Wenk, Lipidomics: new tools and applications, *Cell* 143 (2010) 888–895.
- [14] P.J. Horn, A.R. Korte, P.B. Neogi, E. Love, J. Fuchs, K. Strupat, et al., Spatial mapping of lipids at cellular resolution in embryos of cotton, *Plant Cell* 24 (2012) 622–636.
- [15] H.K. Woodfield, D. Sturtevant, L. Borisjuk, E. Munz, I.A. Guschina, K. Chapman, et al., Spatial and temporal mapping of key lipid species in brassica napus seeds, *Plant Physiol* 173 (2017) 1998–2009.
- [16] S.R. Ellis, M.R.L. Paine, G.B. Eijkel, J.K. Pauling, P. Husen, M.W. Jervelund, et al., Automated, parallel mass spectrometry imaging and structural identification of lipids, *Nat Methods* 15 (2018) 515–518.
- [17] J.F. Frisz, H.A. Klitzing, K. Lou, I.D. Hutcheon, P.K. Weber, J. Zimmerberg, et al., Sphingolipid domains in the plasma membranes of fibroblasts are not enriched with cholesterol, *J Biol Chem* 288 (2013) 16855–16861.
- [18] J.F. Frisz, K. Lou, H.A. Klitzing, W.P. Hanafin, V. Lizunov, R.L. Wilson, et al., Direct chemical evidence for sphingolipid domains in the plasma membranes of fibroblasts, *Proc Natl Acad Sci U S A* 110 (2013) E613–E622.
- [19] S. Mongrand, J. Morel, J. Laroche, S. Claverol, J.P. Carde, M.A. Hartmann, et al., Lipid rafts in higher plant cells: purification and characterization of Triton X-100-insoluble microdomains from tobacco plasma membrane, *J Biol Chem* 279 (2004) 36277–36286.
- [20] M. Uemura, R.A. Joseph, P.L. Steponkus, Cold acclimation of Arabidopsis thaliana (effect on plasma membrane lipid composition and freeze-induced lesions), *Plant Physiol* 109 (1995) 15–30.
- [21] M. Bohn, E. Heinz, S. Luthje, Lipid composition and fluidity of plasma membranes isolated from corn (*Zea mays L.*) roots, *Arch Biochem Biophys* (387) (2001) 35–40.
- [22] M. Uemura, P.L. Steponkus, A contrast of the plasma membrane lipid composition of oat and rye leaves in relation to freezing tolerance, *Plant Physiol* 104 (1994) 479–496.
- [23] M.F. Quartacci, O. Glisic, B. Stevanovic, F. Navari-Izzo, Plasma membrane lipids in the resurrection plant *Ramonda serbica* following dehydration and rehydration, *J Exp Bot* 53 (2002) 2159–2166.
- [24] A.H. Berglund, M.F. Quartacci, L. Calucci, F. Navari-Izzo, C. Pinzino, C. Liljenberg, Alterations of wheat root plasma membrane lipid composition induced by copper stress result in changed physicochemical properties of plasma membrane lipid vesicles, *Biochim Biophys Acta* 1564 (2002) 466–472.
- [25] J.E. Vermeer, T. Munnik, Using genetically encoded fluorescent reporters to image lipid signalling in living plants, *Methods Mol Biol* 1009 (2013) 283–289.
- [26] R. Tejos, M. Sauer, S. Vanneste, M. Palacios-Gomez, H. Li, M. Heilmann, et al., Bipolar plasma membrane distribution of phosphoinositides and their requirement for auxin-mediated cell polarity and patterning in Arabidopsis, *Plant Cell* 26 (2014) 2114–2128.
- [27] M.L. Simon, M.P. Platre, S. Assil, R. van Wijk, W.Y. Chen, J. Chory, et al., A multi-

- colour/multi-affinity marker set to visualize phosphoinositide dynamics in Arabidopsis, *Plant J* 77 (2014) 322–337.
- [28] Y. Yamaoka, Y. Yu, J. Mizoi, Y. Fujiki, K. Saito, M. Nishijima, et al., Phosphatidylserine Synthase1 is required for microspore development in Arabidopsis thaliana, *Plant J* 67 (2011) 648–661.
- [29] T. Hirano, K. Stecker, T. Munnik, H. Xu, M.H. Sato, Visualization of phosphatidylinositol 3,5-bisphosphate dynamics by a tandem ML1N-based fluorescent protein probe in Arabidopsis, *Plant Cell Physiol* 58 (2017) 1185–1195.
- [30] W. van Leeuwen, J.E. Vermeer, T.W. Gadella Jr., T. Munnik, Visualization of phosphatidylinositol 4,5-bisphosphate in the plasma membrane of suspension-cultured tobacco BY-2 cells and whole Arabidopsis seedlings, *Plant J* 52 (2007) 1014–1026.
- [31] F. Furt, S. Konig, J.J. Bessoule, F. Sargueil, R. Zallot, T. Stanislas, et al., Polyphosphoinositides are enriched in plant membrane rafts and form microdomains in the plasma membrane, *Plant Physiol* 152 (2010) 2173–2187.
- [32] M.X. Andersson, M.H. Stridh, K.E. Larsson, C. Liljenberg, A.S. Sandelius, Phosphate-deficient oat replaces a major portion of the plasma membrane phospholipids with the galactolipid digalactosyldiacylglycerol, *FEBS Lett* 537 (2003) 128–132.
- [33] M.X. Andersson, K.E. Larsson, H. Tjellstrom, C. Liljenberg, A.S. Sandelius, Phosphate-limited oat. The plasma membrane and the tonoplast as major targets for phospholipid-to-glycolipid replacement and stimulation of phospholipases in the plasma membrane, *J Biol Chem* 280 (2005) 27578–27586.
- [34] J.E.M. Vermeer, R. van Wijk, J. Goedhart, N. Geldner, J. Chory, T.W.J. Gadella Jr. et al., In vivo imaging of diacylglycerol at the cytoplasmic leaflet of plant membranes, *Plant Cell Physiol* 58 (2017) 1196–1207.
- [35] D.V. Lynch, T.M. Dunn, An introduction to plant sphingolipids and a review of recent advances in understanding their metabolism and function, *New Phytol* 16 (2004) 677–702.
- [36] S. Sonnino, A. Prinetti, Gangliosides as regulators of cell membrane organization and functions, *Adv Exp Med Biol* 688 (2010) 165–184.
- [37] P. Moreau, J.J. Bessoule, S. Mongrand, E. Testet, P. Vincent, C. Cassagne, Lipid trafficking in plant cells, *Prog Lipid Res* 37 (1998) 371–391.
- [38] M.O. Pata, Y.A. Hannun, C.K. Ng, Plant sphingolipids: decoding the enigma of the Sphinx, *New Phytol* 185 (2010) 611–630.
- [39] J.L. Cacas, C. Bure, K. Grosjean, P. Gerbeau-Pissot, J. Lherminier, Y. Rombouts, et al., Revisiting plant plasma membrane lipids in tobacco: a focus on sphingolipids, *Plant Physiol* 170 (2016) 367–384.
- [40] T.A.I. Lenarčič, H. Böhm, V. Hodnik, K. Pirc, A.P. Zavec, M. Podobnik, et al., Eudicot plant—specific sphingolipids determine host selectivity of microbial NLP cytolysins, (2017).
- [41] H.E. Carter, R.H. Gigg, J.H. Law, T. Nakayama, E. Weber, Biochemistry of the sphingolipids. XI. Structure of phytoglycolipide, *J Biol Chem* 233 (1958) 1309–1314.
- [42] C. Bure, J.L. Cacas, S. Mongrand, J.M. Schmitter, Characterization of glycosyl inositol phosphoryl ceramides from plants and fungi by mass spectrometry, *Anal Bioanal Chem* 406 (2014) 995–1010.
- [43] T.C. Hsieh, R.L. Lester, R.A. Laine, Glycophosphoceramide from plants. Purification and characterization of a novel tetracosaric acid derived from tobacco leaf glycolipids, *J Biol Chem* 256 (1981) 7747–7755.
- [44] P. Sperling, E. Heinz, Plant sphingolipids: Structural diversity, biosynthesis, first genes and functions, *Biochim Biophys Acta* 2003 (1632) 1–15.
- [45] C. Bure, J.L. Cacas, F. Wang, K. Gaudin, F. Domergue, S. Mongrand, et al., Fast screening of highly glycosylated plant sphingolipids by tandem mass spectrometry, *Rapid Commun Mass Spectrom* 25 (2011) 3131–3145.
- [46] J.L. Cacas, C. Bure, F. Furt, J.P. Maalouf, A. Badoc, S. Cluzet, et al., Biochemical survey of the polar head of plant glycosylinositolphosphoceramides unravels broad diversity, *Phytochemistry* 96 (2013) 191–200.
- [47] J.C. Mortimer, X. Yu, S. Albrecht, F. Sicilia, M. Huichalaf, D. Ampuero, et al., Abnormal glycosphingolipid mannosylation triggers salicylic acid-mediated responses in Arabidopsis, *Plant Cell* 25 (2013) 1881–1894.
- [48] C. Bure, J.L. Cacas, S. Mongrand, J.M. Schmitter, Characterization of glycosyl inositol phosphoryl ceramides from plants and fungi by mass spectrometry, *Anal Bioanal Chem* 406 (4) (2013) 995–1010.
- [49] L. Fang, T. Ishikawa, E.A. Rennie, G.M. Murawska, J. Lao, J. Yan, et al., Loss of inositol phosphorylceramide sphingolipid mannosylation induces plant immune responses and reduces cellulose content in Arabidopsis, *Plant Cell* 28 (2016) 2991–3004.
- [50] K.D. Lutgeharm, A.N. Kimberlin, R.E. Cahoon, R.L. Cerny, J.A. Napier, J.E. Markham, et al., Sphingolipid metabolism is strikingly different between pollen and leaf in Arabidopsis as revealed by compositional and gene expression profiling, *Phytochemistry* 115 (2015) 121–129.
- [51] F. Tellier, A. Maia-Grondard, I. Schmitz-Afonso, J.D. Faure, Comparative plant sphingolipidomic reveals specific lipids in seeds and oil, *Phytochemistry* 103 (2014) 50–58.
- [52] M. Nagano, T. Ishikawa, M. Fujiwara, Y. Fukao, Y. Kawano, M. Kawai-Yamada, et al., Plasma membrane microdomains are essential for Rac1-RbohB/H-mediated immunity in rice, *Plant Cell* 28 (2016) 1966–1983.
- [53] K. Kaul, R.L. Lester, Characterization of inositol-containing phosphosphingolipids from tobacco leaves: Isolation and Identification of two novel, major lipids: N-acetylglucosamidoglucuronidoinositol phosphorylceramide and glucosamidoglucuronidoinositol phosphorylceramide, *Plant Physiol* 55 (1975) 120–129.
- [54] N. Blaas, H.U. Humpf, Structural profiling and quantitation of glycosyl inositol phosphoceramide in plants with Fourier transform mass spectrometry, *J Agric Food Chem* 61 (2013) 4257–4269.
- [55] T.C. Hsieh, K. Kaul, R.A. Laine, R.L. Lester, Structure of a major glycophosphoceramide from tobacco leaves, PSL-I: 2-deoxy-2-acetamido-D-glucopyranosyl(alpha1 leads to 4)-D-glucuronopyranosyl(alpha1 leads to 2)myoinositol-1-O-phosphoceramide, *Biochemistry* 17 (1978) 3575–3581.
- [56] J.E. Markham, D. Molino, L. Gissot, Y. Bellec, K. Hematy, J. Marion, et al., Sphingolipids containing very-long-chain Fatty acids define a secretory pathway for specific polar plasma membrane protein targeting in Arabidopsis, *Plant Cell* 23 (2011) 2362–2378.
- [57] M. Chen, J.E. Markham, E.B. Cahoon, Sphingolipid Delta8 unsaturation is important for glucosylceramide biosynthesis and low-temperature performance in Arabidopsis, *Plant J* 69 (2012) 769–781.
- [58] T. Mikami, M. Kashiwagi, K. Tsuchihashi, T. Akino, S. Gasa, Substrate specificity and some other enzymatic properties of dihydroceramide desaturase (ceramide synthase) in fetal rat skin, *J Biochem* 123 (1998) 906–911.
- [59] H. Liang, N. Yao, J.T. Song, S. Luo, H. Lu, J.T. Greenberg, Ceramides modulate programmed cell death in plants, *Genes Dev* 17 (2003) 2636–2641.
- [60] J.T. Marques, H.S. Marinho, R.F.M. de Almeida, Sphingolipid hydroxylation in mammals, yeast and plants - an integrated view, *Prog Lipid Res* 71 (2018) 18–42.
- [61] I. Hillig, M. Leipelt, C. Ott, U. Zahringer, D. Warnecke, E. Heinz, Formation of glucosylceramide and sterol glucoside by a UDP-glucose-dependent glucosylceramide synthase from cotton expressed in *Pichia pastoris*, *FEBS Lett* 553 (2003) 365–369.
- [62] W. Wang, X. Yang, S. Tangchaiburana, R. Ndeh, J.E. Markham, Y. Tsegaye, et al., An inositolphosphorylceramide synthase is involved in regulation of plant programmed cell death associated with defense in Arabidopsis, *Plant Cell* 20 (2008) 3163–3179.
- [63] E.A. Rennie, B. Ebert, G.P. Miles, R.E. Cahoon, K.M. Christiansen, S. Stonebloom, et al., Identification of a sphingolipid alpha-glucuronosyltransferase that is essential for pollen function in Arabidopsis, *Plant Cell* 26 (2014) 3314–3325.
- [64] T. Ishikawa, L. Fang, E.A. Rennie, J. Sechet, J. Yan, B. Jing, et al., Glucosamine Inositolphosphorylceramide Transferase1 (GINT1) is a GlcNAc-Containing glycosylinositol phosphorylceramide glycosyltransferase, *Plant Physiol* 177 (2018) 938–952.
- [65] J.O. Blachtutzik, F. Demir, I. Kreuzer, R. Hedrich, G.S. Harms, Methods of staining and visualization of sphingolipid enriched and non-enriched plasma membrane regions of Arabidopsis thaliana with fluorescent dyes and lipid analogues, *Plant Methods* 8 (2012) 28.
- [66] T. Rog, A. Orlowski, A. Llorente, T. Skotland, T. Sylvanne, D. Kauhanen, et al., Interdigitation of long-chain sphingomyelin induces coupling of membrane leaflets in a cholesterol dependent manner, *Biochim Biophys Acta* 2016 (1858) 281–288.
- [67] D.A. Guo, M. Venkatramesh, W.D. Nes, Developmental regulation of sterol biosynthesis in *Zea mays*, *Lipids* 30 (1995) 203–219.
- [68] R.A. Moreau, L. Nystrom, B.D. Whitaker, J.K. Winkler-Moser, D.J. Baer, S.K. Gebauer, et al., Phytosterols and their derivatives: Structural diversity, distribution, metabolism, analysis, and health-promoting uses, *Prog Lipid Res* 70 (2018) 35–61.
- [69] H. Schaller, New aspects of sterol biosynthesis in growth and development of higher plants, *Plant Physiol Biochem* 42 (2004) 465–476.
- [70] M.S. Webb, M. Uemura, P.L. Steponkus, A comparison of freezing injury in oat and rye: Two cereals at the extremes of freezing tolerance, *Plant Physiol* 104 (1994) 467–478.
- [71] A. Ferrer, T. Altabella, M. Arro, A. Boronat, Emerging roles for conjugated sterols in plants, *Prog Lipid Res* 67 (2017) 27–37.
- [72] Y. Boutte, S. Men, M. Grebe, Fluorescent in situ visualization of sterols in Arabidopsis roots, *Nat Protoc* 6 (2011) 446–456.
- [73] M. Ovecka, T. Berson, M. Beck, J. Derksen, J. Samaj, F. Baluska, et al., Structural sterols are involved in both the initiation and tip growth of root hairs in Arabidopsis thaliana, *Plant Cell* 22 (2010) 2999–3019.
- [74] P. Liu, R.L. Li, L. Zhang, Q.L. Wang, K. Niehaus, F. Baluska, et al., Lipid microdomain polarization is required for NADPH oxidase-dependent ROS signaling in *Picea meyeri* pollen tube tip growth, *Plant J* 60 (2009) 303–313.
- [75] L. Bonneau, P. Gerbeau-Pissot, D. Thomas, C. Der, J. Lherminier, S. Bourque, et al., Plasma membrane sterol complexation, generated by filipin, triggers signaling responses in tobacco cells, *Biochim Biophys Acta* 2010 (1798) 2150–2159.
- [76] T. Stanislas, M. Grebe, Y. Boutte, Sterol dynamics during endocytic trafficking in Arabidopsis, *Methods Mol Biol* 1209 (2014) 13–29.
- [77] H. Tjellstrom, L.I. Hellgren, A. Wieslander, A.S. Sandelius, Lipid asymmetry in plant plasma membranes: phosphate deficiency-induced phospholipid replacement is restricted to the cytosolic leaflet, *FASEB J* 24 (2010) 1128–1138.
- [78] S.L. Liu, R. Sheng, J.H. Jung, L. Wang, E. Stec, M.J. O'Connor, et al., Orthogonal lipid sensors identify transbilayer asymmetry of plasma membrane cholesterol, *Nat Chem Biol* 13 (2017) 268–274.
- [79] J.R. Hazel, E.E. Williams, The role of alterations in membrane lipid composition in enabling physiological adaptation of organisms to their physical environment, *Prog Lipid Res* 29 (1990) 167–227.
- [80] K. Jacobson, Z. Derzko, E.S. Wu, Y. Hou, G. Poste, Measurement of the lateral mobility of cell surface components in single, living cells by fluorescence recovery after photobleaching, *J Supramol Struct* 5 (1976) 565(417)–576(428).
- [81] G.S. Ali, K.V. Prasad, I. Day, A.S. Reddy, Ligand-dependent reduction in the membrane mobility of flagellin sensitive2, an Arabidopsis receptor-like kinase, *Plant Cell Physiol* 48 (2007) 1601–1611.
- [82] M. Lankova, J. Humpolickova, S. Vosolsobe, Z. Cit, J. Lacek, M. Covan, et al., Determination of dynamics of plant plasma membrane proteins with fluorescence recovery and raster image correlation spectroscopy, *Microsc Microanal* 22 (2016) 290–299.
- [83] A. Martiniere, I. Lavagi, G. Nageswaran, D.J. Rolfe, L. Maneta-Peyret, D.T. Luu,

- et al., Cell wall constrains lateral diffusion of plant plasma-membrane proteins, *Proc Natl Acad Sci U S A* 109 (2012) 12805–12810.
- [84] R. Machan, M. Hof, Lipid diffusion in planar membranes investigated by fluorescence correlation spectroscopy, *Biochim Biophys Acta* 2010 (1798) 1377–1391.
- [85] P.A. Janney, P.K. Kinnunen, Biophysical properties of lipids and dynamic membranes, *Trends Cell Biol* 16 (2006) 538–546.
- [86] B.R. Lentz, Y. Barenholz, T.E. Thompson, Fluorescence depolarization studies of phase transitions and fluidity in phospholipid bilayers. 1. Single component phosphatidylcholine liposomes, *Biochemistry* 15 (1976) 4521–4528.
- [87] E.R. Moellering, B. Muthan, C. Benning, Freezing tolerance in plants requires lipid remodeling at the outer chloroplast membrane, *Science* 330 (2010) 226–228.
- [88] M.T.Y. Uemura, C. Nakagawara, S. Shigematsu, A. Minami, Y. Kawamura, et al., *Physiol Plant* 126 (2005) 81–89.
- [89] M.F. Thomashow, Plant cold acclimation: Freezing tolerance genes and regulatory mechanisms, *Annu Rev Plant Physiol Plant Mol Biol* 50 (1999) 571–599.
- [90] A. Martiniere, M. Shvedunova, A.J. Thomson, N.H. Evans, S. Penfield, J. Runions, et al., Homeostasis of plasma membrane viscosity in fluctuating temperatures, *New Phytol* 192 (2011) 328–337.
- [91] W.J. Van Blitterswijk, R.P. Van Hoven, P. Emmelot, On the lipid fluidity of malignant lymphoid cell membranes, *Cancer Res* 41 (1981) 3670–3671.
- [92] P. Gerbeau-Pissot, C. Der, D. Thomas, I.A. Anca, K. Grosjean, Y. Roche, et al., Modification of plasma membrane organization in tobacco cells elicited by cryptogein, *Plant Physiol* 164 (2014) 273–286.
- [93] Y. Roche, P. Gerbeau-Pissot, B. Buhot, D. Thomas, L. Bonneau, J. Gresti, et al., Depletion of phytosterols from the plant plasma membrane provides evidence for disruption of lipid rafts, *FASEB J* 22 (2008) 3980–3991.
- [94] Y. Roche, A.S. Klymchenko, P. Gerbeau-Pissot, P. Gervais, Y. Mely, F. Simon-Plas, et al., Behavior of plant plasma membranes under hydrostatic pressure as monitored by fluorescent environment-sensitive probes, *Biochim Biophys Acta* 2010 (1798) 1601–1607.
- [95] M. Shaghghi, M.T. Chen, Y.W. Hsueh, M.J. Zuckermann, J.L. Thewalt, Effect of sterol structure on the physical properties of 1-palmitoyl-2-oleoyl-sn-glycero-3-phosphocholine membranes determined using  $(^2\text{H})$  nuclear magnetic resonance, *Langmuir* 32 (2016) 7654–7663.
- [96] O.G. Mouritsen, L.A. Bagatolli, L. Duelund, O. Garvik, J.H. Ipsen, A.C. Simonsen, Effects of seaweed sterols fucosterol and desmosterol on lipid membranes, *Chem Phys Lipids* 205 (2017) 1–10.
- [97] K.R. Bruckdorfer, R.A. Demel, J. De Gier, L.L. van Deenen, The effect of partial replacements of membrane cholesterol by other steroids on the osmotic fragility and glycerol permeability of erythrocytes, *Biochim Biophys Acta* 183 (1969) 334–345.
- [98] P.A. Edwards, C. Green, Incorporation of plant sterols into membranes and its relation to sterol absorption, *FEBS Lett* 20 (1972) 97–99.
- [99] K. Grosjean, S. Mongrand, L. Beney, F. Simon-Plas, P. Gerbeau-Pissot, Differential effect of plant lipids on membrane organization: specificities of phytosphingolipids and phytosterols, *J Biol Chem* 290 (2015) 5810–5825.
- [100] K.K. Halling, J.P. Slotte, Membrane properties of plant sterols in phospholipid bilayers as determined by differential scanning calorimetry, resonance energy transfer and detergent-induced solubilization, *Biochim Biophys Acta* 2004 (1664) 161–171.
- [101] I. Haralampiev, H.A. Scheidt, D. Huster, P. Muller, The potential of alpha-spi-nasterol to mimic the membrane properties of natural cholesterol, *Molecules* 22 (2017).
- [102] A. Hodzic, M. Rappolt, H. Amenitsch, P. Lagner, G. Pabst, Differential modulation of membrane structure and fluctuations by plant sterols and cholesterol, *Biophys J* 94 (2008) 3935–3944.
- [103] K. Hac-Wydro, P. Wydro, P. Dynarowicz-Latka, M. Paluch, Cholesterol and phytosterols effect on sphingomyelin/phosphatidylcholine model membranes—thermodynamic analysis of the interactions in ternary monolayers, *J Colloid Interface Sci* 329 (2009) 265–272.
- [104] D.A. Mannock, M.G. Benesch, R.N. Lewis, R.N. McElhaney, A comparative calorimetric and spectroscopic study of the effects of cholesterol and of the plant sterols beta-sitosterol and stigmasterol on the thermotropic phase behavior and organization of dipalmitoylphosphatidylcholine bilayer membranes, *Biochim Biophys Acta* 2015 (1848) 1629–1638.
- [105] C.W. Bernsdorff, R., Differential properties of the sterols cholesterol, ergosterol,  $\beta$ -sitosterol, trans-7-dehydrocholesterol, stigmasterol and lanosterol on DPPC bilayer order, *J Phys Chem B* 107 (2003) 10658–10664.
- [106] X. Zhuang, A. Ou, J.B. Klauda, Simulations of simple linoleic acid-containing lipid membranes and models for the soybean plasma membranes, *J Chem Phys* 146 (2017) 215103.
- [107] F. Sena, M. Sotelo-Silveira, S. Astrada, M.A. Botella, L. Malacrida, O. Borsani, Spectral phasor analysis reveals altered membrane order and function of root hair cells in *Arabidopsis thaliana* dry2/sqe1-5 drought hypersensitive mutant, *Plant Physiol Biochem* 119 (2017) 224–231.
- [108] J.B. Mudd, T.T. McManus, Effect of steryl glycosides on the phase transition of dipalmitoyl lecithin, *Plant Physiol* 65 (1980) 78–80.
- [109] K. Grosjean, S. Mongrand, L. Beney, F. Simon-Plas, P. Gerbeau-Pissot, Differential effect of plant lipids on membrane organization: hot features and specificities of phytosphingolipids and phytosterols, *J Biol Chem* 290 (2015) 5810–5825.
- [110] K. Hac-Wydro, M. Flasiński, M. Broniatowski, P. Dynarowicz-Latka, J. Majewski, Properties of beta-sitosterol/DPPC monolayers studied with grazing incidence X-ray diffraction (GIXD) and brewster angle microscopy, *J Colloid Interface Sci* 364 (2011) 133–139.
- [111] K. Hac-Wydro, R. Lenartowicz, P. Dynarowicz-Latka, The influence of plant stanol (beta-sitosterol) on inner leaflet of human erythrocytes membrane modeled with the Langmuir monolayer technique, *Colloids Surf B Biointerfaces* 102 (2013) 178–188.
- [112] R. Sandor, C. Der, K. Grosjean, I. Anca, E. Noiro, N. Leborgne-Castel, et al., Plasma membrane order and fluidity are diversely triggered by elicitors of plant defence, *J Exp Bot* 67 (2016) 5173–5185.
- [113] M. Lonnfors, J.P. Doux, J.A. Killian, T.K. Nyholm, J.P. Slotte, Sterols have higher affinity for sphingomyelin than for phosphatidylcholine bilayers even at equal acyl-chain order, *Biophys J* 100 (2011) 2633–2641.
- [114] E. Sezgin, I. Levental, S. Mayor, C. Eggeling, The mystery of membrane organization: composition, regulation and roles of lipid rafts, *Nat Rev Mol Cell Biol* 18 (2017) 361–374.
- [115] J.T. Marques, A.M. Cordeiro, A.S. Viana, A. Herrmann, H.S. Marinho, R.F. de Almeida, Formation and properties of membrane-ordered domains by phytoceramide: Role of sphingoid base hydroxylation, *Langmuir* 31 (2015) 9410–9421.
- [116] M.P. Platre, Y. Jaillais, Anionic lipids and the maintenance of membrane electrostatics in eukaryotes, *Plant Signal Behav* 12 (2017) e1282022.
- [117] M.L. Simon, M.P. Platre, M.M. Marques-Bueno, L. Armentog, T. Stanislas, V. Bayle, et al., A PtdIns(4)P-driven electrostatic field controls cell membrane identity and signalling in plants, *Nat Plants* 2 (2016) 16089.
- [118] M.P. Platre, L.C. Noack, M. Doumane, V. Bayle, M.L.A. Simon, L. Maneta-Peyret, et al., A combinatorial lipid code shapes the electrostatic landscape of plant endomembranes, *Dev Cell* 45 (2018) 465–480 [e11].
- [119] A. Martiniere, R. Gibrat, H. Sentenac, X. Dumont, I. Gaillard, N. Paris, Uncovering pH at both sides of the root plasma membrane interface using noninvasive imaging, *Proc Natl Acad Sci U S A* 115 (25) (2018) 6488–6493.
- [120] A. Zachowicz, Phospholipids in animal eukaryotic membranes: transverse asymmetry and movement, *Biochem J* 294 (Pt 1) (1993) 1–14.
- [121] M. Murate, T. Kobayashi, Transmembrane asymmetry and lateral domains in biological membranes, *Chem Phys Lipids* 194 (2016) 58–71.
- [122] J.D. Nickels, J.C. Smith, X. Cheng, Lateral organization, bilayer asymmetry, and inter-leaflet coupling of biological membranes, *Chem Phys Lipids* 192 (2015) 87–89.
- [123] M. Murate, T. Kobayashi, Revisiting transbilayer distribution of lipids in the plasma membrane, *Chem Phys Lipids* 194 (2016) 58–71.
- [124] J.H. Ipsen, O.G. Mouritsen, M.J. Zuckermann, Theory of thermal anomalies in the specific heat of lipid bilayers containing cholesterol, *Biophys J* 56 (1989) 661–667.
- [125] O.G. Mouritsen, Theoretical models of phospholipid phase transitions, *Chem Phys Lipids* 57 (1991) 179–194.
- [126] S.L. Veatch, S.L. Keller, Separation of liquid phases in giant vesicles of ternary mixtures of phospholipids and cholesterol, *Biophys J* 85 (2003) 3074–3083.
- [127] P.F. Almeida, Thermodynamics of lipid interactions in complex bilayers, *Biochim Biophys Acta* 2009 (1788) 72–85.
- [128] E. London, How principles of domain formation in model membranes may explain ambiguities concerning lipid raft formation in cells, *Biochim Biophys Acta* 2005 (1746) 203–220.
- [129] J.G. Beck, D. Mathieu, C. Loudet, S. Buchoux, E.J. Dufourc, Plant sterols in "rafts": a better way to regulate membrane thermal shocks, *FASEB J* 21 (2007) 1714–1723.
- [130] E.J. Dufourc, Sterols and membrane dynamics, *J Chem Biol* 1 (2008) 63–77.
- [131] A.S. Klymchenko, R. Kreder, Fluorescent probes for lipid rafts: from model membranes to living cells, *Chem Biol* 21 (2014) 97–113.
- [132] N. Komura, K.G. Suzuki, H. Ando, M. Konishi, M. Koikeda, A. Imamura, et al., Raft-based interactions of gangliosides with a GPI-anchored receptor, *Nat Chem Biol* 12 (2016) 402–410.
- [133] M. Fidorra, A. Garcia, J.H. Ipsen, S. Hartel, L.A. Bagatolli, Lipid domains in giant unilamellar vesicles and their correspondence with equilibrium thermodynamic phases: a quantitative fluorescence microscopy approach, *Biochim Biophys Acta* 2009 (1788) 2142–2149.
- [134] R.D. Klausner, D.E. Wolf, Selectivity of fluorescent lipid analogues for lipid domains, *Biochemistry* 19 (1980) 6199–6203.
- [135] R.M. Mesquita, E. Melo, T.E. Thompson, W.L. Vaz, Partitioning of amphiphiles between coexisting ordered and disordered phases in two-phase lipid bilayer membranes, *Biophys J* 78 (2000) 3019–3025.
- [136] T. Baumgart, G. Hunt, E.R. Farkas, W.W. Webb, G.W. Feigenson, Fluorescence probe partitioning between Lo/Ld phases in lipid membranes, *Biochim Biophys Acta* 2007 (1768) 2182–2194.
- [137] H.I. Ingolfsson, M.N. Melo, F.J. van Eerden, C. Arnarez, C.A. Lopez, T.A. Wassenaar, et al., Lipid organization of the plasma membrane, *J Am Chem Soc* 136 (2014) 14554–14559.
- [138] D.A. Brown, J.K. Rose, Sorting of GPI-anchored proteins to glycolipid-enriched membrane subdomains during transport to the apical cell surface, *Cell* 68 (1992) 533–544.
- [139] E. London, D.A. Brown, Insolubility of lipids in triton X-100: physical origin and relationship to sphingolipid/cholesterol membrane domains (rafts), *Biochim Biophys Acta* 1508 (2000) 182–195.
- [140] R. Schroeder, E. London, D. Brown, Interactions between saturated acyl chains confer detergent resistance on lipids and liposomes/phosphatidylinositol (GPI)-anchored proteins: GPI-anchored proteins in glycosomes and cells show similar behavior, *Proc Natl Acad Sci U S A* 91 (1994) 12130–12134.
- [141] A.E. Garner, D.A. Smith, N.M. Hooper, Visualization of detergent solubilization of membranes: implications for the isolation of rafts, *Biophys J* 94 (2008) 1326–1340.
- [142] H.A. Rinia, B. de Kruijff, Imaging domains in model membranes with atomic force microscopy, *FEBS Lett* 504 (2001) 194–199.
- [143] K. El Kirat, S. Morandat, Cholesterol modulation of membrane resistance to Triton

- X-100 explored by atomic force microscopy, *Biochim Biophys Acta* 2007 (1768) 2300–2309.
- [144] S. Morandat, K. El Kirat, Membrane resistance to Triton X-100 explored by real-time atomic force microscopy, *Langmuir* 22 (2006) 5786–5791.
- [145] S. Keller, A. Tsamaloukas, H. Heerklotz, A quantitative model describing the selective solubilization of membrane domains, *J Am Chem Soc* 127 (2005) 11469–11476.
- [146] H. Ahyayauch, M.I. Collado, F.M. Goni, D. Lichtenberg, Cholesterol reverts Triton X-100 preferential solubilization of sphingomyelin over phosphatidylcholine: a <sup>31</sup>P-NMR study, *FEBS Lett* 583 (2009) 2859–2864.
- [147] G. Staneva, M. Seigneuret, K. Koumanov, G. Trugnan, M.I. Angelova, Detergents induce raft-like domains budding and fission from giant unilamellar heterogeneous vesicles: a direct microscopy observation, *Chem Phys Lipids* 136 (2005) 55–66.
- [148] J. Sot, L.A. Bagatolli, F.M. Goni, A. Alonso, Detergent-resistant, ceramide-enriched domains in sphingomyelin/ceramide bilayers, *Biophys J* 90 (2006) 903–914.
- [149] E.B. Babychuk, A. Draeger, Biochemical characterization of detergent-resistant membranes: a systematic approach, *Biochem J* 397 (2006) 407–416.
- [150] D. Lingwood, K. Simons, Detergent resistance as a tool in membrane research, *Nat Protoc* 2 (2007) 2159–2165.
- [151] A. Rietveld, K. Simons, The differential miscibility of lipids as the basis for the formation of functional membrane rafts, *Biochim Biophys Acta* 1376 (1998) 467–479.
- [152] U. Salzer, R. Prohaska, Stomatin, flotillin-1, and flotillin-2 are major integral proteins of erythrocyte lipid rafts, *Blood* 97 (2001) 1141–1143.
- [153] L.J. Pike, X. Han, K.N. Chung, R.W. Gross, Lipid rafts are enriched in arachidonic acid and plasmenylethanolamine and their composition is independent of caveolin-1 expression: a quantitative electrospray ionization/mass spectrometric analysis, *Biochemistry* 41 (2002) 2075–2088.
- [154] S. Schuck, M. Honsho, K. Ekroos, A. Shevchenko, K. Simons, Resistance of cell membranes to different detergents, *Proc Natl Acad Sci U S A* 100 (2003) 5795–5800.
- [155] F. Pinaud, X. Michalet, G. Iyer, E. Margeat, H.P. Moore, S. Weiss, Dynamic partitioning of a glycosyl-phosphatidylinositol-anchored protein in glycosphingolipid-rich microdomains imaged by single-quantum dot tracking, *Traffic* 10 (2009) 691–712.
- [156] L.J. Foster, Q.W. Chan, Lipid raft proteomics: more than just detergent-resistant membranes, *Subcell Biochem* 43 (2007) 35–47.
- [157] A.G. Ayuyan, F.S. Cohen, Raft composition at physiological temperature and pH in the absence of detergents, *Biophys J* 94 (2008) 2654–2666.
- [158] D.A. Persaud-Sawin, S. Lightcap, G.J. Harry, Isolation of rafts from mouse brain tissue by a detergent-free method, *J Lipid Res* 50 (2009) 759–767.
- [159] S.C. Lee, T.J. Knowles, V.L. Postis, M. Jamshad, R.A. Parslow, Y.P. Lin, et al., A method for detergent-free isolation of membrane proteins in their local lipid environment, *Nat Protoc* 11 (2016) 1149–1162.
- [160] T. Peskan, M. Westermann, R. Oelmüller, Identification of low-density Triton X-100-insoluble plasma membrane microdomains in higher plants, *Eur J Biochem/FEBS* 267 (2000) 6989–6995.
- [161] G.H. Borner, D.J. Sherrier, T. Weimar, L.V. Michaelson, N.D. Hawkins, A. Macaskill, et al., Analysis of detergent-resistant membranes in Arabidopsis. Evidence for plasma membrane lipid rafts, *Plant Physiol* 137 (2005) 104–116.
- [162] M. Laloi, A.M. Perret, L. Chatre, S. Melsler, C. Cantrel, M.N. Vaultier, et al., Insights into the role of specific lipids in the formation and delivery of lipid microdomains to the plasma membrane of plant cells, *Plant Physiol* 143 (2007) 461–472.
- [163] S. Kierszniowska, B. Seiwert, W.X. Schulze, Definition of Arabidopsis sterol-rich membrane microdomains by differential treatment with methyl-beta-cyclodextrin and quantitative proteomics, *Mol Cell Proteomics* 8 (2009) 612–623.
- [164] N.F. Keinath, S. Kierszniowska, J. Lorek, G. Bourdais, S.A. Kessler, H. Shimosato-Asano, et al., PAMP (pathogen-associated molecular pattern)-induced changes in plasma membrane compartmentalization reveal novel components of plant immunity, *J Biol Chem* 285 (2010) 39140–39149.
- [165] H. Zaubner, W. Szymanski, W.X. Schulze, Unraveling sterol-dependent membrane phenotypes by analysis of protein abundance-ratio distributions in different membrane fractions under biochemical and endogenous sterol depletion, *Mol Cell Proteomics* 12 (2013) 3732–3743.
- [166] B. Lefebvre, F. Furt, M.A. Hartmann, L.V. Michaelson, J.P. Carde, F. Sargueil-Boiron, et al., Characterization of lipid rafts from *Medicago truncatula* root plasma membranes: a proteomic study reveals the presence of a raft-associated redox system, *Plant Physiol* 144 (2007) 402–418.
- [167] C. Guillier, J.L. Cacas, G. Recorbet, N. Depretre, A. Mounier, S. Mongrand, et al., Direct purification of detergent-insoluble membranes from *Medicago truncatula* root microsomes: comparison between floatation and sedimentation, *BMC Plant Biol* 14 (2014) 255.
- [168] M. Fujiwara, S. Hamada, M. Hiratsuka, Y. Fukao, T. Kawasaki, K. Shimamoto, Proteome analysis of detergent-resistant membranes (DRMs) associated with OsRac1-mediated innate immunity in rice, *Plant Cell Physiol* 50 (2009) 1191–1200.
- [169] D. Takahashi, Y. Kawamura, M. Uemura, Detergent-resistant plasma membrane proteome to elucidate microdomain functions in plant cells, *Front Plant Sci* 4 (2013) 27.
- [170] E. Gutierrez-Carbonell, D. Takahashi, S. Luthje, J.A. Gonzalez-Reyes, S. Mongrand, B. Contreras-Moreira, et al., A shotgun proteomic approach reveals that fe deficiency causes marked changes in the protein profiles of plasma membrane and detergent-resistant microdomain preparations from *Beta vulgaris* roots, *J Proteome Res* (15) (2016) 2510–2524.
- [171] T. Stanislas, D. Bouyssié, M. Rossignol, S. Vesa, J. Fromentin, J. Morel, et al., Quantitative proteomics reveals a dynamic association of proteins to detergent-resistant membranes upon elicitor signaling in tobacco, *Mol Cell Proteomics* 8 (2009) 2186–2198.
- [172] J. Morel, S. Claverol, S. Mongrand, F. Furt, J. Fromentin, J.J. Bessoule, et al., Proteomics of plant detergent-resistant membranes, *Mol Cell Proteomics* 5 (2006) 1396–1411.
- [173] A. Minami, M. Fujiwara, A. Furuto, Y. Fukao, T. Yamashita, M. Kamo, et al., Alterations in detergent-resistant plasma membrane microdomains in Arabidopsis thaliana during cold acclimation, *Plant Cell Physiol* 50 (2009) 341–359.
- [174] S. König, M. Hoffmann, A. Mosblech, I. Heilmann, Determination of content and fatty acid composition of unlabeled phosphoinositide species by thin-layer chromatography and gas chromatography, *Anal Biochem* 378 (2008) 197–201.
- [175] J. Gronnier, J.M. Crowet, B. Habenstein, M.N. Nasir, V. Bayle, E. Hosity, et al., Structural basis for plant plasma membrane protein dynamics and organization into functional nanodomains, *Elife* 6 (2017).
- [176] L. Carmona-Salazar, M. El Hafidi, N. Gutierrez-Najera, L. Noyola-Martinez, A. Gonzalez-Solis, M. Gavilanes-Ruiz, Fatty acid profiles from the plasma membrane and detergent resistant membranes of two plant species, *Phytochemistry* 109 (2015) 25–35.
- [177] L. Carmona-Salazar, M. El Hafidi, C. Enriquez-Arredondo, C. Vazquez-Vazquez, Gonzalez de la Vara LE, M. Gavilanes-Ruiz, Isolation of detergent-resistant membranes from plant photosynthetic and non-photosynthetic tissues, *Anal Biochem* 417 (2011) 220–227.
- [178] R. Zidovetzki, I. Levitan, Use of cyclodextrins to manipulate plasma membrane cholesterol content: evidence, misconceptions and control strategies, *Biochim Biophys Acta* 2007 (1768) 1311–1324.
- [179] P.G. Nyholm, I. Pascher, S. Sundell, The effect of hydrogen bonds on the conformation of glycosphingolipids. Methylated and unmethylated cerebrosides studied by X-ray single crystal analysis and model calculations, *Chem Phys Lipids* 52 (1990) 1–10.
- [180] H. Lofgren, I. Pascher, Molecular arrangements of sphingolipids. The monolayer behaviour of ceramides, *Chem Phys Lipids* 20 (1977) 273–284.
- [181] P. Sperling, S. Franke, S. Luthje, E. Heinz, Are glucocerebrosides the predominant sphingolipids in plant plasma membranes? *Plant Physiol Biochem* 43 (2005) 1031–1038.
- [182] A. Moscatelli, A. Gagliardi, L. Maneta-Peyret, L. Bini, N. Stroppa, E. Onelli, et al., Characterisation of detergent-insoluble membranes in pollen tubes of *Nicotiana tabacum* (L.), *Biol Open* 4 (2015) 378–399.
- [183] D. Lingwood, K. Simons, Lipid rafts as a membrane-organizing principle, *Science* 327 (2010) 46–50.
- [184] D. Lichtenberg, F.M. Goni, H. Heerklotz, Detergent-resistant membranes should not be identified with membrane rafts, *Trends Biochem Sci* 30 (2005) 430–436.
- [185] J. Malinsky, M. Opekarova, G. Grossmann, W. Tanner, Membrane microdomains, rafts, and detergent-resistant membranes in plants and fungi, *Annu Rev Plant Biol* 64 (2013) 501–529.
- [186] S. Munro, Lipid rafts: elusive or illusive? *Cell* 115 (2003) 377–388.
- [187] W. Tanner, J. Malinsky, M. Opekarova, In plant and animal cells, detergent-resistant membranes do not define functional membrane rafts, *Plant Cell* 23 (2011) 1191–1193.
- [188] E. Noiro, C. Der, J. Lherminier, F. Robert, P. Moricova, K. Kieu, et al., Dynamic changes in the subcellular distribution of the tobacco ROS-producing enzyme RBOHD in response to the oomycete elicitor cryptogin, *J Exp Bot* 65 (2014) 5011–5022.
- [189] J. Lherminier, T. Elmayer, J. Fromentin, K.T. Elaraqui, S. Vesa, J. Morel, et al., NADPH oxidase-mediated reactive oxygen species production: Subcellular localization and reassessment of its role in plant defense, *Mol Plant Microbe Interact* 22 (2009) 868–881.
- [190] C.A. Bucherl, I.K. Jarsch, C. Schudoma, C. Segonzac, M. Mbengue, S. Robatzek, et al., Plant immune and growth receptors share common signalling components but localise to distinct plasma membrane nanodomains, *Elife* 6 (2017).
- [191] S. Raffaele, E. Bayer, D. Lafarge, S. Cluzet, S. German Retana, T. Boubekour, et al., Remorin, a solanaceae protein resident in membrane rafts and plasmodesmata, impairs potato virus X movement, *Plant Cell* 21 (2009) 1541–1555.
- [192] F. Demir, C. Horntrich, J.O. Blachutzyk, S. Scherzer, Y. Reinders, S. Kierszniowska, et al., Arabidopsis nanodomain-delimited ABA signaling pathway regulates the anion channel SLAH3, *Proc Natl Acad Sci U S A* 110 (2013) 8296–8301.
- [193] I.K. Jarsch, S.S. Konrad, T.F. Stratil, S.L. Urbanus, W. Szymanski, P. Braun, et al., Plasma membranes are subcompartmentalized into a plethora of coexisting and diverse microdomains in Arabidopsis and *Nicotiana benthamiana*, *Plant Cell* 26 (2014) 1698–1711.
- [194] K. Simons, M.J. Gerl, Revitalizing membrane rafts: new tools and insights, *Nat Rev Mol Cell Biol* 11 (2010) 688–699.
- [195] T. Ott, Membrane nanodomains and microdomains in plant-microbe interactions, *Curr Opin Plant Biol* 40 (2017) 82–88.
- [196] M. Nakamura, M. Grebe, Outer, inner and planar polarity in the Arabidopsis root, *Curr Opin Plant Biol* 41 (2018) 46–53.
- [197] C. Faulkner, A cellular backline: specialization of host membranes for defence, *J Exp Bot* 66 (2015) 1565–1571.
- [198] L. Galweiler, C. Guan, A. Muller, E. Wisman, K. Mendgen, A. Yephremov, et al., Regulation of polar auxin transport by AtPIN1 in Arabidopsis vascular tissue, *Science* 282 (1998) 2226–2230.
- [199] N. Geldner, Casparian strips, *Current Biol* 23 (2013) R1025–R1026.
- [200] L.C. Noack, Y. Jaillais, Precision targeting by phosphoinositides: How PIs direct endomembrane trafficking in plants, *Curr Opin Plant Biol* 40 (2017) 22–33.
- [201] T. Ischebeck, S. Seiler, I. Heilmann, At the poles across kingdoms: phosphoinositides and polar tip growth, *Protoplasma* 240 (2010) 13–31.

- [202] L. Kalmbach, K. Hematy, D. De Bellis, M. Barberon, S. Fujita, R. Ursache, et al., Transient cell-specific EXO70A1 activity in the CASP domain and Casparian strip localization, *Nat Plants* 3 (2017) 17058.
- [203] J. Tilsner, W. Nicolas, A. Rosado, E.M. Bayer, Staying tight: Plasmodesmal membrane contact sites and the control of cell-to-cell connectivity in plants, *Annu Rev Plant Biol* 67 (2016) 337–364.
- [204] C.L. Thomas, E.M. Bayer, C. Ritzenthaler, L. Fernandez-Calvino, A.J. Maule, Specific targeting of a plasmodesmal protein affecting cell-to-cell communication, *PLoS Biol* 6 (2008) e7.
- [205] C. Simpson, C. Thomas, K. Findlay, E. Bayer, A.J. Maule, An Arabidopsis GPI-anchor plasmodesmal neck protein with callose binding activity and potential to regulate cell-to-cell trafficking, *Plant Cell* 21 (2009) 581–594.
- [206] M. Frescatada-Rosa, T. Stanislas, S.K. Backues, I. Reichardt, S. Men, Y. Boutte, et al., High lipid order of Arabidopsis cell-plate membranes mediated by sterol and DYNAMIN-RELATED PROTEIN1A function, *Plant J* 80 (2014) 745–757.
- [207] J. Kleine-Vehn, K. Wabnick, A. Martiniere, L. Langowski, K. Willig, S. Naramoto, et al., Recycling, clustering, and endocytosis jointly maintain PIN auxin carrier polarity at the plasma membrane, *Mol Syst Biol* 7 (2011) 540.
- [208] E. Rodriguez-Boulan, G. Kreitzer, A. Musch, Organization of vesicular trafficking in epithelia, *Nat Rev Mol Cell Biol* 6 (2005) 233–247.
- [209] D.T. Burnette, P. Sengupta, Y. Dai, J. Lippincott-Schwartz, B. Kachar, Bleaching/blinking assisted localization microscopy for superresolution imaging using standard fluorescent molecules, *Proc Natl Acad Sci U S A* 108 (2011) 21081–21086.
- [210] A. Kusumi, T.A. Tsunoyama, K.M. Hirose, R.S. Kasai, T.K. Fujiwara, Tracking single molecule at work in living cells, *Nat Chem Biol* 10 (2014) 524–532.
- [211] N.M. Curthoys, M. Parent, M. Mlodzianowski, A.J. Nelson, J. Lilieholm, M.B. Butler, et al., Dances with membranes: Breakthroughs from super-resolution imaging, *Curr Top Membr* 75 (2015) 59–123.
- [212] X. Lv, Y. Jing, J. Xiao, Y. Zhang, Y. Zhu, R. Julian, et al., Membrane microdomains and the cytoskeleton constrain AtHIR1 dynamics and facilitate the formation of an AtHIR1-associated immune complex, *Plant J* Vol. 90 (2017) 3–16.
- [213] A. Yoshinari, M. Fujimoto, T. Ueda, N. Inada, S. Naito, J. Takano, DRP1-dependent endocytosis is essential for polar localization and boron-induced degradation of the borate transporter BOR1 in Arabidopsis thaliana, *Plant Cell Physiol* 57 (2016) 1985–2000.
- [214] R. Gutierrez, J.J. Lindeboom, A.R. Paredes, A.M. Emons, D.W. Ehrhardt, Arabidopsis cortical microtubules position cellulose synthase delivery to the plasma membrane and interact with cellulose synthase trafficking compartments, *Nat Cell Biol* 11 (2009) 797–806.
- [215] K. Burstenbinder, B. Moller, R. Plotner, G. Stamm, G. Hause, D. Mitra, et al., The IQD family of calmodulin-binding proteins links calcium signaling to microtubules, membrane subdomains, and the nucleus, *Plant Physiol* 173 (2017) 1692–1708.
- [216] S.J. Hutten, D.S. Hamers, M. Aan den Toorn, W. van Esse, A. Nolles, C.A. Bucherl, et al., Visualization of BR1 and SERK3/BAK1 nanoclusters in Arabidopsis roots, *PLoS One* 12 (2017) e0169905.
- [217] R. Li, P. Liu, Y. Wan, T. Chen, Q. Wang, U. Metzbach, et al., A membrane microdomain-associated protein, Arabidopsis Flot1, is involved in a clathrin-independent endocytic pathway and is required for seedling development, *Plant Cell* 24 (2012) 2105–2122.
- [218] H. Hao, L. Fan, T. Chen, R. Li, X. Li, Q. He, et al., Clathrin and membrane microdomains cooperatively regulate RbohD dynamics and activity in Arabidopsis, *Plant Cell* 26 (2014) 1729–1745.
- [219] J.G.-P.P. Gronnier, V. Germain, S. Mongrand, F. Simon-Plas, Divide and rule: plant plasma membrane organization, *Trends Plant Sci* 23 (10) (2018) 899–917.
- [220] A. Pertsinidis, Y. Zhang, S. Chu, Subnanometre single-molecule localization, registration and distance measurements, *Nature* 466 (2010) 647–651.
- [221] F. Balzarotti, Y. Eilers, K.C. Gwosch, A.H. Gynna, V. Westphal, F.D. Stefani, et al., Nanometer resolution imaging and tracking of fluorescent molecules with minimal photon fluxes, *Science* 355 (2017) 606–612.
- [222] Y. Golan, E. Sherman, Resolving mixed mechanisms of protein subdiffusion at the T cell plasma membrane, *Nat Commun* 8 (2017) 15851.
- [223] F. Persson, M. Linden, C. Unoson, J. Elf, Extracting intracellular diffusive states and transition rates from single-molecule tracking data, *Nat Methods* 10 (2013) 265–269.
- [224] J. Sekeres, P. Pejchar, J. Santrucke, N. Vukasinovic, V. Zarsky, M. Potocky, Analysis of exocyst subunit EXO70 family reveals distinct membrane polar domains in tobacco pollen tubes, *Plant Physiol* 173 (2017) 1659–1675.
- [225] S.S. Konrad, C. Popp, T.F. Stratil, I.K. Jarsch, V. Thallmair, J. Folgmann, et al., S-acylation anchors remorin proteins to the plasma membrane but does not primarily determine their localization in membrane microdomains, *New Phytol* 203 (2014) 758–769.
- [226] B. Sorre, A. Callan-Jones, J.B. Manneville, P. Nassoy, J.F. Joanny, J. Prost, et al., Curvature-driven lipid sorting needs proximity to a demixing point and is aided by proteins, *Proc Natl Acad Sci U S A* 106 (2009) 5622–5626.
- [227] S.N. Pinto, E.L. Laviad, J. Stiban, S.L. Kelly, A.H. Merrill Jr., M. Prieto, et al., Changes in membrane biophysical properties induced by sphingomyelinase depend on the sphingolipid N-acyl chain, *J Lipid Res* 55 (2014) 53–61.
- [228] G.H. Patterson, K. Hirschberg, R.S. Polishchuk, D. Gerlich, R.D. Phair, J. Lippincott-Schwartz, Transport through the Golgi apparatus by rapid partitioning within a two-phase membrane system, *Cell* 133 (2008) 1055–1067.
- [229] J.M. Duran, F. Campelo, J. van Galen, T. Sachsenheimer, J. Sot, M.V. Egorov, et al., Sphingomyelin organization is required for vesicle biogenesis at the Golgi complex, *EMBO J* 31 (2012) 4535–4546.
- [230] F. Campelo, J. van Galen, G. Turacchio, S. Parashuraman, M.M. Kozlov, M.F. Garcia-Parajo, et al., Sphingomyelin metabolism controls the shape and function of the Golgi cisternae, *Elife* 6 (2017).
- [231] S. Melsner, B. Batailler, M. Peyplut, C. Poulou, Y. Bellec, V. Watelet-Boyer, et al., Glucosylceramide biosynthesis is involved in Golgi morphology and protein secretion in plant cells, *Traffic* 11 (2010) 479–490.
- [232] R.W. Klemm, C.S. Ejsing, M.A. Surma, H.J. Kaiser, M.J. Gerl, J.L. Sampaio, et al., Segregation of sphingolipids and sterols during formation of secretory vesicles at the trans-Golgi network, *J Cell Biol* 185 (2009) 601–612.
- [233] Y. Deng, F.E. Rivera-Molina, D.K. Toomre, C.G. Burd, Sphingomyelin is sorted at the trans Golgi network into a distinct class of secretory vesicle, *Proc Natl Acad Sci U S A* 113 (2016) 6677–6682.
- [234] Y. Boutte, M. Frescatada-Rosa, S. Men, C.M. Chow, K. Ebine, A. Gustavsson, et al., Endocytosis restricts Arabidopsis KNOLLE syntaxin to the cell division plane during late cytokinesis, *EMBO J* 29 (2010) 546–558.
- [235] V. Watelet-Boyer, L. Brocard, K. Jonsson, N. Esnay, J. Joubes, F. Domergue, et al., Enrichment of hydroxylated C24- and C26-acyl-chain sphingolipids mediates PIN2 apical sorting at trans-Golgi network subdomains, *Nat Commun* 7 (2016) 12788.
- [236] Y.Q. Gao, J.G. Chen, Z.R. Chen, D. An, Q.Y. Lv, M.L. Han, et al., A new vesicle trafficking regulator CTL1 plays a crucial role in ion homeostasis, *PLoS Biol* 15 (2017) e2002978.
- [237] A. Siddhanta, D. Shields, Secretory vesicle budding from the trans-Golgi network is mediated by phosphatidic acid levels, *J Biol Chem* 273 (1998) 17995–17998.
- [238] H.M. Hankins, Y.Y. Sere, N.S. Diab, A.K. Menon, T.R. Graham, Phosphatidylserine translocation at the yeast trans-Golgi network regulates protein sorting into exocytic vesicles, *Mol Biol Cell* 26 (2015) 4674–4685.
- [239] B. Mesmin, J. Bigay, J. Polidori, D. Jameca, S. Lacas-Gervais, B. Antony, Sterol transfer, PI4P consumption, and control of membrane lipid order by endogenous OSBP, *EMBO J* 36 (2017) 3156–3174.
- [240] D. Gendre, K. Jonsson, Y. Boutte, R.P. Bhalerao, Journey to the cell surface—the central role of the trans-Golgi network in plants, *Protoplasma* 252 (2015) 385–398.
- [241] M.R. Rosquete, D.J. Davis, G. Drakakaki, The plant trans-golgi network: not just a matter of distinction, *Plant Physiol* 176 (2018) 187–198.
- [242] C. Viotti, J. Bubeck, Y.D. Stierhof, M. Krebs, M. Langhans, W. van den Berg, et al., Endocytic and secretory traffic in Arabidopsis merge in the trans-Golgi network/early endosome, an independent and highly dynamic organelle, *Plant Cell* 22 (2010) 1344–1357.
- [243] T. Uemura, Y. Suda, T. Ueda, A. Nakano, Dynamic behavior of the trans-golgi network in root tissues of Arabidopsis revealed by super-resolution live imaging, *Plant Cell Physiol* 55 (2014) 694–703.
- [244] J. Dettmer, A. Hong-Hermesdorf, Y.D. Stierhof, K. Schumacher, Vacuolar H<sup>+</sup>-ATPase activity is required for endocytic and secretory trafficking in Arabidopsis, *Plant Cell* 18 (2006) 715–730.
- [245] K. Grosjean, C. Der, F. Robert, D. Thomas, S. Mongrand, F. Simon-Plas, et al., Interactions between lipids and proteins are critical for plasma membrane ordered domain organization in BY-2 cells, *J Exp Bot* 69 (15) (2018) 3545–3557.
- [246] A. Radhakrishnan, H.M. McConnell, Condensed complexes of cholesterol and phospholipids, *Biophys J* 77 (1999) 1507–1517.
- [247] P.J. Somerharju, J.A. Virtanen, K.K. Eklund, P. Vainio, P.K. Kinnunen, 1-Palmitoyl-2-pyrenedecanoyl glycerophospholipids as membrane probes: evidence for regular distribution in liquid-crystalline phosphatidylcholine bilayers, *Biochemistry* 24 (1985) 2773–2781.
- [248] J. Huang, Exploration of molecular interactions in cholesterol superlattices: Effect of multibody interactions, *Biophys J* 83 (2002) 1014–1025.
- [249] J. Huang, G.W. Feigenson, A microscopic interaction model of maximum solubility of cholesterol in lipid bilayers, *Biophys J* 76 (1999) 2142–2157.
- [250] P. Dhar, E. Eck, J.N. Israelachvili, D.W. Lee, Y. Min, A. Ramachandran, et al., Lipid-protein interactions alter line tensions and domain size distributions in lung surfactant monolayers, *Biophys J* 102 (2012) 56–65.
- [251] O.G. Mouritsen, M. Bloom, Mattress model of lipid-protein interactions in membranes, *Biophys J* 46 (1984) 141–153.
- [252] J.D. Nickels, J.C. Smith, X. Cheng, Lateral organization, bilayer asymmetry, and inter-leaflet coupling of biological membranes, *Chem Phys Lipids* 192 (2015) 87–99.
- [253] T. Fujimoto, I. Parmryd, Interleaflet coupling, pinning, and leaflet asymmetry-major players in plasma membrane nanodomain formation, *Front Cell Dev Biol* 4 (2016) 155.
- [254] E. Chiricozzi, M.G. Ciampa, G. Brasile, F. Compostella, A. Prinetti, H. Nakayama, et al., Direct interaction, instrumental for signaling processes, between LacCer and Lyn in the lipid rafts of neutrophil-like cells, *J Lipid Res* 56 (2015) 129–141.
- [255] R. Raghupathy, A.A. Anilkumar, A. Polley, P.P. Singh, M. Yadav, C. Johnson, et al., Transbilayer lipid interactions mediate nanocoupling of lipid-anchored proteins, *Cell* 161 (2015) 581–594.
- [256] M. Argos, M. Rahman, F. Parvez, J. Dignam, T. Islam, I. Quasem, et al., Baseline comorbidities in a skin cancer prevention trial in Bangladesh, *Eur J Clin Invest* 43 (2013) 579–588.
- [257] N. Yilmaz, T. Kobayashi, Assemblies of pore-forming toxins visualized by atomic force microscopy, *Biochim Biophys Acta* 1858 (2016) 500–511.
- [258] M. Lorizate, B. Brugger, H. Akiyama, B. Glass, B. Muller, G. Anderlueh, et al., Probing HIV-1 membrane liquid order by Laurdan staining reveals producer cell-dependent differences, *J Biol Chem* 284 (2009) 22238–22247.
- [259] B. Brugger, B. Glass, P. Haberkant, I. Leibrecht, F.T. Wieland, H.G. Krausslich, The HIV lipidome: a raft with an unusual composition, *Proc Natl Acad Sci U S A* 103 (2006) 2641–2646.
- [260] I.A. Prior, C. Muncke, R.G. Parton, J.F. Hancock, Direct visualization of Ras proteins in spatially distinct cell surface microdomains, *J Cell Biol* 160 (2003) 165–170.

- [261] Y. Zhou, P. Prakash, H. Liang, K.J. Cho, A.A. Gorfe, J.F. Hancock, Lipid-sorting specificity encoded in k-ras membrane anchor regulates signal output, *Cell* 168 (2017) 239–251 [e16].
- [262] Y. Zhou, C.O. Wong, K.J. Cho, D. van der Hoeven, H. Liang, D.P. Thakur, et al., Signal transduction. Membrane potential modulates plasma membrane phospholipid dynamics and K-Ras signaling, *Science* 349 (2015) 873–876.
- [263] J.D. Jones, J.L. Dangi, The plant immune system, *Nature* 444 (2006) 323–329.
- [264] A.M. Laxalt, T. Munnik, Phospholipid signalling in plant defence, *Curr Opin Plant Biol* 5 (2002) 332–338.
- [265] T. Munnik, J.E. Vermeer, Osmotic stress-induced phosphoinositide and inositol phosphate signalling in plants, *Plant Cell Environ* 33 (2010) 655–669.
- [266] J. Canonne, S. Froidure-Nicolas, S. Rivas, Phospholipases in action during plant defense signaling, *Plant Signal Behav* 6 (2011) 13–18.
- [267] I. Pokotylo, V. Kravets, J. Martinec, E. Ruelland, The phosphatidic acid paradox: too many actions for one molecule class? Lessons from plants, *Prog Lipid Res* 71 (2018) 43–53.
- [268] A.H. van der Luit, T. Piatti, A. van Doorn, A. Musgrave, G. Felix, T. Boller, et al., Elicitation of suspension-cultured tomato cells triggers the formation of phosphatidic acid and diacylglycerol pyrophosphate, *Plant Physiol* 123 (2000) 1507–1516.
- [269] A.M. Laxalt, N. Raho, A.T. Have, L. Lamattina, Nitric oxide is critical for inducing phosphatidic acid accumulation in xylanase-elicited tomato cells, *J Biol Chem* 282 (2007) 21160–21168.
- [270] N. Raho, L. Ramirez, M.L. Lanteri, G. Gonorazky, L. Lamattina, A. ten Have, et al., Phosphatidic acid production in chitosan-elicited tomato cells, via both phospholipase D and phospholipase C/diacylglycerol kinase, requires nitric oxide, *J Plant Physiol* 168 (2011) 534–539.
- [271] S.A. Arisz, C. Testerink, T. Munnik, Plant PA signaling via diacylglycerol kinase, *Biochim Biophys Acta* 1791 (2009) 869–875.
- [272] C. Testerink, T. Munnik, Molecular, cellular, and physiological responses to phosphatidic acid formation in plants, *J Exp Bot* 62 (2011) 2349–2361.
- [273] P.K. Farmer, J.H. Choi, Calcium and phospholipid activation of a recombinant calcium-dependent protein kinase (DcCPK1) from carrot (*Daucus carota* L.), *Biochim Biophys Acta* 1434 (1999) 6–17.
- [274] J. Szczegielniak, M. Klimecka, A. Liwosz, A. Ciesielski, S. Kaczanowski, G. Dobrowolska, et al., A wound-responsive and phospholipid-regulated maize calcium-dependent protein kinase, *Plant Physiol* 139 (2005) 1970–1983.
- [275] T. Munnik, C. Testerink, Plant phospholipid signaling: "in a nutshell", *J Lipid Res* 50 (Suppl) (2009) S260–S265.
- [276] T. Munnik, A.M. Laxalt, Measuring PLD activity in vivo, *Methods Mol Biol* 1009 (2013) 219–231.
- [277] I. Camehl, C. Drzewiecki, J. Vadassery, B. Shahollari, I. Sherameti, C. Forzani, et al., The OX11 kinase pathway mediates Piriformospora indica-induced growth promotion in *Arabidopsis*, *PLoS Pathog* 7 (2011) e1002051.
- [278] I. Pokotylo, Y. Kolesnikov, V. Kravets, A. Zachowski, E. Ruelland, Plant phosphoinositide-dependent phospholipases C: variations around a canonical theme, *Biochimie* 96 (2014) 144–157.
- [279] T.S. Nuhse, A.R. Bottrill, A.M. Jones, S.C. Peck, Quantitative phosphoproteomic analysis of plasma membrane proteins reveals regulatory mechanisms of plant innate immune responses, *Plant J Vol.* 51 (2007) 931–940.
- [280] J.M. D'Ambrosio, D. Couto, G. Fabro, D. Scuffi, L. Lamattina, T. Munnik, et al., Phospholipase C2 affects MAMP-triggered immunity by modulating ROS production, *Plant Physiol* 175 (2017) 970–981.
- [281] M.X. Andersson, O. Kourtchenko, J.L. Dangi, D. Mackey, M. Ellerstrom, Phospholipase-dependent signalling during the AvrRpm1- and AvrRpt2-induced disease resistance responses in *Arabidopsis thaliana*, *Plant J Vol.* 47 (2006) 947–959.
- [282] Z.K.Z. Krčková, M. Daněk, J. Brouzdová, P.P.M. Janda, I. Pokotylo, P.G. Ott, et al., The *Arabidopsis thaliana* non-specific phospholipase C2 is involved in the response to *Pseudomonas syringae* attack, *Ann Bot* 121 (2017) 297–310.
- [283] J.L. Cacas, P. Gerbeau-Pissot, J. Fromentin, C. Cantrel, D. Thomas, E. Jeannette, et al., Diacylglycerol kinases activate tobacco NADPH oxidase-dependent oxidative burst in response to cryptogam, *Plant Cell Environ* 40 (2017) 585–598.
- [284] Y. Kadota, K. Shirasu, C. Zipfel, Regulation of the NADPH oxidase RBOHD during plant immunity, *Plant Cell Physiol* 56 (2015) 1472–1480.
- [285] X. Liang, M. Ma, Z. Zhou, J. Wang, X. Yang, S. Rao, et al., Ligand-triggered de-repression of *Arabidopsis* heterotrimeric G proteins coupled to immune receptor kinases, *Cell Res* 28 (2018) 529–543.
- [286] A.M. Abd-El-Halim, J.H. Vossen, A. van Zeijl, S. Dezhsetan, C. Testerink, M.F. Seidl, et al., Biochemical characterization of the tomato phosphatidylinositol-specific phospholipase C (PI-PLC) family and its role in plant immunity, *Biochim Biophys Acta* 1861 (2016) 1365–1378.
- [287] J. Li, J.L. Henty-Ridilla, B.H. Staiger, B. Day, C.J. Staiger, Capping protein integrates multiple MAMP signalling pathways to modulate actin dynamics during plant innate immunity, *Nat Commun* 6 (2015) 7206.
- [288] Y. Sang, S. Zheng, W. Li, B. Huang, X. Wang, Regulation of plant water loss by manipulating the expression of phospholipase Dalpha, *Plant J Vol.* 28 (2001) 135–144.
- [289] T. Yamaguchi, E. Minami, J. Ueki, N. Shibuya, Elicitor-induced activation of phospholipases plays an important role for the induction of defense responses in suspension-cultured rice cells, *Plant Cell Physiol* 46 (2005) 579–587.
- [290] L. Fan, S. Zheng, D. Cui, X. Wang, Subcellular distribution and tissue expression of phospholipase Dalpha, Dbeta, and Dgamma in *Arabidopsis*, *Plant Physiol* 119 (1999) 1371–1378.
- [291] F. Pinoso, N. Buhot, M. Kwaaitaal, P. Fahlberg, H. Thordal-Christensen, M. Ellerstrom, et al., *Arabidopsis* phospholipase ddelta is involved in basal defense and nonhost resistance to powdery mildew fungi, *Plant Physiol* 163 (2013) 896–906.
- [292] K. Hyodo, T. Taniguchi, Y. Manabe, M. Kaido, K. Mise, T. Sugawara, et al., Phosphatidic acid produced by phospholipase D promotes RNA replication of a plant RNA virus, *PLoS Pathog* 11 (2015) e1004909.
- [293] L. Guo, X. Wang, Crosstalk between phospholipase D and sphingosine kinase in plant stress signaling, *Front Plant Sci* 3 (2012) 51.
- [294] E.C.V. Kooijman, B. de Kruijff, K.N.J. Burger, Modulation of membrane curvature by phosphatidic acid and lysophosphatidic acid, *Traffic* 4 (2003) 162–174.
- [295] M. Roth, Molecular mechanisms of PLD function in membrane traffic, *Traffic* 9 (2008) 1233–1239.
- [296] G.H. Lim, R. Singhal, A. Kachroo, P. Kachroo, Fatty acid- and lipid-mediated signaling in plant defense, *Annu Rev Phytopathol* 55 (2017) 505–536.
- [297] T. Yaeno, O. Matsuda, K. Iba, Role of chloroplast trienoic fatty acids in plant disease defense responses, *Plant J Vol.* 40 (2004) 931–941.
- [298] L.W.X. Madi, L. Kobiler, A. Lichter, D. Prusky, Stress on avocado fruits regulates Δ9-stearoyl ACP desaturase expression, fatty acid composition, antifungal diene level and resistance to *Colletotrichum gloeosporioides* attack, *Physiol Mol Plant Pathol* 62 (2003) 277–283.
- [299] M. Ongena, F. Duby, F. Rossignol, M.L. Fauconnier, J. Dommès, P. Thonart, Stimulation of the lipoxygenase pathway is associated with systemic resistance induced in bean by a nonpathogenic *Pseudomonas* strain, *Mol Plant Microbe Interact* 17 (2004) 1009–1018.
- [300] K. Schrick, S. Fujioka, S. Takatsuto, Y.D. Stierhof, H. Stransky, S. Yoshida, et al., A link between sterol biosynthesis, the cell wall, and cellulose in *Arabidopsis*, *Plant J Vol.* 38 (2004) 227–243.
- [301] L.V. Michaelson, J.A. Napier, D. Molino, J.D. Faure, Plant sphingolipids: their importance in cellular organization and adaptation, *Biochim Biophys Acta* 1861 (2016) 1329–1335.
- [302] S. König, K. Feussner, M. Schwarz, A. Kaever, T. Iven, M. Landesfeind, et al., *Arabidopsis* mutants of sphingolipid fatty acid alpha-hydroxylases accumulate ceramides and salicylates, *New Phytol* 196 (2012) 1086–1097.
- [303] H.K. Abbas, T. Tanaka, W.T. Shier, Biological activities of synthetic analogues of *Alternaria alternata* toxin (AAL-toxin) and fumonisin in plant and mammalian cell cultures, *Phytochemistry* 40 (1995) 1681–1689.
- [304] J.S. Griffiths, S.M. Haslam, T. Yang, S.F. Garczynski, B. Mulloy, H. Morris, et al., Glycolipids as receptors for bacillus thuringiensis crystal toxin, *Science* 307 (2005) 922–925.
- [305] X. Yu, A. Feizpour, N.G. Ramirez, L. Wu, H. Akiyama, F. Xu, et al., Glycosphingolipid-functionalized nanoparticles recapitulate CD169-dependent HIV-1 uptake and trafficking in dendritic cells, *Nat Commun* 5 (2014) 4136.
- [306] J. Gronnier, V. Germain, P. Gouguet, J.L. Cacas, S. Mongrand, GIPC: glycosyl inositol phospho ceramides, the major sphingolipids on earth, *Plant Signal Behav* 11 (2016) e1152438.
- [307] S. Oome, G. Van den Ackerveken, Comparative and functional analysis of the widely occurring family of Nep1-like proteins, *Mol Plant Microbe Interact* 27 (2014) 1081–1094.
- [308] M. Gijzen, T. Nurnberger, Nep1-like proteins from plant pathogens: recruitment and diversification of the NPP1 domain across taxa, *Phytochemistry* 67 (2006) 1800–1807.
- [309] D. Qutob, B. Kemmerling, F. Brunner, I. Kufner, S. Engelhardt, A.A. Gust, et al., Phytotoxicity and innate immune responses induced by Nep1-like proteins, *Plant Cell* 18 (2006) 3721–3744.
- [310] A. Perraki, J.L. Cacas, J.M. Crowet, L. Lins, M. Castroviejo, S. German-Retana, et al., Plasma membrane localization of *Solanum tuberosum* remorin from group 1, homolog 3 is mediated by conformational changes in a novel C-terminal anchor and required for the restriction of potato virus X movement, *Plant Physiol* 160 (2012) 624–637.
- [311] B. Lefebvre, T. Timmers, M. Mbengue, S. Moreau, C. Herve, K. Toth, et al., A remorin protein interacts with symbiotic receptors and regulates bacterial infection, *Proc Natl Acad Sci U S A* 107 (2010) 2343–2348.
- [312] P. Liang, T.F. Stratil, C. Popp, M. Marin, J. Folgmann, K.S. Mysore, et al., Symbiotic root infections in *Medicago truncatula* require remorin-mediated receptor stabilization in membrane nanodomains, *Proc Natl Acad Sci U S A* 115 (2018) 5289–5294.
- [313] V. Srivastava, E. Malm, G. Sundqvist, V. Bulone, Quantitative proteomics reveals that plasma membrane microdomains from poplar cell suspension cultures are enriched in markers of signal transduction, molecular transport, and callose biosynthesis, *Mol Cell Proteomics* 12 (2013) 3874–3885.
- [314] S. Son, C.J. Oh, C.S. An, *Arabidopsis thaliana* remorins interact with SnRK1 and play a role in susceptibility to beet curly top virus and beet severe curly top virus, *Plant Pathol J* 30 (2014) 269–278.
- [315] Bozkurt TO, A. Richardson, Y.F. Dagdas, S. Mongrand, S. Raffaele, The plant membrane-associated REMORIN1.3 accumulates in discrete periaustorial domains and enhances susceptibility to phytophthora infestans, *Plant Physiol* 165 (2014) 1005–1018.
- [316] J. Gui, C. Liu, J. Shen, L. Li, Grain setting defect1, encoding a remorin protein, affects the grain setting in rice through regulating plasmodesmal conductance, *Plant Physiol* 166 (2014) 1463–1478.
- [317] C. Zipfel, G.E. Oldroyd, Plant signalling in symbiosis and immunity, *Nature* 543 (2017) 328–336.
- [318] L. Gomez-Gomez, T. Boller, FLS2: an LRR receptor-like kinase involved in the perception of the bacterial elicitor flagellin in *Arabidopsis*, *Mol Cell* 5 (2000) 1003–1011.
- [319] D. Couto, R. Niebergall, X. Liang, C.A. Bucherl, J. Sklenar, A.P. Macho, et al., The *Arabidopsis* protein phosphatase PP2C38 negatively regulates the central immune

- kinase BIK1, *PLoS Pathog* 12 (2016) e1005811.
- [320] C. Faulkner, E. Petutsch, Y. Benitez-Alfonso, M. Beck, S. Robatzek, V. Lipka, et al., LYM2-dependent chitin perception limits molecular flux via plasmodesmata, *Proc Natl Acad Sci U S A* 110 (2013) 9166–9170.
- [321] R. Zavaliev, X. Dong, B.L. Epel, Glycosylphosphatidylinositol (GPI) modification serves as a primary plasmodesmal sorting signal, *Plant Physiol* 172 (2016) 1061–1073.
- [322] R. Zavaliev, A. Levy, A. Gera, B.L. Epel, Subcellular dynamics and role of Arabidopsis beta-1,3-glucanases in cell-to-cell movement of tobamoviruses, *Mol Plant Microbe Interact* 26 (2013) 1016–1030.
- [323] W. Halperin, W.A. Jensen, Ultrastructural changes during growth and embryogenesis in carrot cell cultures, *J Ultrastruct Res* 18 (1967) 428–443.
- [324] B.D. Rutter, R.W. Innes, Extracellular vesicles as key mediators of plant-microbe interactions, *Curr Opin Plant Biol* 44 (2018) 16–22.
- [325] G. Gonorazky, A.M. Laxalt, C. Testerink, T. Munnik, L. de la Canal, Phosphatidylinositol 4-phosphate accumulates extracellularly upon xylanase treatment in tomato cell suspensions, *Plant Cell Environ* 31 (2008) 1051–1062.
- [326] M. Regente, M. Pinedo, H. San Clemente, T. Balliau, E. Jamet, L. de la Canal, Plant extracellular vesicles are incorporated by a fungal pathogen and inhibit its growth, *J Exp Bot* 68 (2017) 5485–5495.
- [327] C.O. Micali, U. Neumann, D. Grunewald, R. Panstruga, R. O'Connell, Biogenesis of a specialized plant-fungal interface during host cell internalization of *Golovinomyces orontii* haustoria, *Cell Microbiol* 13 (2011) 210–226.
- [328] Q. An, R. Huckelhoven, K.H. Kogel, A.J. van Bel, Multivesicular bodies participate in a cell wall-associated defence response in barley leaves attacked by the pathogenic powdery mildew fungus, *Cell Microbiol* 8 (2006) 1009–1019.
- [329] M. Wang, A. Weiberg, F.M. Lin, B.P. Thomma, H.D. Huang, H. Jin, Bidirectional cross-kingdom RNAi and fungal uptake of external RNAs confer plant protection, *Nat Plants* 2 (2016) 16151.
- [330] T. Zhang, Y.L. Zhao, J.H. Zhao, S. Wang, Y. Jin, Z.Q. Chen, et al., Cotton plants export microRNAs to inhibit virulence gene expression in a fungal pathogen, *Nat Plants* 2 (2016) 16153.
- [331] Q. Cai, L. Qiao, M. Wang, B. He, F.M. Lin, J. Palmquist, et al., Plants send small RNAs in extracellular vesicles to fungal pathogen to silence virulence genes, *Science* 360 (2018) 1126–1129.
- [332] B.D. Rutter, R.W. Innes, Extracellular vesicles isolated from the leaf apoplast carry stress-response proteins, *Plant Physiol* 173 (2017) 728–741.
- [333] G. Gonorazky, A.M. Laxalt, H.L. Dekker, M. Rep, T. Munnik, C. Testerink, et al., Phosphatidylinositol 4-phosphate is associated to extracellular lipoproteic fractions and is detected in tomato apoplastic fluids, *Plant Biol (Stuttg)* 14 (2012) 41–49.
- [334] S. Sabatini, D. Beis, H. Wolkenfelt, J. Murfett, T. Guilfoyle, J. Malamy, et al., An auxin-dependent distal organizer of pattern and polarity in the Arabidopsis root, *Cell* 99 (1999) 463–472.
- [335] E. Benkova, M. Michniewicz, M. Sauer, T. Teichmann, D. Seifertova, G. Jurgens, et al., Local, efflux-dependent auxin gradients as a common module for plant organ formation, *Cell* 115 (2003) 591–602.
- [336] J. Friml, E. Benkova, U. Mayer, K. Palme, G. Muster, Automated whole mount localisation techniques for plant seedlings, *Plant J Vol.* 34 (2003) 115–124.
- [337] V.A. Grieneisen, J. Xu, A.F. Maree, P. Hogeweg, B. Scheres, Auxin transport is sufficient to generate a maximum and gradient guiding root growth, *Nature* 449 (2007) 1008–1013.
- [338] M.J. Bennett, A. Marchant, H.G. Green, S.T. May, S.P. Ward, P.A. Millner, et al., Arabidopsis AUX1 gene: a permease-like regulator of root gravitropism, *Science* 273 (1996) 948–950.
- [339] C. Luschig, R.A. Gaxiola, P. Grisafi, G.R. Fink, EIR1, a root-specific protein involved in auxin transport, is required for gravitropism in Arabidopsis thaliana, *Genes Dev* 12 (1998) 2175–2187.
- [340] J. Petrasek, J. Mravec, R. Bouchard, J.J. Blakeslee, M. Abas, D. Seifertova, et al., PIN proteins perform a rate-limiting function in cellular auxin efflux, *Science* 312 (2006) 914–918.
- [341] J. Wisniewska, J. Xu, D. Seifertova, P.B. Brewer, K. Ruzicka, I. Blilou, et al., Polar PIN localization directs auxin flow in plants, *Science* 312 (2006) 883.
- [342] Y. Yang, U.Z. Hammes, C.G. Taylor, D.P. Schachtman, E. Nielsen, High-affinity auxin transport by the AUX1 influx carrier protein, *Current Biol* 16 (2006) 1123–1127.
- [343] Y. Boutte, K. Jonsson, H.E. McFarlane, E. Johnson, D. Gendre, R. Swarup, et al., ECHIDNA-mediated post-Golgi trafficking of auxin carriers for differential cell elongation, *Proc Natl Acad Sci U S A* 110 (2013) 16259–16264.
- [344] J.G. Wang, S. Li, X.Y. Zhao, L.Z. Zhou, G.Q. Huang, C. Feng, et al., HAPLESS13, the Arabidopsis mu1 adaptin, is essential for protein sorting at the trans-Golgi network/early endosome, *Plant Physiol* 162 (2013) 1897–1910.
- [345] E. Feraru, M.I. Feraru, R. Asaoka, T. Pacionek, R. De Rycke, H. Tanaka, et al., BEX5/RabA1b regulates trans-Golgi network-to-plasma membrane protein trafficking in Arabidopsis, *Plant Cell* 24 (2012) 3074–3086.
- [346] D. Gendre, J. Oh, Y. Boutte, J.G. Best, L. Samuelsen, R. Nilsson, et al., Conserved Arabidopsis ECHIDNA protein mediates trans-Golgi-network trafficking and cell elongation, *Proc Natl Acad Sci U S A* 108 (2011) 8048–8053.
- [347] D. Gendre, H.E. McFarlane, E. Johnson, G. Mouille, A. Sjodin, J. Oh, et al., Trans-Golgi network localized ECHIDNA/Ypt interacting protein complex is required for the secretion of cell wall polysaccharides in Arabidopsis, *Plant Cell* 25 (2013) 2633–2646.
- [348] S. Naramoto, M.S. Otegui, N. Kutsuna, R. de Rycke, T. Dainobu, M. Karampelias, et al., Insights into the localization and function of the membrane trafficking regulator GNOM ARF-GEF at the Golgi apparatus in Arabidopsis, *Plant Cell* 26 (2014) 3062–3076.
- [349] K. Jonsson, Y. Boutte, R.K. Singh, D. Gendre, R.P. Bhalerao, Ethylene regulates differential growth via BIG ARF-GEF-dependent post-golgi secretory trafficking in Arabidopsis, *Plant Cell* 29 (2017) 1039–1052.
- [350] L.E. Sieburth, G.K. Muday, E.J. King, G. Benton, S. Kim, K.E. Metcalf, et al., SCARFACE encodes an ARF-GAP that is required for normal auxin efflux and vein patterning in Arabidopsis, *Plant Cell* 18 (2006) 1396–1411.
- [351] L. Bach, L.V. Michaelson, R. Haslam, Y. Bellec, L. Gissot, J. Marion, et al., The very-long-chain hydroxy fatty acyl-CoA dehydratase PASTICCINO2 is essential and limiting for plant development, *Proc Natl Acad Sci U S A* 105 (2008) 14727–14731.
- [352] F. Roudier, L. Gissot, F. Beaudoin, R. Haslam, L. Michaelson, J. Marion, et al., Very-long-chain fatty acids are involved in polar auxin transport and developmental patterning in Arabidopsis, *Plant Cell* 22 (2010) 364–375.
- [353] V. Willemsen, J. Friml, M. Grebe, A. van den Toorn, K. Palme, B. Scheres, Cell polarity and PIN protein positioning in Arabidopsis require sterol methyltransferase1 function, *Plant Cell* 15 (2003) 612–625.
- [354] S. Men, Y. Boutte, Y. Ikeda, X. Li, K. Palme, Y.D. Stierhof, et al., Sterol-dependent endocytosis mediates post-cytokinetic acquisition of PIN2 auxin efflux carrier polarity, *Nat Cell Biol* 10 (2008) 237–244.
- [355] J. Kleine-Vehn, P. Dhonukshe, R. Swarup, M. Bennett, J. Friml, Subcellular trafficking of the Arabidopsis auxin influx carrier AUX1 uses a novel pathway distinct from PIN1, *Plant Cell* 18 (2006) 3171–3181.
- [356] A.S. Mialoundama, N. Jadid, J. Brunel, T. Di Pascoli, D. Heintz, M. Erhardt, et al., Arabidopsis ERG28 tethers the sterol C4-demethylation complex to prevent accumulation of a biosynthetic intermediate that interferes with polar auxin transport, *Plant Cell* 25 (2013) 4879–4893.
- [357] X. Zhang, S. Sun, X. Nie, Y. Boutte, M. Grison, P. Li, et al., Sterol methyl oxidases affect embryo development via auxin-associated mechanisms, *Plant Physiol* 171 (2016) 468–482.
- [358] E. Darwish, C. Testerink, M. Khalil, O. El-Shihy, T. Munnik, Phospholipid signaling responses in salt-stressed rice leaves, *Plant Cell Physiol* 50 (2009) 986–997.
- [359] M. Mishkind, J.E. Vermeer, E. Darwish, T. Munnik, Heat stress activates phospholipase D and triggers PIP accumulation at the plasma membrane and nucleus, *Plant J Vol.* 60 (2009) 10–21.
- [360] H.J. Meijer, J.A. van Himbergen, A. Musgrave, T. Munnik, Acclimation to salt modifies the activation of several osmotic stress-activated lipid signalling pathways in *Chlamydomonas*, *Phytochemistry* 135 (2017) 64–72.
- [361] Q. Hou, G. Ufer, D. Bartels, Lipid signalling in plant responses to abiotic stress, *Plant Cell Environ* 39 (2016) 1029–1048.
- [362] M. Li, Y. Hong, X. Wang, Phospholipase D- and phosphatidic acid-mediated signaling in plants, *Biochim Biophys Acta* 1791 (2009) 927–935.
- [363] M. Heilmann, I. Heilmann, Plant phosphoinositides-complex networks controlling growth and adaptation, *Biochim Biophys Acta* 1851 (2015) 759–769.
- [364] X. Wang, K.D. Chapman, Lipid signaling in plants, *Front Plant Sci* 4 (2013) 216.
- [365] W. Zhang, C. Qin, J. Zhao, X. Wang, Phospholipase D alpha 1-derived phosphatidic acid interacts with ABI1 phosphatase 2C and regulates abscisic acid signaling, *Proc Natl Acad Sci U S A* 101 (2004) 9508–9513.
- [366] M. Diaz, M.J. Sanchez-Barrena, J.M. Gonzalez-Rubio, L. Rodriguez, D. Fernandez, R. Antoni, et al., Calcium-dependent oligomerization of CAR proteins at cell membrane modulates ABA signaling, *Proc Natl Acad Sci U S A* 113 (2016) E396–E405.
- [367] W.J. Nicolas, M.S. Grison, S. Trepout, A. Gaston, M. Fouche, F.P. Cordelieres, et al., Architecture and permeability of post-cytokinesis plasmodesmata lacking cytoplasmic sleeves, *Nat Plants* 3 (2017) 17082.
- [368] S. Lahiri, A. Toulmay, W.A. Prinz, Membrane contact sites, gateways for lipid homeostasis, *Curr Opin Cell Biol* 33 (2015) 82–87.
- [369] M.S. Grison, L. Fernandez-Calvino, S. Mongrand, E.M. Bayer, Isolation of plasmodesmata from Arabidopsis suspension culture cells, *Methods Mol Biol* 1217 (2015) 83–93.
- [370] M. Deleu, J.M. Crowet, M.N. Nasir, L. Lins, Complementary biophysical tools to investigate lipid specificity in the interaction between bioactive molecules and the plasma membrane: a review, *Biochim Biophys Acta* 1838 (2014) 3171–3190.
- [371] D. Martinez, A. Legrand, J. Gronnier, M. Decossas, P. Gouguet, O. Lambert, et al., Coiled-coil oligomerization controls localization of the plasma membrane REMORINS, *J Struct Biol* S1047-8477 (18) (2018) 30046–30047.
- [372] A. Pandey, K. Shin, R.E. Patterson, X.Q. Liu, J.K. Rainey, Current strategies for protein production and purification enabling membrane protein structural biology, *Biochem Cell Biol* 94 (2016) 507–527.
- [373] S.A. Sarver, R.B. Keithley, D.C. Essaka, H. Tanaka, Y. Yoshimura, M.M. Palcic, et al., Preparation and electrophoretic separation of Bodipy-Fl-labeled glycosphingolipids, *J Chromatogr A* 1229 (2012) 268–273.
- [374] H.T. Cheng, London E. Megha, Preparation and properties of asymmetric vesicles that mimic cell membranes: effect upon lipid raft formation and transmembrane helix orientation, *J Biol Chem* 284 (2009) 6079–6092.
- [375] K. Pluhackova, R.A. Bockmann, Biomembranes in atomistic and coarse-grained simulations, *J Phys Condens Matter* 27 (2015) 323103.
- [376] A.P. Lyubartsev, A.L. Rabinovich, Force field development for lipid membrane simulations, *Biochim Biophys Acta* 1858 (2016) 2483–2497.
- [377] T.A. Wassenaar, H.I. Ingolfsson, M. Priess, S.J. Marrink, L.V. Schafer, Mixing MARTINI: Electrostatic coupling in hybrid atomistic-coarse-grained biomolecular simulations, *J Phys Chem B* 117 (2013) 3516–3530.
- [378] D. Poger, B. Caron, A.E. Mark, Validating lipid force fields against experimental data: Progress, challenges and perspectives, *Biochim Biophys Acta* 1858 (2016) 1556–1565.
- [379] C.A. Lopez, Z. Sovova, F.J. van Eerden, A.H. de Vries, S.J. Marrink, Martini force field parameters for glycolipids, *J Chem Theory Comput* 9 (2013) 1694–1708.

- [380] E. Izquierdo, A. Delgado, Click chemistry in sphingolipid research, *Chem Phys Lipids* 215 (2018) 71–83.
- [381] M.D. Best, Click chemistry and bioorthogonal reactions: Unprecedented selectivity in the labeling of biological molecules, *Biochemistry* 48 (2009) 6571–6584.
- [382] T. Stanislas, M.P. Platre, M. Liu, L.E.S. Rambaud-Lavigne, Y. Jaillais, O. Hamant, A phosphoinositide map at the shoot apical meristem in *Arabidopsis thaliana*, *BMC Biol* 16 (2018) 20.
- [383] Y. Ma, E. Pandzic, P.R. Nicovich, Y. Yamamoto, J. Kwiatek, S.V. Paeon, et al., An intermolecular FRET sensor detects the dynamics of T cell receptor clustering, *Nat Commun* 8 (2017) 15100.
- [384] Y. Ma, K. Poole, J. Goyette, K. Gaus, Introducing membrane charge and membrane potential to T cell signaling, *Front Immunol* 8 (2017) 1513.
- [385] S. Oncul, A.S. Klymchenko, O.A. Kucherak, A.P. Demchenko, S. Martin, M. Dontenwill, et al., Liquid ordered phase in cell membranes evidenced by a hydration-sensitive probe: effects of cholesterol depletion and apoptosis, *Biochim Biophys Acta* 1798 (2010) 1436–1443.
- [386] P. Tarazona, K. Feussner, I. Feussner, An enhanced plant lipidomics method based on multiplexed liquid chromatography-mass spectrometry reveals additional insights into cold- and drought-induced membrane remodeling, *Plant J* Vol. 84 (2015) 621–633.
- [387] A. Ray, N. Jatana, L. Thukral, Lipidated proteins: Spotlight on protein-membrane binding interfaces, *Prog Biophys Mol Biol* 128 (2017) 74–84.
- [388] P. Prakash, Y. Zhou, H. Liang, J.F. Hancock, A.A. Gorfe, Oncogenic K-Ras binds to an anionic membrane in two distinct orientations: a molecular dynamics analysis, *Biophys J* 110 (2016) 1125–1138.
- [389] A. Sayyed-Ahmad, K.J. Cho, J.F. Hancock, A.A. Gorfe, Computational equilibrium thermodynamic and kinetic analysis of K-Ras dimerization through an effector binding surface suggests limited functional role, *J Phys Chem B* 120 (2016) 8547–8556.
- [390] T. Tian, A. Harding, K. Inder, S. Plowman, R.G. Parton, J.F. Hancock, Plasma membrane nanoswitches generate high-fidelity Ras signal transduction, *Nat Cell Biol* 9 (2007) 905–914.
- [391] S.V. Paeon, T. Tabarin, Y. Yamamoto, Y. Ma, P.R. Nicovich, J.S. Bridgeman, et al., Functional role of T-cell receptor nanoclusters in signal initiation and antigen discrimination, *Proc Natl Acad Sci U S A* 113 (2016) E5454–E5463.
- [392] D.J. Williamson, D.M. Owen, J. Rossy, A. Magenau, M. Wehrmann, J.J. Gooding, et al., Pre-existing clusters of the adaptor Lat do not participate in early T cell signaling events, *Nat Immunol* 12 (2011) 655–662.
- [393] T. Zech, C.S. Ejsing, K. Gaus, B. de Wet, A. Shevchenko, K. Simons, et al., Accumulation of raft lipids in T-cell plasma membrane domains engaged in TCR signalling, *EMBO J* 28 (2009) 466–476.
- [394] C. Rentero, T. Zech, C.M. Quinn, K. Engelhardt, D. Williamson, T. Grewal, et al., Functional implications of plasma membrane condensation for T cell activation, *PLoS One* 3 (2008) e2262.
- [395] M. Kinoshita, K.G. Suzuki, N. Matsumori, M. Takada, H. Ano, K. Morigaki, et al., Raft-based sphingomyelin interactions revealed by new fluorescent sphingomyelin analogs, *J Cell Biol* 216 (2017) 1183–1204.
- [396] A. Kusumi, T.K. Fujiwara, R. Chadda, M. Xie, T.A. Tsunoyama, Z. Kalay, et al., Dynamic organizing principles of the plasma membrane that regulate signal transduction: Commemorating the fortieth anniversary of singer and Nicolson's fluid-mosaic model, *Annu Rev Cell Dev Biol* 28 (2012) 215–250.
- [397] A. Kusumi, K. Suzuki, Toward understanding the dynamics of membrane-raft-based molecular interactions, *Biochim Biophys Acta* 1746 (2005) 234–251.
- [398] M. Fujimoto, Y. Suda, S. Vernhettes, A. Nakano, T. Ueda, Phosphatidylinositol 3-kinase and 4-kinase have distinct roles in intracellular trafficking of cellulose synthase complexes in *Arabidopsis thaliana*, *Plant Cell Physiol* 56 (2015) 287–298.
- [399] T. Hirano, T. Munnik, M.H. Sato, Phosphatidylinositol 3-Phosphate 5-Kinase, FAB1/PIKfyve kinase mediates endosome maturation to establish endosome-cortical microtubule interaction in *Arabidopsis*, *Plant Physiol* 169 (2015) 1961–1974.
- [400] A. Aubert, J. Marion, C. Boulogne, M. Bourge, S. Abreu, Y. Bellec, et al., Sphingolipids involvement in plant endomembrane differentiation: The BY2 case, *Plant J* Vol. 65 (2011) 958–971.
- [401] E. Wang, W.P. Norred, C.W. Bacon, R.T. Riley, A.H. Merrill Jr., Inhibition of sphingolipid biosynthesis by fumonisins. Implications for diseases associated with *Fusarium moniliforme*, *J Biol Chem* 266 (1991) 14486–14490.
- [402] F. Kruger, M. Krebs, C. Viotti, M. Langhans, K. Schumacher, D.G. Robinson, PDMP induces rapid changes in vacuole morphology in *Arabidopsis* root cells, *J Exp Bot* 64 (2013) 529–540.
- [403] B. Nieto, O. Fores, M. Arro, A. Ferrer, *Arabidopsis* 3-hydroxy-3-methylglutaryl-CoA reductase is regulated at the post-translational level in response to alterations of the sphingolipid and the sterol biosynthetic pathways, *Phytochemistry* 70 (2009) 53–59.
- [404] J.G. Mina, Y. Okada, N.K. Wansadhipathi-Kannangara, S. Pratt, H. Shams-Eldin, R.T. Schwarz, et al., Functional analyses of differentially expressed isoforms of the *Arabidopsis* inositol phosphorylceramide synthase, *Plant Mol Biol* 73 (2010) 399–407.
- [405] T. Baba, A. Yamamoto, M. Tagaya, K. Tani, A lysophospholipid acyltransferase antagonist, CI-976, creates novel membrane tubules marked by intracellular phospholipase A1 KIAA0725p, *Mol Cell Biochem* 376 (2013) 151–161.
- [406] W.J. Brown, H. Plutner, D. Drecktrah, B.L. Judson, W.E. Balch, The lysophospholipid acyltransferase antagonist CI-976 inhibits a late step in COPII vesicle budding, *Traffic* 9 (2008) 786–797.
- [407] K. Chambers, B. Judson, W.J. Brown, A unique lysophospholipid acyltransferase (LPAT) antagonist, CI-976, affects secretory and endocytic membrane trafficking pathways, *J Cell Sci* 118 (2005) 3061–3071.
- [408] P. Wu, H.B. Gao, L.L. Zhang, H.W. Xue, W.H. Lin, Phosphatidic acid regulates BZR1 activity and brassinosteroid signal of *Arabidopsis*, *Mol Plant* 7 (2014) 445–447.
- [409] C.M. Motes, P. Pechter, C.M. Yoo, Y.S. Wang, K.D. Chapman, E.B. Blancaflor, Differential effects of two phospholipase D inhibitors, 1-butanol and N-acyl ethanolamine, on *in vivo* cytoskeletal organization and *Arabidopsis* seedling growth, *Protoplasma* 226 (2005) 109–123.
- [410] G. Li, H.W. Xue, *Arabidopsis* PLDzeta2 regulates vesicle trafficking and is required for auxin response, *Plant Cell* 19 (2007) 281–295.
- [411] I. Staxen, C. Pical, L.T. Montgomery, J.E. Gray, A.M. Hetherington, M.R. McAinsh, Abscisic acid induces oscillations in guard-cell cytosolic free calcium that involve phosphoinositide-specific phospholipase C, *Proc Natl Acad Sci U S A* 96 (1999) 1779–1784.

## Thesis Objectives

In plants as in animals, there are three main classes of lipids in plasma membrane: glycerophospholipids, sterols and sphingolipids. These classes of lipids are shared by all living organisms, but plants exhibit some striking characteristics. While animal plasma membrane (PM) essentially comprises cholesterol, diverse structures and abilities to organize PM are present in plants. Plant sphingolipids are of four major classes: ceramides (CER), glucosylceramide (gluCERgluCer), Glycosyl Inositol Phosphoryl Ceramides (GIPC) and free Long Chain Bases (LCBs), representing ca., 2%, 34%, 64% and 0.5 % of total sphingolipids, respectively in *Arabidopsis thaliana* (Markham, Li, Cahoon, & Jaworski, 2006). As such, GIPCs are the major sphingolipid on earth. First described as phytoglycolipid (PGL) in 1964 by HE Carter (Carter, Brooks, Gigg, Strobach, & Suami, 1964), a broad study of the GIPC polar head of 23 plant species from algae to monocots (Buré, Cacas, Mongrand, & Schmitter, 2014) further showed that polar head structures are largely unknown and versatile for the different biological taxa. The vast structural diversity of GIPC has never been studied, as GIPCs are not soluble in classical lipid extraction solvents. As such this lipid has been forgotten for almost 25 years until the mid-2000 (Markham et al., 2006), still much remain to be investigated about the structure and role of GIPCs.

Plants PM exhibits a striking and to date mysterious ability to ensure these functions across a wide range of temperatures, from negative ones to 40°C: this makes the understanding of this membrane organization a fascinating challenge. The unexpected and outstanding complexity of PM organization, and the essential role of lipids in organization and intrinsic properties of PM, appeared crucial for ensuring its physiological functions. The abundance and the particular structure of GIPCs with its (h)VLCFA of 22 to 28 carbon atoms, (h)VLCFA, as well as their close interactions with sterols put them as a good candidate to be involved in phase transition regulation of the PM.

The relevance to understand more about GIPCs cannot be underestimated. Biophysics seems to be the tool by excellence to study the interactions of lipids with other molecules helping to develop new strategies to understand the role of lipids in plant PM. The principal aims of my thesis were to obtain GIPC samples from different species so as to investigate how GIPCs are structured, the polar head group, the number of sugars in the head group. Then we investigated how GIPCs are organized in the membrane and their role in modulating lipid domains through particular interactions with sterols. My thesis is based on the study of GIPCs, where I was able to investigate the biochemical properties of GIPCs as well as their biophysical characteristics.

Most of the experiments were performed in Bordeaux at the LBM for purification and lipidomic assays, at the IECB for the NMR experiments, at the CBMN for the cryo-EM

observations and on the BIC platform for all microscopy experiments. I was also able, for several weeks during the 3 years of my thesis, to learn and perform biophysic assays such as Langmuir Trough Isotherm compression technique as well as molecular modelling, in Gembloux, Belgium at the Laboratoire de Biophysique Moléculaire aux Interfaces (LBMI) with our collaborators Laurence Lins and Magali Deleu . With our collaborator Eric Lesniewska in Dijon at the Université de Bourgogne Franche-Comté, I was able to visit his lab for five days to perform Atomic Force Microscopy and Nano-IR assays. I also collaborated with Laurent Heux and Yotam Navon at the CERMAV in Grenoble to obtain data of Neutron Reflectivity experiments on GIPC organisation in model membranes. GIPCs were sent to them by mail and Yotam performed the different experiments. To investigate more about sugar head group identity of GIPCs, I also collaborated with Jenny Mortimer at the University of California, Berkeley where assays were performed on GIPC series that I isolated and sent for analysis.

## **Chapter I. Multipolar approaches into deciphering GIPC structure and its role in membrane organisation**

In this chapter, presented as a draft of a paper to be submitted soon, I focused on optimizing the protocols for the extraction, purification and isolation of plant GIPCs. Through different trial and errors of sequencing experimental steps extracted from old to more recent papers, I devised a protocol that optimized the purification of GIPCs. I analysed GIPCs purity by GC-MS assay on the fatty acid and sugar content, and HPTLC. These results gave an indication of the (h)VLCFA content which was correlated with GIPC amount and GIPC series in the samples. GIPC molecules underwent hydrolysis to free the sugar moieties of the head group and analysed in GC-MS and HPAE.

To investigate more about the biophysical characteristic of GIPCs, I performed at the LBMI in Gembloux, the interaction of GIPCs with phytosterols (free and conjugated phytosterol) in Compression Isotherm Langmuir Trough assays. Molecular Modelling using Hypermatrix was also used to see the different parameters of the interactions. This gave an insight on the specific GIPC/sterol interaction that takes place in nanodomains. By AFM and Nano-IR experiments, performed in Dijon, I showed that on supported monolayer containing GIPC, sitosterol is important for the formation of domain-like structures, which is not the case for stigmasterol and conjugated sterols (SG and ASG).

I also made liposomes with GIPC, to find out that GIPC alone was not able to form membrane bilayers, but makes crystals. We further showed that the presence of phospholipids and sterols is required for the formation of liposomes. We were able to make MLVs and GUVs containing GIPCs. Deposited on solid support to form supported lipid bilayers (SLB), these GIPC-containing bilayers were analysed by Neutron Reflectivity to characterize the properties of the bilayer. The vesicles were

also observed under Cryo-EM and different structures were observed depending on the sterol identity. It seems that sterol affects the thickness of membrane containing GIPCs.

Inspired by the study of the effect of phytosterols on phase transition using model membranes (Beck, Mathieu, Loudet, Buchoux, & Dufourc, 2007b), I investigated the effect of sterol in the presence of GIPCs on phase transition. The experiments were performed at the IECB with Axelle Grelard and Jean-Paul Douliez on liposomes containing deuterated POPC, GIPC and sterol (sitosterol or stigmasterol) – see Additional Data of Chapter 1.

## **Chapter II. Role of VLCFA and hydroxylation in PM marker mobility**

This chapter deals with the role of VLCFA and hydroxylation of GIPC in the *in vivo* mobility of proteins and lipids of the PM in root epidermal cells of *Arabidopsis thaliana*. Minimum protein markers were described by Alexandre Martinière (Martinière et al., 2012), WAVE-lines and PIP-Lines lipid probes were provided by Yvon Jaillais's group in Lyon. *Arabidopsis* lines expressing the PM markers were generated as well as mutant lacking the FAH gene, important for the hydroxylation of fatty acid. A pharmaceutical approach using Metazachlor (Mz), a drug shortening fatty acid chain length was also used.

This part of my thesis was done in collaboration with Minoru Nagano (Saitama university, Japan), who spent 1 year as a visiting scientist at our lab, and Yohann Boutté (LBM, Bordeaux). Minoru performed all the FRAP experiments. I also generated lines of double mutants and analysed their fluorescence under confocal microscopy. I performed the lipid analysis of PM lipids purified from Mz-treated plants (GC-MS and LC-MS) with Laetitia Fouillen (LBM, Bordeaux).

Christophe Der and Françoise Simon-Plas, at INRA Dijon analysed with di-ANEPPDH, an environment-sensitive fluorescent probe, the effect of metazachlor on the PM fluidity in wild type and *fah* mutants. di-ANEPPDH fluorescent measures the degree of order of membrane, and we showed that this dye mostly probes the outer leaflet of the plasma membrane.

## **Chapter III. GIPC, receptor to microbial NLP, determine host sensitivity**

Thorsten Nürnberger (University of Tübingen, Germany) team works on (Nep1-like protein) NLP toxins. These toxins are produced by bacteria, oomycetes and fungi causing necrosis in eudicot plants but not monocot. The NLP toxins are quite similar to animal actinoporin that binds with sphingomyelin and cause cell lysis. My contribution to this work started during my Master degree internship on the project that became my

phD thesis project. I generated milligrams of GIPCs from cauliflower and leek which are eudicots and monocots respectively and also analysed the mean molecular area of these GIPCs through Langmuir Trough Compression assay to investigate how an added sugar group (present in GIPC from monocot but not eudicots) can influence the amount of space occupied by GIPC. This result was a crucial information in this paper showing how the conformation of a sugar moieties of a GIPC molecule can have dramatic role in plant-pathogen interaction.

This work has been published in *Science* in 2017, where I am 18<sup>th</sup> authors on 25 authors.

Lenarčič T, Albert I, Böhm H, Hodnik V, Pirc K, Zavec AB, Podobnik M, Pahovnik D, Žagar E, Pruitt R, Greimel P, Yamaji-Hasegawa A, Kobayashi T, Zienkiewicz A, Gömann J, Mortimer J, Fang L, **Mamode-Cassim A**, Deleu M, Lins L, Oecking C, Feussner I, Mongrand S, Anderluh G\*, Nürnberger T,\* (2017) Eudicot plant-specific sphingolipids determine host selectivity of microbial NLP cytolysins. *Science*, Dec 15;358(6369):1431-1434. \*co- corresponding authors

To follow up this work and to investigate more about the mode of action of NLPs, I went to Gembloux at the LBMi to perform Langmuir trough compression isotherms experiments with lipid monolayer mimicking the outer-leaflet of plant PM in presence of NLPs. NLPs were produced, extracted and purified from *Pichia pastoris* in Tübingen and sent to Gembloux by our collaborator Isabel Albert from Nürnberger Lab. This experiment was part of a larger scheme in order to understand more about the binding process of NLPs to GIPCs. The different GIPC series interact differently with NLPs – see Additional Data of Chapter 3.

#### **Chapter IV. Miscellaneous**

I participated in the redaction of a News & Views with Sébastien Mongrand on a paper published in *Nature plants* on the development of a FRET biosensors of Phosphatidic Acid (PA) in plants, called PAleon.

## Chapter I

# Multipolar approaches into deciphering GPCR structure and its role in membrane organisation

In chapter 1, you shall find a draft of a paper to be submitted soon. This publication will contain the main findings of my thesis through a multi-disciplinary approach. The primary aim of my PhD project is the optimization of the protocols for the extraction, purification and isolation of plant GIPCs. Through different trial and errors of sequencing experimental steps extracted from old to more recent papers, I devised a protocol that optimized the purification of GIPCs. GC-MS and HPTLC assays were used to assess GIPC purity. These analyses gave an indication of the (h) VLCFA content which was correlated with GIPC amount, and GIPC series content in the samples.

To investigate more about the characteristic of GIPCs, I performed biophysics assays at the LBMI (Laboratoire Biophysique Moléculaire aux Interfaces), Université de Liège, Gembloux (Laurence Lins and Magali Deleu). I studied the interaction of GIPCs with sterols (both free and conjugated sterols) using Compression Isotherm Langmuir Trough assays. Molecular Modelling using HyperMatrix (HM) was also used to see the different parameters of the interactions. This gave an insight on the specific GIPC/sterol interaction that takes place in nanodomains. By AFM and Nano-IR experiments, performed in Dijon (Eric Lesniewska, Institut Carnot de Bourgogne and Françoise Simon-Plas/Christophe Der, unité Agroécologie), I showed that on supported monolayer containing GIPCs, sitosterol is important for the formation of domain-like structures, which is not the case for stigmasterol and conjugated sterols (SG and ASG).

I also made liposomes with GIPC, to find out that GIPC alone was not able to form membrane bilayer, but made crystals. We further showed that the presence of phospholipids and sterols is required for the formation of liposomes. We were able to make MLVs and GUVs containing GIPCs. Deposited on solid support to form supported lipid bilayer (SLB), these GIPC-containing bilayers were analysed by Neutron Reflectivity to characterize the properties of the bilayer At ILL Grenoble in collaboration with CERMAV laboratory (Yotam Navon, Laurent Heux. The vesicles were also observed under Cryo-EM and different structures were observed depending on the sterol identity. It seems that sterol affects the thickness of membrane containing GIPCs (done on the cryo-EM facilities of CBMN Pessac, Marion Decossas).

Inspired by the study of the effect of phytosterols on phase transition using model membranes (Beck et al., 2007b), I investigated the effect of sterols in the presence of GIPCs on phase transition during change of temperature. The experiments were performed at the IECB with Axelle Grelard and Jean-Paul

Douliez on liposomes containing deuterated POPC, GIPC and sterol (sitosterol or stigmasterol) – see Additional Data of Chapter 1.

The first step of my PhD was to obtain GIPCs pure enough to characterize the molecule, since GIPCs are not commercially available. The chemical synthesis of this molecule is difficult due to the complexity of its structure and the lack of information and studies on the molecule. So my first challenge starting my PhD was to set up a protocol for the scaling up of GIPC extraction and purification. The protocol described in the proposed paper of this chapter is the product of one and a half year of long trial and error to obtain the perfect sequence of steps that give time-efficient reasonable yield. The following is a summary of what did not work on some of the most published GIPC extraction protocols.

After testing the protocols published in recent years, it was clear that most of them were not adequate for purifying large amount of GIPC. One published protocol for GIPC extraction (Mortimer et al., 2013) used plant material incubated in a mix of solvent and ammoniac defined as buffer A (chloroform/methanol/ammoniac/water [10:60:6:24 v/v/v/v]) overnight at 21°C. The next day, after centrifugation, the supernatant was transferred to a weak AEX SPE cartridge (Strata X-AW; Phenomenex). The column was before, equilibrated with methanol. The following series of wash steps were performed using one column volume: chloroform, chloroform/methanol (2:1, 1:1, and 1:2 v/v), and methanol and the cartridge was allowed to dry overnight. While the apolar lipids are washed away, GIPCs bind to the cartridge due to ionic forces. Bound GIPCs were eluted with the buffer A and the elution was dried under a N<sub>2</sub> stream. This protocol although published several times did not work in our hands. The problematic part was that the loading solvent and elution solvent of the SPE column were buffer A, such that almost all lipids were eluted at the first two washes.

I then tried the protocol published by (Blaas & Humpf, 2013). The first step of this extraction procedure was to lyophilize plant material as only the dry mass is treated with solvent during extraction. It was noted that using large amount of plant material, involved finding the right material to lyophilize. Space and material were the limiting factors of this step. Once lyophilized, we proceeded to extracting sphingolipids in 2-propanol/n-hexane/water in a ratio of 55:20:25 (v/v/v) for 1 h at room temperature on a shaker. This extraction solvent was described in (Markham & Jaworski, 2007) and is a classic method of extracting sphingolipids. When mixing lyophilized plant material with the solvent mix, a

slurry mixture was obtained. After filtration under vacuum, the filtrate was again extracted with 2-propanol/n-hexane/water and filtered. A third extraction of the filtrate was performed with chloroform/methanol (2:1, v/v) using an Ultra-Turrax at the highest adjustment for 5 min followed by 30 min on a shaker. The mixture was again filtered, and all filtrates were concentrated. We could not proceed further as, despite all attempts, the filter paper was completely clogged and only a third of the filtrate was collected. This represented a loss of 80% of GIPCs. It seems that once plant material was lyophilized, it became very difficult to extract GIPCs. To compare, extracts of sphingolipids from fresh plant material and lyophilized one using the same solvent mix propanol/n-hexane/water (55:20:25, v/v/v) were compared. The yield of GIPC was slightly higher when non-lyophilized material was used. It appeared that hydration was an important component during extraction.

The extraction process of (Rennie et al., 2014) began with the lyophilization of plant material which was then ground and resuspended in water. Lipids were first extracted with  $\text{CHCl}_3/\text{CH}_3\text{OH}/4\text{M NH}_4\text{OH}$  (9:7:2, v/v/v) with 0.2M  $\text{C}_2\text{H}_3\text{O}_2\text{NH}_4$  at 37°C and centrifuged to separate the organic from the aqueous phase. The top aqueous phase was collected, cooled to -20°C, and then centrifuged again. After centrifugation, the bottom phase was collected as the crude GIPC fraction and dried under a  $\text{N}_2$  stream. This protocol did not work in our hands. After lipid analysis by HPTLC, no GIPC band was detected in the bottom phase fraction. An intermediate phase was also formed after the first centrifugation, making the collect of the top aqueous phase difficult. This once again highlights that lyophilization was not the best option.

The problem with lyophilization could be due to the close interaction of GIPC with the cell wall, such that by removing moisture, the cell wall and GIPCs stick together such that it becomes difficult to extract GIPC afterwards as the material becomes fibrous like paper. The team that studied the interaction of GIPC and cell component rhamnogalacturonan II published an extraction protocol of GIPC (Voxeur & Fry, 2014a). It involved a butan-1-ol/water (1:1) phase partitioning to discard cell wall contaminants in the aqueous phase. The problem arises as we scale up to increase GIPC yield. A thick cloudy intermediate phase is formed containing 90% of total GIPC. We tried adding aqueous hydrochloric acid to break RGII-boron-GIPC bridges as suggested in the publication, however the concentration of aqueous hydrochloric acid used to destroy the boron bond, also breaks the head group of GIPCs. HPTLC analysis showed the appearance of intermediate bands above those of GIPC series A, suggesting the presence of GIPC with cleaved polar heads. An increase of GIPC series A and B at the

expense of polyglycosylated GIPCs, was also observed upon treatment with acid. To avoid compromising the structural integrity of GIPCs, the protocol was abandoned in our purification process.

Inspired from the following publications: (H E Carter & Koob, 1969; Kaul & Lester, 1975; Markham & Jaworski, 2007), the right combination of steps to have an effective yield to purity ratio was set up. The protocol is illustrated in Figure 2. The yield before the purification step is about 85%. Step 3 describes the purification step of GIPCs (according to Kaul and Lester, 1975). It consists of fixing GIPCs on a homemade silica column activated by chloroform. Using two column volumes of chloroform and chloroform/methanol (2:1 v/v), apolar lipids such as sterol, GluCer and phospholipids are discarded as shown in the HPTLC analysis of collected sample, supplementary data S1. Solvent mixtures containing CHCl<sub>3</sub>/MeOH/H<sub>2</sub>O at different volume ratios were prepared and labelled A and B. A linear gradient of solvent A and solvent B is used to eluate the different GIPC series based on their polarity. Eluates containing the same GIPC series are pooled together. For tobacco GIPC for instance, pool  $\alpha$  contains mostly PSL1 GIPC series A,  $\beta$  contains both GIPC series A and B,  $\gamma$  contains mainly series B, C, D, E and F (polyglycosylated GIPCs) (Figure 3).

## **Title: Multiple approaches to study the role of plant sphingolipids GIPC in plasma membrane organization**

*Running title: plant sphingolipids GIPC*

Adiilah Mamode Cassim <sup>1</sup>, Yotam Navon <sup>2</sup>, Minoru Nagano<sup>9</sup>, Yu Gao <sup>3</sup>, Marion Decossas<sup>4</sup>, Laetitia Fouillen<sup>1</sup>, Pierre Van Delft<sup>1</sup>, Claire Bréhélin<sup>1</sup>, Jean-Paul Douliez <sup>5</sup>, Françoise Simon-Plas <sup>7</sup>, Eric Lesniewska <sup>6</sup>, Laurent Heux <sup>2</sup>, Lilly Maneta-Peyret<sup>1</sup>, Jenny Mortimer <sup>3</sup>, Magali Deleu <sup>8</sup>, Laurence Lins <sup>8</sup>, Sébastien Mongrand<sup>1\*</sup>

1, Laboratoire de Biogénèse Membranaire, UMR 5200, CNRS, Université de Bordeaux, 71 Avenue Edouard Bourlaux, 33883 Villenave d'Ornon Cedex, France

2, Centre de Recherches sur les Macromolécules Végétales (CERMAV), Univ. Grenoble Alpes, CNRS F-38000 Grenoble, France

3, Joint BioEnergy Institute, Emeryville, California 94608; Biological Systems and Engineering, Lawrence Berkeley National Laboratory, Berkeley, California 94720; Department of Chemical and Biomolecular Engineering, University of California, Berkeley, California 94720

4, Institute of Chemistry & Biology of Membranes & Nanoobjects (UMR5248 CBMN), CNRS, Univ. Bordeaux, Institut Polytechnique Bordeaux, All. Geoffroy Saint-Hilaire, 33600 Pessac, France

5, Biologie du Fruit et Pathologie UMR 1332 INRA, Univ. Bordeaux, 71 Avenue Edouard Bourlaux, 33883 Villenave d'Ornon Cedex, France

6, Institut Carnot de Bourgogne, Centre National de la Recherche Scientifique, UMR 5209, Univ. Bourgogne, Faculté Sciences Mirande, Dijon, France

7, Agroécologie, AgroSup Dijon, INRA, Univ. Bourgogne Franche-Comté, F-21000 Dijon, ERL 6003 CNRS, Dijon, France

8, Laboratoire de Biophysique Moléculaire aux Interfaces, Université de Liège, B-5030 Gembloux, Belgium

9, College of Life Sciences, University of Ritsumeikan, 56-1 Tojiin Kitamachi, Kita Ward, Kyoto, Japan

- Corresponding author : [sebastien.mongrand@u-bordeaux.fr](mailto:sebastien.mongrand@u-bordeaux.fr)

## **Abstract**

Plant PM is an essential barrier between the cell and the external environment. PM is stable but adaptable, crucial for signal perception and transmission. It consists of an asymmetrical lipid bilayer made up of three different classes of lipid: sphingolipids, sterols and phospholipids. The most abundant sphingolipid in plant PM is GlycosylInositolPhosphorylCeramide (GIPC) representing up to 50-60% of total sphingolipids in plants. GIPCs are assumed to be almost exclusively in the outer leaflet of the PM. In this study, we investigate the structure of GIPC and its role in membrane organization. Since GIPCs are not commercially available, we develop a protocol to extract and isolate GIPC-enriched fractions from eudicots (cauliflower and tobacco) and monocots (leek and rice). Lipidomic analysis confirmed the presence of different GIPC series containing mostly h24/t18:1 as the most abundant ceramide. The glycan head groups of the different GIPC series from monocots and dicots were analyzed showing different sugar components. Biophysics tools such as Langmuir, AFM and molecular modelling were used to investigate the physical properties of GIPC and its interaction with free and conjugated phytosterols. We demonstrate the importance of molecular structure in these interactions. We showed that GIPC increases the thickness and electronegativity of model membrane through different complementary approaches

## **Keywords:**

Plant PM, GIPC, biophysics, phytosterol, extraction, lipidomic, glycan group, molecular modelling, Atomic Force Microscopy, Langmuir, neutron reflectivity

## Introduction

The plant plasma membrane model is made up of an asymmetric distribution of lipids and proteins. There are three main classes of lipids: phytosterols, sphingolipids and phospholipids with a great level of molecular complexity, see (Cacas et al., 2016a) (Yetukuri, Ekroos, Vidal-Puig, & Orešič, 2008). In plants, the major sphingolipid is Glycosyl Inositol Phosphoryl Ceramide (GIPCs). GIPCs, in plant and fungi were discovered during the 1950's (CARTER, GIGG, LAW, NAKAYAMA, & WEBER, 1958). They are composed of a ceramide moiety and a glycan polar head group. The structural diversity of GIPCs also lies in the hydroxylation, degree and position of saturation of their fatty acid chain and LCB (Pata, Hannun, & Ng, 2010). Plant GIPCs consist mainly of an LCB t18:0 (trihydroxylated saturated LCB of 18 carbon atoms) or a t18:1 (trihydroxylated and monounsaturated LCB of 18 carbon atoms) amidified to a Very Long Chain Fatty Acid (VLCFA) or 2-hydroxylated VLCFA (hVLCFA) (Cacas et al., 2016a)(Buré et al., 2011). The presence of VLCFA increases the hydrophobicity of sphingolipids, likely important for the interdigitation with the inner leaflet as described from animal gangliosides (Manna et al., 2017). In the plant PM, 95% of VLCFA and hVLCFA are amidified to a LCB to make GIPC (Cacas et al., 2016a).

GIPCs are classified into series based on degree of glycosylation of their polar head group (Buré et al., 2011). The head group of GIPC consists of a phosphate linked to an inositol to which glycan moieties are bound. The basic structure of the GIPC's polar head is an inositol phosphoryl ceramide (IPC) backbone linked to a glucuronic acid (GlcA). GIPC series A with 2 sugars is defined as a sugar unit bound to the GlcA-IPC form (Buré et al., 2011). In the 1960s, the first characterization of GIPC structure was made in tobacco plant (Hsieh, Lester, & Laine, 1981; Kaul & Lester, 1978). In order to do so, they used hundreds of kilograms of plant materials and litres of solvents to extract GIPC. They fully resolved the exact number and type of sugars as well as the nature of the sugar

bond. For instance, GIPC series A of tobacco, has the most basic known structure:  $\text{GlcNAc}(\alpha 1 \rightarrow 4)\text{GlcA}(\alpha 1 \rightarrow 2)\text{inositol-1-O-phosphorylceramide}$ . Additional sugar moieties such as glucosamine (GlcN), N-acetyl-glucosamine (GlcNAc), arabinose (Ara), galactose (Gal) and mannose (Man) may lead to glycan patterns of three to seven sugars, so-called GIPC series B to F. GIPC found in corn seeds and *Erodium* display branched polar heads, see for review (Sperling & Heinz, 2003)(Buré, Cacas, Badoc, Mongrand, & Schmitter, 2016). GIPC series are species- and tissue- specific. In *Arabidopsis*, series A Man-GlcA-IPC is predominant in leaves (Buré et al., 2014, 2011), whereas GlcN(Ac)-GlcA-IPC are mainly in seeds and leaves, as well as in cultured tissues of rice and tobacco (Buré et al., 2011; Nagano et al., 2012; Tellier, Maia-Grondard, Schmitz-Afonso, & Faure, 2014). In monocots, the predominant GIPC series is series B (Buré et al., 2011). Nevertheless, their core structures are yet to be deciphered. A broad study of the GIPC polar head of 23 plant species from algae to monocots further showed that polar head structures are largely unknown and versatile for the different biological taxa (Cacas et al., 2013). Kaul and Lester calculated the ratio between carbohydrate/LCB/Inositol in purified polyglycosylated GIPCs and showed that GIPCs may contain up to 19–20 sugars (Kaul & Lester, 1975). The polar head is responsible for the high polarity of the GIPC, accounting for its insolubility in traditional lipid extraction solvents, such as chloroform/methanol. GIPCs, although being one of the fundamental component of the plant PM model is hardly studied due to its absence on the commercial market. The old published protocols used quite a lot of material involving litres of solvents, which is not feasible in modern labs. More recently published protocols did not yield enough pure material for characterization. In this project, we devise a new protocol to obtain GIPC-enriched samples from plants of different clades, monocots and eudicots. The aim being to study the structure of GIPC and its role in PM organization.

Multiple studies have suggested the presence of GIPC in nanodomains (Cacas et al., 2016a; Markham et al., 2011). Lipid domains are lateral partitioning; due

to the different lipid, molecular species are unhomogeneously distributed within lipid bilayers. The lateral segregation observed in plant PM might be due to differential phase behaviours of different lipid species (Sampaio et al., 2009). They were reported in model membrane using biophysical approaches and super resolution microscopy (Levental & Veatch, 2016). Lipid domains or liquid-ordered (Lo) phases are formed from saturated phospholipids and sphingolipids in the presence of cholesterol, while liquid-disordered (Ld) phases are formed mainly from unsaturated phospholipids (Baumgart, Hunt, Farkas, Webb, & Feigenson, 2007; Lingwood & Simons, 2010). In Lo phases, the high degree of conformational order is imposed on the acyl tails of lipids by the rigid ring structure of cholesterol. This increases the thickness of the lipid bilayer and lipid packing, although lipids remain laterally mobile (Mannock, Lewis, McMullen, & McElhaney, 2010). Sterols and sphingolipid/sterol interactions have recently been reported as important determinants of lipid partitioning and organization within membranes (Beck, Mathieu, Loudet, Buchoux, & Dufourc, 2007a; Gerbeau-Pissot et al., 2014b; Grosjean, Mongrand, Beney, Simon-Plas, & Gerbeau-Pissot, 2015a). In its huge lipid diversity, plant PM contains of 30–50% phospholipids, 20–50% sterols, and 6–30% sphingolipids, depending on plant species and organs (Furt, Lefebvre, Cullimore, Bessoule, & Mongrand, 2007). Higher plant species contain a wide range of sterols (free and conjugated) whereby sitosterol, stigmasterol, and campesterol often predominate (Moreau et al., 2018). These phytosterols play significant roles in regulating the order level of the membrane such that ternary mixtures (sterol/sphingolipid/saturated PC) have a lesser temperature sensitivity to thermal variations compared to system mimicking lipid rafts of animal and fungi (Beck et al., 2007a). Sitosterol was shown to have the most important effect in lipid ordering (Beck et al., 2007a; Cacas et al., 2016a; Grosjean et al., 2015a). Conjugated form of sitosterol and stigmasterol is proposed as reinforcing the membrane cohesion by additional attractive van der Waals interactions with the acyl chains of sphingolipids and phospholipids (Beck et al., 2007a). To measure the order level of the leaflets,

the most prominent tools are environment-sensitive probes. Di-4-ANEPPDHQ marks the lipid bilayer with its chromophore, which is aligned to the surrounding tails of the lipid molecules and its head group oriented toward lipid polar heads. Membrane packing around the dye molecules affects its emission spectrum, by sensing exposure to level of hydration of the lipid bilayer (Jin, Millard, Wuskell, Clark, & Loew, 2005; Jin et al., 2006). This probe was used in various studies to show that the spatial distribution of the order level of membrane areas by ratiometric analysis of the green to red emission spectrum (Gerbeau-Pissot et al., 2014a; Grosjean et al., 2015a). It was shown that various phytosterols have the ability to modulate the proportion of  $L_0$  phases and membrane heterogeneity, with the notable exception of stigmasterol. Thus, GIPCs in synergy with sterols may organize and promote large ordered domains such that both have important roles in PM subcompartmentalization and membrane dynamics (Grosjean et al., 2015a).

In this study, we set up a protocol to obtain GIPC enriched samples so as to obtain enough materials for the physical characterization of the molecules. Using biophysics tools such as Langmuir trough, molecular modelling, atomic force microscopy, supported lipid bilayers, GUVs, dynamic light scattering, zeta-potential, cryo-EM and neutron reflectivity, we aim to uncover the role of GIPCs in model membrane structuring in synergy with sterols.

## Results

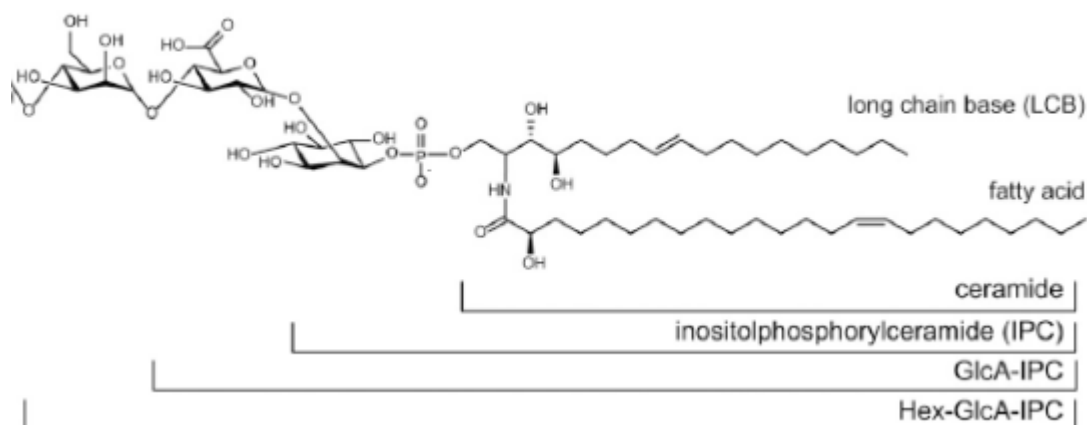
### Extraction and Purification of GIPC-enriched fractions from different plant species tissue and cell culture

The structure of GIPC is illustrated in Figure 1A. The main GIPC molecule has a ceramide with a t18:1 or t18:0 as LCBs which is amidified by a hVLCFA of about 24 carbon as the acyl chain. The ceramide is attached to a head group with a phosphoryl group, a glucuronic acid and several sugar moieties such as GlucA, GlucNAc, Man, etc. The head group defined the different GIPC series dependant on the plant species and tissues. Previous papers of Buré et al, 2014 and Cacas et al, 2016 have shown the diversity of GIPC in plants (Buré et al., 2014; Cacas et al., 2016b). Eudicots contain main GIPC series A with two sugar moieties, while monocots contain GIPC series B mainly, with three sugar as polar head group (Buré et al., 2014).

GIPC are not commercially available. In order to purify large amount of GIPCs, we first appreciate the amount of GIPCs by quantifying the non-hydroxylated and 2-hydroxylated (h)VLCFA, diagnostic of plant's GIPC (Cacas et al., 2016a). Because milligrams of material were needed for the characterization of GIPCs, we choose plant tissues abundantly available to give the highest yield. Four species were selected: Cauliflower head (*Brassica oleracea*) and tobacco cell culture Bright-Yellow 2 (BY-2) which are eudicots, as well as leek white leaves (*Allium porrum*) and rice cell culture (*Oryza sativa*) which are monocots. White part of plant tissues and cell cultures were used to avoid contamination by abundant chloroplastic lipids and pigments. Cauliflower and rice cell culture have the highest GIPC content with an estimated 4.3 mg and 3.4 mg per fresh weight respectively (Figure 1B). Leek has the least amount of GIPC with a mean estimated content of 0.4 mg/ml per fresh weight.

GIPCs were extracted from each material to get a diverse GIPC series pool for characterization. In order to maximize the yield, several trials were performed to test the different published protocols of GIPCs ((L. Fang et al., 2016). Steps from three protocols were sequenced to obtain the best yield of GIPC. These protocols were extracted from (H E Carter & Koob, 1969), (Markham & Jaworski, 2007) and (Kaul and Lester, Plant Physiol. 1975). Figure 2 shows the extraction and purification process to obtain GIPC-enriched fractions of cauliflower (Bo-GIPC), tobacco culture cell BY-2 (Nt-GIPC), leek (Ap-GIPC) and rice (Os-GIPC). Some fine-tuning was done to maximize

A



B

		Plant Species	Estimated GIPC by (h)VLCFA content (mg/g fw)	Main GIPC series as per Cacas et al., 2016
Eudicots	Plant (white part)	<i>Brassica oleracea</i> (n=5)	4.3 ± 0.9	A
	Cell culture	<i>Nicotiana bentamiana</i> (BY-2) (n=3)	0.6 ± 0.2	A B C D E F
Monocots	Plant (white part)	<i>Allium porrum</i> (n=3)	0.4 ± 0.1	B
	Cell culture	<i>Oryza sativa</i> (n=3)	3.4 ± 0.2	B

**Figure 1. A. GIPC structure** of series A (2 sugar after the inositol group)

**B. GIPCs content of different plant species:** *Brassica oleracea* (cauliflower), *Nicotiana tabacum* (BY-2 cell culture), *Allium porrum* (leek) and *Oryza sativa* (rice cell culture). The GIPC content in mg per g of fresh weight was estimated by calculating the plant sample (h)VLCFA (hydroxylated Very Long Chain Fatty Acid) from FAMES content by GC-MS. The type of GIPC was defined by HPTLC analysis based on Cacas et al., 2016. Three to five independent samples were processed.

**Extraction process of sphingolipid    Purification process of GIPCs**

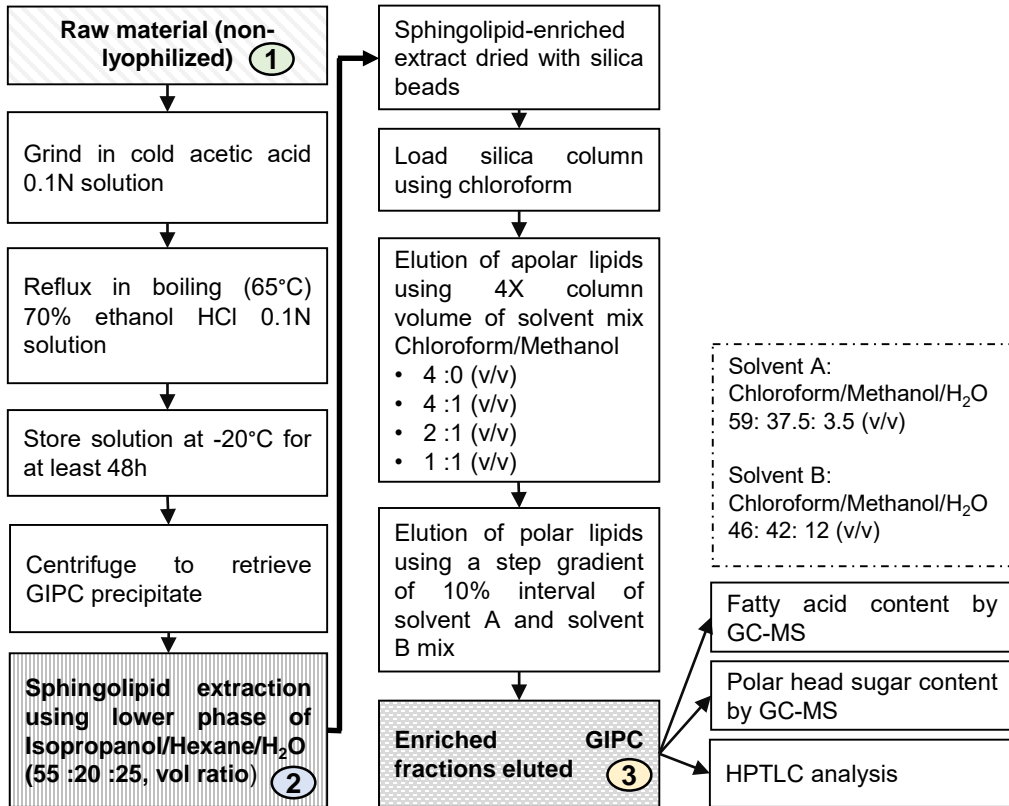


**Figure 2. Extraction and purification protocols of GIPCs.** GIPC purification scheme, adapted from Carter & Koob, Kaul & Lester and Markham et al.. The three steps labelled 1, 2 and 3, respectively are important milestones in the GIPC isolation steps.

the yield such as refluxing in boiling ethanol for 20 min and using large lab-made silica column to process several hundreds of grams of material, see Material and Methods. The column chromatography was performed by depositing on the packed column the sphingolipid extract directly dried in silica. The column was then washed by 4 volumes of column using a mix of chloroform/methanol with increasing polarity to get rid of sterols, glucosylceramide and phospholipids. For the elution of GIPCs, a step gradient of two solutions with different volume ratio of chloroform/methanol/water was used (Figure 2). Hence, molecules of increasing polarity are eluted in the last fractions. All washed and eluted fractions were collected and analysed by High Performance Thin Layer Chromatography (HPTLC) as shown in Supplementary data 1. The HPTLC protocol used for lipid migration allows the clear separation of sterols, phospholipids and GIPC series. HPTLC is a quick and reliable way to select fractions containing GIPCs with few sterol and phospholipid contamination. To check the quality and quantify GIPCs, samplings were done at steps labelled 1, 2 and 3. These steps were key to determine the success of the extraction and purification protocol.

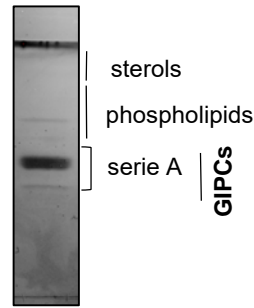
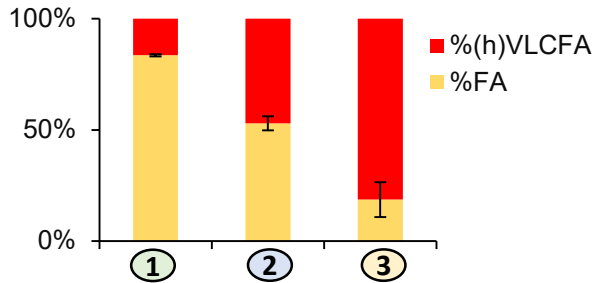
### **Fatty acid and sugar content of GIPC-enriched fractions**

To estimate the GIPC content and the amount of contamination by phospholipids (containing medium chain 16-18 carbon atom FA), samples were trans-esterified in hot methanol/sulfuric acid solution to release both fatty acid-esterified glycerolipids and fatty acid-amidified sphingolipids. The samples were then derivatized in hot BSTFA-TMCS. Gas Chromatograph-Mass Spectrometry (GC-MS) using C17 and h14 as internal standards, quantified total fatty acid content as internal standards. The percentage of fatty acid with medium chain length (%FA) and (hydroxylated) very long chain length %(h)VLCFA was calculated from 2 to 3 independent experiments. Samples after step 1 (raw plant material), step 2 (sphingolipid extract) and step 3 (GIPC-enriched fractions), were analysed for their fatty acid content at each step (Figure 3A). As we proceeded through the purification steps, it can be noted that the amount of medium chain FA decreased as the amount of (h)VLCFA increased (Figure 3A), the latter being correlated to an increase in sphingolipid more precisely GIPCs as shown by high performance chromatography assay (HPTLC) (Figure 3B). At step 2, the percentage of (h)VLCF in the sphingolipid extract was around 50%

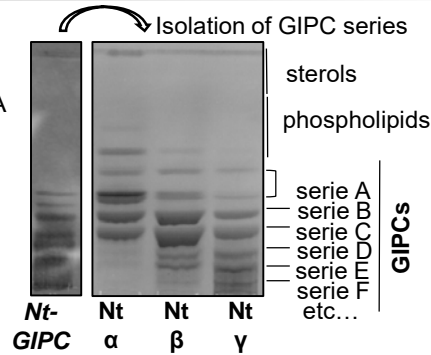
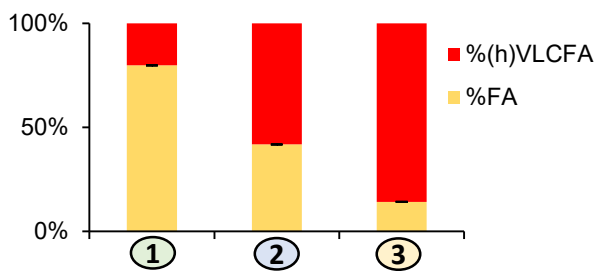
## A. GC-MS analysis of FAMES

## B. HPTLC assay of lipid content

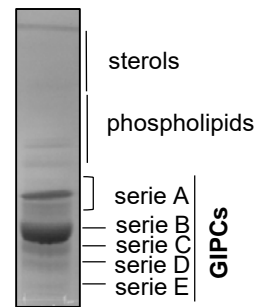
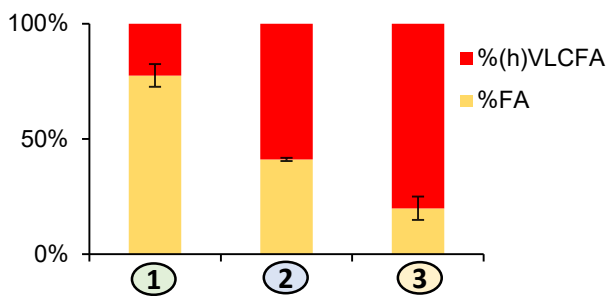
### I. *Bo*-GIPC (cauliflower)



### II. *Nt*-GIPC (BY-2)



### III. *Ap*-GIPC (leek)



### IV. *Os*-GIPC (rice)

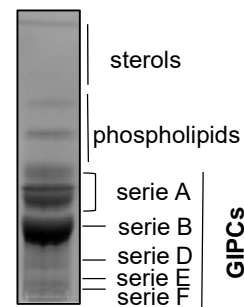
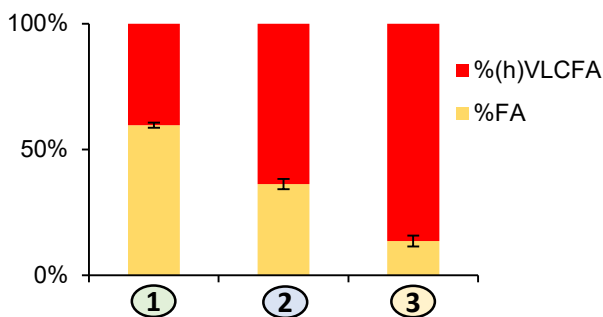


**Figure 3. Gas Chromatography- Mass Spectrometry (GC-MS) analysis of fatty acid content (A) and High Performance Thin Layer Chromatography (HPTLC) assay of lipid content (B) after steps  $\alpha$ ,  $\beta$  and  $\gamma$  of the extraction and purification process (see Figure 2).**

A. Aliquots of (I) *Bo*-cauliflower, (II) *Nt*-BY-2, (III) *Ap*-leek and (IV) *Os*-rice samples at step 1,2 and 3 underwent trans-methylation to release fatty acid before derivatization by BSTFA, the resulting FAMES were analysed by GC-MS and the fatty acid content calculated (n=3). FA refer to fatty acid of 16 to 18 carbon atoms fatty acids and (h)VLCFA refer to hydroxylated or non-hydroxylated very long chain fatty acid of 20 to 28 carbon atoms. The amount of GIPC in each sample were extrapolated from the (h)VLCFA content. Data shown for 3 independent replicas  $\pm$  SD. B. HPTLC assay shows the lipid content of GIPC-enriched samples after step 3. Cauliflower (I) contains mainly GIPC series A, BY-2 (*Nt*-GIPC) sample were further separated by column chromatography to isolate the different GIPC series. *Nt* (1) GIPC-enriched sample contains mainly series A, B and C while *Nt* (2) and *Nt*(3) show presence of polyglycosylated GIPCs (series D, E ,F, etc). Leek (III) and rice (IV) samples contain mainly GIPC series B.

and at the final step, the amount of (h)VLCFA was at about 80% for all GIPC-enriched extract (Figure 3A). The detailed FA composition of the GIPC-enriched fractions of all four species is provided in supplementary data 2. It was estimated that the enrichment in GIPC between the first and last step of the extraction and purification process, was 5-fold for Bo-GIPC, 4.2-fold for Nt-GIPC, 3.6-fold for Ap-GIPC but only 2-fold for Os-GIPC.

The GIPC-enriched samples were analysed by HPTLC to verify the lipid component present in the fractions. Bands on TLC plate clearly showed the predominant GIPCs present in the samples. Only traces of sterols and phospholipids were observed, and Glucosylceramide was not detected. As reported in (Buré et al., 2011), eudicots contained mainly series A, monocots series B and plant cell culture a mix of GIPCs with highly glycosylated ones. Bo-GIPC enriched fraction contained one major band of GIPC series A. Nt-GIPC fraction contained GIPC series A to F, with two bands of series A closely packed together, representing PSL1 (with N-acetyl glucosamine) and PSL2 (with glucosamine) of GIPC series A as described in (Kaul & Lester, 1975) (Figure 3B). These fractions were a pool of three fractions Nt-GIPC (fraction  $\alpha$ ), Nt-GIPC (fraction  $\beta$ ) and Nt-GIPC (fraction  $\gamma$ ). These fractions were collected after elution of step 3 and clearly showed the presence of polyglycosylated GIPC in Nt-GIPC (fraction  $\beta$ ) and Nt-GIPC (fraction  $\gamma$ ) enriched-fractions (Figure 3B). As expected, Ap-GIPC enriched fraction contained mainly GIPC series B, same for Os-GIPC enriched which contained also slight presence of series A and polyglycosylated GIPCs (Figure 3B).

The GIPC predominantly present in GIPC-enriched fractions contained different (h)VLCFA species depending on the sample. It appeared that the Bo-GIPC enriched fraction consisted in h24, h24:1 and h26 as main fatty acyl chain. Nt-GIPC enriched fractions contained GIPC with h24, h22, h23 and h25 acyl chain. Ap-GIPC enriched fractions had C24, h24, h22 and C22 as main acyl chain. Lastly, Os-GIPC enriched fraction consisted of GIPC with C24, C22, C20 and h24 as main fatty acids (Figure 4A).

We also investigated the sugar moieties present in GIPC-enriched fractions from both the monocots and eudicots samples by High performance anion exchange chromatography (HPAEC) with pulsed Pulsed Amperometric Detection (PAD), a

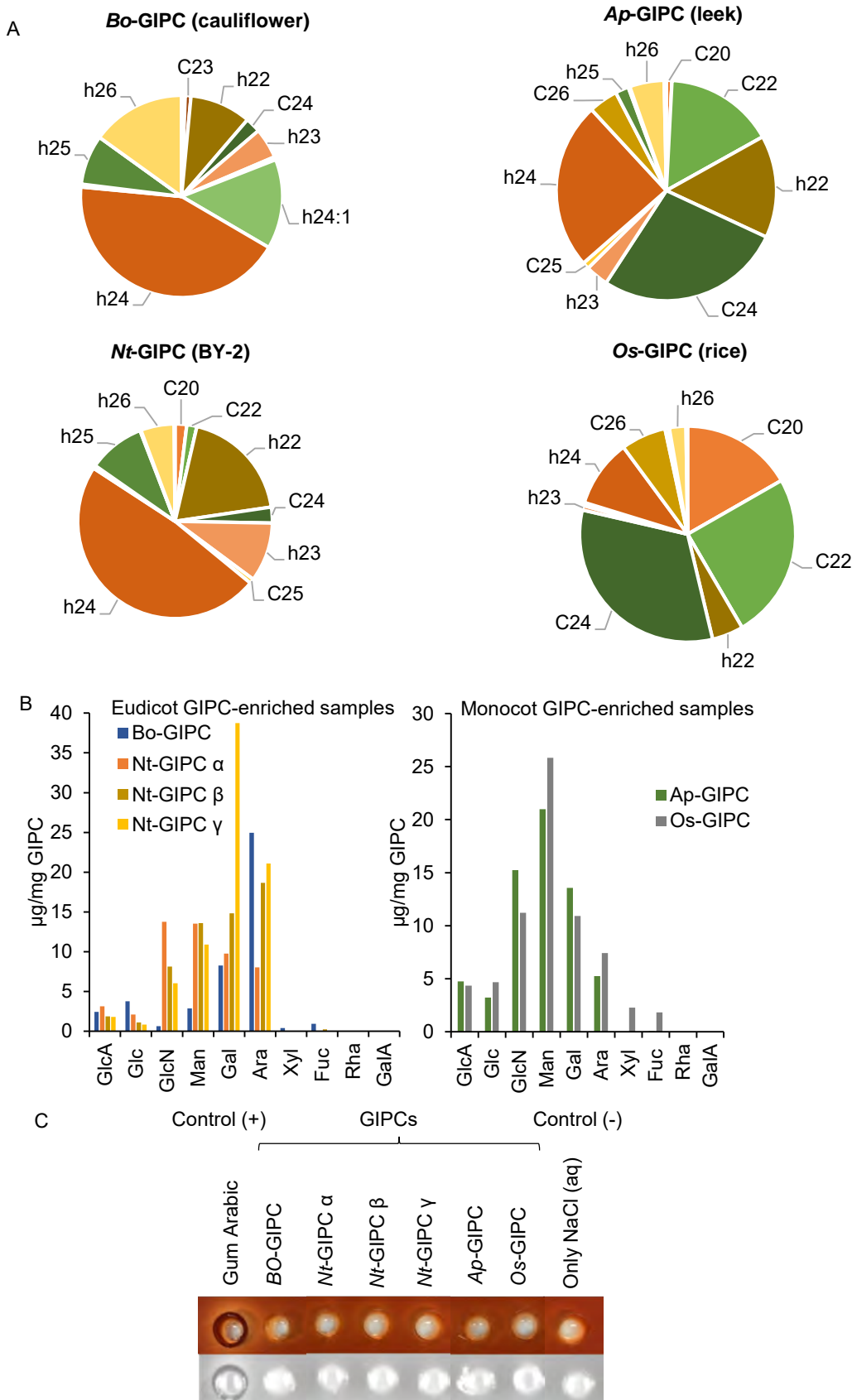


**Figure 4.** A. Very long-chain fatty acid (VLCFA) and hydroxylated VLCFA (hVLCFA) content of GIPC enriched samples from cauliflower, BY-2 cell culture, leek and rice cell culture. The fatty acids were released from the GIPC enriched samples by transmethylation followed by derivatization using BSTFA, before GC-MS analysis. B. HPAEC analysis of GIPC-enriched samples shows glycan content after TFA hydrolysis. Abbreviations are as followed: GlcA: glucuronic acid; Glc: glucose; GlcN: glucosamine; Man: mannose; Gal: galactose; Ara: arabinose; Xyl: xylose; Fuc: fucose; Rha: rhamnose; GalA: galacturonic acid. C. Yariv reactivity test of GIPC-enriched samples to detect arabino-galactanes (AGPs) content. No AGPs were detected. 50µg of each sample (1mg/ml) was deposited in each well, the picture was taken 48h after initiating the reaction.

technique used to measure carbohydrate (Figure 4B). As a control, to ensure that sugar content was not damaged by hydrolysis during sample preparation, the sugar content for BO-GIPC enriched fraction was analysed 1h, 3h and 4h after hydroxylation. Results showed that hydrolysis has no to very little effect on sugar moieties of GIPC fractions (Supplementary data 3).

As expected all GIPC-enriched fraction contained Glucuronic acid and inositol found in all GIPC previously characterized [see for review, (Mamode Cassim et al., 2019)]. Bo-GIPC enriched fraction not only contains Glucose (Glc) and mannose (Man) previously found in Brassicaceae species (L. Fang et al., 2016), but also large amount of arabinose (Ara) and galactose (Gal). These latter sugars, never described in Brassicaceae such as Arabidopsis, could be a real specificity of Bo-GIPC's polar head, or a cell wall contamination of the GIPC-enriched fraction, see below.

The different fractions of Nt-GIPC series have a complex glycan content. Nt-GIPC (fraction  $\alpha$ ) contained glucuronic acid (GlcA), glucosamine (GlcN) and mannose (Man) (Figure 4B). Note here that N-acetyl glucosamine is hydrolysed during the extraction procedure and is mixed with glucosamine. Galactose (Gal) and arabinose (Ara) became the main glycan moieties in fractions  $\beta$  and  $\gamma$  as described for highly glycosylated GIPC, series D and further, in (Kaul & Lester, 1978). Monocot GIPC-enriched sample, both Ap-GIPC and Os-GIPC contained mainly Man, Gal and GlcN at relatively same amount, GlcA and Arabinose at lower amount (Figure 4B).

From previous studies, GIPC seems to be in close contact with the cell wall components and particularly Rhamnogalacturonan II, RGII (Voxeur & Fry, 2014b), but we did not detect neither galacturonic acid (GalA) and rhamnose (Rha), two main component of pectins, suggesting no major pectin contamination (Figure 4B). But we detected a large amount of arabinose and galactose (Figure 4B) so we performed a Yariv test to check out for the presence the arabino-galactane (AG) as contaminants in the GIPC-enriched fractions (Figure 4C). No clearance of the zone was observed in the different samples in the Yariv reactivity test (Kitazawa et al., 2013), suggesting no AGs in the 50  $\mu$ g of each sample deposited in the well. Gum Arabic and saline buffer were used as control (Figure 4C). The contamination by protein was also tested by Bradford.

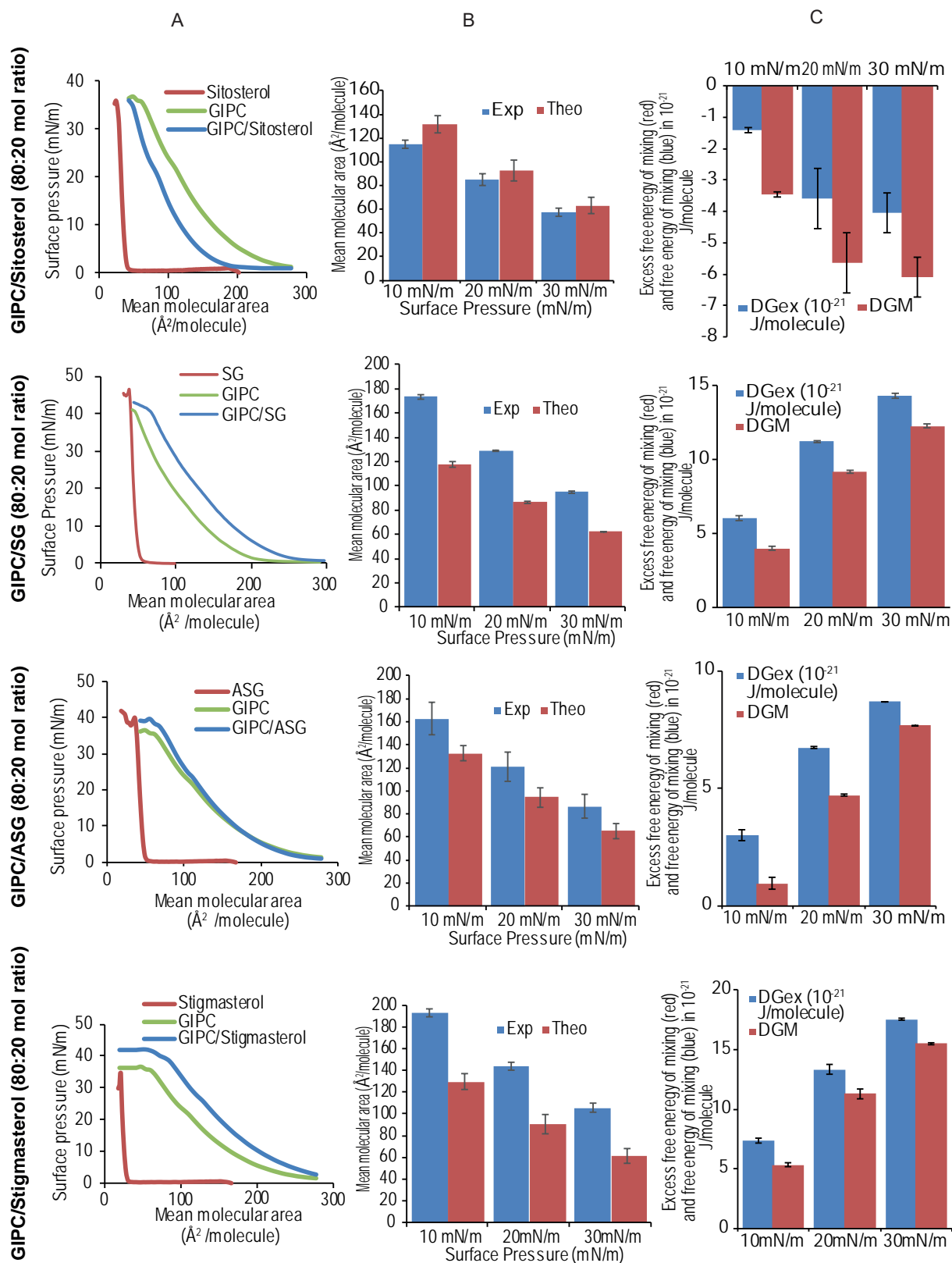


**Figure 5: Surface pressure-area (P-A) isotherms, at the air-aqueous phase interface, of pure GIPC and sterol monolayers and of mixed GIPC/sterol monolayer prepared at a molar ratio of 0.80.** A, The isotherms were recorded at 25°C in an aqueous subphase composed by 10 mM Tris buffer at pH 7. Duplicate experiments using independent preparations yielded similar results. B, Comparison of the experimental (blue bars) and theoretical (red bars) mean molecular areas at a surface pressure of 10, 20, and 30 mN/m<sup>2</sup> for a GIPC/sterol molar ratio of 0.80. The theoretical value is obtained according to the additivity rule:  $A_{12} = A_1X_1 + A_2X_2$ , where  $A_{12}$  is the mean molecular area for ideal mixing of the two components at a given P,  $A_1$  and  $A_2$  are the molecular areas of the respective components in their pure monolayers at the same P, and  $X_1$  and  $X_2$  are the molar ratios of components 1 and 2 in the mixed monolayers. C, Excess free energy of mixing (DGex; blue bars) and free energy of mixing (DGM; red bars) of the mixed monolayer GIPC/sterol at a molar ratio of 0.80 for various surface pressures. DGex and DGM were calculated according to the equations as shown in (Maget-Dana, 1999; Eeman et al., 2005). Abbreviations are as follows: SG, steryl glucoside (sitosterol, glucose head group); ASG, acyl steryl glucoside (sitosterol, glucose head group with C18:2 acyl chain)

Up to 30  $\mu\text{g}$  of GIPC were tested by Bradford method and no protein was detected (data not shown).

### **Biophysical characterisation of GIPC-Sterol interaction and molecular modelling**

The Langmuir trough compression technique applied on a monolayer model at the air-water interface has been used extensively to characterize the lipid-lipid interactions at the micrometric level (Deleu et al., 2014). As previously published in (Cacas et al., 2016a), the biophysical characteristic of GIPC series A alone or together with sitosterol was conducted and the energetic calculations suggested a preferential interaction of GIPC with sitosterol defined as 'cooperative effect'. We went further in our investigation of the characterization of the interaction of Bo-GIPC (cauliflower) with phytosterols by conducting biophysical experiments to characterize the outer leaflet organization with free and conjugated sterols (SG, sitoSteryI Glucoside and ASG, Acyl (18:2) sitoSteryI Glucoside). The ratio of GIPC:sterol (80:20 mol ratio) is conform to the estimated ratio of the lipids in the outer leaflet of the PM (Cacas et al., 2016a)(Tjellstrom et al., 2010). The compression isotherm of Bo-GIPC (green line) (Fig. 5A) shows a low and relatively constant surface pressure in large molecular areas, corresponding to a 'gaseous' state. Compression of a monolayer with purely GIPC (green line) induced a progressive increase in surface pressure, indicating the appearance of a liquid-expanded state, which is characterized by a certain degree of cooperative interaction between the molecules at the interface (Fig. 5A). The two-dimensional compressibility modulus ( $C_s^{-1}=38.3 \text{ mN m}^{-1}$  in the 160- to 110-  $\text{\AA}^2$  per molecular region). The mean interfacial area of Bo-GIPC is  $212.9 \pm 4.9 \text{ \AA}^2$  at its expanded form and at its most condensed form is  $60.0 \pm 14.6 \text{ \AA}^2$ . These results are in agreement with the results obtained with BY-2 GIPC (Cacas et al., 2016b).

The interaction of Bo-GIPC mixed with different sterols was assessed by the thermodynamic analysis of the compression isotherms of mixed GIPC-sterol monolayers. In this comparative study, we adhere to the rule of additivity, which suggests that if two molecules within a mixed monolayer are immiscible, the area occupied by the mixed film will be the sum of the areas of the separated components.

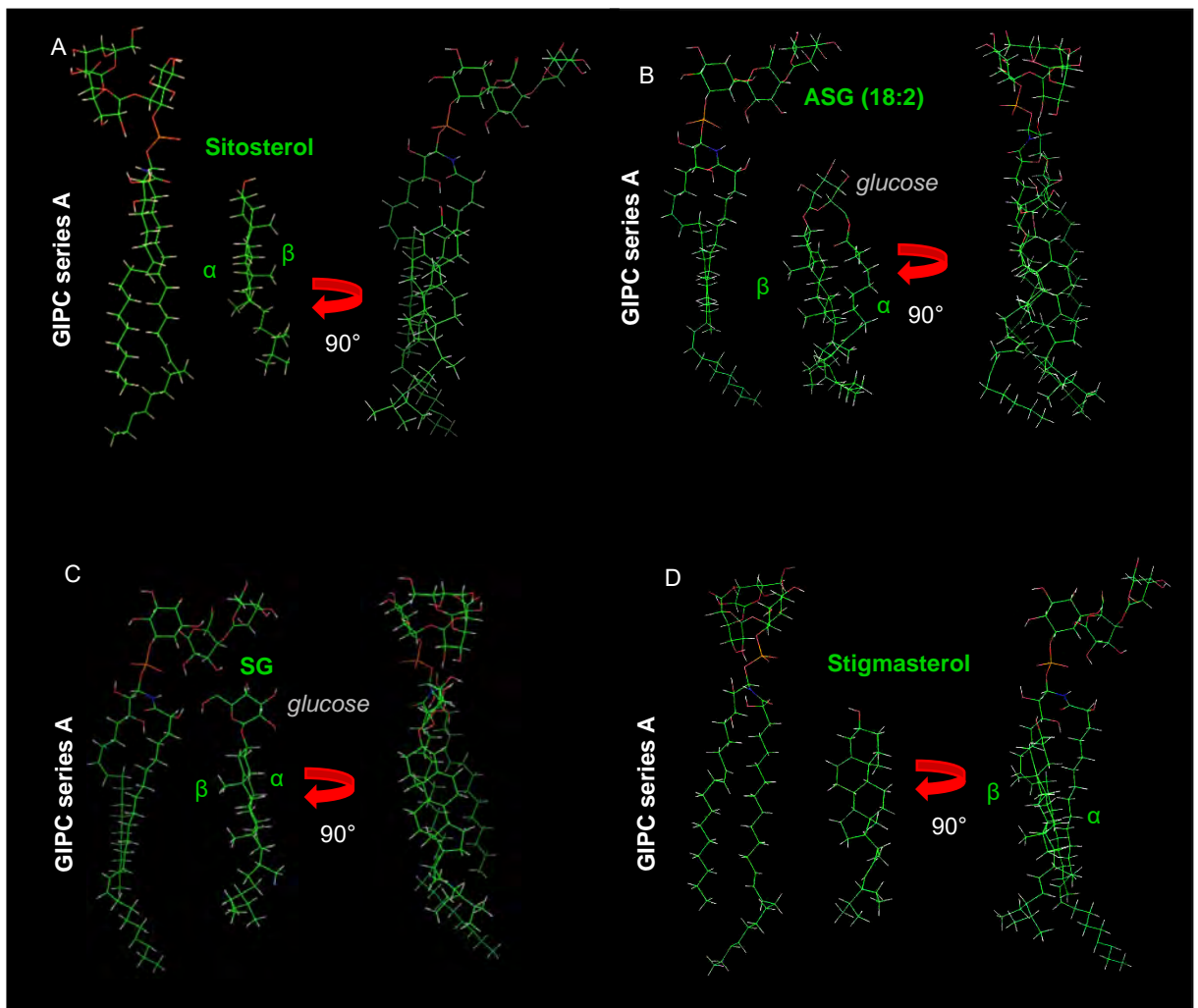


**Figure 6: Hypermatrix Modeling interaction of GIPC and sterols.** Theoretical interactions calculated by HyperMatrix method with one molecule of GIPC serie A t18:0/h24:0 and one molecule of either A, sitosterol, or B, Acyl Steryl Glucoside, ASG (sitosterol, with glucose head group/18:2 acyl chain), or C, Steryl Glucoside, SG (sitosterol, with glucose head group), or D, stigmasterol

The only deviation to that rule is in the case of specific interaction between the two molecules (Maget-Dana, 1999). The mean molecular area of the mixed monolayer Bo-GIPC:sitosterol (80:20) was lower than the calculated theoretical value (using the rule of additivity), irrespective of the considered surface pressure (10, 20 and 30 mN m<sup>-1</sup>) (Figure 5B). This cooperative effect of sitosterol in presence of Bo-GIPC confirms the data in Cacas et al., 2016 with tobacco GIPCs.

The trend was however reversed for mixed monolayer Bo-GIPC:SG (80:20), Bo-GIPC:ASG (80:20) and Bo-GIPC:stigmasterol (80:20), where the mean molecular area is significantly higher than the theoretical value irrespective of the surface pressure (Figure 5B). The most significant difference between the experimental and theoretical mean molecular area was obtained for the mixed monolayer Bo-GIPC:stigmasterol (80:20). It is interesting to note that the only structural difference between sitosterol and stigmasterol is the presence of a double bond at C22 in stigmasterol. The mixed monolayer GIPC:ASG (80:20) had a comparable mean molecular area to GIPC molecule at low surface area (Figure 5A) and the average difference between the mean molecular area and its theoretical value is 30 Å<sup>2</sup> per molecule for all three surface pressures (Figure 5B). We calculated the compressibility modulus to evaluate the stability of the mixed lipid monolayer. The compressibility modulus is the inverse of the monolayer elasticity. The two-dimensional compressibility modulus for the mixed monolayer of GIPC/sitosterol is,  $C_s^{-1}=32.4 \pm 0.74$  mN m<sup>-1</sup> in the 120- to 90 Å<sup>2</sup> per molecular region, for GIPC/stigmasterol  $C_s^{-1}=28.1 \pm 0.02$  mN m<sup>-1</sup> in the 160- to 140 Å<sup>2</sup> per molecular region, for GIPC/SG  $C_s^{-1}=28.6 \pm 0.09$  mN m<sup>-1</sup> in the 150- to 110 Å<sup>2</sup> per molecular region and for the mixed monolayer of GIPC/ASG is  $C_s^{-1}= 27.14 \pm 0.24$  mN m<sup>-1</sup> in the 140- to 120 Å<sup>2</sup> per molecular region. The lower the compressibility modulus, the higher is the interfacial elasticity, and consequently, the lower is the monolayer stability. There is not much difference between the compressibility modulus of GIPC/stigmasterol, GIPC/ASG and GIPC/SG. Interestingly, monolayer GIPC/sitosterol was more stable compared to the other monolayers.

In order to appreciate the interaction and thermodynamic stability of the two components, the excess free energy of the mixing ( $\Delta G_{ex}$ ) and the free energy of mixing ( $\Delta G_M$ ) were calculated for all four mixed monolayers. The negative value of  $\Delta G_{ex}$  for the mixed monolayer GIPC:sitosterol (80:20) suggests a strong attractive interaction

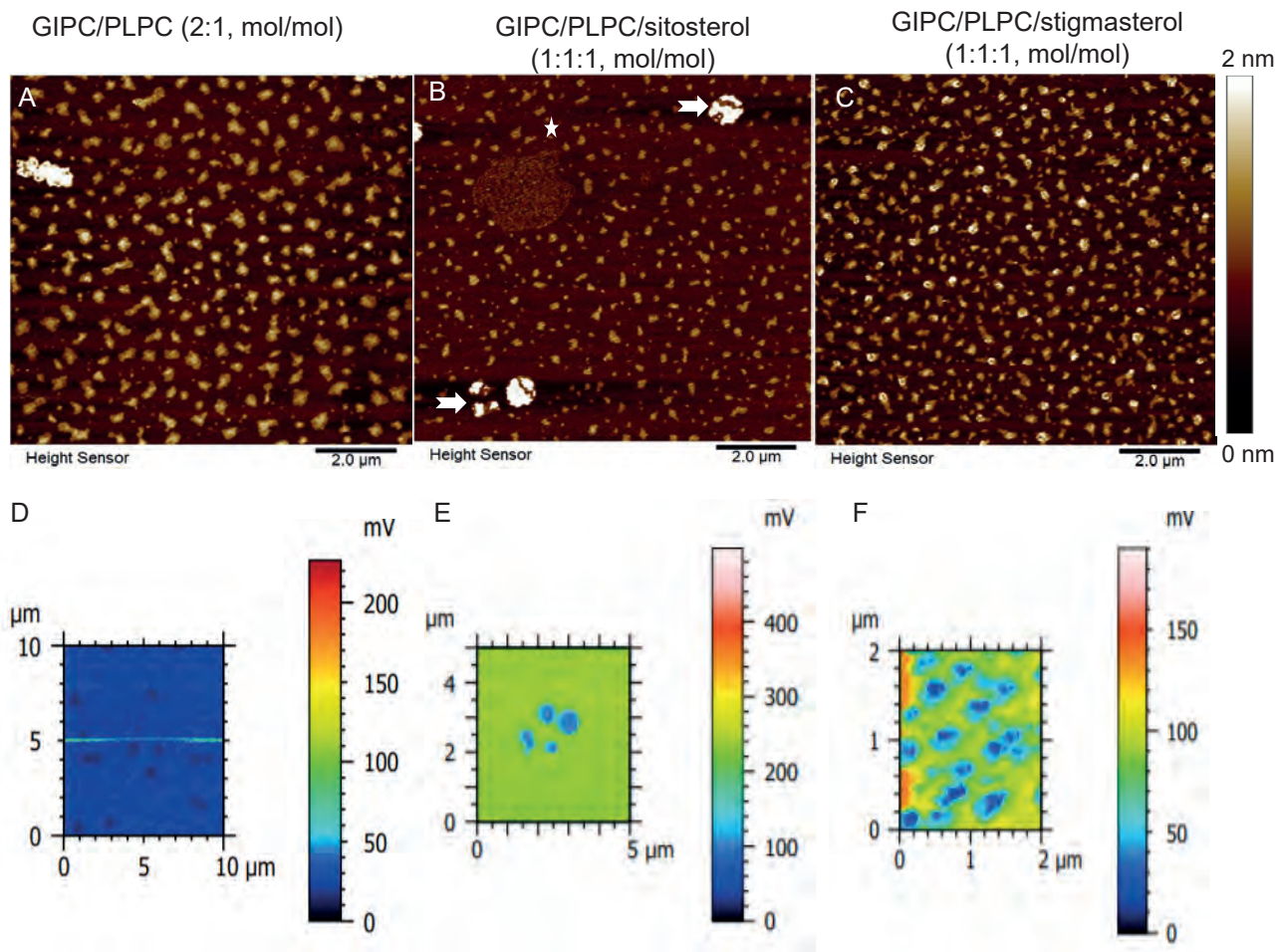
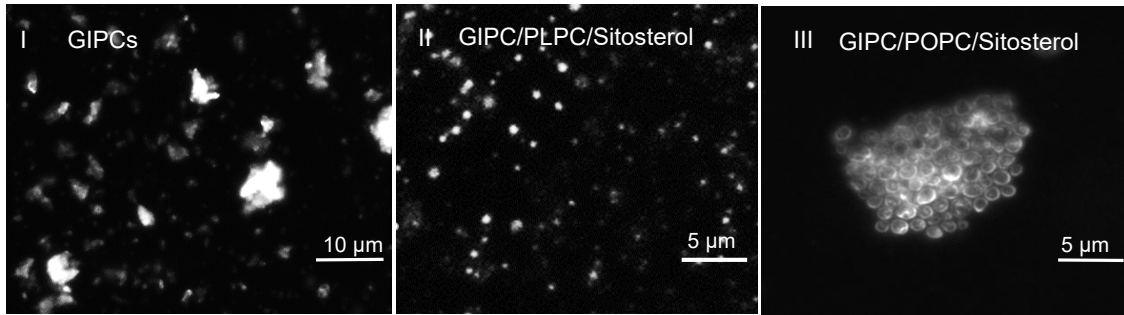


**Figure 7: Influence of sterol in nanodomain organisation in monolayer membrane containing GIPC.** Atomic Force Microscopy topographic analysis (A to C, scan size 10  $\mu\text{m}$ ) and Nano-Infrared observations (Nano-IR) (D to F) images of lipid films transferred on mica plate at an initial surface pressure of 10mN/m. The lipid monolayer contains: GIPC/PLPC (2:1) (A and D), GIPC/PLPC/Sitosterol (B to E) and GIPC/PLPC/Stigmasterol (C and F). NanoIR images (D to F) indicate the amplitude of IR signal. Different colors refer to different molecular signatures of the monolayer.

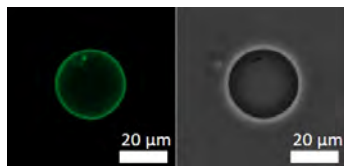
between the two components and the negative value of  $\Delta GM$  indicates that the mixed monolayer is thermodynamically stable (Figure 5C) as suggested by (Cacas et al., 2016b). The positive value of  $\Delta G_{ex}$  and of  $\Delta GM$  for the mixed monolayers GIPC:SG (80:20), GIPC:ASG (80:20) and GIPC/Stigmasterol (80:20) are both positive in all three mixed monolayers (Figure 5C) showing strong repulsion between the molecules within the monolayer and the thermodynamic instability of the mixed monolayer.

Hypermatrix is a simple theoretical docking method used to calculate specific interactions between a molecule with itself and other lipids. The calculations of the different interacting forces help to understand the organization of the molecules. The interaction of one molecule of GIPC series A with t18:0/h124:0 and one molecule of sterol was generated *in silico* using Hypermatrix and analysed. The sterols used were the four molecules studied by Langmuir trough i.e.  $\beta$ -sitosterol, ASG with a  $\beta$ -sitosterol, glucose head group esterified by 18:2 acyl chain, SG composed of  $\beta$ -sitosterol and glucose head group, and stigmasterol (Figure 6). The interactions of the different sterols and one GIPC molecule were calculated. The molecules displayed very different configurations. The difference between the spatial organization of GIPC/sitosterol and GIPC/stigmasterol is striking: the alpha-side of the sterol moieties of sitosterol is directed towards the acyl chains of GIPC whereas the sterol rings of stigmasterol are positioned at a perpendicular angle with respect to GIPC acyl chains. Hence, the structural difference of the desaturation on C22 in stigmasterol seems to alter its interaction with GIPC (Figure 6), being in very good agreement with the non-cooperativity effect observed experimentally in monolayer compression experiments. The conjugated sterol, ASG has its acyl chain in direct interaction with the alpha side of its sterol rings, such that the beta-side of the sterol cycle interacts with GIPC acyl chains (Figure 6B). The acyl chain is responsible for hydrophobic interactions thus orienting the acyl chain away from the GIPC molecule such that the atoms interact with minimum energy. For sterol glucoside (SG), the beta side of the sterol group is oriented towards GIPC. It is interesting to note the the sugar head group of GIPC is bent favouring interaction with the glucose head group of SG (Figure 6C).

### A. Freeze-thaw method



### B. Teflon method GUVs GIPC/DOPC/Sitosterol (1/1/1; mol ratio)



### C. DLS and $\zeta$ -potential (GIPC/DOPC/Sitosterol)

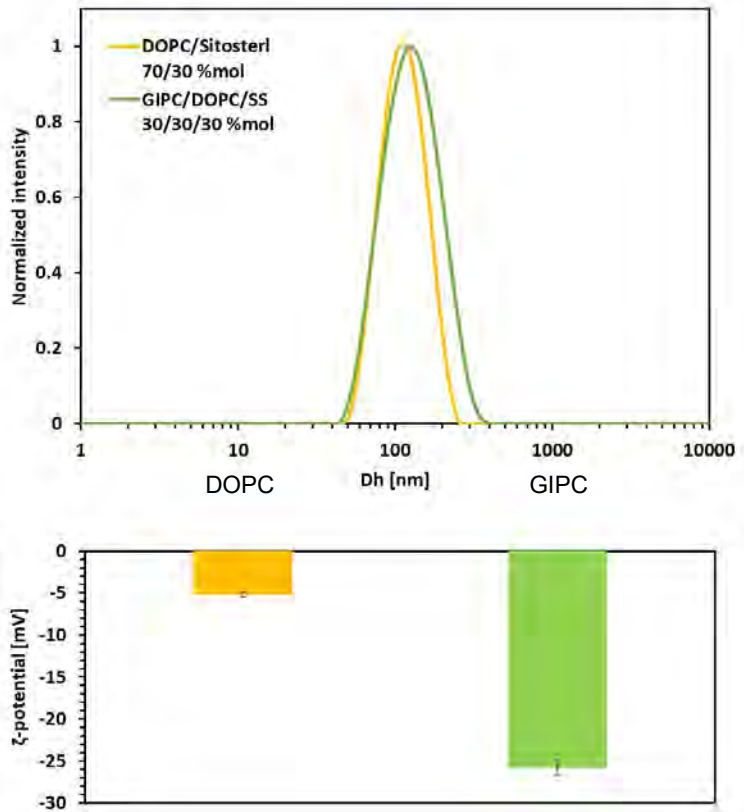


**Figure 8.** A, Bo-GIPC containing-liposomes in buffer solution after 3 cycles of freeze and thaw. Enriched Bo-GIPC (cauliflower), underwent freeze ( $-20^{\circ}\text{C}$ , 20 min) and thaw ( $50^{\circ}\text{C}$ , 20 min) cycles three times GIPC in TBS buffer pH 5,8 with or without phospholipid and sitosterol at a concentration of 1 mg/ml. (I) GIPCs alone form crystals in a saline buffer solution. A lipid mix, at a concentration of 1mg/ml, of GIPC/PLPC/Sitosterol or GIPC/POPC/Sitosterol (1:1:1, mol/mol), shown in (II) and (III) respectively, forms vesicles of approx. 2  $\mu\text{m}$ . **B.** Fluorescence and phase contrast microscopy images of Giant unilamellar vesicles (GUVs) of GIPC/DOPC/Sitosterol (1:1:1, mol/mol). The lipid mix was labeled by NBD-PC at 0.1%. mol. **C.** Dynamic light scattering (DLS) and  $\zeta$ -potential of liposomes containing DOPC/Sitosterol (7:3, mol ratio) (yellow) and GIPC/DOPC/Sitosterol (1:1:1, mol ratio) (green), respectively provide the size which is around 100nm and  $\zeta$ -potential values of -28mV in the presence of GIPC

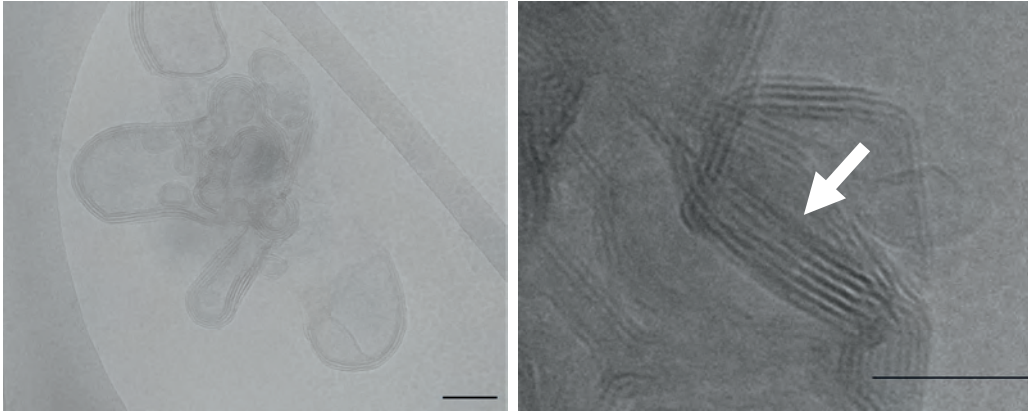
## **Lipid segregation observed in AFM is dependent on both GIPC and phytosterol**

Monolayers previously obtained were transferred on mica plates by the method of Langmuir-Blodgett. Atomic Force Microscopy (AFM) assay on model monolayer containing Bo-GIPC (cauliflower GIPC enriched sample), showed differential segregation of lipids in the presence of sterols and GIPC (Figure 7 A-C). The mean height and width of the observed structures were calculated after analysis of five different areas of the sample. Using the NanoIR assay, we were able to assess the distribution of particles of different molecular signatures in the structures observed (Figure 7 D-F). A monolayer of GIPC:PLPC (1:2, mol ratio) showed structures of a mean width of 515 nm of about 1.5 nm high (Figure 7A). These structures were not present in PLPC monolayer (supplementary data 4A). The GIPC signature can be seen as agglomerates in the nanoIR image (Figure 7D). Mixed monolayer GIPC:PLPC:sitosterol (1:2:1) formed structures of 890 nm wide of 2 nm high (arrows in Figure 7B). The nanoIR image showed a co-existence of GIPC and sitosterol forming these structures in a PLPC background (Figure 7E). Sitosterol seemed to also form fibrils of sterols (star in Figure 7B). These fibre-like structures were also observed in PLPC:stigmasterol (4:1) monolayer (Supplementary data 4A). Sitosterol promoted the formation of wider circular domain-like structures of 2nm in height in the presence of GIPC. Sitosterol with PLPC formed a flat uniform monolayer (Supplementary data 4). Domain-like structures were dissipated in the presence of stigmasterol. Indeed mixed monolayer GIPC:PLPC:stigmasterol (1:2:1) contained smaller structures of width 330 nm and 1.3 nm high (Figure 7C). The nanoIR imaging showed dissipation of stigmasterol signature around GIPC agglomerates (Figure 7F). Stigmasterol seemed to disperse GIPC agglomeration hence forming smaller structures. Without GIPC, PLPC:stigmasterol (1:1) did not form similar structures (Supplementary data 4). These data paved the way to understand more the synergic effect of GIPC and sitosterol in organizing domain-like structures in model bilayers.

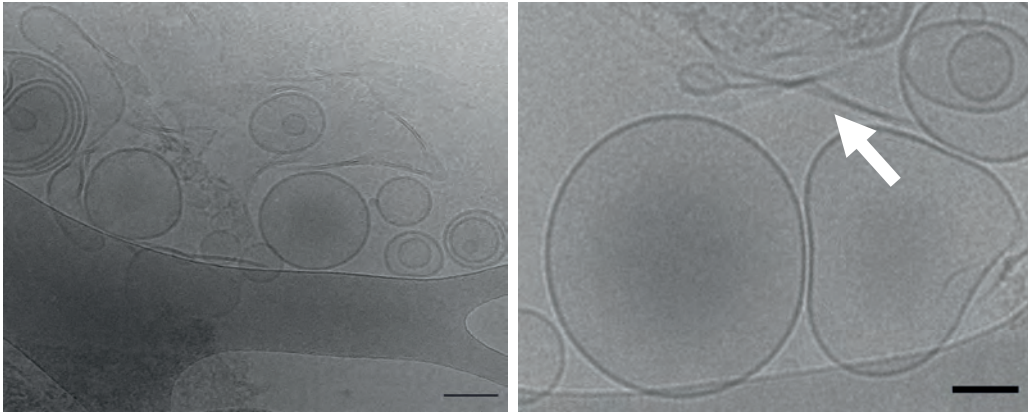
### **Effect of GIPC on membrane organization and thickness**

To investigate more about the properties of GIPC using model bilayers, we tried to make liposomes with Bo-GIPC by freeze/thawing. We found that GIPC are made

A. GIPC/POPC-d31



B. GIPC/POPC-d31/Sitosterol



C. GIPC/POPC-d31/Stigmasterol

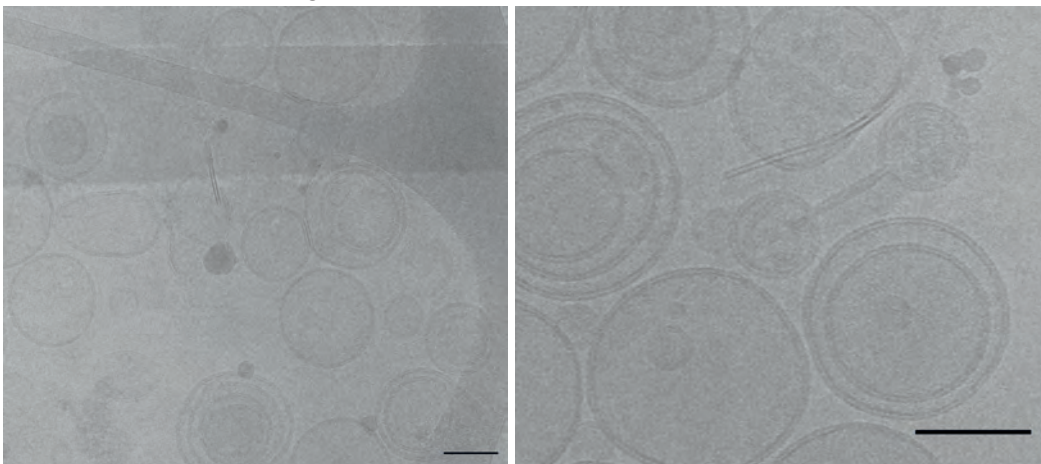


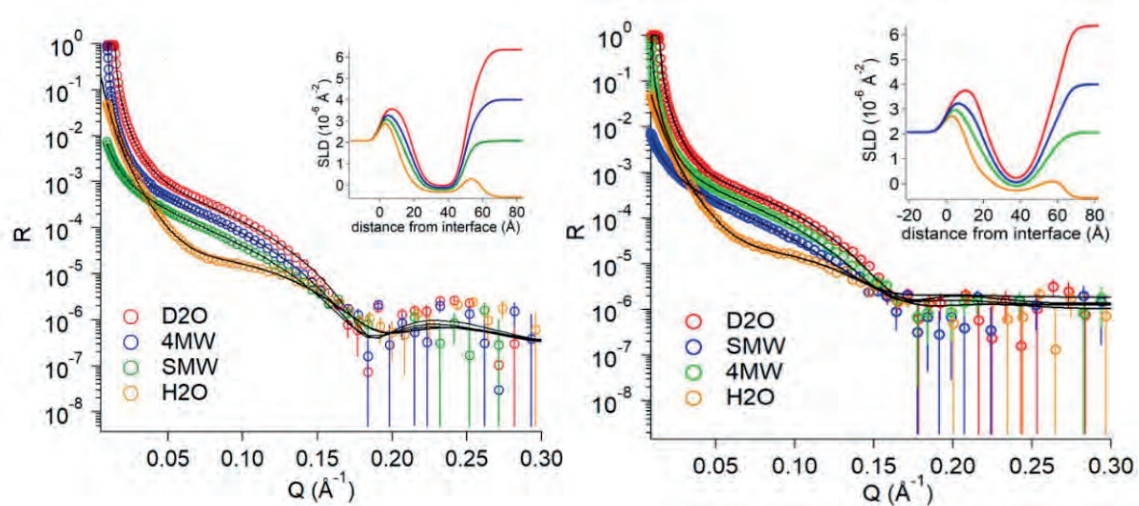
**Figure 9:** Liposomes shapes varies with lipid composition of liposomes. A, Cryo-EM images of liposomes containing: GIPC:POPC-d31(2:1), shows multilamellar structures. with bilayers of 7.5 nm thick. B, GIPC/POPC-d31/Sitosterol (1:1:1) indicates mostly large bilayer liposomes of 6 nm thick with the presence of structures with high rigidity bilayer. C, GIPC/POPC-d31/Stigmasterol (1:1:1) present similar structures. Lipid concentration 0.3 mg/ml. scale bar, 100 nm. POPC-d31 is a deuterated POPC on the carbon of the palmitoyl chain : 16:0-d31-18:1 PC

crystal-like structure but not vesicles (Figure 8A). We also tried with Nt-GIPC and obtained similar results (Supplementary data 5A). Only by adding phospholipids of short fatty acyl chain we observe liposomes (Supplementary data 5A). To be closer to mimicking the outer leaflet of the PM, we generated liposomes with a ternary system of GIPC:phospholipid:sitosterol (1:1:1). As phospholipids, we tried PLPC, POPC or DOPC, in all cases the ternary system yielded liposomes using the freeze-thaw method with liquid nitrogen and water bath of 60°C (Figure 8A) (Supplementary data 5B). Giant unilamellar vesicles (GUVs) were made, using the Teflon method by (Kubsch, Robinson, Steinkühler, & Dimova, 2017) with ternary mix GIPC/DOPC/sitosterol (Figure 8B). The incorporation of GIPC in the liposomes were analysed by dynamic light scattering (DSL) and quartz crystal microbalance with dissipation monitoring (QCM-D), which gave respectively the diameter of the liposomes and the zeta-potential of the GIPC-containing liposomes (Figure 8C). The addition of GIPC did not seem to affect the diameter of liposomes, which was about 100nm. Since GIPC is negatively charged due to the presence of phosphate group and the glucuronic acid, the zeta-potential of the liposomes containing GIPC were measured to be around -26 mV, while DOPC/sitosterol alone had a potential of -5mV. It seemed therefore that GIPC play an important role in the potential of plant PM, which might influence its interaction with different actors of the cell wall for example.

Further investigation by cryo-EM showed that depending on the content of ternary mix containing Bo-GIPC, the bilayer structures formed differed. We first analysed liposomes made by the freeze/thaw method (Figure 9). While GIPC:dPOPC formed multilamellar structures with bilayers of 7 to 8 nm thick, GIPC:dPOPC:sitosterol formed more regular-shaped liposomes of 6 nm thick (Figure 9). Rigid bilayer structures can also be seen (arrow in figure 9). GIPC:dPOPC:stigmasterol seemed to form vesicles similar to GIPC:dPOPC:sitosterol. It appeared that sterols dissipate stacked structures that are observed in GIPC:dPOPC alone.

Finally, we investigated influence of GIPC on membrane thickness by neutron reflectivity (Figure 10A). Liposomes containing 30% of GIPC were no entirely deposited on the plates, therefore to increase the amount of deposition we generated liposomes with 15% of GIPC. It could be that 30% of GIPC in the lipid mix modified the bilayer properties such that it does not adhere to the membrane.

A



B

Parameter	POPC/Sitosterol	GIPC/POPC/Sitosterol
Bilayer formation	Yes	Yes
% solvent in the tails	5	5
Inner Sugar (Å)	-	4
Inner Head (Å)	8	8
Tail (Å)	31	31
Outer Head (Å)	8	8
Outer Sugar (Å)	-	4

C

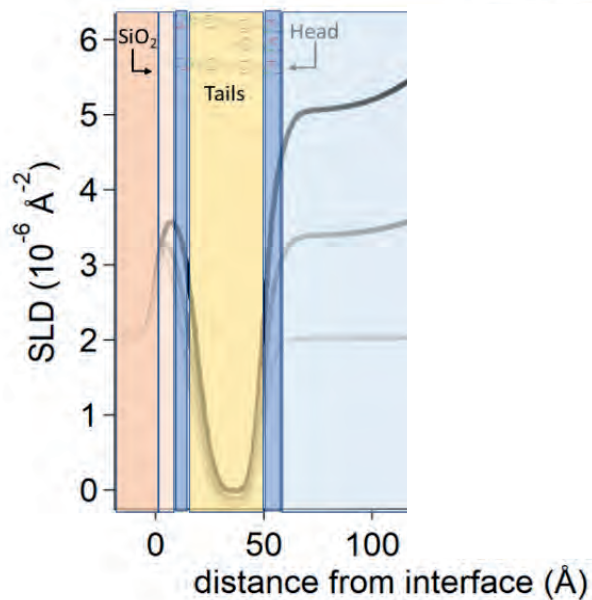


**Figure 10: Reflectivity profiles and calculated Scattering length density (SLD) following lipid bilayer deposition of (i) POPC/Sitosterol (70:30, mol/mol) and (ii) GIPC/POPC/Sitosterol (55:15:30, mol/mol). The multilayer model was composed from the silicon substrate ( $SLD=2.07 \cdot 10^{-6} \text{Å}^{-2}$ ) covered with a layer of silicon oxide ( $SLD=3.47 \cdot 10^{-6} \text{Å}^{-2}$ ). (B) Structural parameters of the lipid bilayers obtained after fitting of reflectivity data. (C) Scheme showing the SLD profile overlaid on the multilayer model as obtained for POPC membrane.**

15% containing GIPC liposomes were thus used to make a supported bilayer (SBL) and analysed by neutron reflectivity. The scattering length density (SLD) were generated, after model fitting, giving the profile of how the polar head and acyl tail were organized in the bilayer. The addition of GIPC seemed to increase by 8 Å the thickness of the bilayer due to the 4 Å of sugar head group (Figure 10B). Refer to the tables of supplementary data 6 for more details of the structural parameters that were generated. Figure 10C shows a schematic representation of the different thickness of the lipids head and tails of GIPC-containing SBL.

## Discussion

### Fine tuning GIPC purification

This paper describes a protocol for the purification of GIPC. It has been inspired from three publications (H E Carter & Koob, 1969),(Kaul & Lester, 1975) and (Markham & Jaworski, 2007), whereby the steps were rearranged in order to get rid of all sterols and glycerolipids along the extraction procedure and retain GIPCs which are eluted in the column purification steps. For better yield and purity, we still have to fine-tune the purification and extraction process of GIPCs, nevertheless we were able to obtain 30 mg of material of 85% purity from 4 distinct plant materials. In the near future, it will also be important to purify different GIPC series individually, such as to study their polar head composition and to understand their biological roles. To do so, preparative chromatography needs to be developed such as by elution with the solvent with the right polarity.

In all enriched GIPC fractions (*Bo*-GIPC, *Nt*-GIPC, *Ap*-GIPC and *Os*-GIPC) galacturonic acid and rhamnose are absent suggesting no contamination by pectins, and particularly RGII known that bind GIPC, see (Voxeur & Fry, 2014b) (refer to Figure 4B). We detected arabinose and galactose in *Bo*-GIPC and especially in large amount in *Nt*-GIPC (fraction  $\gamma$ ) (Figure 4B). Both of these sugars are main constituents of Rhamnogalacturonan I, RGI. To test for the presence of RGI we performed a Yariv test, this test did not detect presence of AGs. We hypothesized from literature that GIPC of cauliflower potentially have hexoses as sugar moieties of polar head and not pentose (Buré et al., 2014). Hence, could arabinose be a contamination from cell wall RGI? Cauliflower being from the *brassicacea* family as *Arabidopsis*, the biosynthesis of the polar head group might involve enzymes that will add hexoses to the sugar head group such as GMT1. The latter transfers a mannose to the core structure GlcA-Ins-P-Cer in vegetative tissues of *Arabidopsis* (L. Fang et al., 2016). As for *Arabidopsis* seeds and pollen, rice and tobacco, the work of (Ishikawa et al., 2018) shows that GINT1, another glycosyltransferase adds a GlcNAc instead of a Man to the core structure of GIPC. However, we cannot conclude whether Ara and Gal are contaminations or intricate sugar moieties of GIPC. The polar head sugar diversity of GIPCs are species-dependent (Buré et al., 2011). For instance the increasing large amount of galactose and arabinose

in Nt-GIPC(fraction  $\alpha$ ), Nt-GIPC(fraction  $\beta$ ) and Nt-GIPC(fraction  $\gamma$ ) has been described in (Kaul & Lester, 1978) where GIPCs of tobacco leaves contain up to 4 arabinose and 2 galactose attached to the GIPC structures GlcN/GlcNAc-GlcA-Ins-P-Cer, see (Kaul & Lester, 1978). Hence, it is correct to assume that the large amount of Ara and Gal of Nt-GIPC(fraction  $\gamma$ ) accounts for polyglycosylated GIPC of up to GIPC series E of Ara-Ara-Gal-Gal-Man-GlcN/GlcNAc-GlcA-Ins-P-Cer.

The full structure and diversity of sugar moieties in GIPCs polar head remain to be understood and investigated. Such diversity cannot be futile. The importance of GIPC polar head structure is highlighted in plant/pathogen interactions. GIPCs are receptors to necrotic toxin, Necrosis and ethylene-inducing peptide 1-like (NLPs) such that plant enriched in GIPC series A are sensitive to NLPs while those enriched in GIPC series B are insensitive to NLPs, hence conferring resistance against pathogens secreting NLPs (Lenarčič et al. 2017). The protocol of this study, although not perfect, is simpler, time-efficient, with reasonable yield, compared to the old publications where large amounts of solvents were used. Material can be generated for  $^1\text{H}$  and  $^{13}\text{C}$  NMR analysis to decipher the number, the bonds and the types of sugar residues of plant GIPC polar head group, as was done for fungi GIPC (Simenel, Coddeville, Delepierre, Latgé, & Fontaine, 2008). While the purification of polyglycosylated GIPC is challenging, it paves the way to analyse different GIPC series as described in (Gutierrez et al., 2007).

### **GIPC interaction with sterols in membrane order**

We showed that GIPC interacts differentially with sterols by biophysical techniques of Langmuir compression isotherms, molecular modelling and AFM. We confirmed that GIPC with sitosterol had a cooperative effect as shown by (Cacas et al., 2016a) and showed that stigmasterol had the reverse effect, known as non-cooperative effect (Figure 5). These differential interactions are structure dependent. Just adding a glucose head group (SG) and an acyl chain (ASG) or an unsaturation (C22 in stigmasterol) to the sitosterol sterol moieties change the interaction with GIPCs and modify the characterisation of model membrane (Figure 5, 6 and 7). The interaction between SG and GIPC seems slightly non-cooperative while ASG and GIPC have a

cooperative effect (Figure 5). In drought stressed plants, there are accumulation of GIPCs, ASG and SG (Tarazona, Feussner, & Feussner, 2015). It is suggested that glycosylated sterols in addition to GIPC, contribute to dehydration responses by providing sugar head groups (Tarazona et al., 2015). The specific interaction with GIPC due to their different backbones may confer special membrane physicochemical properties that remain to be investigated.

The structural difference between sitosterol and stigmasterol is an unsaturation on C22. This has dramatic effect on membrane fluidity as discussed in (Grosjean et al., 2015a). Using model membranes and environment-sensitive probes, they showed that plant lipids promote various spatial organization of membrane and that sitosterol promotes lipid ordered (lo) phases while stigmasterol has a low ordering effect and is correlated with low level of lo phases. Plant sterols and sphingolipid make lipid rafts which are signalling platforms (Mongrand et al., 2004) (Cacas et al., 2016a) (Gronnier, Gerbeau-Pissot, Germain, Mongrand, & Simon-Plas, 2018). These structures can be clearly seen as domain-shaped structures in model monolayers containing sitosterol and GIPC that interact with each other (Figure 7). This interaction might translate into liquid ordered phases. Stigmasterol, on the other hand, tends to sequester small structures containing GIPC which might contribute to deter lo and domain formation.

Compared to animals, plants are poikilotherm organisms and have to adapt the viscosity of their membrane when temperature varies. By modulating the fluidity of their membrane to be functionally viable, plants can adapt to temperature fluctuations. These properties of altering the membrane fluidity can explain why plants can readily convert sitosterol to stigmasterol by expressing C22 desaturase CYP710 during temperature acclimation (Morikawa et al., 2006). Sensitivity to temperature model membranes mimicking membrane domains with phytosterols and glucosylcerebroside is lower compared to the temperature sensitivity of the system with cholesterol and sphingomyelin typical to animal (Beck et al., 2007a). Specific plant cell membrane components like sitosterol, stigmasterol and glucosylcerebrosides, are produced to adapt to temperature to make membrane-associated biological processes possible (Beck et al., 2007a). Here we use GIPCs which represent 50% of sphingolipids in plant PM (Cacas et al., 2016a). It seems that GIPCs are more conducive to enable thermal adaptation and regulation of homeoviscosity in interaction with sterols in plant PM.

It will be interesting to further investigate how GIPC is involved in modulating PM fluidity in thermal adaptation.

### **GIPCs alone form crystal-like structures, but not liposomes**

With the aim to study the physical properties of GIPC, we attempted to make liposomes. Liposomes are spherical lipid bilayers whose composition depends on the desired model of study. GIPCs having large polar heads and very long chain fatty acid that tend to agglomerate and make crystal-like structures similar to pure sterols. In order to make liposomes and further study GIPCs, secondary mix with phospholipids or ternary mix with phospholipids and sterols were used. To be closer to biological PM model, we use lipid mix of GIPC/phospholipid/sterol at a molar ratio of 1:1:1. As expected for lipid with hydroxylated very long chain fatty acid, GIPC forms thicker membrane in model membrane. GIPC increases the membrane thickness by few nm as shown by neutron reflectivity on supported bilayer. AFM analysis of monolayer lipid mix showed particular structural organization in presence of GIPC and sterols suspected to be nanodomains. Liposomes containing GIPCs, observed under cryo-EM are around 6-7 nm for the ternary mix, which correspond to the thickness of purified PM from *Medicago truncatula* and tobacco (Lefebvre et al., 2007)(Mongrand et al., 2004). The rigid structures of 7 nm resembled the purified Detergent Insoluble Membranes (DIMs) described as parallel membrane sheets of 6.5 nm thick (Lefebvre et al., 2007)(Mongrand et al., 2004). In order to confirm so, we can treat the liposomes samples with triton X100 to see if the rigid structures dissolve away.

One important feature of the PM is its electrostatic charges. PM purification using polymers phase separation PEG/Dextran relies on the fact that PM is highly negatively charged and PM right-side-out (RSO) fraction are attracted to the positively charged PEG phase (Morré & Morre, 2000). The membrane surface charge (MSC) is regulated by lipids and post transcriptional modification of proteins such as phosphorylation (Goldenberg & Steinberg, 2010). The zeta-potential of GIPC-containing liposomes is -26 mV, five times higher than a PC-containing bilayer, likely due to the large electronegativity of GIPC conferred by its phosphate group and GlcA residue of the polar head. Therefore, GIPC being mostly located in the outer leaflet of the PM (Cacas et al., 2016a), we demonstrated here that GIPCs contribute strongly in conferring electronegative charges to the outer leaflet of the PM.

## **GIPC structure in membrane organization**

Recent studies provide new insight on the important role of GIPC structure in plants through genetic approach (L. Fang et al., 2016; Ishikawa et al., 2018; Mortimer et al., 2013). By generating mutants combined with the multidisciplinary approach used in this study like AFM, neutron scattering, DLS and QCM-D, we can uncover more about GIPC intricate structure and its biological implications. The modification of the ceramide length and hydroxylation of GIPC might alter the organization of the membrane like sphingomyelin (SM) in animal cell responsible for interdigitating between the bilayers and domain formation with cholesterol (Róg et al., 2016) (London & Brown, 2000). The closest homologue in term of membrane structuring role of plant GIPC series A and B could be SM, even if the latter –absent in plant PM- is made up of a phosphocholine head group. The theoretical model of plant PM showed GIPC as the major sphingolipid in the outer leaflet, just like SM and a lateral segregation to form liquid ordered phases with phytosterols (Cacas et al., 2016a)(Tjellstrom et al., 2010). Structurally, GIPC are homologous to animal gangliosides that are absent in plants. Gangliosides are acidic glycolipids containing sialic acid in their polar head that play an important role in immunity, modulating cellular signal transduction in the PM, essential brain and retinal functions in animal cells (Sonnino & Prinetti, 2010)(Sibille et al., 2016). It is possible that polyglycosylated GIPCs have the same role of gangliosides that are heavily glycosylated. It is hence worth investing into understanding the glycosylation patterns and enzymes involved in GIPC biosynthesis. The present study paves the way to tackle the function of plant glycosylated sphingolipids in membrane organisation and function.

## **Material and Method**

### **Plant Material**

Cauliflower and leek were store-bought. Wild-type tobacco (cv. Bright Yellow) cell culture were obtained by (Cacas et al., 2013). Rice cultured cells were obtained as described in (Nagano et al., 2012).

### **Extraction and purification of GIPCs**

Leafy green parts of cauliflower and leek were removed to prevent contamination by galactolipid mainly present in chloroplasts. The plant material (about 250 g fresh weight) were blended with 5 litres of cold 0.1 N aqueous acetic acid in a chilled stainless-steel Waring Blendor at low, medium and high speed for 30s each. The slurry was filtered through 16 layers of acid-washed miracloth. The residue was extracted once (twice for leek) again in the same manner. The aqueous acetic acid filtrate was discarded. The residue was air-dried overnight under a fume hood and was then refluxed with 2 litres of hot 70% ethanol (0.1 N in HCl) for 20 min. The slurry was filtered hot through 16 layers of miracloth pre-washed with acidic ethanol (press well to remove all liquid). This process was repeated twice more using a total of 5 litres of acidic ethanol. The combined filtrates were chilled at - 20°C for 48h. The precipitate was removed by centrifugation at 30,000 g (14000 rpm at using a Sorvall SLA-1500 rotor) at 4°C for 15 min. Sphingolipids were then extracted from the precipitates in hot isopropanol/hexane/water (55:20:25, v/v). The solution was homogenized using an Ultra-Turrax for 20 s and incubated at 60°C for 20 min. After centrifugation at 3000 g for 10 min, the supernatant was decanted to another tube and the residue extracted twice more with the hot solvent. A total of 100 ml of solvent was used at this step. The supernatants were combined and its lipid content was analysed by TLC and GC-MS to evaluate the amount of GIPC content.

Porous silica beads (Silica gel for chromatography 60 A, 75-125  $\mu$ m, Acros Organics), were used throughout for packing the column chromatography. The column consists of 70 ml of silica beads, sand of Fontainbleau followed by the sphingolipid sample dried in 20 ml of silica beads (see Figure 2). The column was washed and equilibrated with chloroform. Apolar lipids were washed with a mix of chloroform/methanol of different volume ratios of increasing polarity (4:1 then 3:1 and 2:1). The volume used was equivalent to 4-fold the volume of the column. The column was then eluted with a step gradient of chloroform:methanol:water. Solvent A was chloroform:methanol:water (59:37.5:3.5, v/v) and the solvent B chloroform:methanol:water (46:42:12, v/v). The step gradient elution started with 100% A to end with 100% B, with 10% intervals. The volume of elution corresponds to 2-fold the volume of the column. 1/100<sup>th</sup> of each elution fractions were collected and dried for GC-MS and TLC analysis to test the purity of the fractions (see below HPTLC of eluted fractions). Once the latter was determined, fractions containing the same type of GIPCs were pooled and dried. The estimated

quantity of GIPC is assessed by calculating the amount of (h)VLCFA ((hydroxylated-) Very Long Chain Fatty Acid). (h)VLCFA represents 1/3 of total GIPC molecular mass.

### **Fatty Acid Analysis**

Each sample was transmethylated at 110°C overnight in methanol containing 5% (v/v) sulfuric acid and spiked with 10 mg of heptadecanoic acid (c17:0) and 10 mg of 2-hydroxy-tetradecanoic acid (h14:0) as internal standards. After cooling, 3 mL of NaCl (2.5%, w/v) was added, and the released fatty acyl chains were extracted in hexane. Extracts were washed with 3 mL of saline solution (200 mM NaCl and 200 mM Tris, pH 8), dried under a gentle stream of nitrogen, and dissolved in 150 mL of BSTFA and trimethylchlorosilane. Free hydroxyl groups were derivatized at 110°C for 30min, surplus BSTFA-trimethylchlorosilane was evaporated under nitrogen, and samples were dissolved in hexane for analysis using GC-MS under the same conditions as described (Buré et al., 2011). Quantification of fatty acids and hydroxyl acids was based on peak areas, which were derived from total ion current, and using the respective internal standards.

### **Langmuir Trough**

GIPC-enriched fractions were purified in this study. A solution at 0.4 mM in chloroform:methanol:water (30:60:8) was prepared. Sterols and PLPC were purchased from Avanti Polar Lipids. They were dissolved at 0.4 mM in chloroform:methanol (2:1). The surface pressure-area (P-A) isotherms were recorded by means of an automated Langmuir trough (KSV Minitrough [width, 75 mm; area, 24.225 mm<sup>2</sup>]; KSV Instruments) equipped with a platinum plate attached to a Wilhelmy-type balance. The GIPC sample was heated to 60°C for 15 min for a better solubilization. Pure solutions and lipid mixtures were spread (fixed volume of 30 mL) as tiny droplets to produce a uniform monolayer on a Tris:NaCl 10:150 mM (Millipore) subphase adjusted to pH 7 with HCl. After evaporation of the solvent (15 min), monolayers were compressed at a rate of 5 mm/min and at a temperature of 22°C ± 1°C. Before each experiment, the cleanliness of the system was confirmed by checking the surface pressure over the surface compression of the pure subphase. The reproducibility of the P-A isotherms was checked by repeated recordings, and the relative SD in surface pressure and area was found to be 3% or less.

### **Molecular modelling Approaches**

The Hypermatrix docking procedure was used to study the monolayer formed by GIPC and its interaction with sterols, as already described in (Cacas et al., 2016a). Briefly, one GIPC molecule is positioned and fixed for the whole calculation at the centre of the system, oriented at the hydrophobic /hydrophilic interface. The inter- acting GIPC (for GIPC monolayer) or sterols (for mixed monolayer) is also oriented at the hydrophobic/hydrophilic interface, and by rotations and translations, more than 107 positions of the interacting molecule around the central molecule are calculated. The

most stable matching is used to decide the position of the first interacting molecule. The position of the second one is then defined as the next most energetically favourable orientation stored in the matrix, taking steric and energetic constraints due to the presence of the first molecule into account. Refer to (Cacas et al., 2016a) for more details.

### **Liposomes preparation (Freeze and thaw method)**

The lipid solution of 1mg/ml (GIPC/PLPC or POPC or DOPC/Stigmasterol or Sitosterol) at different molar ratio, was dried and resuspended in water. Several cycles of freeze and thaw were done with freezing occurring in liquid nitrogen for 5 min and thawing at 50°C for 15min.

### **LUV preparation for DLS and $\zeta$ -Potential**

The lipid solution (GIPC/DOPC/Sterol) in 3/1 v/v THF/H<sub>2</sub>O methanol mixture was transferred into a round-bottom flask and the organic solvent was removed by evaporation under high vacuum pumping for 2 h, until complete evaporation of the solvent. The lipid film was then hydrated in an appropriate amount of buffer solution at room temperature, well above the melting point of the lipids, to yield suspensions with concentrations in the 0.5–2.8 mM range. Multilamellar vesicles were then obtained by vortexing for 30 min. The resulting suspensions were then successively extruded 20 times through 200 and 100 nm polycarbonate membranes using a mini-extruder (Avanti Polar Lipids). The vesicle size distribution and  $\zeta$ -potential were finally characterized by light scattering.

### **DLS and $\zeta$ -potential values**

Dynamic Light Scattering (DLS) and  $\zeta$ -Potential. DLS measurements were performed with a Malvern NanoZS instrument operating with a 2 mW HeNe laser at a wavelength of 632.8 nm and detection at an angle of 173°. All measurements were performed in a temperature-controlled chamber at 20 °C ( $\pm 0.05$  °C). Three measurements of 15 runs each were usually averaged. The intensity size distribution was obtained from the analysis of the correlation function using the multiple narrow mode algorithm of the Malvern DTS software.

The electrophoretic mobility of vesicles and CNCs was measured by using the same Malvern NanoZS apparatus performing at 17° from which the  $\zeta$ -potential values are determined by applying the Henry equation. The  $\zeta$ -potential values and the  $\zeta$ -deviation were averaged over at least three measurements with at least 30 runs per measurement. They were expressed as mean  $\pm$  SD ( $n \geq 3$ ).

### **GUV preparation (Teflon method)**

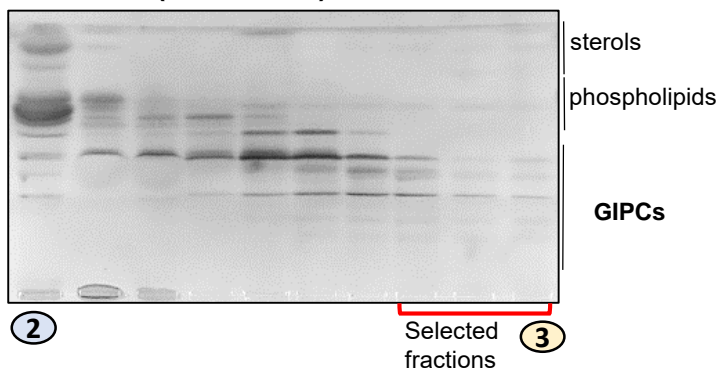
GUV were prepared as previously described by Dimova (Kubsch et al., 2017). Briefly, 50  $\mu$ L of lipid mixture (1 mg mL<sup>-1</sup>) dissolved in organic solvent mixture were deposited

on a pre-cleaned Teflon disk and the solvent was evaporated with vacuum for 2 hr. The disk was then placed in a 4 mL sealed glass vial with 200 mM sucrose and 50 mM NaCl at 60°C for 12 hours, until a cloudy deposit was formed. For microscopy observation, one volume of the vesicle suspension was mixed with 4 volumes of iso-osmolar glucose/NaCl solution for better contrast.

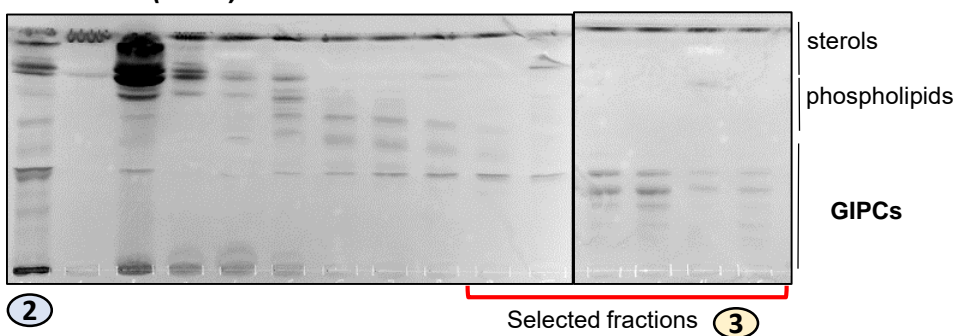
### **Cryogenic Electronic Microscopy (Cryo-EM)**

For cryo-EM studies, lacey carbon formvar 300mesh copper grids were used. They were first submitted to a standard glow discharged procedure (3mbar, 3mA for 40sec). Plunge freezing was realized using the EM-GP apparatus (Leica). Four microliters of the sample (description / concentration) was deposited on the grid and immediately blotted for 2 sec with a whatmann paper grade 5 before plunging into a liquid ethane bath cooled with liquid nitrogen (-184°C). The settings of the chamber were fixed at 70% humidity and 20°C. Deuterated POPC (POPC-<sup>2</sup>H<sub>31</sub>) were bought from Avanti, GIPC were prepared from cauliflower. Sitosterol and stigmasterol were store bought from Avanti. Specimens were observed at -170 °C using a cryo holder (626, Gatan, USA), with a ThermoFisher FEI Tecnai F20 electron microscope operating at 200 kV under low-dose conditions. Images were acquired with an Eagle 4k x 4k camera (ThermoFisher FEI).

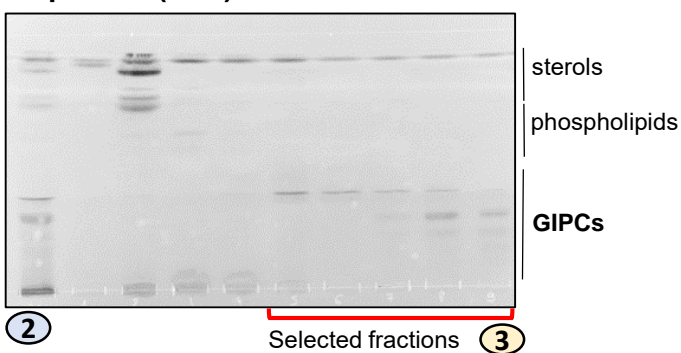
### ***Bo*-GIPC (cauliflower)**



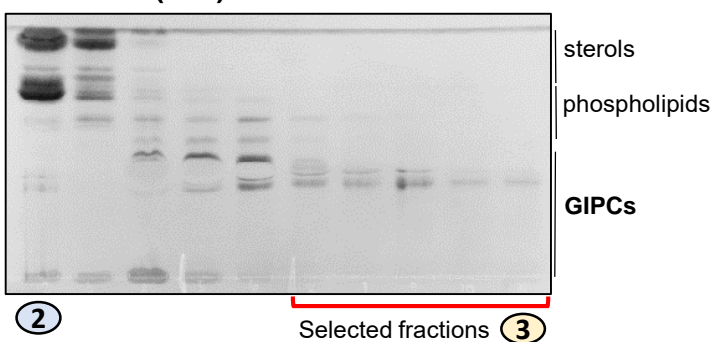
### ***Nt*-GIPC (BY-2)**



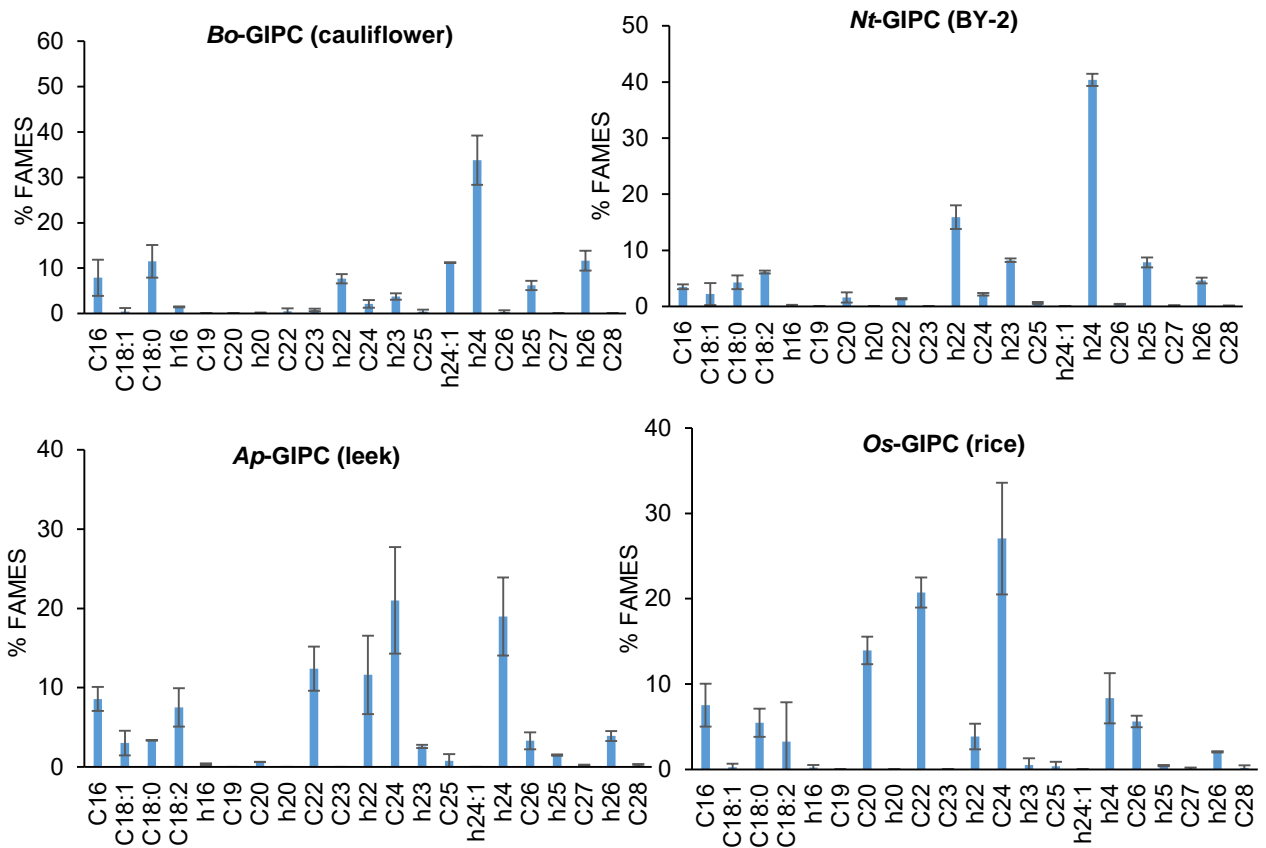
### ***Ap*-GIPC (leek)**



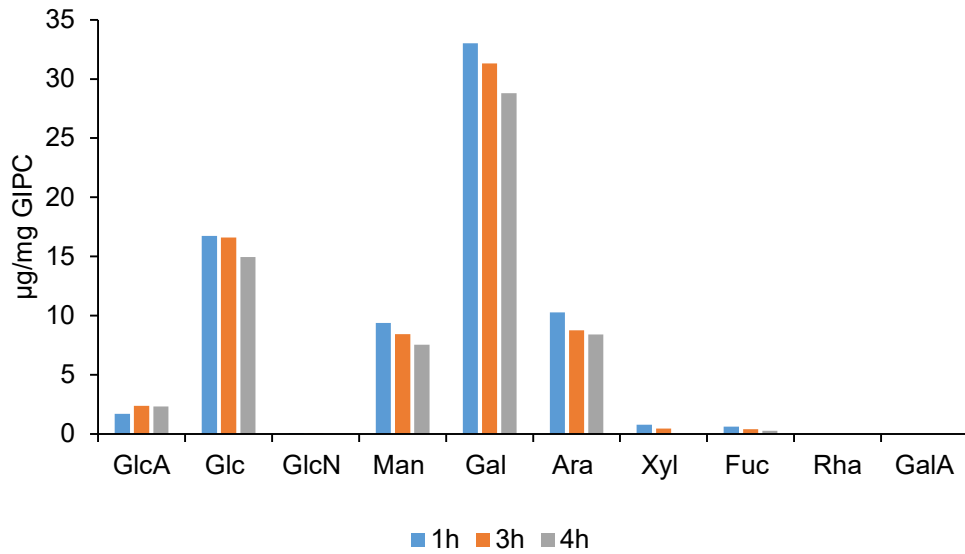
### ***Os*-GIPC (rice)**



**Supplementary data 1: High performance thin layer chromatography (HPTLC) assay of eluted fractions collected during the GIPC purification process** (described in Figure 2). (2) refers to the crude extract deposited on the silica column. Fractions containing GIPC without visible contamination of sterols and phospholipids were selected and pooled to make up fraction (3)

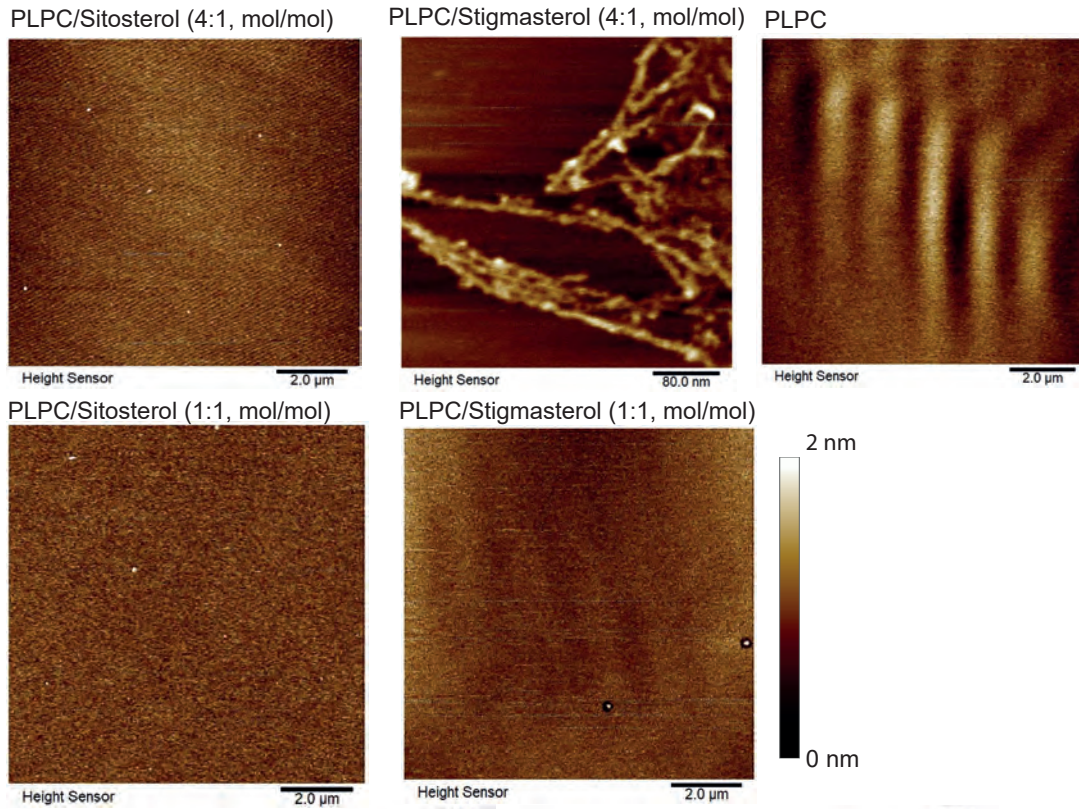


**Supplementary data 2: Fatty acid contents of GIPC-enriched fractions purified from cauliflower, BY-2 cell culture, leek and rice cell culture.** The fatty acid content was quantified after releasing fatty acid by transmethylation of GIPC-enriched samples, followed by derivatization by BSTFA before GC-MS analysis. The most abundant pool of fatty acid are hydroxylated fatty acid >20 carbons (hVLCFA) for *Bo*-GIPC and *Nt*-GIPC enriched-samples and non-hydroxylated fatty acid >20 carbons (VLCFA) for *Ap*-GIPC and *Os*-GIPC enriched-sample. The data are means of three independent experiments  $\pm$  SD.

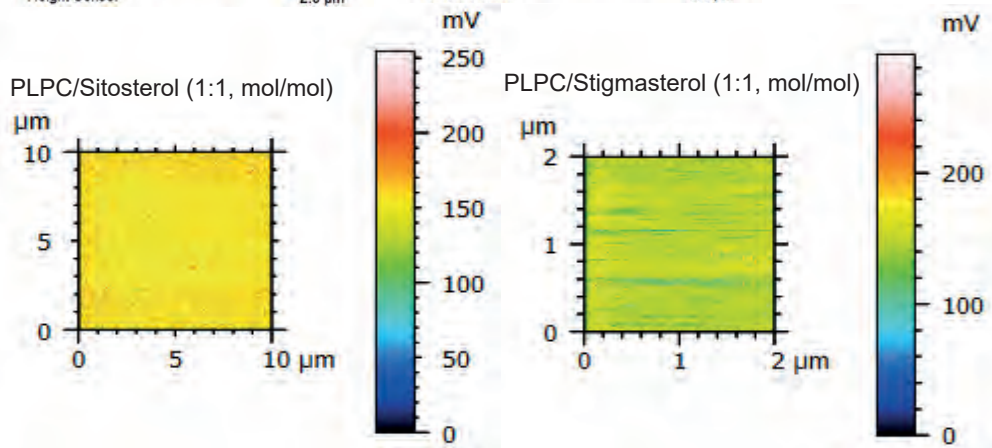


**Supplementary data 3: Determining glycan content by HPAE analysis of GIPC-enriched samples.** A slight change in sugar amount was seen after 1h, 3h and 4h of TFA hydrolysis. (GlcA: glucuronic acid; Glc: glucose; GlcN: glucosamine; Man: mannose; Gal: galactose; Ara: arabinose; Xyl: xylose; Fuc: fucose; Rha: L-rhamnose; GalA: galacturonic acid)

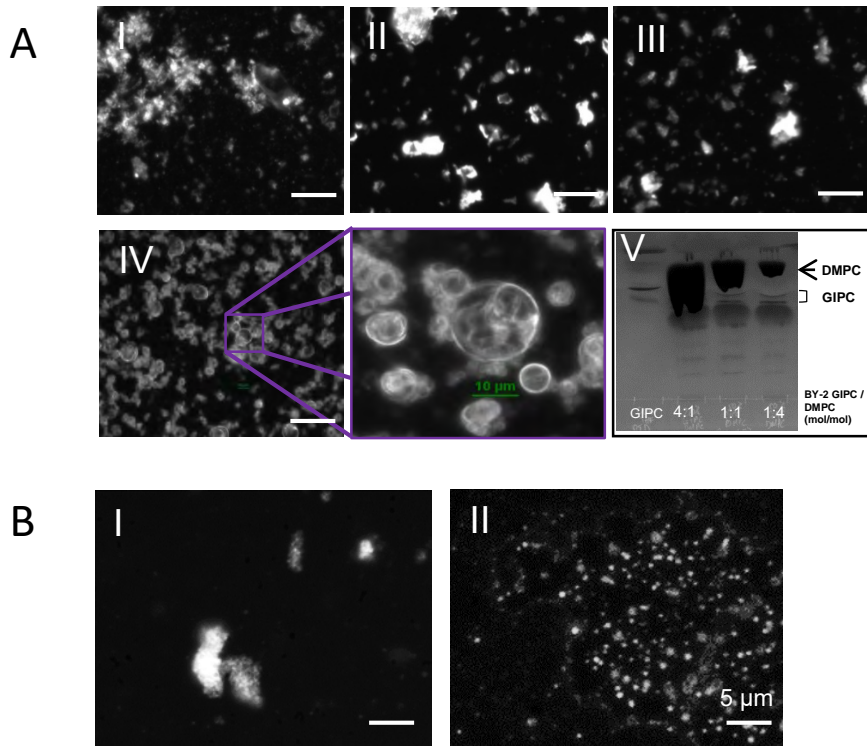
A



B



**Supplementary data 4:** A. Atomic Force Microscopy topographic images of lipid monolayer containing PLPC or PLPC/Sitosterol or stigmasterol at different molar ratio. No distinguishable structure was observed amid fiber-like structures for PLPC/Stigmasterol (4:1, mol/mol). Scan size is 10 $\mu$ m with the exception of PLPC/Stigmasterol (4:1, mol/mol) scan size 400nm. B. NanoIR images display low amplitude signal and no particular difference in molecular signature.



**Supplementary data 5. Fluorescent microscopy observations of Nt-GIPC containing liposomes in water at RT, pH 7.** A, Liposomes obtained after 3 cycles of freeze in liquid nitrogen and thaw (water bath at 60°C) containing (I) Nt-GIPCs 2mg/ml; (II) Nt-GIPC/ 1,2-dimyristoyl-sn-glycero-3-phosphocholine (DMPC) (4:1 mol/mol) at 2mg/ml; (III) Nt-GIPC/ DMPC (1:1 mol/mol) at 2mg/ml shows crystals; (IV) Nt-GIPC/DMPC molar ratio (1:4 mol/mol) at 2mg/ml forms liposomes of 10μm. (V) HPTLC analysis of lipid mixture confirms the presence of GIPC and DMPC in the liposome mix observed. The higher the GIPC content, the higher the occurrence of crystal formation. GIPCs can form liposomes with phospholipids of short acyl chains when the latter is four-folds more abundant in the mix. B, Liposomes of Bo-cauliflower GIPC/POPC/Sitosterol (1:1:1 mol/mol) at 1mg/ml in TBS 1X. Clusters as shown in (I) were obtained after three cycles of 20min freezing at -20°C and thawing in a water bath at 60°C. Liposomes in (II) were formed after three cycles of freezing in liquid N<sub>2</sub> and 20min heating in a water bath at 60°C; no cluster was observed. The type of freeze/thaw determines the size and shape of liposomes formed.

Table 1

POPC/Sitosterol	SLD ( $10^{-6}\text{\AA}^{-2}$ )	Thickness ( $\text{\AA}$ )	Solvent (%)	Roughness ( $\text{\AA}$ )
SiO <sub>2</sub>	3.47	10	3	3
Head	1.8	8	45	3
tails	-0.31	31	5	5
head	1.8	8	39	4

Table 2

GIPC/POPC/Sitosterol	SLD ( $10^{-6}\text{\AA}^{-2}$ )	Thickness ( $\text{\AA}$ )	Solvent (%)	Roughness ( $\text{\AA}$ )
SiO <sub>2</sub>	3.47	10	1	3
Sugar	1.9	4	80	3
Head	1.8	8	50	3
tails	-0.31	31	5	7
head	1.8	8	45	6
Sugar	1.9	4	80	5

**Supplementary data 6: Structural parameters after multilayer model fitting of reflectivity profiles of lipid bilayer.** Scattering length density (SLD), thickness, solvent and roughness profiles of POPC/Sitosterol (Table 1) and GIPC/POPC/Sitosterol (Table 2). The addition of GIPC in the bilayer increases the membrane thickness by 8  $\text{\AA}$ .

## References

- Baumgart, T., Hunt, G., Farkas, E. R., Webb, W. W., & Feigenson, G. W. (2007). Fluorescence probe partitioning between Lo/Ld phases in lipid membranes. *Biochimica et Biophysica Acta - Biomembranes*, 1768(9), 2182–2194. <https://doi.org/10.1016/j.bbamem.2007.05.012>
- Beck, J. G., Mathieu, D., Loudet, C., Buchoux, S., & Dufourc, E. J. (2007). Plant sterols in “rafts”: a better way to regulate membrane thermal shocks. *The FASEB Journal*, 21(8), 1714–1723. <https://doi.org/10.1096/fj.06-7809com>
- Buré, C., Cacas, J. L., Badoc, A., Mongrand, S., & Schmitter, J. M. (2016). Branched glycosylated inositolphosphosphingolipid structures in plants revealed by MS3analysis. *Journal of Mass Spectrometry*. <https://doi.org/10.1002/jms.3758>
- Buré, C., Cacas, J. L., Mongrand, S., & Schmitter, J. M. (2014). Characterization of glycosyl inositol phosphoryl ceramides from plants and fungi by mass spectrometry. *Analytical and Bioanalytical Chemistry*, Vol. 406, pp. 995–1010. <https://doi.org/10.1007/s00216-013-7130-8>
- Buré, C., Cacas, J. L., Wang, F., Gaudin, K., Domergue, F., Mongrand, S., & Schmitter, J. M. (2011). Fast screening of highly glycosylated plant sphingolipids by tandem mass spectrometry. *Rapid Communications in Mass Spectrometry*. <https://doi.org/10.1002/rcm.5206>
- Cacas, J. L., Buré, C., Furt, F., Maalouf, J. P., Badoc, A., Cluzet, S., ... Mongrand, S. (2013). Biochemical survey of the polar head of plant glycosylinositolphosphoceramides unravels broad diversity. *Phytochemistry*. <https://doi.org/10.1016/j.phytochem.2013.08.002>
- Cacas, J. L., Buré, C., Grosjean, K., Gerbeau-Pissot, P., Lherminier, J., Rombouts, Y., ... Mongrand, S. (2016a). Revisiting plant plasma membrane lipids in tobacco: A focus on sphingolipids. *Plant Physiology*, 170(1), 367–384. <https://doi.org/10.1104/pp.15.00564>
- Cacas, J. L., Buré, C., Grosjean, K., Gerbeau-Pissot, P., Lherminier, J., Rombouts, Y., ... Mongrand, S. (2016b). Revisiting plant plasma membrane lipids in tobacco: A focus on sphingolipids. *Plant Physiology*, 170(1), 367–384. <https://doi.org/10.1104/pp.15.00564>
- CARTER, H. E., GIGG, R. H., LAW, J. H., NAKAYAMA, T., & WEBER, E. (1958). Biochemistry of the sphingolipides. XI. Structure of phytoglycolipide. *The Journal of Biological Chemistry*, 233(6), 1309–1314. Retrieved from <http://www.jbc.org/>
- Carter, H. E., & Koob, J. L. (1969). Sphingolipids in bean leaves (*Phaseolus vulgaris*). *Journal of Lipid Research*, 10(4), 363–369.
- Deleu, M., Crowet, J. M., Nasir, M. N., & Lins, L. (2014). Complementary biophysical tools to investigate lipid specificity in the interaction between bioactive molecules and the plasma membrane: A review. *Biochimica et Biophysica Acta - Biomembranes*, 1838(12), 3171–3190. <https://doi.org/10.1016/j.bbamem.2014.08.023>
- Fang, L., Ishikawa, T., Rennie, E. A., Murawska, G. M., Lao, J., Yan, J., ... Mortimer, J. C. (2016). Loss of Inositol Phosphorylceramide Sphingolipid Mannosylation

Induces Plant Immune Responses and Reduces Cellulose Content in Arabidopsis. *The Plant Cell*. <https://doi.org/10.1105/tpc.16.00186>

- Furt, F., Lefebvre, B., Cullimore, J., Bessoule, J. J., & Mongrand, S. (2007). Plant lipid rafts: Fluctuat nec mergitur. *Plant Signaling and Behavior*, 2(6), 508–511. <https://doi.org/10.4161/psb.2.6.4636>
- Gerbeau-Pissot, P., Der, C., Thomas, D., Anca, I.-A., Grosjean, K., Roche, Y., ... Simon-Plas, F. (2014a). Modification of Plasma Membrane Organization in Tobacco Cells Elicited by Cryptogein. *PLANT PHYSIOLOGY*, 164(1), 273–286. <https://doi.org/10.1104/pp.113.225755>
- Gerbeau-Pissot, P., Der, C., Thomas, D., Anca, I. A., Grosjean, K., Roche, Y., ... Simon-Plas, F. (2014b). Modification of plasma membrane organization in tobacco cells elicited by cryptogein. *Plant Physiology*, 164(1), 273–286. <https://doi.org/10.1104/pp.113.225755>
- Goldenberg, N. M., & Steinberg, B. E. (2010, February 15). Surface charge: A key determinant of protein localization and function. *Cancer Research*, Vol. 70, pp. 1277–1280. <https://doi.org/10.1158/0008-5472.CAN-09-2905>
- Gronnier, J., Gerbeau-Pissot, P., Germain, V., Mongrand, S., & Simon-Plas, F. (2018, October 1). Divide and Rule: Plant Plasma Membrane Organization. *Trends in Plant Science*, Vol. 23, pp. 899–917. <https://doi.org/10.1016/j.tplants.2018.07.007>
- Grosjean, K., Mongrand, S., Beney, L., Simon-Plas, F., & Gerbeau-Pissot, P. (2015). Differential effect of plant lipids on membrane organization specificities of phytosphingolipids and phytosterols. *Journal of Biological Chemistry*, 290(9), 5810–5825. <https://doi.org/10.1074/jbc.M114.598805>
- Gutierrez, A. L. S., Farage, L., Melo, M. N., Mohana-Borges, R. S., Guerardel, Y., Coddeville, B., ... Guerardel, Y. (2007). Characterization of glycoinositolphosphoryl ceramide structure mutant strains of *Cryptococcus neoformans*. *Glycobiology*. <https://doi.org/10.1093/glycob/cwm030>
- Hsieh, T. C., Lester, R. L., & Laine, R. A. (1981). Glycophosphoceramides from plants. Purification and characterization of a novel tetrasaccharide derived from tobacco leaf glycolipids. *Journal of Biological Chemistry*.
- Ishikawa, T., Fang, L., Rennie, E. A., Sechet, J., Yan, J., Jing, B., ... Mortimer, J. C. (2018). GLUCOSAMINE INOSITOLPHOSPHORYLCERAMIDTRANSFERASE1 (GINT1) is a GlcNAc-containing glycosylinositol phosphorylceramide glycosyltransferase. *Plant Physiology*, 177(3), 938–952. <https://doi.org/10.1104/pp.18.00396>
- Jin, L., Millard, A. C., Wuskell, J. P., Clark, H. A., & Loew, L. M. (2005). Cholesterol-enriched lipid domains can be visualized by di-4-ANEPPDHQ with linear and nonlinear optics. *Biophysical Journal*, 89(1). <https://doi.org/10.1529/biophysj.105.064816>
- Jin, L., Millard, A. C., Wuskell, J. P., Dong, X., Wu, D., Clark, H. A., & Loew, L. M. (2006). Characterization and application of a new optical probe for membrane lipid domains. *Biophysical Journal*, 90(7), 2563–2575. <https://doi.org/10.1529/biophysj.105.072884>

- Kaul, K., & Lester, R. L. (1975). Characterization of Inositol-containing Phosphosphingolipids from Tobacco Leaves. *Plant Physiology*, 55(1), 120–129. <https://doi.org/10.1104/pp.55.1.120>
- Kaul, K., & Lester, R. L. (1978). Isolation of Six Novel Phosphoinositol-Containing Sphingolipids from Tobacco Leaves. *Biochemistry*, 17(17), 3569–3575. <https://doi.org/10.1021/bi00610a023>
- Kitazawa, K., Tryfona, T., Yoshimi, Y., Hayashi, Y., Kawauchi, S., Antonov, L., ... Kotake, T. (2013).  $\beta$ -Galactosyl Yariv Reagent Binds to the  $\beta$ -1,3-Galactan of Arabinogalactan Proteins. *Plant Physiology*, 161(3), 1117–1126. <https://doi.org/10.1104/pp.112.211722>
- Kubsch, B., Robinson, T., Steinkühler, J., & Dimova, R. (2017). Phase behavior of charged vesicles under symmetric and asymmetric solution conditions monitored with fluorescence microscopy. *Journal of Visualized Experiments*, 2017(128). <https://doi.org/10.3791/56034>
- Lefebvre, B., Furt, F., Hartmann, M.-A., Michaelson, L. V., Carde, J.-P., Sargueil-Boiron, F., ... Mongrand, S. (2007). Characterization of Lipid Rafts from *Medicago truncatula* Root Plasma Membranes: A Proteomic Study Reveals the Presence of a Raft-Associated Redox System. *PLANT PHYSIOLOGY*, 144(1), 402–418. <https://doi.org/10.1104/pp.106.094102>
- Lenarčič, T., Albert, I., Böhm, H., Hodnik, V., Pirc, K., Zavec, A. B., ... Nürnberger, T. (2017). Eudicot plant-specific sphingolipids determine host selectivity of microbial NLP cytolysins. *Science*, 358(6369), 1431–1434. <https://doi.org/10.1126/science.aan6874>
- Levental, I., & Veatch, S. L. (2016, December 4). The Continuing Mystery of Lipid Rafts. *Journal of Molecular Biology*, Vol. 428, pp. 4749–4764. <https://doi.org/10.1016/j.jmb.2016.08.022>
- Lingwood, D., & Simons, K. (2010, January 1). Lipid rafts as a membrane-organizing principle. *Science*, Vol. 327, pp. 46–50. <https://doi.org/10.1126/science.1174621>
- London, E., & Brown, D. A. (2000). Insolubility of lipids in Triton X-100: physical origin and relationship to sphingolipid/cholesterol membrane domains (rafts). *Biochimica et Biophysica Acta (BBA) - Biomembranes*, 1508(1–2), 182–195. [https://doi.org/10.1016/S0304-4157\(00\)00007-1](https://doi.org/10.1016/S0304-4157(00)00007-1)
- Maget-Dana, R. (1999). The monolayer technique: A potent tool for studying the interfacial properties of antimicrobial and membrane-lytic peptides and their interactions with lipid membranes. In *Biochimica et Biophysica Acta - Biomembranes* (Vol. 1462). [https://doi.org/10.1016/S0005-2736\(99\)00203-5](https://doi.org/10.1016/S0005-2736(99)00203-5)
- Mamode Cassim, A., Gouguet, P., Gronnier, J., Laurent, N., Germain, V., Grison, M., ... Mongrand, S. (2019). Plant lipids: Key players of plasma membrane organization and function. *Progress in Lipid Research*, 73(November 2018), 1–27. <https://doi.org/10.1016/j.plipres.2018.11.002>
- Manna, M., Javanainen, M., Monne, H. M. S., Gabius, H. J., Rog, T., & Vattulainen, I. (2017). Long-chain GM1 gangliosides alter transmembrane domain registration through interdigitation. *Biochimica et Biophysica Acta - Biomembranes*, 1859(5), 870–878. <https://doi.org/10.1016/j.bbamem.2017.01.033>

- Mannock, D. A., Lewis, R. N. A. H., McMullen, T. P. W., & McElhaney, R. N. (2010, June). The effect of variations in phospholipid and sterol structure on the nature of lipid-sterol interactions in lipid bilayer model membranes. *Chemistry and Physics of Lipids*, Vol. 163, pp. 403–448.  
<https://doi.org/10.1016/j.chemphyslip.2010.03.011>
- Markham, J. E., & Jaworski, J. G. (2007). Rapid measurement of sphingolipids from *Arabidopsis thaliana* by reversed-phase high-performance liquid chromatography coupled to electrospray ionization tandem mass spectrometry. *Rapid Communications in Mass Spectrometry*. <https://doi.org/10.1002/rcm.2962>
- Markham, J. E., Molino, D., Gissot, L., Bellec, Y., Hématy, K., Marion, J., ... Faure, J.-D. (2011). Sphingolipids Containing Very-Long-Chain Fatty Acids Define a Secretory Pathway for Specific Polar Plasma Membrane Protein Targeting in *Arabidopsis*. *The Plant Cell*. <https://doi.org/10.1105/tpc.110.080473>
- Mongrand, S., Morel, J., Laroche, J., Claverol, S., Carde, J. P., Hartmann, M. A., ... Bessoule, J. J. (2004). Lipid rafts in higher plant cells: Purification and characterization of triton X-100-insoluble microdomains from tobacco plasma membrane. *Journal of Biological Chemistry*, 279(35), 36277–36286.  
<https://doi.org/10.1074/jbc.M403440200>
- Moreau, R. A., Nyström, L., Whitaker, B. D., Winkler-Moser, J. K., Baer, D. J., Gebauer, S. K., & Hicks, K. B. (2018, April 1). Phytosterols and their derivatives: Structural diversity, distribution, metabolism, analysis, and health-promoting uses. *Progress in Lipid Research*, Vol. 70, pp. 35–61.  
<https://doi.org/10.1016/j.plipres.2018.04.001>
- Morikawa, T., Mizutani, M., Aoki, N., Watanabe, B., Saga, H., Saito, S., ... Ohta, D. (2006). Cytochrome P450 CYP710A encodes the sterol C-22 desaturase in *Arabidopsis* and tomato. *Plant Cell*, 18(4), 1008–1022.  
<https://doi.org/10.1105/tpc.105.036012>
- Morré, D. M., & Morre, D. J. (2000). Aqueous two-phase partition applied to the isolation of plasma membranes and Golgi apparatus from cultured mammalian cells. *Journal of Chromatography B: Biomedical Sciences and Applications*, 743(1–2), 377–387. [https://doi.org/10.1016/S0378-4347\(00\)00058-X](https://doi.org/10.1016/S0378-4347(00)00058-X)
- Mortimer, J. C., Yu, X., Albrecht, S., Sicilia, F., Huichalaf, M., Ampuero, D., ... Dupree, P. (2013). Abnormal glycosphingolipid mannosylation triggers salicylic acid-mediated responses in *Arabidopsis*. *Plant Cell*, 25(5), 1881–1894.  
<https://doi.org/10.1105/tpc.113.111500>
- Nagano, M., Takahara, K., Fujimoto, M., Tsutsumi, N., Uchimiya, H., & Kawai-Yamada, M. (2012). *Arabidopsis* sphingolipid fatty acid 2-hydroxylases (AtFAH1 and AtFAH2) are functionally differentiated in fatty acid 2-hydroxylation and stress responses. *Plant Physiology*, 159(3), 1138–1148.  
<https://doi.org/10.1104/pp.112.199547>
- Pata, M. O., Hannun, Y. A., & Ng, C. K. Y. (2010). Plant sphingolipids: Decoding the enigma of the Sphinx. *New Phytologist*, Vol. 185, pp. 611–630.  
<https://doi.org/10.1111/j.1469-8137.2009.03123.x>
- Róg, T., Orłowski, A., Llorente, A., Skotland, T., Sylvänne, T., Kauhanen, D., ...

- Vattulainen, I. (2016). Interdigitation of long-chain sphingomyelin induces coupling of membrane leaflets in a cholesterol dependent manner. *Biochimica et Biophysica Acta - Biomembranes*, 1858(2), 281–288. <https://doi.org/10.1016/j.bbamem.2015.12.003>
- Sampaio, J. L., Levental, I., Lingwood, D., Simons, K., Rajendran, L., Kalvodova, L., & Kaiser, H.-J. (2009). Order of lipid phases in model and plasma membranes. *Proceedings of the National Academy of Sciences*, 106(39), 16645–16650. <https://doi.org/10.1073/pnas.0908987106>
- Sibille, E., Berdeaux, O., Martine, L., Bron, A. M., Creuzot-Garcher, C. P., He, Z., ... Masson, E. A. Y. (2016). Ganglioside profiling of the human retina: Comparison with other ocular structures, brain and plasma reveals tissue specificities. *PLoS ONE*. <https://doi.org/10.1371/journal.pone.0168794>
- Simenel, C., Coddeville, B., Delepierre, M., Latgé, J. P., & Fontaine, T. (2008). Glycosylinositolphosphoceramides in *Aspergillus Fumigatus*. *Glycobiology*. <https://doi.org/10.1093/glycob/cwm122>
- Sonnino, S., & Prinetti, A. (2010). Gangliosides as regulators of cell membrane organization and functions. *Advances in Experimental Medicine and Biology*, 688, 165–184. [https://doi.org/10.1007/978-1-4419-6741-1\\_12](https://doi.org/10.1007/978-1-4419-6741-1_12)
- Sperling, P., & Heinz, E. (2003). Plant sphingolipids: Structural diversity, biosynthesis, first genes and functions. *Biochimica et Biophysica Acta - Molecular and Cell Biology of Lipids*. [https://doi.org/10.1016/S1388-1981\(03\)00033-7](https://doi.org/10.1016/S1388-1981(03)00033-7)
- Tarazona, P., Feussner, K., & Feussner, I. (2015). An enhanced plant lipidomics method based on multiplexed liquid chromatography-mass spectrometry reveals additional insights into cold- and drought-induced membrane remodeling. *Plant Journal*, 84(3), 621–633. <https://doi.org/10.1111/tpj.13013>
- Tellier, F., Maia-Grondard, A., Schmitz-Afonso, I., & Faure, J. D. (2014). Comparative plant sphingolipidomic reveals specific lipids in seeds and oil. *Phytochemistry*. <https://doi.org/10.1016/j.phytochem.2014.03.023>
- Tjellstrom, H., Hellgren, L. I., Wieslander, A., & Sandelius, A. S. (2010). Lipid asymmetry in plant plasma membranes: phosphate deficiency-induced phospholipid replacement is restricted to the cytosolic leaflet. *The FASEB Journal*. <https://doi.org/10.1096/fj.09-139410>
- Voxeur, A., & Fry, S. C. (2014). Glycosylinositol phosphorylceramides from *Rosa* cell cultures are boron-bridged in the plasma membrane and form complexes with rhamnogalacturonan II. *Plant Journal*. <https://doi.org/10.1111/tpj.12547>
- Yetukuri, L., Ekroos, K., Vidal-Puig, A., & Orešič, M. (2008). Informatics and computational strategies for the study of lipids. *Mol. BioSyst.*, 4(2), 121–127. <https://doi.org/10.1039/B715468B>

**Acknowledgements.**

We thank Catherine Sarazin and Sébastien Buchoux for critical reading and advice, and Laure Beven for bright field microscopy.

## Additional data

### **A survey to analyse the structure of tobacco GIPC polar head by liquid-state <sup>1</sup>H-NMR**

As it will be described in chapter 3, the structure of GIPC polar head group has a huge implication in its role as receptors for necrotic toxin NLPs (Lenarčič et al., 2017a, 2019). Our recent publication (Lenarčič et al., 2017a) showed that the sensitivity and resistance to NLPs lies in the GIPC series sugar structure. Eudicots containing mainly GIPC series A (2 sugar moieties after the inositol group) are prone to necrosis upon NLP binding, while monocots are resistant to the cytolytic toxin as they contain mainly GIPC series B (3 sugar moieties after the inositol group). Our biophysics experiments and molecular modelling showed that in monocots (leek GIPC-enriched fractions), the additional sugar molecule is arranged perpendicular to the horizontal plane of the membrane such that the toxin on binding far away from the PM to induce necrosis. Understanding the structure of GIPC sugar head might yield important information about the important role of GIPC in plant/pathogen interactions.

The following report presents the results of experiments done with BY-2 GIPC-enriched samples in order to obtain information on the polar head structure of By-2 GIPCs. The aim was to use liquid-state <sup>1</sup>H-NMR to understand the identity of the sugar moieties, type of bonds between the glycan components of GIPC polar head group. I purified few milligrams GIPC-enriched fractions from tobacco BY-2 cells and sent them for analysis to our collaborator in Lille, Dr Emmanuel Maës at the Unité de Glycobiologie Structurale et Fonctionnelle, CNRS UMR 8576, Lille.

The first step for solid-state <sup>1</sup>H-NMR analysis was to remove the polar head group. This was done by acidic methanolysis. I provided twice tobacco GIPC-enriched fractions since the first samples were not pure enough to extrapolate results. Tobacco GIPC was used as they were already characterized by chromatography in the old papers of (H. E. Carter, Strobach, & Hawthorne, 1969; Kaul & Lester, 1978). Since NMR analysis was never done on plant GIPC fractions, we wanted to do so with a GIPC which has an already published structure. We were inspired by the publication of (Gutierrez et al., 2007) which use liquid-state NMR to characterize fungi GIPCs.

The results of our NMR experiments were not conclusive which might be blamed on the insufficient amount of GIPCs, as well as the insufficient purity. The acidic hydrolysis might have also damaged the sugar moieties to such an extent that they were no longer detected. The report attributed the amount of Arabinose, Galactose and Mannose found in the polyglycosylated fraction (Figure 7, samples F3 and F4) to partial contamination of the samples. The signal threshold was too close to the baseline to be conclusive. We argued that the presence of these sugars might actually be part of the polar head group structure of tobacco GIPC as (Kaul & Lester, 1975) propose a polyglycosylated structure of tobacco GIPC enriched in arabinose and galactose. (H. E. Carter et al., 1969) also propose the presence of mannose after hydrolysis of GIPC samples. The Yariv test done on the BY-2 samples (refer to Figure 4 of chapter 1) showed absence of arabinogalactan. Could there be other contaminants that we neglect to identify?

We hence have to work towards improving our extraction and purification protocol so as to obtain better quality GIPC for solid state NMR analysis. The ultimate objective is to obtain the molecular identity and bond orientation of a vast array of GIPC polar head group to supply information for molecular modelling and simulations in order to represent GIPC in plant PM models.

Here follows the pdf report of the platform written by Emmanuel Maës:

## FINAL REPORT (PAG17015)

### STRUCTURAL STUDY OF POLAR HEADS OF GLYCOLIPIDS (GIPC) FROM BY-2 CULTURE CELLS (NICOTENIA TABACUM)

UNITE DE GLYCOBIOLOGIE STRUCTURALE ET FONCTIONNELLE  
UMR 8576 DU CNRS  
F- 59655 VILLENEUVE D'ASCQ

Tel : 03 20 33 63 47

Fax : 03 20 43 65 55

[Plateforme-PAGES@univ-lille1.fr](mailto:Plateforme-PAGES@univ-lille1.fr)



Direction de l'Unité : Pr Christophe D'Hulst

Administratrice : Mme Martine Ratajczak

Direction Scientifique : Dr Yann Guérardel

Direction Technique : Dr Emmanuel Maes

Intervenant(s) : Dr Emmanuel Maes, Dr Yann Guérardel

## I- BY2 FRACTION (FIRST SENDING)

Nmr spectra were acquired in appropriate solvent (CDCl<sub>3</sub>:CD<sub>3</sub>OD:D<sub>2</sub>O) showing an high complexity of the mixture. In order to elucidate the main structure of this sample, we decided to saponify it. Saponification done with KOH 0.5 N during 6h at room 100°C. The fraction was purified through C18 sep-pak<sup>®</sup> cartridge from waters<sup>®</sup>. The column was firstly eluted with 5 mL of water and secondly by 5 mL of acetonitrile. The acetonitrile fraction further analyzed by GC-FID and GC-MS after derivatization whereas, prior to analyses, water fraction passed through molecular sieving BioGel<sup>®</sup> P2 column. 3 water fractions were obtained and analyzed by nmr and GC-MS.

In order to determine sugar composition we analyzed compound by two ways, firstly we did itol-acetate derivates after acidic hydrolysis and secondly trimethylsilyl (TMS) derivates after methanolysis. Finally, to obtain linkage analysis we did partially methylated and acetylated alditols derivates (PMAA) after total methylation, hydrolysis, reducing and finally peracétylation.

### 1- ITOL ACETATE DERIVATES

As shown on Fig. 1A, 2 main peaks identified based on electronic impact spectra (Fig 1B and Fig 1C). The peak at 22.74 min has identified as penta-acetyl pentitol and that at 30.65 as hexa-acetyl hexitol. The both retention times and the analyses of fragmentation spectra comparing to both standard derivates, *i.e.* pentitol and hexitol prove that were an arabinitol and galactitol derivates respectively. Moreover, three minor peaks eluted between 29.5 to 30.5 min correspond to hexa-acetyl of inositol, mannitol and glucitol residues respectively. The integration of mains peaks indicated that arabinitol and galactitol residues represent 43.5 % and 47.9% of total identified residues, whereas inositol, mannitol and glucitol represente 1.5, 1.6 and 5.4 % respectively of total identified residues and considered as traces.

No hexosamine and no uronic acid identified by this method.

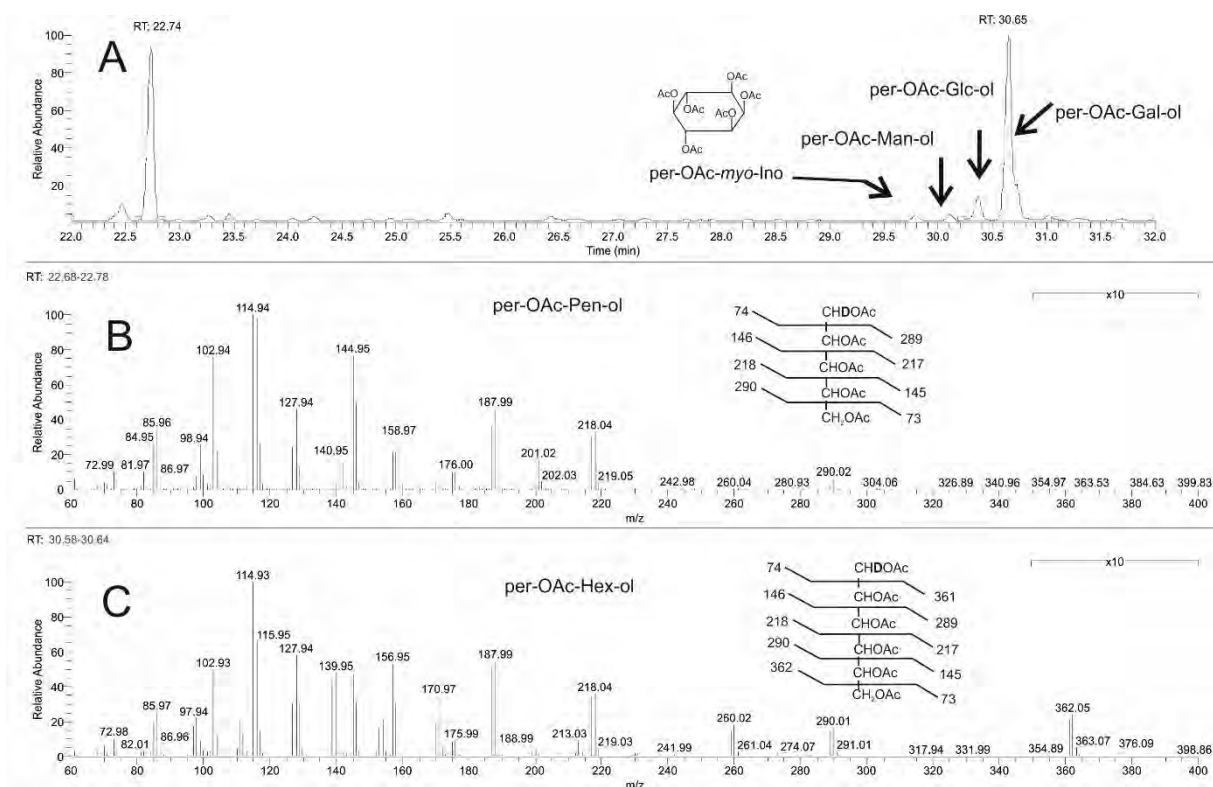


Figure 1 : Part of TIC chromatogram from GC-MS in impact electronic mode for acetonitrile fraction of BY2 Itol-acetate derivatives

## 2- TRIMETHYL SILYL DERIVATES

In order to confirm the Itol-acetate results we did trimethylsilyl derivatives method that was much more sensitive. Thus, sample subjected to methanolysis following by heptan extraction to put off lipids, and finally trimethylsilylation done. Based on retention time and electronic impact spectra from GC-MS analysis, as shown Fig. 2, allowed us identify four sugars residues Ara, Gal, Glc and GlcA and one Ino. Relative ratio of monosaccharides reported in table 1, these information obtained by integrated areas of their corresponding peaks. Moreover, some sugars possessed some retention times corresponding to their configuration as pyranne or furane cycles and their anomeries (*i.e.*  $\alpha$ - and  $\beta$ -).

Table 1 : Relative proportion of monosaccharides in molecule from GC-MS analyses

	Ara	Ino	Glc	GlcA	Gal
<b>areas</b>	40303757	1505470	6515577	1270907	54799282
<b>%</b>	38.6	1.4	6.2	1.2	52.5
<b>With Ino set to 1</b>	26.8	1.0	4.3	0.8	36.4

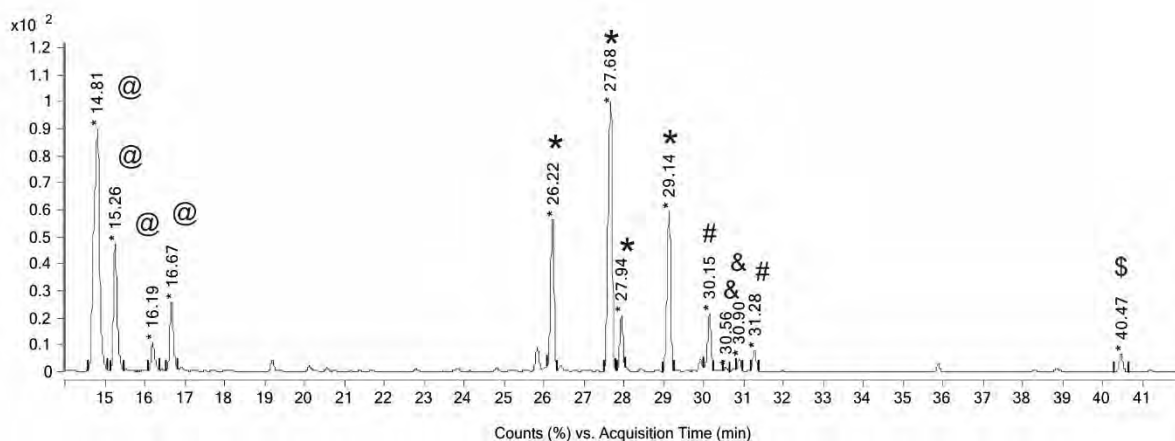


Figure 2 : Part of TIC chromatogram from GC-MS in impact electronic mode for acetonitrile fraction BY2 TMS derivatives. @ : Arabinoses, \* : Galactoses, # : Glucoses, & : Glucuronic acids, \$ : Inositol

Such composition leading us to think an arabinogalactane molecule linked to GIPC core without ceramide part deleted after saponification. No hexosamine was identified.

### 3- PARTIALLY METHYLATED AND ACETYLATED ALDITOLS (PMAA) DERIVATES

In order to know the linkages between sugars; we performed an analysis of partially methylated and acetylated alditols from sugars. The methylation analysis done according to Hakomori's method where methylation derivation obtained with sodium hydride in anhydrous DMSO and methyl iodide.

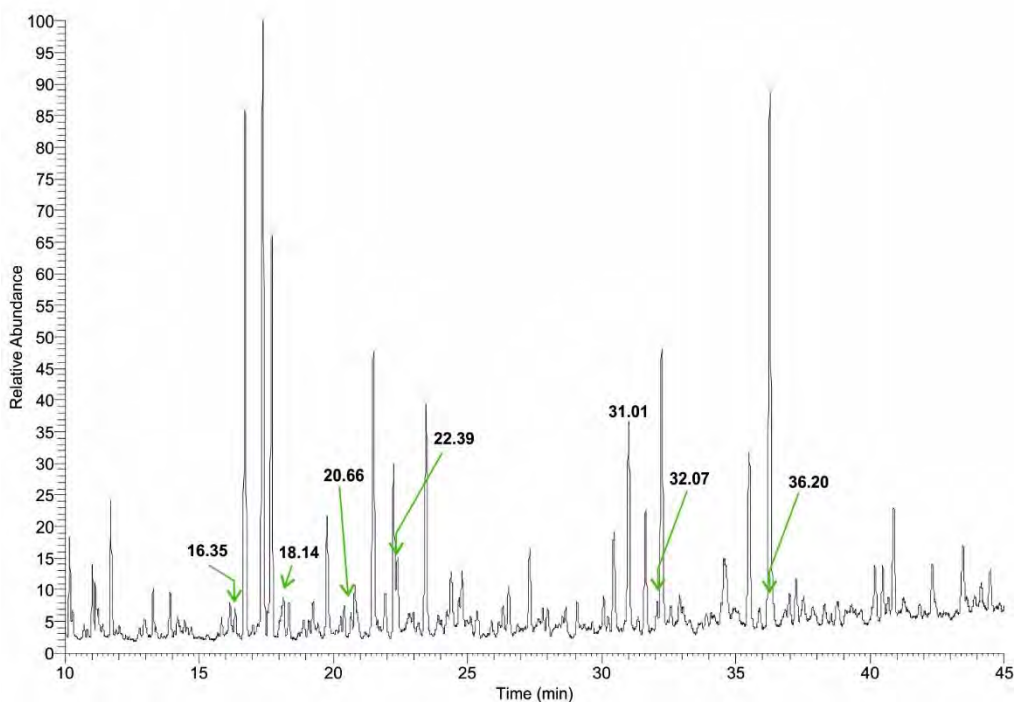


Figure 3 : TIC of Partially Methylated and Acetylated Alditol (PMAA) derivatives obtained by electronic impact source of GC-MS spectrometer. Arrows indicate retention time of identified molecules

The TIC chromatogram (Fig. 3) shows the complex mixture of volatile derivatives including non-sugar molecules and containing GIPC fraction. Seven kind of monosaccharide derivatives identified based on their characteristic fragmentation; main ions reported in table 2. The presence of terminal pentoses as well as furan and pyranic forms identified as proved by the presence or absence of typical ions, *i.e.* concomitant absence of  $m/z$  45 and presence of  $m/z$  117 allowed identifying pyranic form of pentose. In the same way, we have identified a 2-O-substituted pentose thanks to its  $m/z$  set fragmentation values 161, 190 and 101. Moreover a 3,6-di-O-substituted hexosyl residue with the  $m/z$  set values 189, 234 and 305 related to 6-O-galactosyl residue has been detected and so on. No terminal galactose identified indicating firstly an absence of ramification of internal galactosyl sequence or secondly all possible terminal galactoses substituted by Arabinose

Table 2 : Partially Methylated and Acetylated Alditol derivatives (PMAA) identified by impact electronic mass spectrometry. *m/z* ions in bold characters represents most important ions for identification

Retention time (min)	PMAA residues	Corresponding sugars	Characteristic ions			Absent ion
16.35	1,4 di-O-acetyl-2,3,5 tri-O-Methyl pentitol	t-Araf	118	161	45	
18.15	1,5 di-O-acetyl-2,3,4 tri-O-Methyl pentitol	t-Arap	161	162	<b>117</b>	<b>45</b>
20.66	1,2,4-tri-O-acetyl-3,5-di-O-methyl-pentitol	2-Araf	<b>161</b>	190	<b>101</b>	
22.39	1,4,5 tri-O-acetyl-2,3 di-O-Methyl pentitol	5-Araf or 4-Arap	118	189	162	
31.01	1,2,4,5 tetra-O-acetyl-3 mono-O-Methyl pentitol	2,5-Araf or 2,4-Arap	189	190		
32.07	1,5,6-tri-O-acetyl-2,3,4-tri-O-Methyl Hexitol	6-Galp	<b>118</b>	189	<b>233</b>	
36.20	1,3,5,6-tetra-O-acetyl-2,4-di-O-methyl-Hexitol	3,6-Galp	<b>189</b>	<b>234</b>	<b>305</b>	45

## 4 NMR STUDIES

NMR spectra were very complex but they allowed us firstly to define anomeric form of the some monosaccharides, secondly to prove the both presence of furanic and pyranic forms for monosaccharides and thirdly to confirm some substitution features.

### 3.1 Proton nmr of BY2 fraction, C18 acetonitrile elution

We recorded 1D <sup>1</sup>H-NMR spectra before and after saponification (Fig 4), the results were relevant since we observe that trace, after saponification, represent molecule with lower molecular weight than before saponification. Indeed, signals between 3 to 1 ppm represented large alkyl chains, founded in fatty acid chains, and shown a large chemical shift anisotropy. Surprisingly, some alkyl chains remained on the molecule despite the saponification. It was possible that chain was differently linked and thus more resistant to saponification. However, we identified between 6 to 3 ppm, signals corresponding to carbohydrate significant signals recovered after saponification and purification on C18 column.

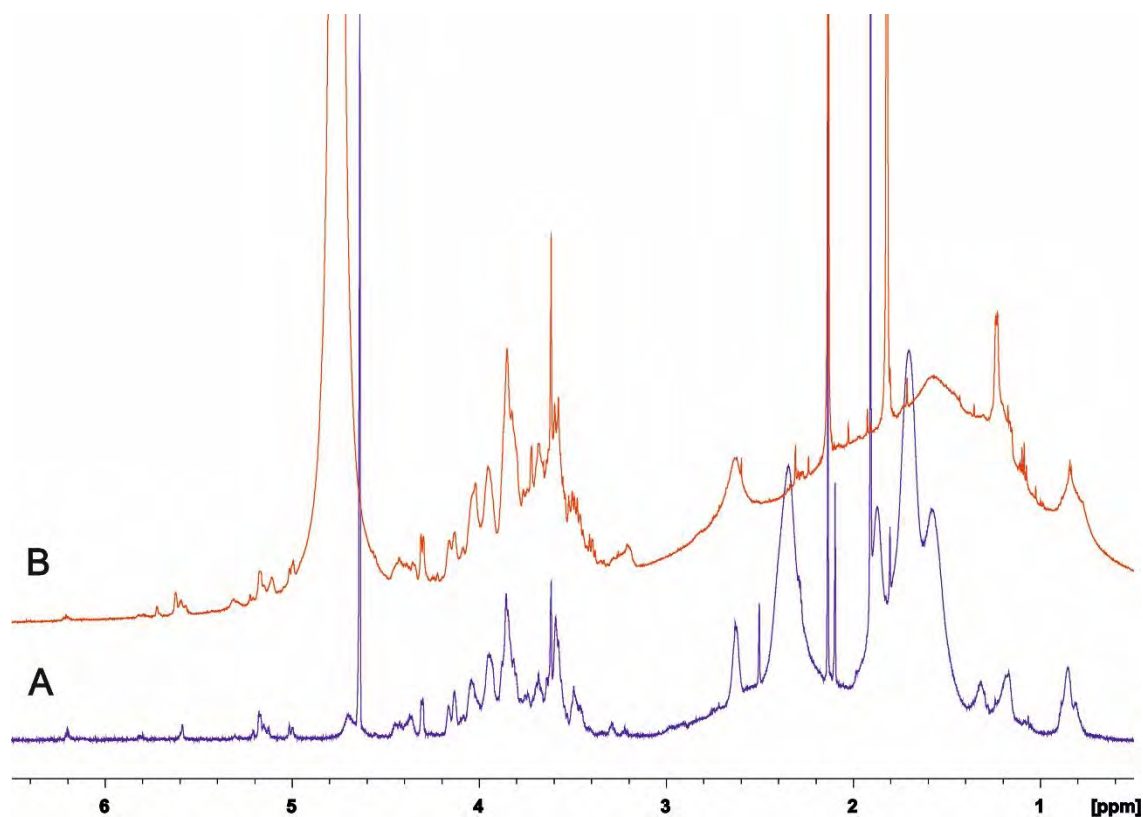


Figure 4 :  $^1\text{H}$ -nmr spectra of molecule before (red B) and after (A blue) saponification.

In order to elucidate spin system of carbohydrate we recorded a set of nmr experiments like homonuclear correlation spectroscopy (*i.e.* COSY and TOCSY experiments) and heteronuclear correlation Fig. 5 (*i.e.*  $^1\text{H}$ - $^{13}\text{C}$  edited HSQC).

Unfortunately, nmr spectra were not nice quality to elucidate complete sequence. However, we confirmed that both main carbohydrates were  $\beta$ -Galactopyranosyl and  $\alpha$ -Arabinofuranosyl residues. Anomeric proton of  $\beta$ -Gal resonated between 4.40 to 4.52 ppm and their  $^{13}\text{C}$  chemical shift at 104.6 ppm whereas anomeric protons of  $\alpha$ -Araf resonated at 5.09 and 5.26 ppm and anomeric carbons at 109.1 and 110.4 respectively. We demonstrated the presence of both O-3-monosubstituted and O-3, O-6 disubstituted  $\beta$ -Gal as proved its H3-C3 chemical shift at 3.74-81.5 ppm and their H6,6' resonating around  $\delta$  3.92,3.67 and C6 at  $\delta$  67.5-67.8. In the same way, the downfield shifted of the C2 and some C5 of  $\alpha$ -Arabino-furanoside indicated their respective substitution at these positions.

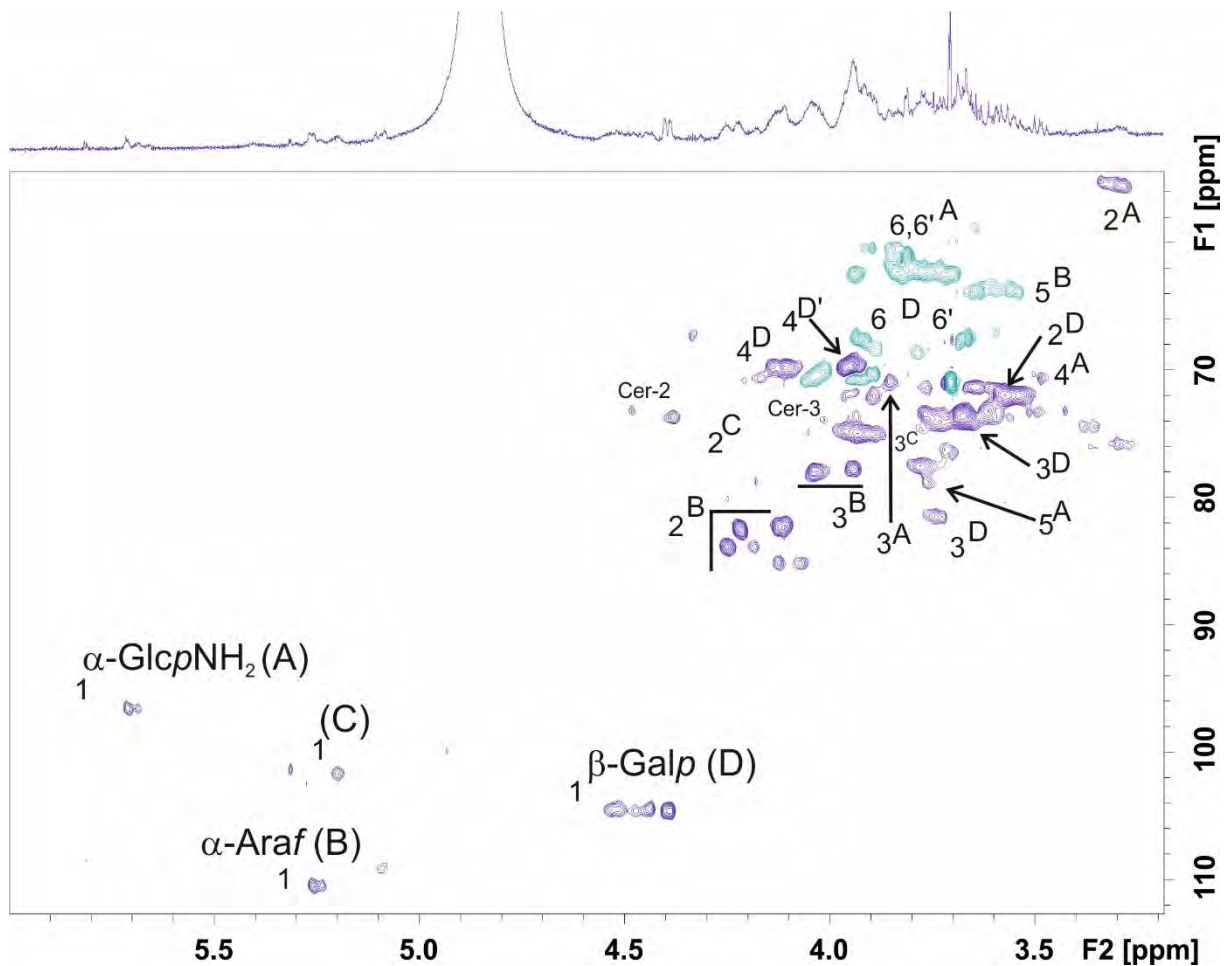


Figure 5 : part of  $^1\text{H}$ - $^{13}\text{C}$  edited HSQC, green signals corresponded to secondary alcohol bearing carbons. Letters correspond to identified residues, i.e. A =  $\alpha$ -GlcNH<sub>2</sub>, B =  $\alpha$ -Araf, C=may be uronic acid and D=  $\beta$ -Galp

The unit A was supposed as an  $\alpha$ -GlcNH<sub>2</sub>, since H<sub>2</sub>-C<sub>2</sub> correlation resonated at 3.33-55.3, with two spin system indicating two states of substitutions. Carefulness, this unit could also be a nitrogen bearing carbon of a ceramide molecule. Unfortunately, the poor quality of nmr spectra forbidden the clean reading of their entire spin systems. In the same way, the unit C was unlabeled since its spin system appeared not clear but it could be uronic acid.

### 3.2 Protons nmr of water fraction after saponification

Amount of samples were too few to engage extensive 2D nmr experiments.

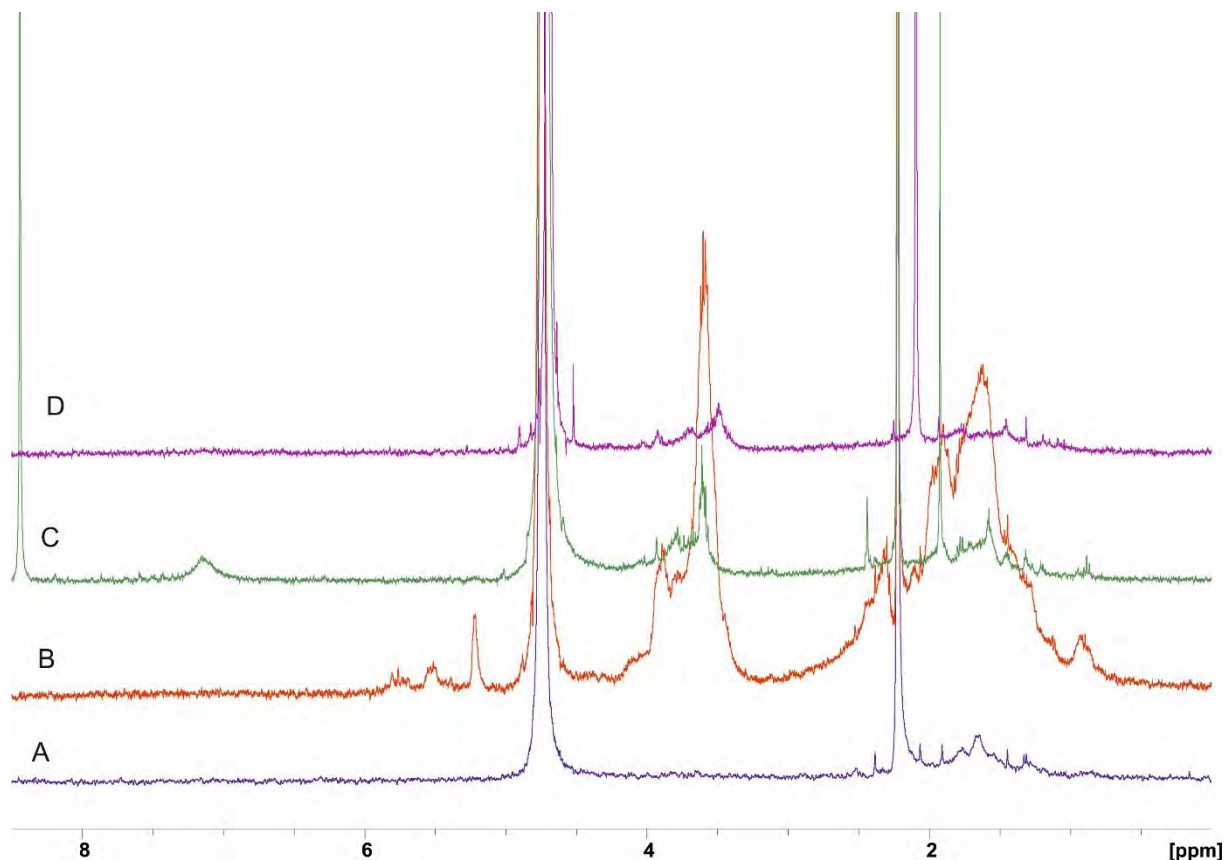


Figure 6 :  $^1\text{H-NMR}$  spectra of different fractions eluted from Bio-Gel P2 chromatography. A, first eluted fraction, D last eluted fraction.

As shown Fig 6, the fraction B seemed the main sugar-containing fraction. The amount of material was too few to record extensive 2D nmr experiment, however, we recorded low resolved tocsy experiment allowed us to show that B fraction contained highly hydroxylated alkyl chains and not sugars. Unfortunately, not all other fractions contained not enough material to continue structural investigation.

## II- BY2 FIVE FRACTIONS (SECOND SENDING)

In a second part, we analyzed five fractions labeled F1 to F5. In order to compare molecular composition, we did TMS derivates of these fractions (Fig. 6).

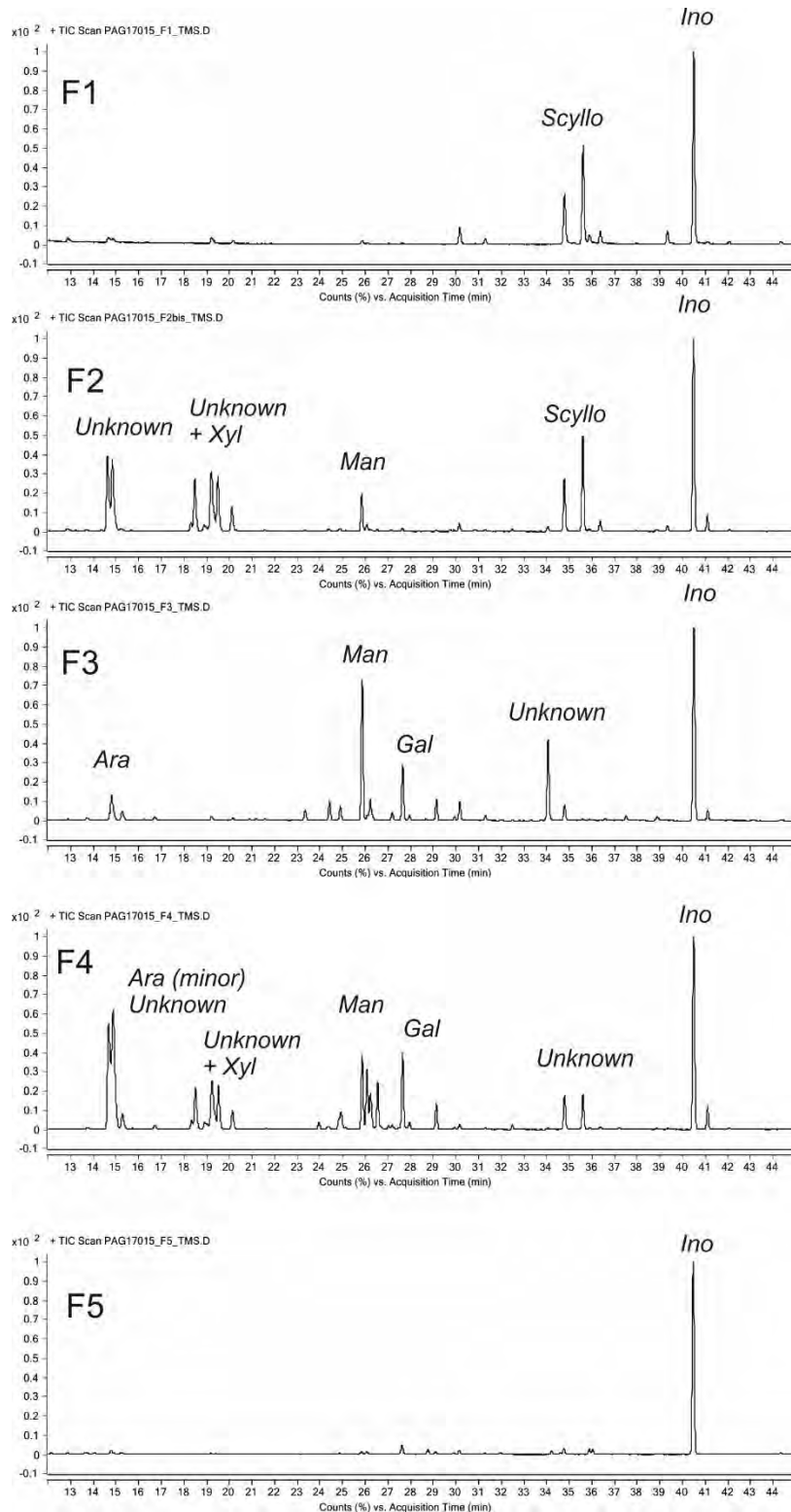


Figure 7 : GC-MS chromatograms of TMS derivates of BY2 F1 to F5 fraction, Ino added as internal standard

On Fig 6, we observe that fractions are heterogeneous, some peaks remained unresolved and didn't correspond to classical sugar, some more investigations must

be done. Indeed, nmr fraction of F1, F2, F3 and F5 were done but the sugar ratio is really poor compare to lipid part. Fig 7 shows 1D nmr experiment of fraction F2, after 2D experiments, the anomeric zone corresponds to protons correlated with  $-CH_2-$  as observed for 2 deoxysugars (e.g. 2-d-Rib), but the chemical shifts of both carbons and protons (HSQC spectrum not shown) were incompatible with this case of figure. In our opinion, it is possible firstly, that it is highly hydroxylated glycolipids or secondely that it is other kind of sugar, like apiose, branched pentose largely found in plants. Indeed, the nmr trace remained compatible with this [ref Gloagen *et al J. Nat. Prod.* (2010),**73**, 6,1087-92]. Unfortunately, we don't possess this sugar in pure form to do standard analysis for TMS.

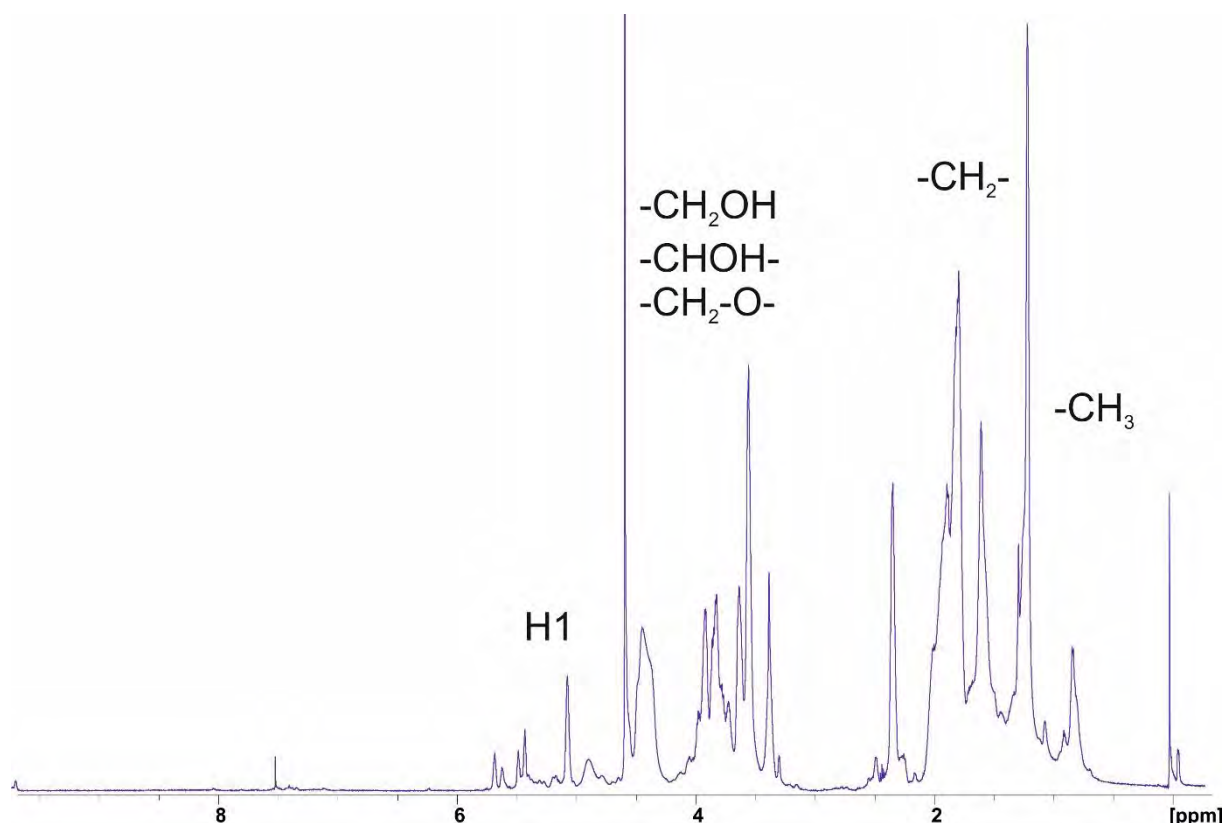


Figure 8 : <sup>1</sup>H-NMR spectrum of BY2 F2 fraction

### III GENERAL CONCLUSION

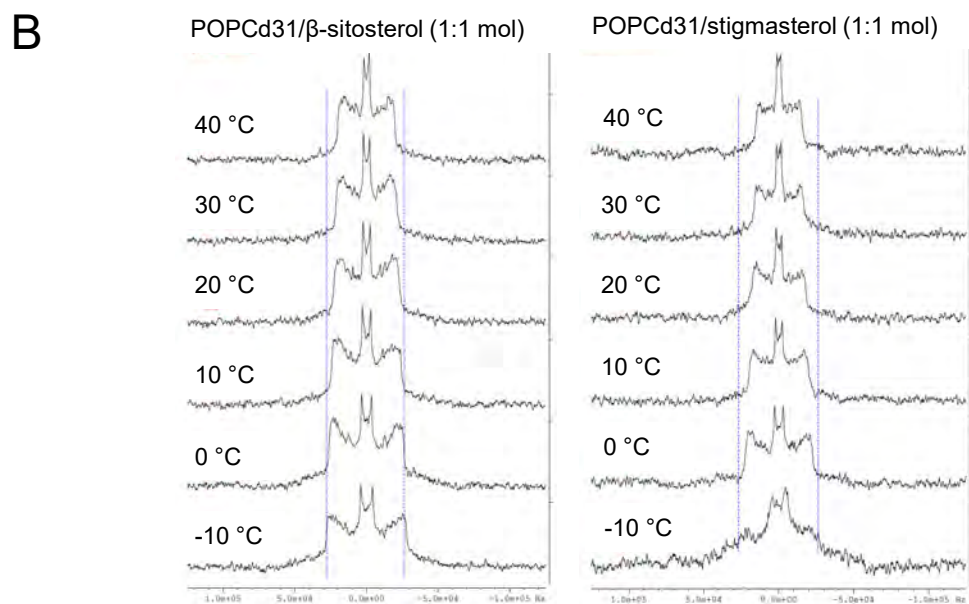
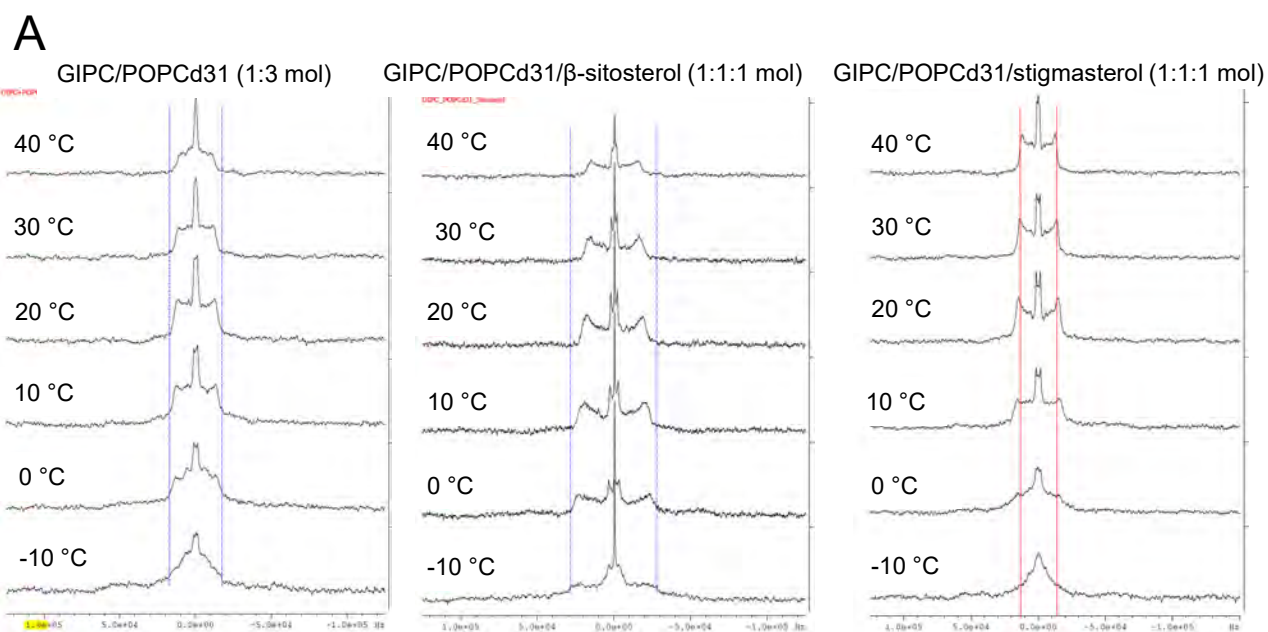
In this work, we identified arabinogalactan type polysaccharide as main molecule. The simultaneous presence of typical monosaccharides constituting GIPC with both arabinosyl and galactosyl residues allowed us to think that arabinogalactane is linked throughout the GIPC anchor into the membrane. Unfortunately, we have not real proof of this conclusion since not extensive nmr has been possible. Moreover, it could be possible to have some atypical sugars as apiose

related monosaccharides but both proton and carbon chemical shifts could be confused with poly-hydroxylated acyl chains. Thus it was not possible to give an complete structure of analyzed samples with these pooled data.

## **Phase transition of GIPC containing-vesicles analysed by liquid state $^2\text{H}$ -NMR and $^{31}\text{P}$ -NMR**

From past studies on GIPC as well as our recent experiments, it was strongly suggested that GIPC preferentially interact with sterols to form potentially nanodomains (please refers to Chapter 1 Figures 5 and 7) (Cacas et al., 2016a). The cooperative effect with  $\beta$ -sitosterol and non-cooperative effect with stigmasterol might definitely account for important physiological role, involving lipid packing in the PM. Stigmasterol is synthesized from  $\beta$ -sitosterol by the cytochrome P450 CYP710, a desaturase responsible for the C22 desaturation (Morikawa et al., 2006). This enzyme activity is important during plant/pathogen interactions and thermal adaptation (heat and cold). Stigmasterol formation is also triggered through the perception of pathogen-associated molecular patterns such as flagellin and lipopolysaccharides, and through production of reactive oxygen species, but does not depend on the salicylic acid, jasmonic acid or ethylene defence pathways. There is an increased amount of stigmasterol in leaves after pathogen attack. Plant disease susceptibility is promoted through stimulation of sterol C22 desaturation in leaves of Arabidopsis, which increases the stigmasterol to  $\beta$ -sitosterol ratio in plant membranes (Griebel & Zeier, 2010). Is this conversion and accumulation of stigmasterol in membrane associated with fluidity? Could the plant susceptibility be associated with increased membrane fluidity due to stigmasterol? Could it be that stigmasterol is shortly involved in fluidifying the membrane to recruit new components for defence again pathogens?

(Grosjean, Mongrand, Beney, Simon-Plas, & Gerbeau-Pissot, 2015b) showed the effect of sterols on the order level of membrane using environment-sensitive dye. With a nonintrusive method, (Beck et al., 2007a) uses solid-state  $^2\text{H}$ -NMR spectroscopy to demonstrate the role of phytosterol in abolishing membrane phase transitions in varying temperatures. Solid-state  $^2\text{H}$ -NMR spectroscopy gives information on the order parameters of lipid bilayers. They used binary and ternary systems of saturated PC, phytosterol and sphingolipid to show that the lamellar gel-to-fluid phase transition is almost or completely abolished in the presence of sterols. In ternary system mimicking fungi, mammalian and plant rafts, the latter prove to be sensitive to thermal variation. In this work, they used glucosylceramide, stigmasterol, sitosterol, 24-methylcholesterol and cholesterol



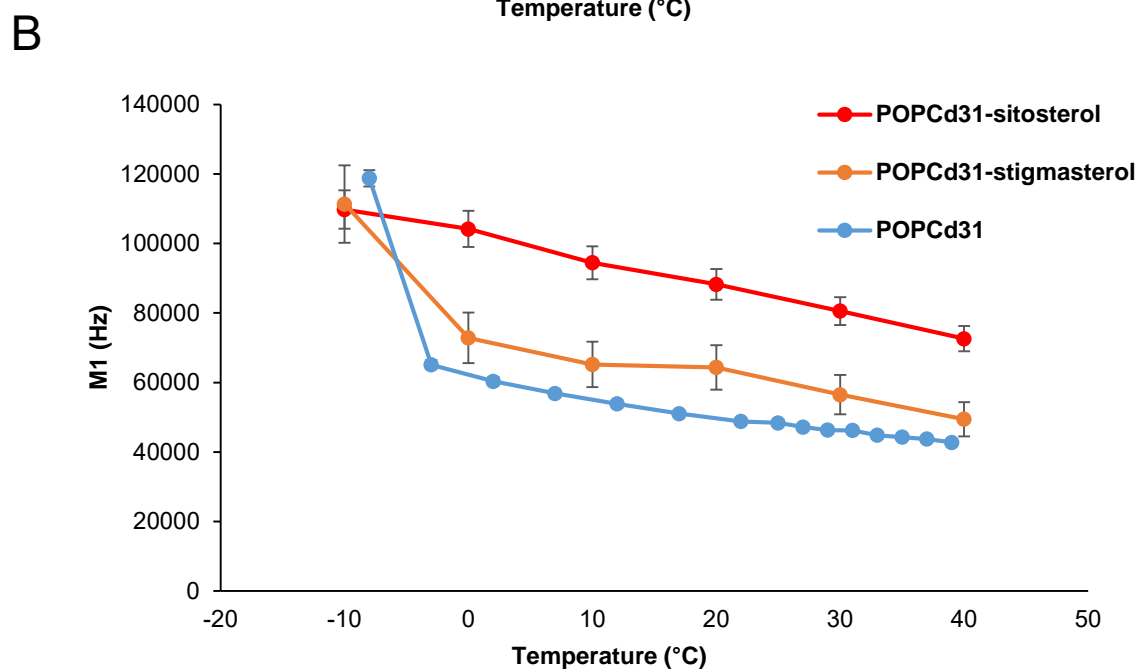
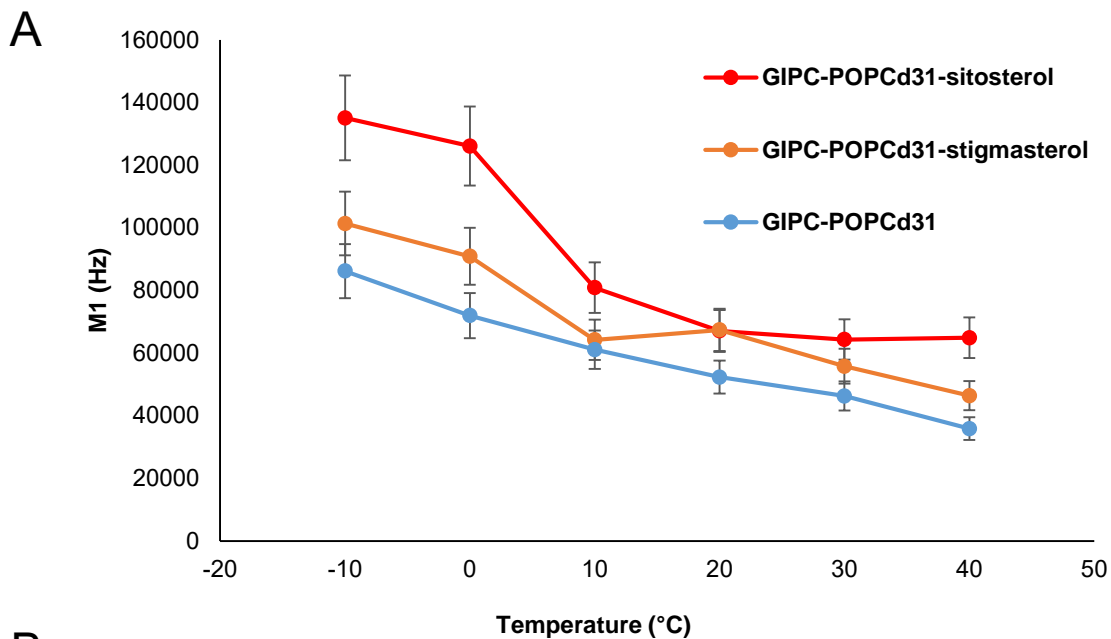
**Additional data Figure 1.  $^2\text{H}$ -NMR powder spectra of lipid mix containing GIPCs (A) GIPC/d-POPC (1:3 mol ratio), GIPC/d-POPC/ $\beta$ -sitosterol (1:1:1 mol ratio), GIPC/d-POPC/Stigmasterol (1:1:1 mol ratio); and as control binary lipid mix (B) d-POPC/ $\beta$ -sitosterol (1:1 mol/mol) and d-POPC/Stigmasterol (1:1 mol/mol)**

to mimick tobacco BY-2 DRMs as described in (Mongrand et al., 2004).

Since it is strongly suggested that GIPCs are the most abundant sphingolipid in plants, localised in the PM (Cacas et al., 2016a), we aim at finding how GIPCs are involved in membrane phase transition. Will replacing glucosylceramide with GIPCs have an increased effect on abolishing gel-to-fluid phase transition?

We used GIPC-enriched fractions from cauliflower to make binary and ternary system using deuterated palmitoyl oleoyl phosphatidylcholine with 31 deuterium on the palmitoyl chain (d-POPC; POPC- $^{2}\text{H}_{31}$ ). We choose to use POPC as it is a phospholipid with a long chain fatty acid with an unsaturation found in plant PM, and most importantly commercially available deuterated. The POPC phase transition is  $-2^{\circ}\text{C}$ . (note that PLPC is the most abundant phospholipid in plants but its deuterated form is not commercially available). All our systems were suspended in de-deuterated water so as to see only the d-POPC signal in  $^{2}\text{H}$ -NMR. We made liposomes using the freeze/thaw method as previously described. The liposomes used for the  $^{2}\text{H}$ -NMR experiments are the ones observed under cryo-EM in Chapter 1, Figure 9. Axelle Grelard performed the  $^{2}\text{H}$ -NMR and  $^{31}\text{P}$ -NMR experiments and data treatment. I went to the IECB on several occasions to drop the liposomes and with the help of Axelle I learned the simplified theoretical and practical science behind solid-state  $^{2}\text{H}$ -NMR. I observed from afar the loading of the rotor containing the sample into the NMR field.

Figure 1 shows the selected NMR spectra of lipid mix system containing GIPC (Figure 1 A) and control system without GIPC (Figure 1 B), while fluctuating the temperature from  $-10^{\circ}\text{C}$  to  $40^{\circ}\text{C}$ . Those are plausible thermal variations, that plants are constantly being submitted to in nature. The ternary mix consists of GIPC/d-POPC/ $\beta$ -sitosterol (1:1:1, mol ratio) and GIPC/d-POPC/stigmasterol (1:1:1, mol ratio), mimicking the outer leaflet of the PM. The binary systems consist of GIPC/d-POPC (1:3, mol ratio), d-POPC/ $\beta$ -sitosterol (1:1, mol ratio) and dPOPC/stigmasterol (1:1; mol ratio). I used 3 times more d-POPC in the GIPC/d-POPC binary mix, so as to obtain liposomes as GIPC alone form crystals as described previously. Figure 2 shows the first moments calculated from  $^{2}\text{H}$ -NMR powder spectra of samples GIPC containing samples (Figure 2 A) and samples without GIPC (Figure 2 B). The M1 gives indication on the deuterated



**Additional data Figure 2. Moment of  $^2\text{H}$ -NMR spectra showing membrane ordering vs temperature in binary and tertiary lipid mix containing (A) GIPC/d-POPC (1:3 mol ratio), GIPC/d-POPC/Sitosterol (1:1:1 mol ratio), GIPC/d-POPC/Stigmasterol (1:1:1 mol ratio). As control, lipid mix (B) d-POPC, Sitosterol/d-POPC (1:1 mol ratio), and Stigmasterol/d-POPC (1:1 mol ratio) were investigated.**

(C-D) chain dynamics. We can hence appreciate the phase transition of the membrane such that a low M1 corresponds to a fluid (ld) phase and high M1 to a rigid (lo) phase. The thermal variation shows an abolished phase transition upon adding GIPC to d-POPC (Figure 2, lines in blue). This means that GIPCs are able to fluidify the membrane at low temperatures (-10°C to 0°C). However, in these experiments, we did not take measurements between -10°C to 0°C and the phase transition temperature ( $T_m$ ) of POPC is -2°C. It might be wiser to use a deuterated phospholipid with higher  $T_m$  such as 14:0-16:0 PC ( $T_m=35^\circ\text{C}$ ) or 16:0 PC (DPPC) ( $T_m=41^\circ\text{C}$ ) as used in (Beck et al., 2007a). However, these phospholipids have too short carbon chain to be representative of plant phospholipid. GIPC with its unsaturation (24:1), hydroxyl groups (tri-hydroxylated ceramide), amide function might decrease the order level of the d-POPC chain such that at low temperature the bilayer has a lower M1. The phase transition in the presence of GIPCs is easily abolished, compared to bilayer of dPOPC.

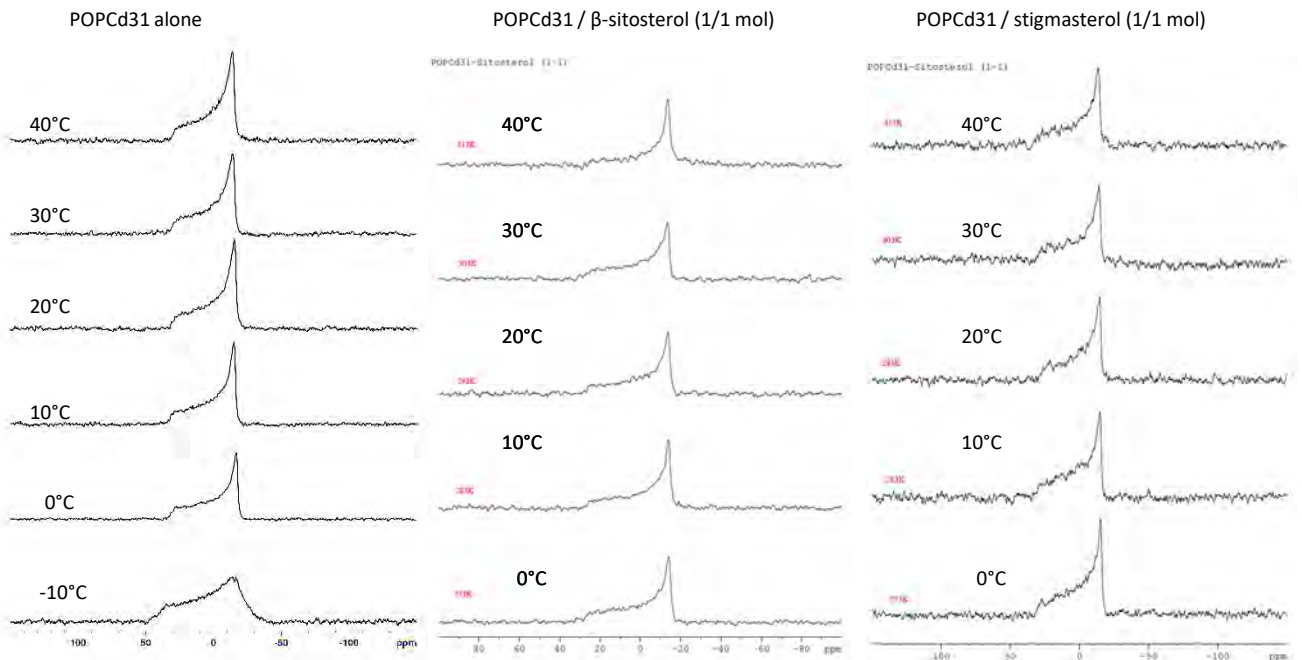
It is also interesting to note that the sterols in the ternary systems behave differently compared to the ternary system described in (Beck et al., 2007a), (Figure 2 A). Sitosterol seems to be more lo compared to stigmasterol which has a lower ordering level (Figure 2 A). At 20°C, both ternary systems have the same M1.

I did not include the above results in the paper of chapter 1 as they were performed on only one set of samples, with GIPC-enriched fractions from two independent extraction process. It is arguable that some of the results between sitosterol and stigmasterol are not comparable as the two ternary mix contain GIPC from two independent extraction batch. d-POPC/GIPC/Stigmasterol and d-POPC/GIPC are from the same GIPC enriched fraction. More importantly, they contain contaminants that cause the apparition of extra unknown phosphorous signal in  $^{31}\text{P}$ -NMR (Figure 3) in the d-POPC/GIPC/sitosterol (1:1:1 mol ratio) system. Such signal could be due to the presence of hexagonal phase, but such hexagonal phases were not observed by cryo-EM in the same liposome preparations (see draft of the paper above, Figure 9).

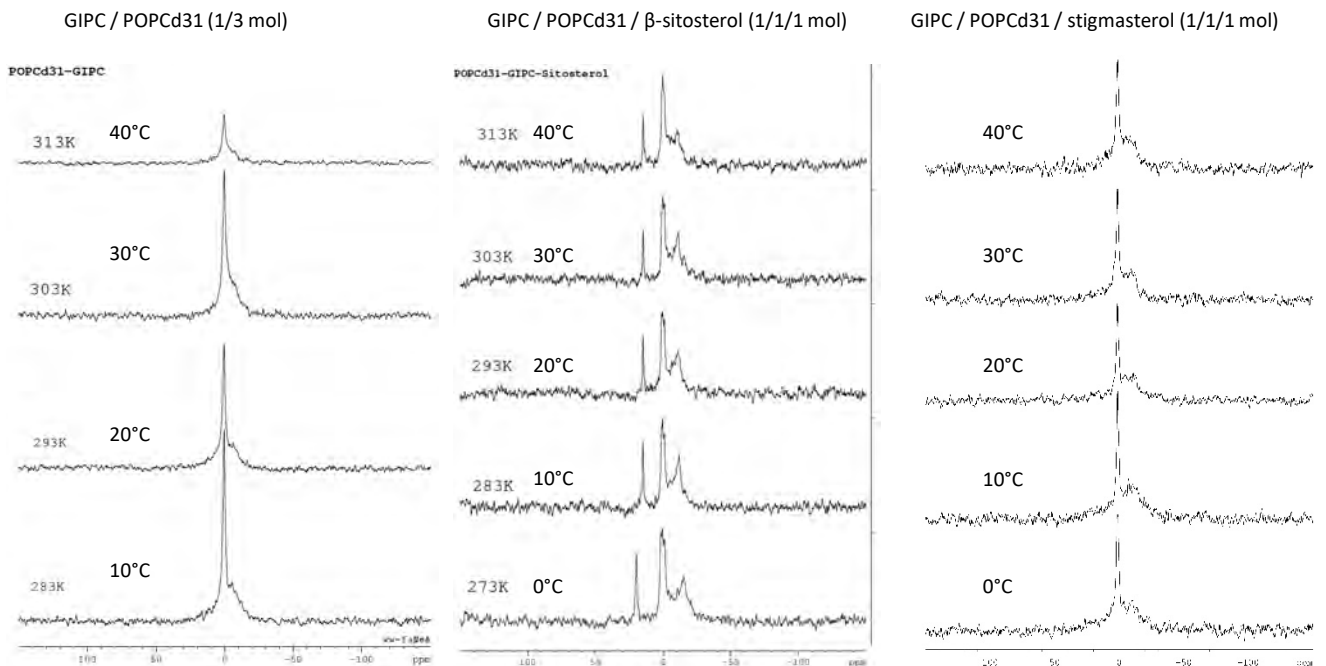
In the next future, we will need to further improve the purity of our GIPC fractions to get rid of this unknown phosphorous signal.

# solid-state $^{31}\text{P}$ NMR on liposomes

## Without GIPC



## With GIPC



**Additional data Figure 3.  $^{31}\text{P}$ -NMR spectra of lipid mix control d-POPC and binary lipid mix control: d-POPC/ $\beta$ -sitosterol (1:1 mol/mol) and d-POPC/Stigmasterol (1:1 mol/mol) and spectra of lipid mix containing GIPCs: GIPC/d-POPC (1:3 mol ratio), GIPC/d-POPC/ $\beta$ -sitosterol (1:1:1 mol ratio), GIPC/d-POPC/Stigmasterol (1:1:1 mol ratio)**



## Chapter 2

# Role of VLCFA and hydroxylation in PM marker mobility

In this chapter, we shall see the role of very long chain fatty acid (VLCFA) and hydroxylation of PM lipid GIPC in the *in vivo* mobility of proteins and lipids of the plasma membrane (PM) of root epidermal cells of *Arabidopsis thaliana* (At). Minimal protein markers described by Alexandre Martinière (Martiniere et al., 2012) were used as well as WAVE-lines and PIP-Lines lipid probes were provided by Yvon Jaillais's group in Lyon. *Arabidopsis* lines expressing the PM markers were generated in a wild-type background as well as in mutants lacking the FAH gene, important for the hydroxylation of fatty acid. We used a pharmaceutical approach to shorten VLCFA chain length using the drug Metazachlor (Mz).

This part of my thesis was done in collaboration with Minoru Nagano (Saitama university, Japan), who spent 1 year as a visiting scientist in our lab, and Yohann Boutté (LBM, Bordeaux). Minoru performed all of the FRAP experiments and started generating genetic lines at the LBM. He also continued on working on generating third and fourth generations of transgenic lines at his new lab at the University of Ritsumeikan, Kyoto, Japan. I also generated lines of double mutant *fah1-fah2* expressing GPI-GFP using the floral dipping techniques. I also analysed their fluorescence under confocal microscopy. I performed lipidomic analysis of PM lipids purified from Mz-treated plants (GC-MS and LC-MS/MS), and LC-MS/MS in collaboration with Laetitia Fouillen (LBM, lipidomic platform, Bordeaux).

Christophe Der and Françoise Simon-Plas, at INRA Dijon analysed with di-ANEPPDH, an environment-sensitive fluorescent probe, the effect of metazachlor on the PM fluidity in wild type and *fah* mutants. di-ANEPPDH fluorescence measures the degree of order of membrane, and they showed that this dye mostly probes the outer leaflet of the plant PM.

Overall this project is still underway and we are looking forward to complete the FRAP analysis and lipidomic analyses soon. We faced a lot of huddles in generating the appropriate genetic lines since some of the plasmids used were quite old. However, we now have all of the genetic lines and most of the FRAP experiments are done. We expect to be able to publish by next year.

The plant plasma membrane is stable, robust but yet adaptable to its environment. With the development of a battery of methods in proteomics, lipidomics and microscopy, we are able to increase our understanding of the PM in both plants and animals. The PM is a complex system, with different molecular species of lipids and proteins that are heterogeneously distributed throughout the bilayer. The molecular organization of the PM allows a combination of long-term stability and short-term dynamics allowing the transmission of signals and the adaptation of the PM to be a signalling platform transmitting signals between the surrounding cell environment to the cell. In animal cells, the compositional heterogeneity of PM lipids is well established. For instance, human erythrocyte PM, considered as the archetype animal cell PM, contains mostly phosphatidylcholine (PC) and sphingolipids in the outer-leaflet while the inner leaflet consists of phosphatidylserine (PS), phosphatidylethanolamine (PE) and phosphatidylinositol (PI) (Zachowski, 1993). PS is associated with high content of VLCFA. Minor lipids such as PIPs and PA are in the inner leaflet while outer leaflet consists of predominantly sphingomyelin and glycerosphingolipids such as gangliosides. There is also a lateral segregation in the PM due to the segregation of lipids in liquid ordered (lo)- liquid disordered (ld) phases giving rise to membrane domains or 'rafts' (Simons & Vaz, 2004). These domains are fundamental for the good functioning of the mammalian cells (Simons & Gerl, 2010). The cell membrane contains various lipids of different acyl chain length/saturation/hydroxylation and sterol levels, which can cause small, transient regions of lo regions locally. (Swamy et al., 2006) showed by various approaches such as local probes, spin-labelled lipids and electron-spin resonance techniques, the existence of a fraction of membrane lipids exhibiting lo-like conformations in live cells. As for transbilayer lipid asymmetry, it is maintained by the activity of lipid translocases such as scramblases, flippases and floppases, allowing the movement of the lipids between the leaflets, much faster than the slow random diffusion of lipids. The diversity of the acyl chain length also leads to the connection of the bilayer known as interdigitation.

(Raghupathy et al., 2015) showed that there is a bilayer coupling, a lipid interaction mediated by long-chain interdigitation between the outer and inner leaflet of the PM lipids of mammalian cells. They demonstrated that it requires long acyl chains of outer

leaflet lipid, GPI anchor proteins (GPI-APs) and identified inner leaflet lipid phosphatidylserine (PS), as responsible for this mechanism. They showed that this connection is stabilized by cholesterol and occurs when the two lipid species involved are immobilized. More precisely, they did molecular dynamic (MD) simulations to show that interdigitation of VLCFA can occur even in membranes above their main transition temperature, that is in *l<sub>d</sub>* phase, as long as VLCFA-containing lipids are immobilized at one of the leaflets. It was demonstrated by the use of synthetic linker PS-actin that the immobilization may occur due to inner leaflet PS binding to actin structures at physiological conditions in live-cells.

In plants, the structure of the PM remains a model as it is more difficult to access to the plant directly like live animal cell, due to the presence of the cell wall. The models proposed consist of sphingolipids and sterols mainly in the outer leaflet and phospholipids in the inner-membrane, with lateral segregation of sphingolipids and phytosterols to form lipid domains (Cacas et al., 2016a; Tjellstrom et al., 2010)(Takeda & Kasamo, 2001). In plants, there are neither sphingomyelin nor gangliosides, the two main sphingolipid classes in animal PM. Plant sphingolipids are of four major classes: ceramides (CER), glucosylceramide (gluCer), Glycosyl Inositol Phosphoryl Ceramides (GIPC) and free Long Chain Bases (LCBs), representing ca., 2%, 34%, 64% and 0.5% of total sphingolipids, respectively in *Arabidopsis thaliana* (Markham et al., 2006). GIPCs are the main component of the plant outer leaflet (Cacas et al., 2016a). They consist of a ceramide attached to a glycan polar head group. GIPCs show diversity in their structure mainly in: 1/ the length, the number and position of hydroxylations and unsaturations in the FA chain; 2/ the hydroxylation degree, saturation and position of double bond(s) in the LCB; 3/ the nature and the number of glycans, and the type of glycosidic links between the glycans that compose the polar head group (Pata et al., 2010)(Buré et al., 2014). Globally, plant GIPC consists of a ceramide moiety made up mainly of a t18:0 (trihydroxylated saturated LCB of 18 carbon atoms) or a t18:1 (trihydroxylated and monounsaturated LCB of 18 carbon atoms) as LCB, amidified to a Very Long Chain Fatty Acid (VLCFA) or 2-hydroxylated VLCFA (hVLCFA). (Cacas et al., 2016a) showed that 95 mol% of PM VLCFA and hVLCFA are amidified in GIPC. When it comes to phospholipids, PC, PE, PI consist mostly of 16 to 18-carbon species combined. PS is the only phospholipid with significant amounts of VLCFA. VLCFAs

represents 30% of total PS in roots while 1% of PC and 5% of PE (Bach & Faure, 2010)(Yamaoka et al., 2011). The dynamic of PS can be monitored by the use of lipid anionic sensors (Platre et al., 2018). A recent paper by Jaillais' team showed that PS is important for the stabilization of Rho of Plants 6 (ROP6) protein in nanodomains and cell signalling. This protein is from the Rho/Rhas superfamily implicated in the regulation of cell signalling, trafficking, polarity and cytoskeleton dynamics. They showed that PS is present in nanodomains and is necessary for ROP6 lateral segregation and stabilisation into these domains. They argued that this stabilization of ROP6 in PS-nanoclusters constitutes the functional signalling unit of the protein (Platre et al., 2019a).

Polyphosphoinositides or phosphatidylinositol-phosphates (PIPs) are another minor lipid class, which are composed of a PI backbone phosphorylated by up to 3 inositol residues. They are involved in cell signalling and trafficking and can be used as markers of cell compartments (Tejos et al., 2014). Their localisation and dynamics can be studied by the use of biosensors (Vermeer & Munnik, 2013). The "PIP-lines" generated by (Simon et al., 2014) in *Arabidopsis thaliana*, are phosphoinositide biosensors with various fluorophores, allowing the rapid visualisation of PIP dynamics *in vivo*. It is thus possible to visualize PIPs such as phosphatidylinositol-4-phosphate (PI4P), phosphatidylinositol-3-phosphate (PI3P), phosphatidylinositol-4,5-bisphosphate (PI4,5P<sub>2</sub>), phosphatidylinositol-3,5-bisphosphate (PI3,5P<sub>2</sub>), phosphatidylinositol-3,4,5-triphosphate (PI3,4,5P<sub>3</sub>) (Hirano, Stecker, Munnik, Xu, & Sato, 2017; Van Leeuwen, Vermeer, Gadella, & Munnik, 2007).

All of these lipid anionic reporters have a high binding affinity with their respective lipid target in the membranes. What we observe is the on and off interaction of the marker with its lipid ligand. We need to consider that since these markers are expressed *in vivo*, and are in competition with the lipid's endogenous binding partners. The marker might affect the way that lipids interact under normal conditions with their usual partners. A marker with a too high affinity to the lipid target might displace the endogenous protein ligand, abolishing its function and causing undesirable phenotypes. The cell might also respond to the endogenous protein displacement with an upregulation of the lipid causing yet another undesirable effect that can be misinterpreted as useful data. It is hence important to use the minimum anionic lipid

sensors so as to obtain adequate imaging without influencing the normal cell functioning (Heilmann, 2016).

*In vivo*, we can also study membranes through the use of environment-sensitive dye that can detect membrane lo domains such as di-4-ANEPPDQH (Gerbeau-Pissot, Der, Grebe, & Stanislas, 2016). Di-4-ANEPPDQH is a fluorescent probe sensitive to lipid order phases that can be used to quantify the level of membrane order using ratiometric fluorescence microscopy to map localized lo levels. It is a probe that exhibits a shift in its emission spectrum. This shift does not depend on the local composition of the membrane but rather on the different lipid packing phases (Jin et al., 2005) (Dinic, Biverståhl, Mäler, & Parmryd, 2011). (Gerbeau-Pissot et al., 2016) describe a protocol for ratiometric live imaging using di-4-ANEPPDQH to quantify membrane lo during plant cell division in cultured cells and *Arabidopsis thaliana* roots. The Dijon team previously characterized the PM order level in tobacco cells as well as the spatial distribution of Lo phases on the plant membrane and variations upon treatment with the elicitor cryptogein (Gerbeau-Pissot et al., 2014a). Most recently, the study of (Grosjean et al., 2018) used the environment-sensitive probe to investigate the membrane order at a local level in BY-2 tobacco cell. To identify mechanisms and cell components involved in maintaining ordered membrane organization, they use the lipid packing-sensitive probe on different models: model membrane GUVs, GUVs of native PM, protoplasts, treated living cells with affected cytoskeleton and intact tobacco BY-2 cells. We also used di-4-ANEPPDQH to show the importance of sterols and GIPC in lipid packing in LUVs (Cacas et al., 2016a).

(Pinto, Silva, De Almeida, & Prieto, 2008) showed the importance of very long chain ceramide in the formation and segregation of gel domains. The behaviour and morphology were associated to the formation of multiple, interdigitated gel phases in mammalian cell model. Another study on mammalian very long chain sphingolipids showed the importance of C24 sphingomyelin in lateral organization of live cell PM as well as the partitioning of cholesterol in the PM (Courtney et al., 2017). In plants, (Luttgeharm, Chen, et al., 2015) showed the importance of VLCFA- and trihydroxylated-sphingolipids in both growth and cell division of using LOH1 and LOH3 overexpressing plants. (Molino et al., 2014) demonstrated that membrane VLCFA-sphingolipids of 24 carbons are important in the regulation of Golgi vesicular trafficking

in *Arabidopsis*. They also affect cell division and shape in tobacco BY-2. *Trans* Golgi-network secretory vesicles are shown to be enriched in sterols and alpha-hydroxylated VLCFA containing 24 or 26 carbon atoms (h24 or h26) (Wattelet-Boyer et al., 2016). By altering the pool of VLCFA in sphingolipids, the morphology of TGN-associated secretory vesicles is impacted. The membrane apical polarity mediated by PIN2 is lost, due to the secretory blockage of PIN2 in secretory vesicles (Wattelet-Boyer et al., 2016). The importance of VLCFA in the plant is also highlighted in responses to stress. The elongation of VLCFA goes through the ER-localized membrane protein complex of four enzymes (Haslam & Kunst, 2013). The successive action of  $\beta$ -ketoacyl-CoA synthase (KCS),  $\beta$ -ketoacyl-CoA reductase (KCR),  $\beta$ -hydroxyacyl-CoA dehydratase (HCD) and enoyl-CoA reductase (ECR). KCS is tissue-specific and coded by a multigenic family of 21 members (Joubès et al., 2008). The genes coding for KCS were shown to be sensitive to stresses such as dehydration, light, salt, cold and osmotic stresses (Joubès et al., 2008). In *Arabidopsis*, endogenous levels of VLCFA increase during induced resistance to bacterial pathogen (Raffaele et al., 2008). hVLCFA may also be involved in stress acclimation (Nagano et al., 2012). *Arabidopsis* BAX INHIBITORS-1 (At-BI1), an ER-resident cell death regulator can interact with the cytochrome-b5, associated electron donor, with FATTY ACID HYDROXYLASE1 (FAH1). The enzyme catalyses the hydroxylation of VLCFA. The overexpression of At-BI1 was correlated with a high hVLCFA content and decreased cell death under stressful conditions. *fah1* knock-down plants however have decreased hVLCFA amounts and enhanced sensitivity to hydrogen peroxide. This suggests that FAH1 might be activated by BI1 to protect the cells from cell death against oxidative stress (Nagano et al., 2012).

Our project aims at understanding the effect of both VLCFA and hydroxylation of lipids, mainly GIPCs, the most abundant sphingolipids in plant PM, in the dynamics of membrane proteins. To investigate the effect of VLCFA in the mobility and fluidity of the two leaflets of the PM, we used the drug metazachlor (Mz) on *Arabidopsis thaliana* plants as described in (Wattelet-Boyer et al., 2016). Mz is an inhibitor of KCS responsible for the elongation of VLCFA acyl chain. We did not use a genetic approach as *kcs* mutants have weak phenotype. We also show the importance of hydroxylation in PM markers mobility by generating *fah* mutant plants expressing the PM markers.

Di-4-ANEPPDQH also helped in determining the effect of sphingolipid hydroxylation in membrane fluidity.

## Results

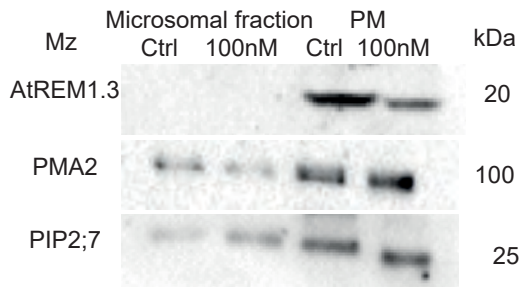
### Metazachlor treatment modifies sphingolipid pool in purified PM

The first step was to purify by PEG-Dextran phase partitioning PM from 10-days old *Arabidopsis thaliana* (*At*) plants grown in liquid medium. We used control treatment or 100nM metazachlor treated seedlings. The microsomal fraction and PM fraction of each condition were collected. We verified the purity of the PM fractions by western-blot. The western-blot assay showed the enrichment of three PM markers AtREM1.3 (PM protein remorin of 20kDa), PMA2 (a PM ATPase of 104 kDa) and PIP2;7 (aquaporin, PM intrinsic protein of 25 kDa) in the PM fractions of both the control and Mz-treated plants (Figure 1A). Neither Golgi (Sec21), nor vacuolar (V-ATPase) proteins were detected in the PM fractions, but their presence was observed in the microsomal fractions (data not shown).

The GC-MS analysis of the total fatty acid content of each PM fraction was first analysed. Fatty acid content of sample fractions was hydrolysed from lipids by overnight transmethylation at 85°C, followed by derivatisation by BSTFA, before GC-MS analysis. Results showed most dramatic decrease of FA with 24 or more carbon atoms, mainly C24, h24 and h24:1 (Supplementary data S1), and an increasing of C16 to C20 FA.

The PM fractions were then analysed by LC/MS-MS after a specific extraction of sphingolipids and hot methylamine treatment to remove glycerolipids. Sphingolipid analysis showed the presence of two main species in the control, GIPC series A t18:1 as LCB and either a h24:1 or a h24:0 as (h)VLCFA (Figure 1B). However, the treatment with Mz showed a strong shift in the sphingolipid profile with a strong increase of GIPC with long fatty acid chains, notably h16 and h20. Although GIPC with LCB t18:1 remained the most abundant species after Mz treatment, it was worth noting the increased presence of GIPC with LCB d18:1 and d18:0 (Figure 1B). Therefore, this change significantly altered the h16:0, h24, h24:1 and h26 acyl chain. These results correlated with the previous paper of (Wattelet-Boyer et al., 2016) which showed that, Mz caused an increase in the acyl chain of less than 24 carbons and a decrease of acyl chain with more than 24 carbons in the total sphingolipid composition of *At* roots.

A. Western-blot of purified PM from At treated and non-treated by Metazachlor



B. LC-MS/MS analysis of At PM

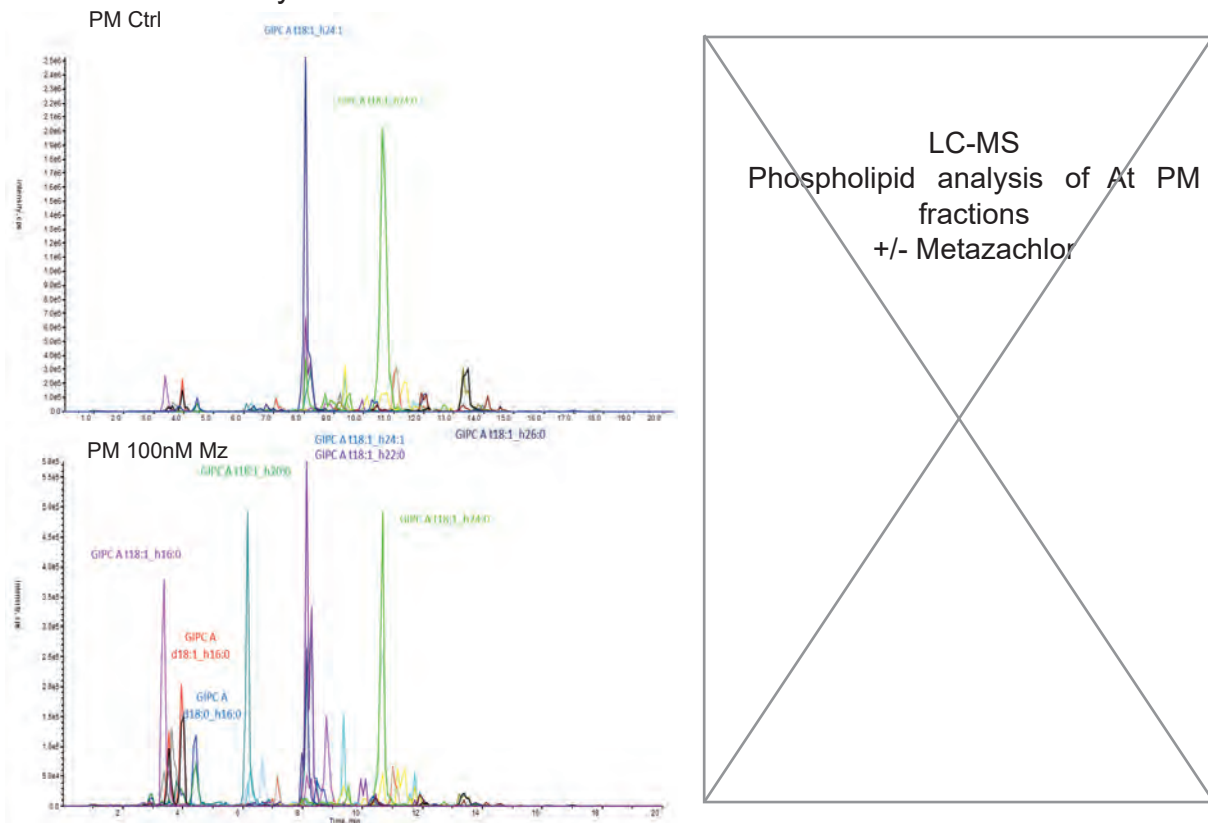
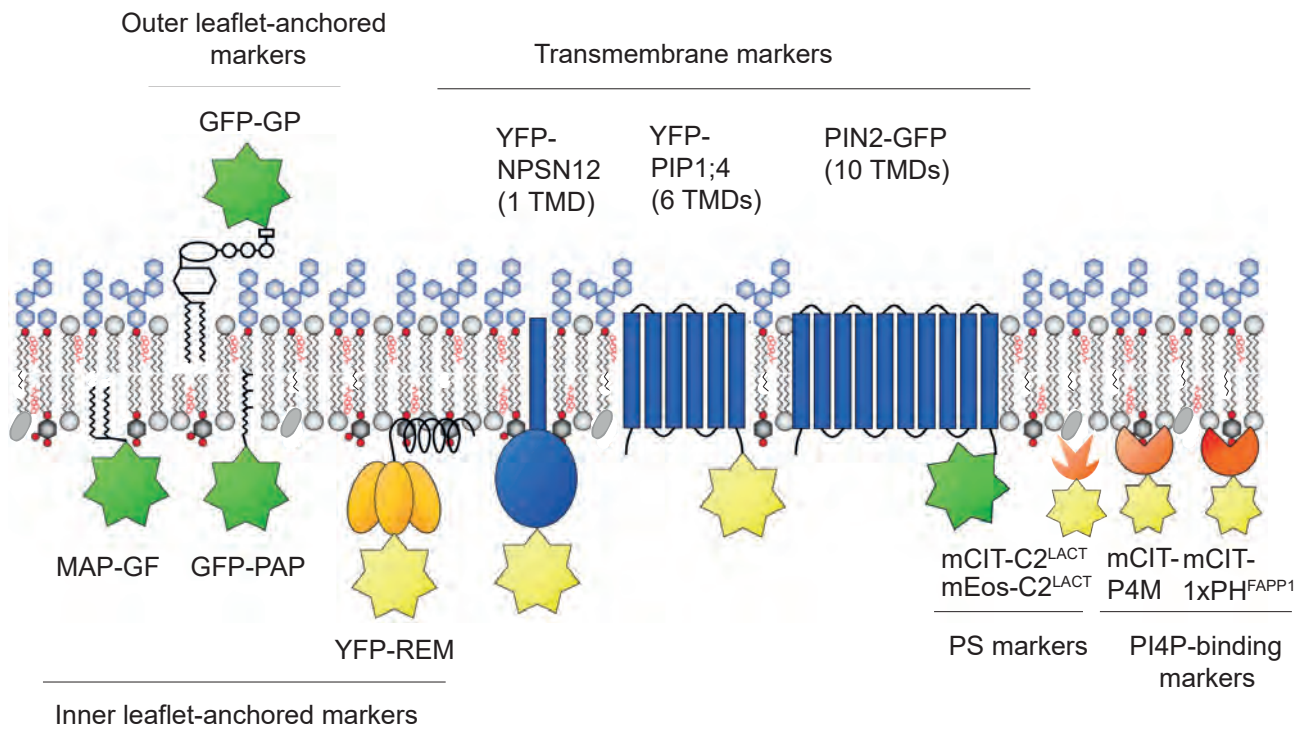


Figure 1: Arabidopsis thaliana plasma membrane (PM) were purified from 6-day old plant, treated with 100 nM of metazachlor (100nM Mz), or non-treated control (Ctrl). The purity of the PM was assessed by Western Blot (A) with the presence of PM markers in the PM fractions. Abbreviations: REM, remorin; PMA, plasma membrane ATPase; PIP2;7, plasma membrane intrinsic protein. LC-MS/MS analysis of sphingolipid (B, left) of the PM fractions of metazachlor treated and non-treated displays an abundance of GIPCs and a shift towards GIPC species with shorter fatty acid length.

In order to further investigate about the effect of Mz on PM phospholipid, we planned to perform LC-MS/MS analysis to analyse the glycerophospholipid composition of our At PM fractions, with a special focus on PS located in the inner leaflet of the PM and known to be the phospholipid containing VLCFA (Maneta-Peyret et al., 2014). As stated before, in animal cells, PS VLCFA are essential for domain formation (Raghupathy et al., 2015).

### **PM membrane markers are visible after Mz treatment of wild type and in *At fah* mutants**

We next measured the dynamic of a set of markers tagged with GFP, located either specifically in the inner leaflet or in the outer leaflet of the PM, or markers containing several transmembrane domains (TMD). Figure 2 shows a conceptual model of the PM as an asymmetrical bilayer with sphingolipids, GIPC, mainly located in the outer leaflet, and phospholipids specially PS as well as phosphatidyl inositol phosphate (PI4P) located in the inner leaflet according to (Cacas et al., 2016a). Sterols locate between the acyl chains of both leaflets but predominantly in the outer leaflet (Figure 2) according to (Tjellstrom et al., 2010). We used a multiple set of markers and probes to study the dynamics of the two leaflets of the PM in *At* roots. For instance, we used minimal protein constructs anchored in the membrane developed by (Martiniere et al., 2012) which include a glycosylphosphatidylinositol-anchored GFP (GFP-GPI) as outer-membrane marker, a myristoylated and palmitoylated GFP (MAP-GFP) and a prenylated GFP (GFP-PAP) as inner-leaflet markers. Full protein remorin (REM) fused with YFP (YFP-AtREM102 and YFP-REM1.3) were also used to mark the inner-leaflet. We also used plants expressing transmembrane markers YFP-NPSN12 and YFP-PIP1;4 which were from a collection of fluorescent proteins developed by (Geldner et al., 2009) known as 'WAVE-lines' (Figure 2). In addition, plants, expressing transmembrane fluorescent marker PIN2 fused with GFP (PIN2-GFP) were also generated. While these markers give us a comprehensive understanding of the lateral movement of protein in the leaflets, we also wanted to see the behaviour of two important inner leaflet lipids namely PS and PI4P. We generated *At* lines expressing PS marker the C2 domain of lactadherin (C2<sup>LACT</sup>) fused with mCitrine (mCIT-C2<sup>LACT</sup>)



MAP: myristoylated and palmitoylated  
 PAP: prenylated  
 GPI: glycosylphosphatidylinositol-anchored  
 NPSN12: syntaxin  
 PIP1,4: aquaporin  
 PIN2: auxin efflux carrier

Figure 2: Schematic representation of the plasma membrane markers used to determine the lateral mobility of PM proteins and lipids. Minimal constructs anchored proteins from Martinière et al., 2012, include the outer-leaflet marker glycosylphosphatidylinositol-anchored GFP (GFP-GPI), inner-leaflet markers myristoylated and palmitoylated GFP (MAP-GFP), prenylated GFP (GFP-PAP). Inner-leaflet markers also include YFP fused with remorine (YFP-REM). Transmembrane markers are Wave-line markers YFP-NPSN12 and YFP-PIP1;4, as well as PIN2-GFP. Lipid lateral diffusion is assessed by using PS-markers and PI4P-binding markers.

and C2<sup>LACT</sup> fused with mEos fluorescent (mEos- C2<sup>LACT</sup>) (Platre et al., 2018). As for PI4P reporters, we used 'PIP-line' marker mCIT-1XPH<sup>FAPP1</sup> (Simon et al., 2014) and P4M reporter (Figure 2). P4M reporter consists of a SidC, an effector protein of *Legionella pneumophila* with its 20-kDa "P4C" fragment (Hilbi, Weber, & Finsel, 2011). It is a robust and specific probe for PI4P.

Before undertaking FRAP experiments to study the markers recovery, we tested the fluorescence of *Arabidopsis* lines expressing all the markers at 6 days old. Confocal microscopy observations showed fluorescence of all reporters in the PM, at the level of the root tip except for GFP-PAP whose fluorescence was also detected in the root elongation zone (EZ) (Supplementary data 2).

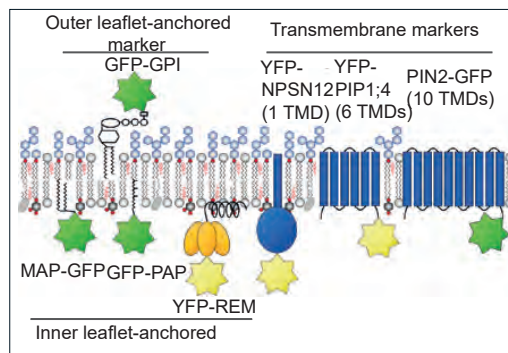
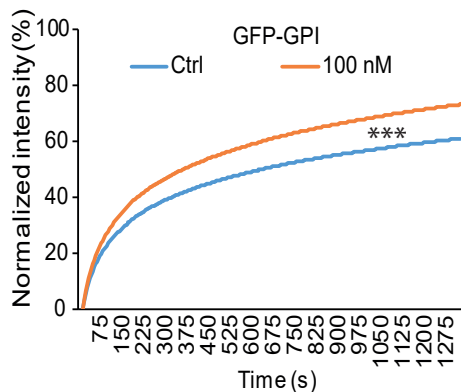
### **The recovery of PM marker GPI-GFP is significantly higher in metazachlor-treated plants**

We investigated the mobility of the PM reporters through FRAP analysis on *Arabidopsis thaliana* roots at 6 days old, treated or not with 100nM of metazachlor. The amount of metazachlor used for treatment of At seedlings where at a final concentration of 100nM as 50nM metazachlor did not strongly affect PM marker mobility nor lipid profile when compared to the control (0nM Mz). FRAP analysis was performed on 10 to 20 plants per condition. The time of recovery after bleaching was recorded until the stabilization of the fluorescence intensity in a plateau. The intensity was normalized to the background autofluorescence and data was fitted. Fluorescence recovery post-bleaching in outer-leaflet marker, GPI-GFP were significantly ( $p < 0.0001$ ) less in Mz-treated roots (Figure 3). This means that Mz clearly increased the lateral mobility of outer-leaflet marker GFP-GPI. This increase was however neither observed for the inner-leaflet markers (MAP-GFP, GFP-PAP, YFP-AtREM1.2 or YFP-REM1.3), nor for the TMD markers (YFP-NPSN12, YFP-PIP1;4, PIN2-GFP) (Figure 3). This result strongly suggests that the length of VLCFA of GIPC regulates the outer leaflet dynamic of proteins.

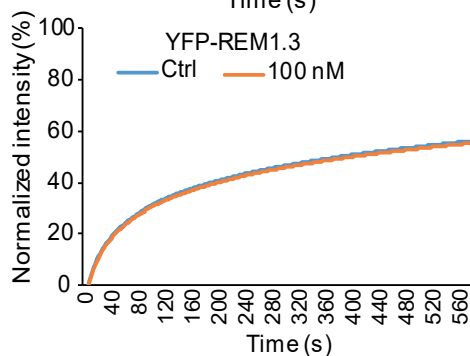
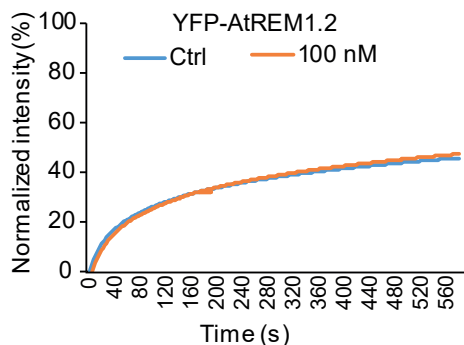
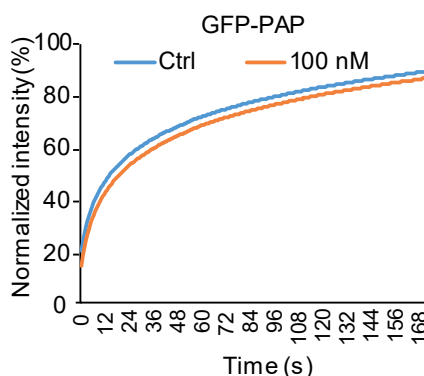
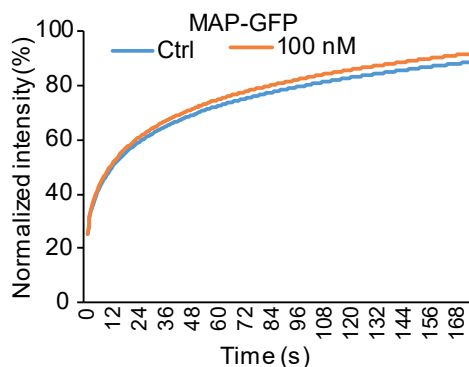
To further challenge the role of the hydroxylation of VLCFA of GIPC that was shown to be important to regulate PM degree of order (Nagano et al., 2012), we also generated

# Protein Markers expressed in At wild-type plants

## Outer-leaflet markers



## Inner-leaflet markers



## Transmembrane markers

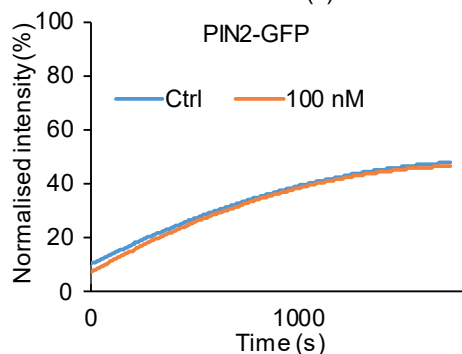
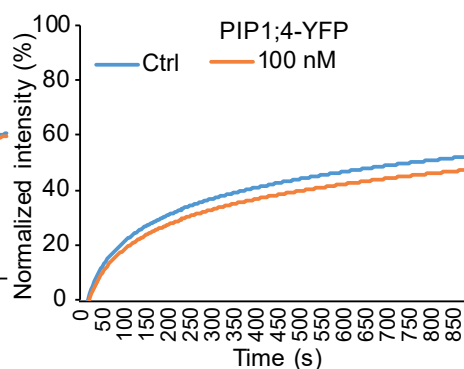
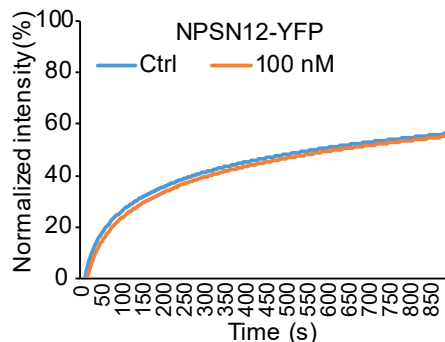
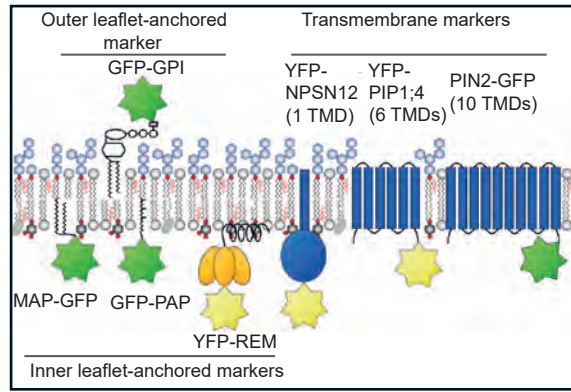


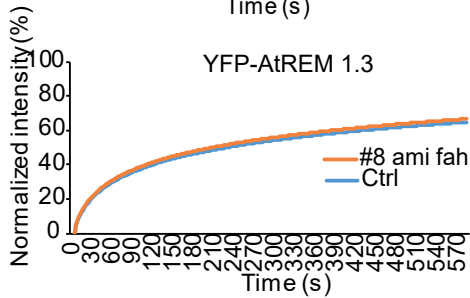
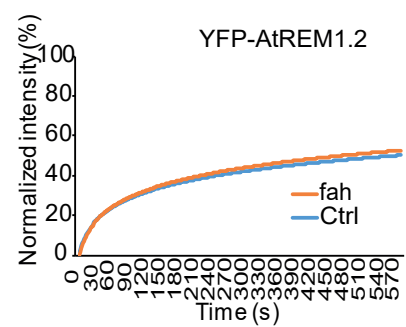
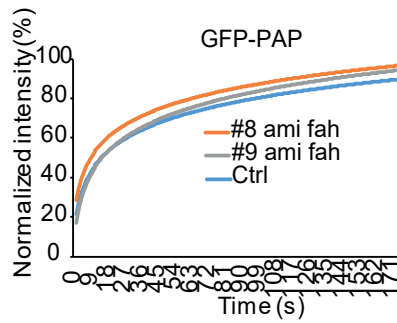
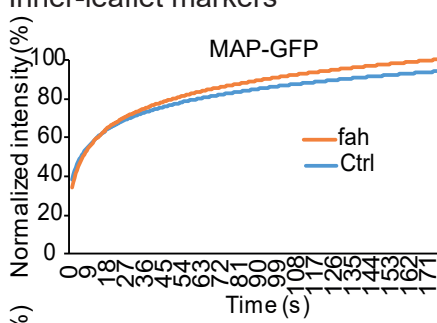
Figure 3: Curve-fitting FRAP data illustrates the range of diffusion of membrane protein markers on metazachlor treated (100 nM) and non-treated (Ctrl) plants.

# Protein Markers expressed in At fah mutant plants

## Outer-leaflet marker



## Inner-leaflet markers



## Transmembrane markers

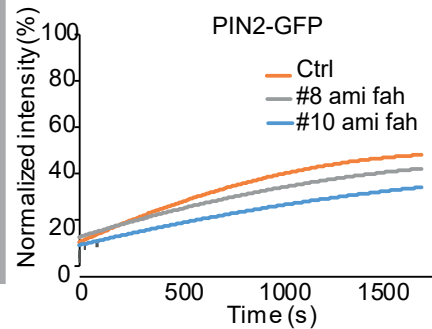
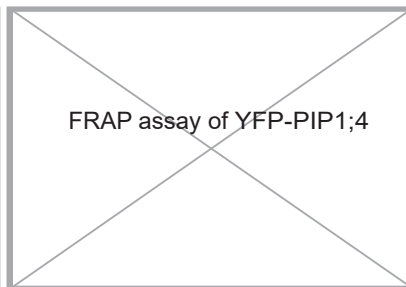
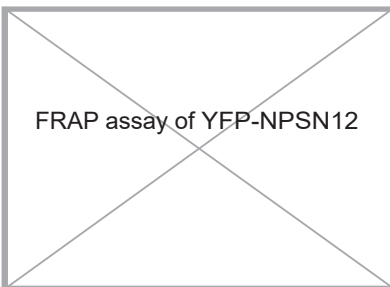


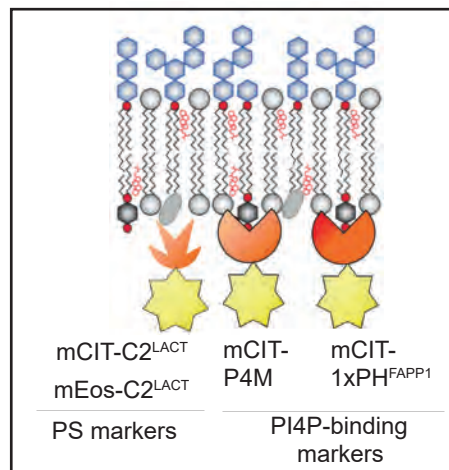
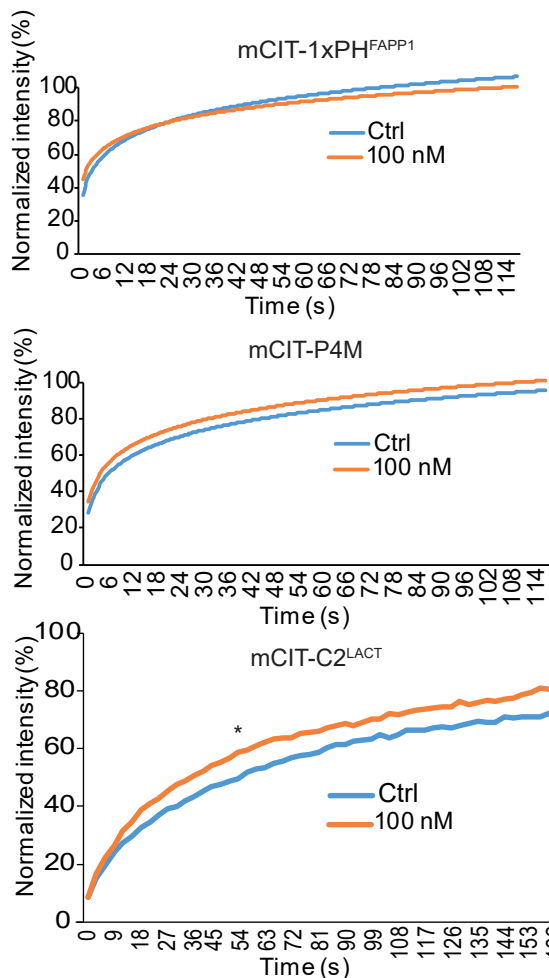
Figure 4: Curve-fitting FRAP data shows the range of diffusion of membrane protein markers in At fah mutants and plants with no fah mutation (Ctrl). Gray boxes are experiments to be done.

*At fah* mutants expressing the different fluorescent reporters. The generation of lines expressing some PM reporters in a *fah* mutant background is still underway. This is illustrated by grey boxes in figure 4. So far, we showed that there is no significant difference in the recovery post-bleaching of *fah* mutants expressing inner-leaflet markers (Figure 4). No significant difference was either observed for PIN2-GFP recovery in control and *fah* mutants. We are now looking forward the generation of GFP-GPI marker in *fah* mutants.

### **Anionic lipid sensors and metazachlor treatment**

Lipid biosensors mCIT-1XPH<sup>FAPP1</sup> and mCIT-P4M recovery after bleaching was not affected by Mz treatment (Figure 5). For PS reporter mCIT-C2<sup>LACT</sup>, a slight difference in the recovery could be observed between 75 s and 115 s but this difference was not consistent all over the recovery data points. Hence, we believe that if any, Mz has a minor effect on PS movement. These results have to be further investigated and reproduced to conclude. As said before, the biosensors used here may not be only representative for lateral movement of the lipids they are targeting when performing FRAP experiments due to the fact that they can associate and dissociate rather fast from their targeted lipid. Thus, other methods should be employed to explore lateral diffusion of anionic lipids within a membrane as we don't believe that FRAP experiment would completely reflect lateral movement, oppositely to protein-GFP fusion which are covalently bound. Therefore, we are looking forward to performing single particle tracking-photoactivated localization microscopy (SPT-PALM) on lines expressing mEos-C2<sup>LACT</sup> treated with Mz to investigate the effect of shortening the acyl chain on PS mobility and segregation. These experiments are in line of the recent paper of Yvon Jaillais's group (Platre et al., 2019b) who showed that PS is necessary for auxin-induced stabilization of ROP6 into nanodomains, and we wanted to understand whether this stabilization is VLCFA-dependant or not.

A. Lipid biosensors expressed in At Col-0



SPT-PALM assay of mEos-C2<sup>LACT</sup>

B. Lipid biosensors expressed in At fah mutants

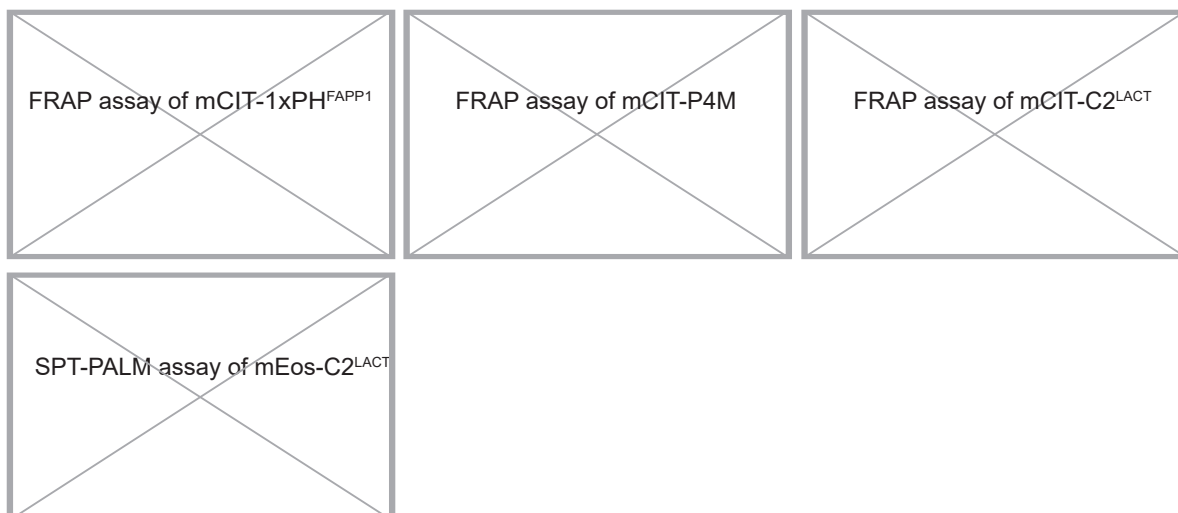


Figure 5: Curve-fitting FRAP data illustrates the range of diffusion of membrane lipid biosensors on metazachlor treated (100 nM) and non-treated control (Ctrl) of At plants (A) and of At fah mutant (B). No significant mobility difference is observed when wild-type plants undergo metazachlor treatment. (B) represents experiments are underway as all marker lines are not yet available. Gray boxes represents experimental assays to be performed for a more conclusive study of lipid marker mobility.

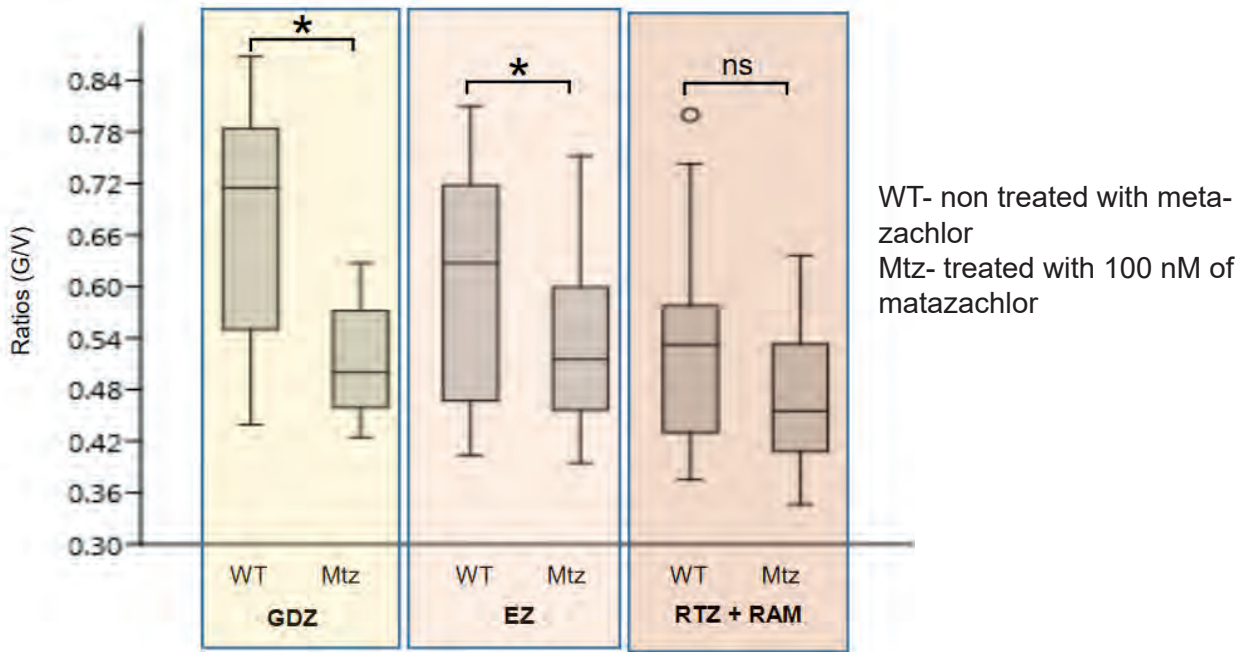
## **PM outer-leaflet order decreases with Metazachlor treatment**

Environment sensitive dye di-4-ANEPPDHQ was used to determine the membrane degree order of PM of *At* root (Jin et al., 2005). Its fluorescence properties change such that the red to green ratio (RG) is inversely correlated with the membrane order level (Jin et al., 2006). We first checked which leaflets are probed by di-4-ANEPPDHQ. To do so, Tobacco (BY-2) cells incubated in the dye showed quenching of the fluorescence after incubation by non-permeable trypan blue (Supplementary data 3). At 1min or 10min after incubation in trypan blue, the quenching percentage of the fluorescence was quite the same suggesting that the dye remained on the outer-leaflet only of the PM (Supplementary data 3). Therefore, we can conclude that the PM order detected by di-4-ANEPPDHQ seemed to be mostly that of the outer-leaflet (Supplementary data 3).

*At* roots were incubated in di-4-ANEPPDHQ and its fluorescence was observed in all regions of the root (Supplementary data 4). The treatment of *At* root cells with 100nM of metazachlor (Mz) seemed to decrease significantly the RG ratio in the growth differentiation zone (GDZ) of the root as well as in the elongation zone (EZ), but not in the root transition zone (RTZ) and root apical meristem (RAM) (Figure 6A). This suggested that Mz by decreasing the acyl chain length of the hVLCFA of GIPCs, increased the outer membrane order. In *fah* mutant, there seemed to be no significant difference between the control (WT) and *fah* mutant (Mut) RG ratio, hence no significant difference (Figure 6B). It was worth noting that the PM order in *fah* mutant, decreased as we got closer to the RTZ and RAM regions suggesting the importance of hydroxylation in membrane ordering (Figure 6B).

To summarize, the reduction of VLCFA in the GIPC of the PM increases the dynamic of the outer leaflet markers. Counterintuitively, the degree of order is also increased, suggesting that these two parameters may not be closely connected. All the results described 'to be done' along the presentation of the results should be finished in the next months. We will draft a paper and send it for submission where I will be co-first author.

A. At wild-type treated and non-treated with metazachlor



B. At *fah* mutants

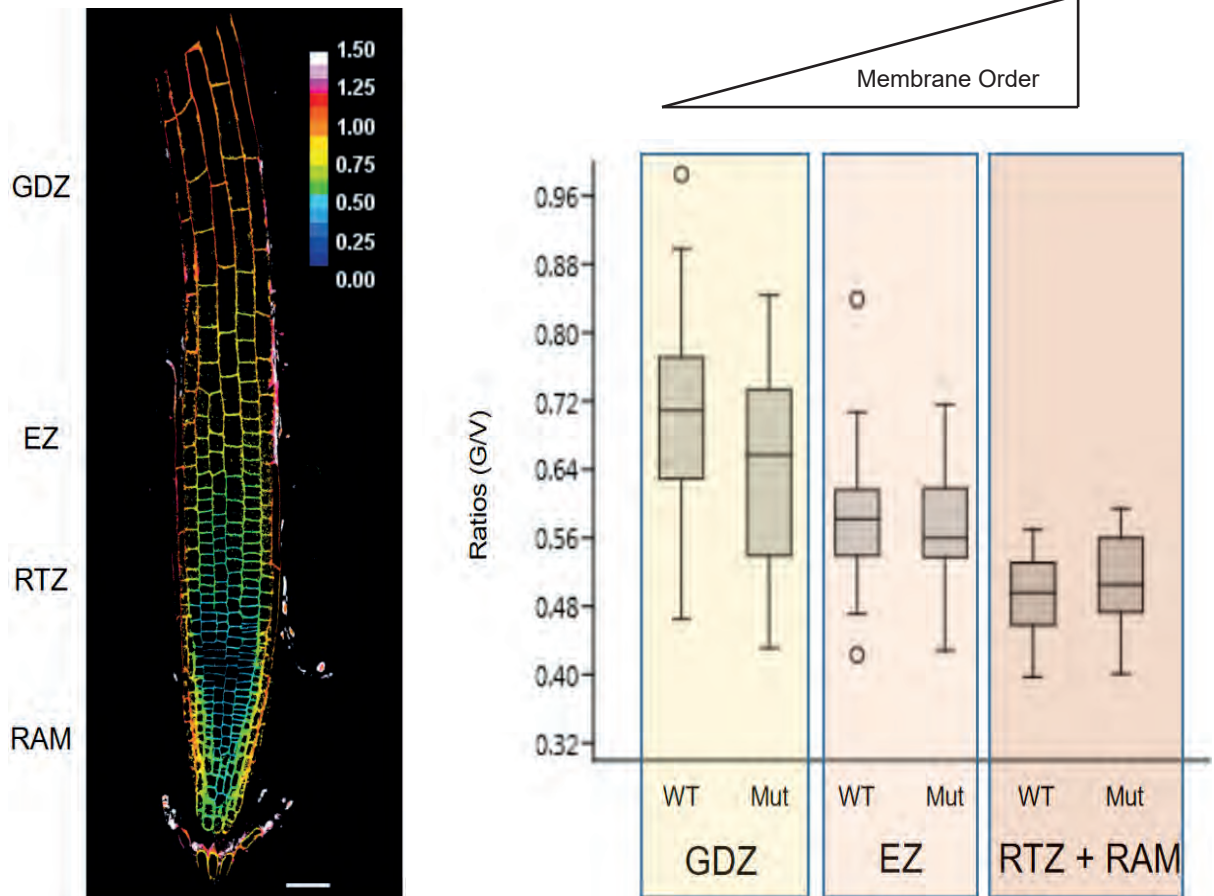
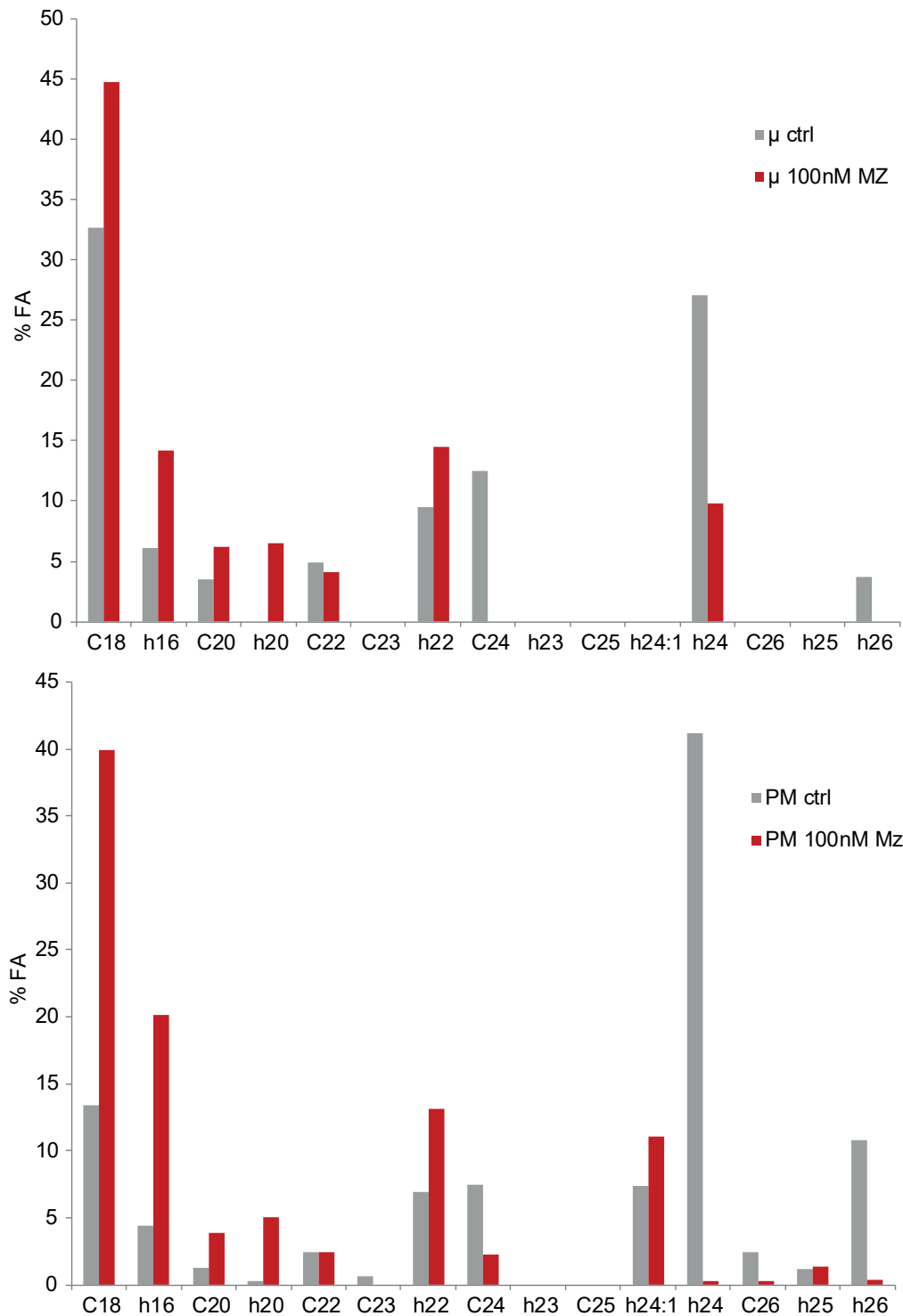
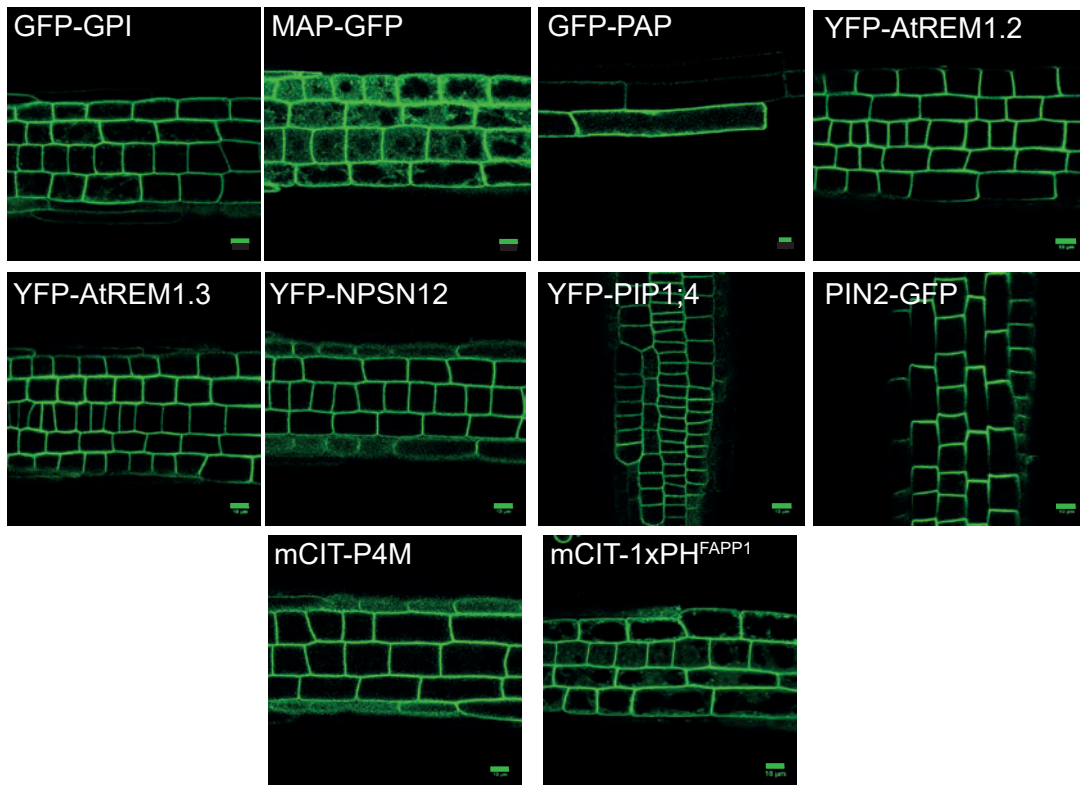


Figure 6: Membrane order determined using fluorescent probe di-4-anepdhq in *At* wild-type and *At fah* mutants. *A.thaliana* plants were incubated with di-4-anepdhq and the green to red ratio (G/V) measured. (A) Metazachlor treatment of the plants does not alter the G/V ratio in the RTZ and RAM regions. (B) *At fah* mutant show a decrease in G/V ratio the closer RTZ region. Data were recorded for 6 independent experiments of n=19 for each condition per experiment. Abbreviations are as follows: GDZ, growth differentiation zone; EZ, elongation zone; RTZ, root transition zone; ; RAM, root apical meristem

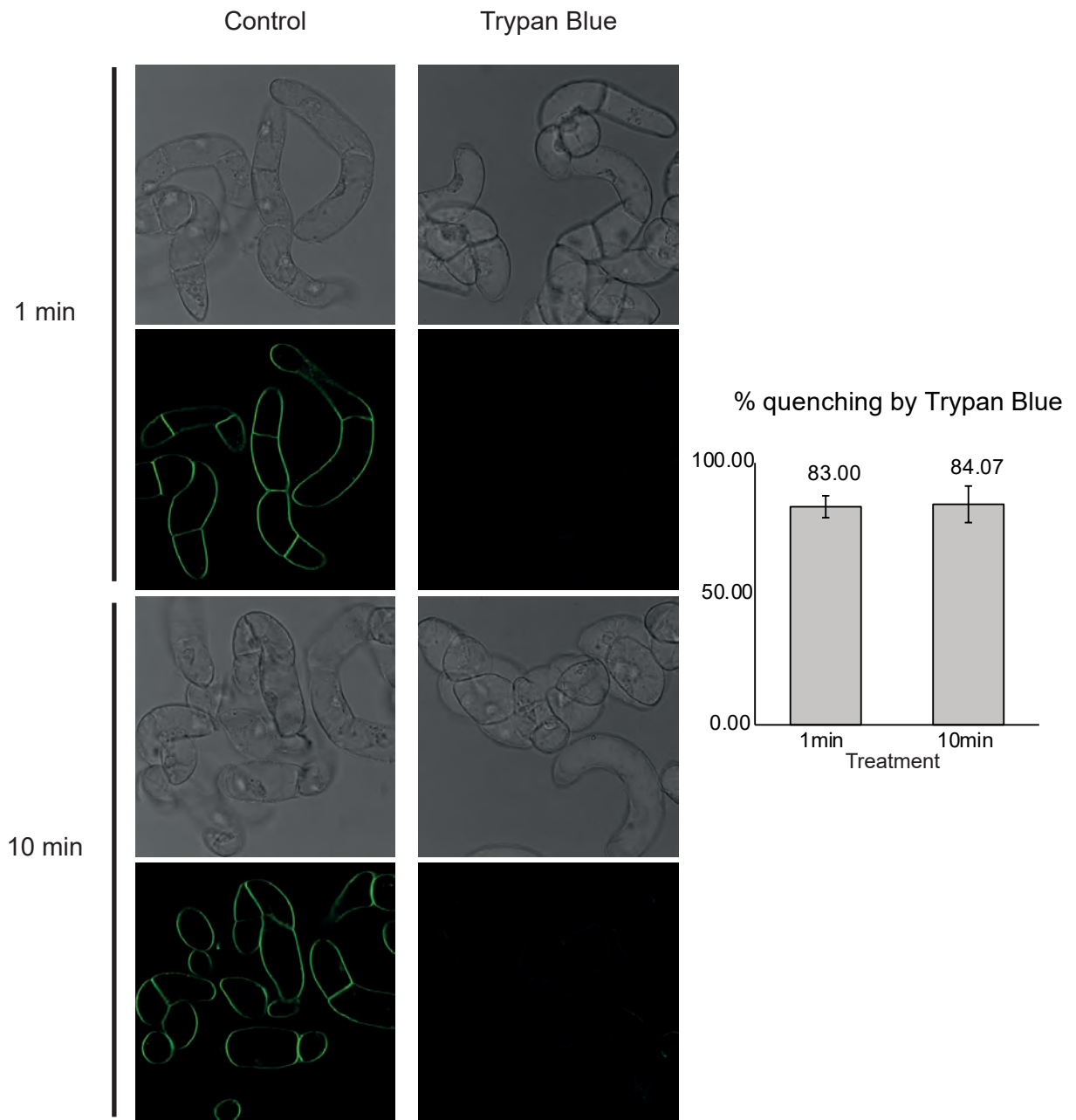
## Supplementary Data



Supplementary data 1, S1 : Fatty acid content of (A) microsomal fractions and (B) PM fractions, treated with metazachlor (Mz) at 100 nM and non-treated (Ctrl). The fatty acid content was quantified by GC-MS after transmethylation of the samples followed by derivatization by BSTFA. Metazachlor treatment (100 nM) does not modify quantitatively the lipid pool but rather is responsible for a shift towards shorter fatty acid chain both in PM and microsomal fractions.

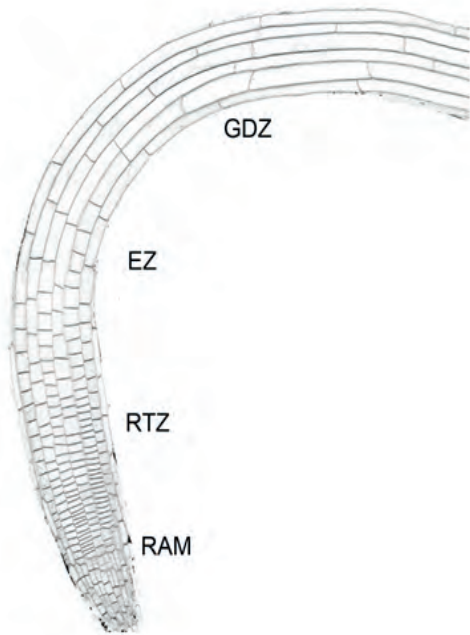


Supplementary data 2, S2: Confocal Microscopy observations confirm the presence of fluorescent markers at the root tip and root elongation zone for prenylated-GFP (GFP-PAP) marker. Observations were done on 6 days-old *Arabidopsis thaliana* plant grown on MS medium. Scale bar, 10 micrometers.

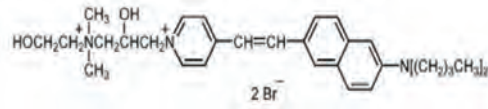


Supplementary data 3, S3: Tobacco (BY-2) cells marked with fluorescent marker di-4-ANEPPDHQ is quenched in the presence of trypan blue by 83 to 84% showing presence of fluorescent on the outer leaflet of the membrane.

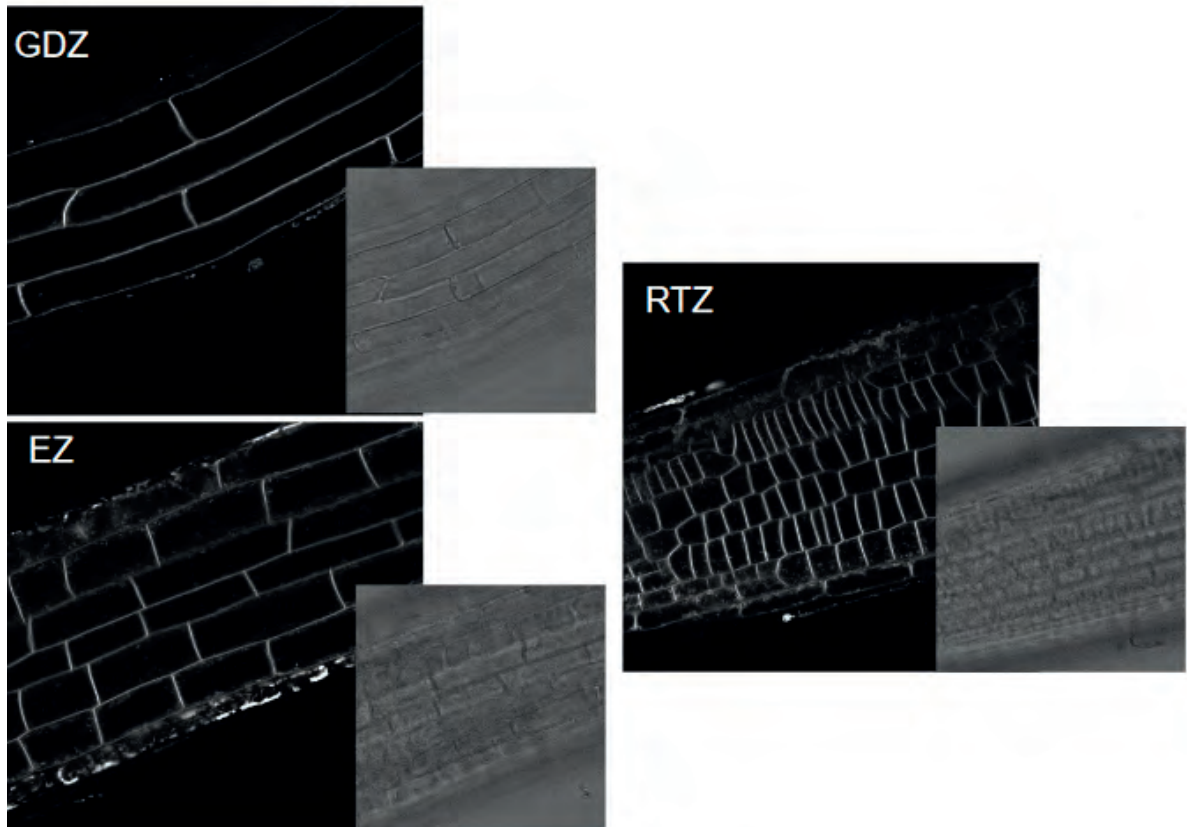
A



Di-4-anepdhdq probe



B



Supplementary data 4, S4: Schematic representation of a *A. thaliana* root sections and chemical equation of the di-4-anepdhdq probe (A). Di-4-anepdhdq probe are highly visible in PM of all three regions of the root (B). Abbreviations are as follows: GDZ, growth differentiation zone; EZ, elongation zone; RTZ, root transition zone, ; RAM, root apical meristem

## Discussion and Perspectives

### Metazachlor treatment and PM lipids

In this project, we studied how alteration of the fatty acid structure of PM lipids can alter the organisation and dynamic of the PM more specifically the mobility of its components. *At* PM was obtained using phase partitioning with PEG/Dextran. The PM is highly electronegative. Based on this characteristic, the PM is attracted to the positively charge PEG phase (Morré & Morre, 2000). Since PEG/Dextran phase partitioning is based on membrane negative charges, PEG phase contains mostly PM. Both leaflets of PM are highly negatively charged due to the presence of PI4P and GIPCs (Simon et al., 2014).

Previous studies showed that there are specific recruitment of proteins with specific post-translational modifications, such as myristoylation, palmitoylation, or presence of a glycosylphosphatidylinositol anchor in PM domains (Morel et al., 2006). (Martiniere et al., 2012) showed that for the two inner leaflet markers, myristoylated and palmitoylated GFP (MAP-GFP) are in detergent insoluble membrane (DIM) while prenylated GFP (GFP-PAP) occurred mostly in non-DIM fractions. The only difference between the two markers are the lipid motif of their acyl tail. Could the lipid structure of PM components (proteins or lipids) affect their mobility, lateral diffusion and segregation in nanodomains? We focused on the role of two important structural components of lipid in PM organisation: VLCFAs and hydroxylation. Very long chain fatty acid (VLCFA), is defined as fatty acid with acyl chain with more than 18 carbon atoms. In plants, there are strong suggestions that GIPCs are the most abundant sphingolipid enriched in the outer leaflet of the PM (Cacas et al., 2016a). PS is an anionic phospholipid, rich in VLCFAs, that accumulates in the inner leaflet of the PM and endosomes (Platre et al., 2018). We hypothesized that altering the acyl chain length and hydroxylation degree of GIPCs of the outer leaflet and perhaps acyl chain length of PS of the inner membrane, modifies PM lateral diffusion and phases.

In the PM control fraction, GIPC acyl chain consists of a ceramide containing three hydroxylations and a hVLCA (Figure 1). This confirms the results of (Wattelet-Boyer et al., 2016) which showed that in *Arabidopsis* root, FAs of GIPCs contained 83.5% of hFAs and mainly of VLCFA (more than 20 carbon atoms).

Our LC-MS/MS analysis effectively showed that in both control and MZ treated, PM GIPCs are enriched in hVLCFA.

Metazachlor (Mz) is a chloracetamide-based herbicide that inhibits VLCFA synthesis by targeting the 3-ketoacyl CoA synthase (KCS) enzymes of the elongase complex. On the pre-existing FAs chain, the complex condenses two carbons at a time to elongate the acyl chain (Tresch, Heilmann, Christiansen, Looser, & Grossmann, 2012). Lipid analysis by LC-MS/MS of PM fractions showed a shift of (h)VLCFA from 24 carbon atoms towards 20 carbon atoms or less in Mz treated samples. This shift in FA>22 to FA<22 was also observed in GC-MS lipid analysis. It is also important to note that Mz does not affect quantitatively the GIPC content in the fractions but rather qualitatively as shown in (Wattelet-Boyer et al., 2016).

When it comes to the degree of hydroxylation, control PM fraction contains only t18:1 GIPC while Mz-treated fractions displayed the presence of both trihydroxylated LCB (t18:1) and dihydroxylated LCB (d18:1 or d18:0). The depletion of VLCFA-GIPC resulted in an increase of d18:1- or d18:0/C16-GIPC. In wild type, the C16-specific ceramide synthase LOH2 uses dihydroxylated LCB, d18:1/d18:0 to synthesize GluCer (Luttgeharm, Kimberlin, et al., 2015). Could Mz hijack LOH2 for the synthesis of C16/20-GIPC instead of GluCer? We need to analyse the lipid composition of WT plants in more detailed. Moreover, we also have to analyse the lipid composition (LC-MS/MS and GC-MS) of *At fah* mutants to determine whether the PM fractions have the same lipid profile as described in (Nagano et al., 2012) where they use total plant lipid extract.

Among the phospholipids of the PM, PE and PC are the most abundant phospholipids in *Arabidopsis* representing each ca. 15 mol% of membrane lipids. However, they are both mainly composed of C16 and C18 and VLCFAs represent only 1.7% and 3.4% of total fatty acids in PC and PE, respectively (Furt, Simon-Plas, & Mongrand, 2010)(Yamaoka et al., 2011). On the other side, even if PS accounts only for 3 mol% of membrane lipids in *Arabidopsis* leaves, it contains VLCFAs such as arachidic acid (C20:0), eicosenoic acid (C20:1), behenic acid (C22:0), erucic acid (C22:1), and lignoceric acid (C24:0). These VLCFAs account for 34.7% of total fatty acids in PS

(Furt et al., 2010)(Yamaoka et al., 2011)(Maneta-Peyret et al., 2014). It is important to know to what extent Mz affects PS acyl chain length to further investigate its effect on PM lateral diffusion. This is why we plan to perform LC-MS/MS analysis of phospholipids to compare the lipid acyl chain composition between PM control and PM Mz treated fractions. It may be that there is a similar shift of PS VLCFAs towards medium length chain fatty acid, as it was the case for GIPCs.

Metazachlor targets several KCS enzymes among which KCS2, KCS17 and KCS20 are highly expressed or expressed at medium level in primary roots (Joubès et al., 2008). In roots, KCS4 and KCS9 are highly expressed or expressed at medium level (Hruz et al., 2008; Joubès et al., 2008). (Lee et al., 2009) showed that in double mutant *kcs2,20* the reduction of C22- and C24-containing FAs is accompanied by the accumulation of C20-containing FAs. (Kim et al., 2013) determined that *kcs9* knockout mutant displayed a reduction of C24-containing FAs and an accumulation of C20- and C22-containing FAs. This mutant showed similar lipid component profile as Mz-treated fractions (Supplementary data, S1). We hence developed *At* lines of *kcs9* mutants expressing the various PM markers (Figure 2) to investigate the effect of VLCFAs in PM lateral diffusion of PM markers by genetic approach to complement the pharmaceutical approach.

We also develop, for FRAP analysis, other Arabidopsis lines of lipid defective mutants expressing the lipid markers: *ipcs 1.2 amiRNA*, *sld1sld2*, *ads2* and *gmt1*. While Inositol Phosphoryl Ceramide Synthase (IPCS) and GIPC Mannosyl-Transferase1 (GMT1) are enzymes affecting the grafting of the polar head, LCB  $\Delta 8$  desaturase (SLD) and Acyl- CoA Desaturase (ADS2) are involved in the ceramide desaturation of sphingolipids. More precisely, ADS2 is responsible to add unsaturation on very long chain fatty acid, such as the h24:1 unsaturation in GIPC. In *ads2* mutants, there is a specific deficiency in the VLCFA unsaturated ceramides in Arabidopsis (Xie et al., 2015). *ads2* mutants are sensitive to dark and light treatment showing the importance of very long chain species in controlling submergence tolerance (Xie et al., 2015). AtSLD1 and AtSLD2 are expressed in the ER and target  $\Delta 8$  desaturase of gluCer. GluCer LCB are significantly enriched in d18:1 $\Delta$  8cis/trans and d18:21 $\Delta$  8cis/trans (combined with a C16 to form the ceramide) and may also contain a t18:1 $\Delta$ 8cis. In contrast, GIPCs are predominantly composed of t18:1 $\Delta$ 8trans LCB combined with a very long-chain fatty acid, as well

as some t18:0 LCB, absent from gluCers. Double mutants *sld1sld2* do not contain LCB  $\Delta 8$  desaturation revealing 50% reduction in gluCer levels and a corresponding increase in GIPCs containing mainly t18:0 LCB. This mutant phenotype is restored by complementation with a wild-type AtSLD1 (Ming Chen et al., 2012). Using the double mutant will increase the amount of t18:0 GIPC in the PM. However, since the double mutants are impacted on their growth, it is quite delicate to make them express the PM markers. Inositolphosphorylceramide synthase, IPCS is the enzyme involved in attaching a phosphoinositol to the ceramide base, to form inositol phosphatidyl ceramide triggering GIPC synthesis in the Golgi. The lack of IPCS causes the accumulation of ceramide and HR response and cell death. Expression of the PM markers in this mutant might give more information on the importance of GIPC in PM organisation.

The cell wall restricts lateral mobility of membrane proteins (Martiniere et al., 2012). It will be interesting to see whether outer leaflet GIPC polar head group is involved in this process. *In vitro* experiments have shown that GIPCs make complexes with the rhamnogalacturonane II (RGII) of the cell wall (Voxeur & Fry, 2014a). Although not all glycosyl transferases involved in GIPC biosynthesis are identified, they seemed to be close to those in the cell-wall pectin biosynthesis (Voxeur, André, Breton, & Lerouge, 2012). We can hypothesize that GIPC acts as a scaffold in maintaining a cell wall-PM continuum, such that by genetically modified GIPC polar head, we can affect the lateral mobility of PM proteins. And if the modification of GIPC head group also affects PS mobility, could there be interdigitation involved between the two leaflets as suggested in animal model by (Raghupathy et al., 2015)? By using *Arabidopsis* mutants such as *gint1*, *gonst1* and *gmt1*, we can investigate the importance of glycosylation, especially that of polyglycosylated GIPCs in PM protein mobility of both leaflets (L. Fang et al., 2016; Ishikawa et al., 2018; Mortimer et al., 2013). Mutated lines of *gmt1* expressing the different PM markers developed by Minoru Nagano are ready for FRAP analysis.

During this project, we measured two parameters: the lateral diffusion of markers in a restricted area of the root PM by photobleaching using FRAP and the order of the PM leaflet by using environment-sensitive probe ANEPPDHQ. It is important to note that these two parameters can be mutually exclusive. For instance, (Martiniere et al., 2012) showed that even if GPI-GFP and MAP-GFP are both in DIMs, they have contrasting mobility with MAP-GFP having a recovering intensity 3.5 times faster than GPI-GFP.

This showed no direct relationship between membrane subcompartmentation and mobility in PM.

### **FRAP analysis and GPI-GFP lateral mobility affected by metazachlor treatment**

Of all the FRAP analyses done using PM markers in the various conditions, only outer-leaflet GPI-GFP mobility showed a significant difference with Mz treatment (Figure 3). GPI-GFP recovery was significantly increased by Mz treatment. In order to conclude that the PM outer leaflet proteins are more dynamic upon Mz treatment, we need to use other plant PM outer leaflet markers. The marker that we used to tag the outer leaflet of the PM is a minimal protein GPI fused with a GFP. It will be interesting to do FRAP with the full native protein of the outer leaflet PM tagged with a fluorophore. We will use GIPC fused GPI-anchored PD proteins, PDCB (Plasmodesma Callose Binding) and PDBG (Plasmodesma Beta-Glucanase) as used in (Grison et al., 2015) and will analyse the recovery post-bleaching in PM with shortened sphingolipid acyl chain, either treated with metazachlor or in *At fah* mutant.

The PS sensor, mCIT-C2<sup>LACT</sup> recovery showed an increase although not significantly related to Mz treatment. This particular FRAP analysis was performed in Japan by Minoru Nagano. The team of Yohann Boutté carried out the experiments here using the same seeds and Mz treatment condition. They did not find any difference in postbleaching recovery between mock and Mz treatment. This increase could be related to varied experimental conditions.

With ongoing experiments and incomplete set of data, we cannot draw a model to show which exact components are involved in PM mobility, however we can argue several scenarios that remain to be tested. For instance, is GPI-GFP chain altered by metazachlor such that its shortened chain is related to its increase in mobility? This can be tested by doing immunopurification of GPI-GFP of PM fractions to compare control and Mz treatment conditions. The fatty acids of the fractions would be liberated by transmethylation, followed by derivatization before GC-MS analysis of lipids. If Mz

alters GPI-GFP acyl chain length, the complementary genetic approach using *kcs9* mutant will be compared with GPI-GFP mobility in Mz treated condition and mutants.

In the case that Mz does not affect GPI-GFP acyl chain and that the increase mobility of the GPI-GFP PM marker is the direct effect of Mz on the surrounding VLCFA lipids of the PM, it could be that GIPC with shorted acyl chain no longer interacts the same way with GPI which hence moves faster. It could also be the impact of Mz on interdigitation. Interdigitation is the phenomenon that link VLCFA of one leaflet into the other such that there is a connection between the two leaflets. The study of (Platre et al., 2019a) just as that of (Raghupathy et al., 2015) highlight the importance of PS in nanodomain clusters and protein immobilization. We may suppose that, upon shortening VLCFA, there is no more interdigitation, hence GPI mobility increases even though PS mobility is not affected. It could be that Mz deter nanodomain formation, through the structural alterations of its components. Hence, GPI not being clustered in these domains, is able to move around more easily. But we do not see recovery difference for inner leaflet MAP-GFP although the latter is also present in nanodomains. Could it be that the components of nanodomains of both leaflets have different mobilities? FRAP experiments have its limitations. It measures the recovery of fluorescence for a relatively small region through both PM leaflets. The anionic probes used have a certain affinity for their targets *in vivo* as there is competition with other molecules as described in (Heilmann, 2016). This is also the case for minimal PM markers, we do not know how they interact differentially with neighbouring proteins.

To study more in details about the behaviour of particles, particularly their mobility the best method is to use super resolution microscopy for single particle tracking. This will give information on the confinement/diffusion behaviour of the each marker. We prepared At lines expressing the PS probe mEos-C2<sup>LACT</sup> to track PS mobility through its rate of diffusion but also its confinement in specific local region. The diffusion is related to the speed of motion of the particle within the limit of the experiment and the confinement is related to the amount of time the particle is packed in domain.

### **Order of the phases in the PM leaflets**

Using di-4-ANEPPDHQ as an environmental sensitive probe specific to the

outer leaflet, we showed that metazachlor treatment increases the overall order of the outer leaflet. It will be interesting to see the phase order of the inner leaflet and how Mz alters it. GPMVs using inside out fractions can be made and di-4-ANEPPDHQ used to examine the order degree of the inner leaflet. We can also use another membrane dye that reports packing. Laurdan displays a spectral red shift in emission between the liquid-ordered and -disordered phases, as well as a shortening of its fluorescence lifetime. It can be used as a control to confirm the di-4-ANEPPDHQ results. It seems contradictory to our expectation that the GFP-GPI seems very mobile in a more-ordered phase. We mentioned above that mobility and phase order can be contrasting as demonstrated in (Martinière et al., 2012). We can also hypothesize that shorter chain GIPCs interact better with phytosterols, since there is fewer conformational hindrance with the VLCFA of the GIPCs, hence increasing degree of order.

The degree of order of the leaflet is an overall one. We don't know how many separated phases and how are organized membrane domains or 'raft' in the leaflet. Past studies have investigated domain organization in intact cell membranes through the mobility of membrane components (Dietrich, Yang, Fujiwara, Kusumi, & Jacobson, 2002; Kusumi, Ike, Nakada, Murase, & Fujiwara, 2005; Owen, Williamson, Magenau, & Gaus, 2012). It seems that PM lipids and proteins showed anomalous diffusion behaviour in cells. This was attributed to the partitioning of the diffusing components into raft domains. Most of these studies use a set of different methods. For instance in the study of (Owen et al., 2012) on HeLa cells, they simultaneously recorded membrane order from Laurdan's emission profile and protein diffusion using fluorescence correlation spectroscopy (FCS). They hence correlated membrane order to protein diffusion. To see clustering and particle movement, they also did super-resolution photoactivated localization microscopy (PALM). (Eggeling et al., 2009) used stimulated emission (STED)-fluorescence correlation spectroscopy (FCS) to observe the average time taken by single molecules to diffuse a defined area. They observed that the slowly diffusing components were present even in very small spot sizes. This suggested that single molecules can partition into very small membrane domains. The study of single particle movement and confinement behaviours by super resolution single particle tracking is one of the answers into understanding the intricate role of PM protein diffusion and clustering.

Our project opens doors towards the understanding of PM protein and lipid behaviours in both leaflets and how PM lipid structures might influence the membrane organization and behaviour of neighbouring molecules. The field of rafts and membrane domains is ever evolving with new techniques, probes and methods devised to elucidate the mechanism involved in nanodomain formation, components, lifespan and physiological role. These new advents open new doors into elucidating the mystery of PM leaflet asymmetry as so far our understanding of membrane asymmetry is purely passed on presumed models (Cacas et al., 2016a; Tjellstrom et al., 2010) Takeda aussi. Plant PM despite being particularly difficult to study due to the presence of the cell wall, is a key element to understand cell function and integrity.

This paper where I will be co-first author with Minoru Nagano will be published next year.

## **Material and Methods**

### **Plant Materials**

#### **Tobacco BY-2 cell culture**

BY-2 cells (*Nicotiana tabacum* cv. Bright Yellow 2) were grown in Murashige and Skoog medium, pH 5.6, containing Murashige and Skoog salt, 1 mg/liter thiamine HCl, 0.2 mg/liter 2,4-dichlorophenylacetic acid, 100 mg/liter myo-inositol, 30 g/liter sucrose, 200 mg/liter  $\text{KH}_2\text{PO}_4$ , and 2 g/l MES. Cells were maintained by weekly dilution (2:80) into fresh medium.

#### **Arabidopsis seedling liquid culture**

Arabidopsis seeds were directly grown in liquid medium containing MES for 10 days on agitation.

#### **Treatments of *At* seedlings for FRAP**

For metazachlor (Greyhound Chromatography and Allied Chemicals) treatment, seedlings were grown on MS plates containing the drug at 50nM in most experiments, except when specified. Metazachlor was added from a 100mM stock in dimethylsulfoxide, an intermediate stock concentration at 100 mM was used extemporarily to make the plates. For cycloheximide (CHX) and BFA treatments, seedlings were treated in liquid medium (LM) containing 1XMS, 1% sucrose, 2.5mM morpholinoethanesulfonic acid pH 5.8. In BFA experiments, seedlings were first pretreated with 50 mM CHX (Sigma) for 90 min and then treated with 50 mM CHX and 50 mM BFA for 90 min. Washout experiments were performed by washing in LM implemented with 50 mM CHX for 90 min.

#### **Arabidopsis PM purification protocol**

All steps were performed at 4°C. PM isolation PM fractions were obtained from seedlings grown in hydroponic medium by membrane partitioning in an aqueous polymer two-phase system with polyethylene glycol 3350/ dextran T-500 (6.6% each), according to Mongrand et al. (2004). Protein content was quantified using the Bradford method, in order to obtain an aliquoted solution of 10 mg ml<sup>-1</sup> final concentration.

## **Fatty acid analysis**

Each sample was transmethylated at 110°C overnight in methanol containing 5% (v/v) sulfuric acid and spiked with 10 mg of heptadecanoic acid (c17:0) and 10 mg of 2-hydroxy-tetradecanoic acid (h14:0) as internal standards. After cooling, 3 mL of NaCl (2.5%, w/v) was added, and the released fatty acyl chains were extracted in hexane. Extracts were washed with 3 mL of saline solution (200 mM NaCl and 200 mM Tris, pH 8), dried under a gentle stream of nitrogen, and dissolved in 150 mL of BSTFA and trimethylchlorosilane. Free hydroxyl groups were derivatized at 110°C for 30min, surplus BSTFA-trimethylchlorosilane was evaporated under nitrogen, and samples were dissolved in hexane for analysis using GC-MS under the same conditions as described (Buré et al., 2011). Quantification of fatty acids and hydroxyl acids was based on peak areas, which were derived from total ion current (Rehman et al., 2008), and using the respective internal standards. LC-MS/MS analysis of sphingolipid

## **Western-blot**

All steps were performed at room temperature. After electrophoresis separation (1 h, 20 mA/gel), proteins were electroblotted onto nitrocellulose membrane (20 min, 15 V; Trans-blot SD semidry transfer cell; Bio-Rad) in a buffer containing 30 mM Tris, 192 mM glycine, and 20% methanol. Membranes were blocked for 1 h with 5% powdered milk in Tris-buffered saline (TBS)-Tween (2 mM Tris, 15 mM NaCl, 0.05% Tween 20, pH 7.6), washed for 7 min three times in TBS Tween, and then incubated for 1 h with primary antibody.

## **FRAP experiments**

The relative mobile fraction of different fluorescent proteins was assessed by FRAP following the technique of (Martiniere et al., 2012) as follows. The relative mobile fraction at time 60 s postbleaching (l60s) of different fluorescent proteins was. Circular regions of interest (ROIs) (radius 4.3 µm) were bleached in median optical sections of the fluorescent PM. Recovery of fluorescence was recorded during 60 or 120 s with a delay of 1.5 s between frames. Fluorescence intensity data were

normalized using the equation described in (Martiniere et al., 2012). Experiments were performed on 10-15 samples for each condition.

## Chapter 3

**GIPC, receptor to microbial NLP,  
determine host sensitivity**

In this chapter, we shall see the role of GIPCs as receptors to toxins called necrosis and ethylene-inducing peptide 1 (Nep 1)-like proteins (NLP) and that of GIPC polar head diversity playing an important role in the sensitivity of plants to these toxins.

The teams of Thorsten Nürnberger in Germany and Gregor Anderluh in Slovenia work on NLP toxins. These toxins are secreted by several phytopathogenic microorganisms causing necrosis in eudicot, but not in monocot plants. The NLP toxins share similar structure with animal actinoporin that binds to sphingomyelin (SM) and cause cell lysis. While the abundant sphingolipid in animal is SM, plant GIPCs shared a number of similarities to SM. So the affinity of NLP to GIPC was tested. My contribution to this work started during my MSc degree internship on the project that later evolved into my PhD thesis project. I worked on optimizing the extraction process of GIPC and generated milligrams of GIPCs from mainly cauliflower (eudicot) and leek (monocot) at the LBM, Bordeaux, see chapter 1. I then went to the LBMi, Université de Liège, Gembloux in Belgium to characterize my GIPC samples, more precisely the spatial differences of GIPC series A and B. The aim was to find how an added sugar group (present in GIPC from monocot but not eudicots) can influence the amount of space occupied by the molecule. I measured the mean molecular area of these GIPCs through Langmuir trough compression isotherm assays. The result obtained showing that both GIPC series A and B occupied similar mean molecular area, was crucial information for the submitted version of the paper. The experimental results were backed by modelling showing a perpendicular orientation of the sugar moieties of GIPC series B above the horizontal plane, rather than perpendicular. This highlighted how the structure of the GIPC molecule with an added sugar residue can have dramatic role in plant-pathogen interaction.

This work is published in *Science* 2017, where I am 18th author on 25 authors. My contribution to the paper involved producing the GIPC extracts from cauliflower and leek for the experiments and Langmuir trough experiment of supplementary data, particularly Figure S15.

Lenarčič T, Albert I, Böhm H, Hodnik V, Pirc K, Zavec AB, Podobnik M, Pahovnik D, Žagar E, Pruitt R, Greimel P, Yamaji-Hasegawa A, Kobayashi T, Zienkiewicz A, Gömann J, Mortimer J, Fang L, **Mamode-Cassim A**, Deleu M, Lins L, Oecking C,

Feussner I, Mongrand S, Anderluh G\*, Nürnberger T\* (2017) Eudicot plant-specific sphingolipids determine host selectivity of microbial NLP cytolysins. *Science*, Dec 15;358(6369):1431-1434. \*co- corresponding authors



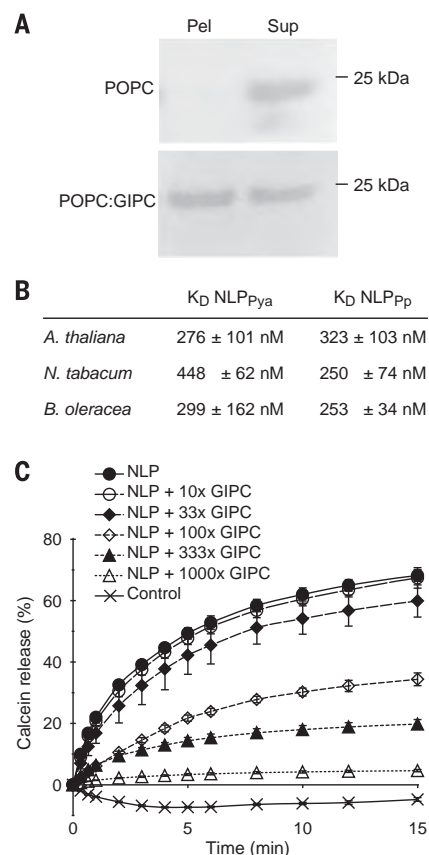


**Fig. 2. Binding of NLP proteins to plant**

**GIPCs.** (A) NLP<sub>PyA</sub> binding to POPC and POPC:GIPCs 1:1 (m:m) multilamellar vesicles monitored by means of liposome sedimentation. Pel, pellet; Sup, supernatant. (B) Surface plasmon resonance analysis of NLP<sub>PP</sub> or NLP<sub>PyA</sub> binding to GIPCs ( $n = 3$ ). (C) Cauliflower GIPC-mediated inhibition of NLP<sub>PP</sub>-induced (100 nM) calcein release from purified *Arabidopsis* plasma membrane vesicles. GIPCs:NLP<sub>PP</sub> molar ratios are given. Values represent means ± SD of three replicates.

preparations with dissociation constants (Fig. 2B and fig. S4) similar to NLP concentrations required to cause leaf necrosis (fig. S1D) (3). Soluble *Arabidopsis* GIPCs also bound chip-immobilized NLP<sub>PyA</sub>, but metazoan sphingomyelin and POPC did not (fig. S5). Preincubation of NLP<sub>PP</sub> with GIPCs reduced its cytolytic activity in a GIPC-concentration-dependent manner (Fig. 2C). This suggests that saturating the toxin with its receptor prevented vesicle lysis, implying physical interaction between NLP and its receptor, GIPC.

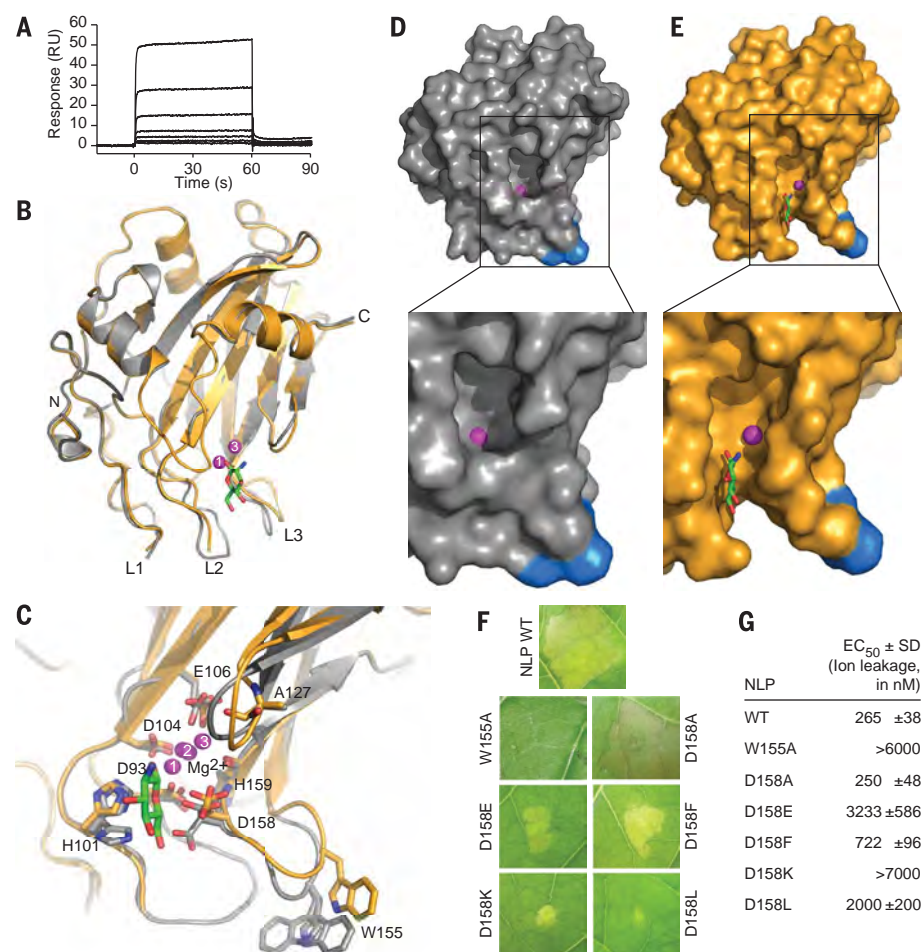


**Fig. 3. Structural and functional analysis of a GlcN-NLP<sub>PyA</sub> complex.** (A) Surface plasmon resonance analysis of GlcN binding (5 mM to 78.1 μM, from top to bottom in twofold dilutions) to immobilized NLP<sub>PyA</sub>. (B and C) Structural comparison of apo-NLP<sub>PyA</sub> (gray) and GlcN-NLP<sub>PyA</sub> complex (orange). (B) GlcN is displayed in green sticks. Loops at the bottom are designated as L1, L2, and L3. Mg<sup>2+</sup> ions are shown in magenta spheres: state 1, position in apo-NLP<sub>PyA</sub>; state 2, positions in other three polypeptide chains from the asymmetric unit that did not bind hexose; state 3, position in GlcN-bound NLP<sub>PyA</sub>. (C) Amino acids involved in Mg<sup>2+</sup> coordination and GlcN binding and residue W155 are shown in sticks. (D and E) Conformational changes presented by protein surfaces. (D) apo-NLP<sub>PyA</sub> structure (gray). (E) GlcN-bound form of NLP<sub>PyA</sub> (orange). Mg<sup>2+</sup> and GlcN are as in (C), and W155 is depicted as a blue surface. (F) Tobacco leaf necroses caused by wild-type NLP<sub>PyA</sub> and NLP<sub>PyA</sub> mutant proteins (200 nM). (G) Quantification of cell death as in (F) by means of ion leakage measurement.

We next assayed whether NLP<sub>PyA</sub> can bind free sugars corresponding to the terminal saccharides found in tobacco GIPC head groups. NLP<sub>PyA</sub> bound GlcN and its epimer mannosamine (ManN) (Fig. 3A and fig. S6A), but at concentrations higher than those required to bind intact GIPCs (Fig. 2B).

To address how GIPC hexoses contact NLP<sub>PyA</sub> toxins, we determined crystal structures of NLP<sub>PyA</sub> in complex with either GlcN or ManN (Fig. 3B, figs. S6B and S7, and table S1). In both cases, we found electron density indicating a bound sugar in one out of four polypeptide chains in the

<sup>1</sup>Department for Molecular Biology and Nanobiotechnology, National Institute of Chemistry, Hajdrihova 19, 1000 Ljubljana, Slovenia. <sup>2</sup>Centre of Plant Molecular Biology, Eberhard-Karls-University Tübingen, Auf der Morgenstelle 32, 72076 Tübingen, Germany. <sup>3</sup>Department of Biology, Biotechnical Faculty, University of Ljubljana, Jamnikarjeva 101, 1000 Ljubljana, Slovenia. <sup>4</sup>Department of Polymer Chemistry and Technology, National Institute of Chemistry, Hajdrihova 19, 1000 Ljubljana, Slovenia. <sup>5</sup>Lipid Biology Laboratory, RIKEN, Wako Saitama 351-0198, Japan. <sup>6</sup>Laboratory for Cell Function Dynamics, Brain Science Institute, RIKEN Institute, Wako, Saitama 351-0198, Japan. <sup>7</sup>Molecular Membrane Neuroscience, Brain Science Institute, RIKEN Institute, Wako, Saitama 351-0198, Japan. <sup>8</sup>UMR 7213 CNRS, University of Strasbourg, 67401 Illkirch, France. <sup>9</sup>Department of Plant Biochemistry, Albrecht-von-Haller-Institute for Plant Sciences, University of Göttingen, Germany. <sup>10</sup>Göttingen Center for Molecular Biosciences, University of Göttingen, Germany. <sup>11</sup>Joint Bioenergy Institute, Emeryville, CA 94608, USA. <sup>12</sup>Biosciences Division, Lawrence Berkeley National Laboratory, Berkeley, CA 94720, USA. <sup>13</sup>Laboratoire de Biogenèse Membranaire, UMR 5200 CNRS-Université de Bordeaux, 71 Avenue Edouard Bourlaux, 33883 Villenave-d'Ornon Cedex, France. <sup>14</sup>Laboratory of Molecular Biophysics at Interfaces, University of Liège, Gembloux, Belgium.

\*These authors contributed equally to this work.

†Corresponding author. Email: gregor.anderluh@ki.si (G.A.); nuernberger@uni-tuebingen.de (T.N.)

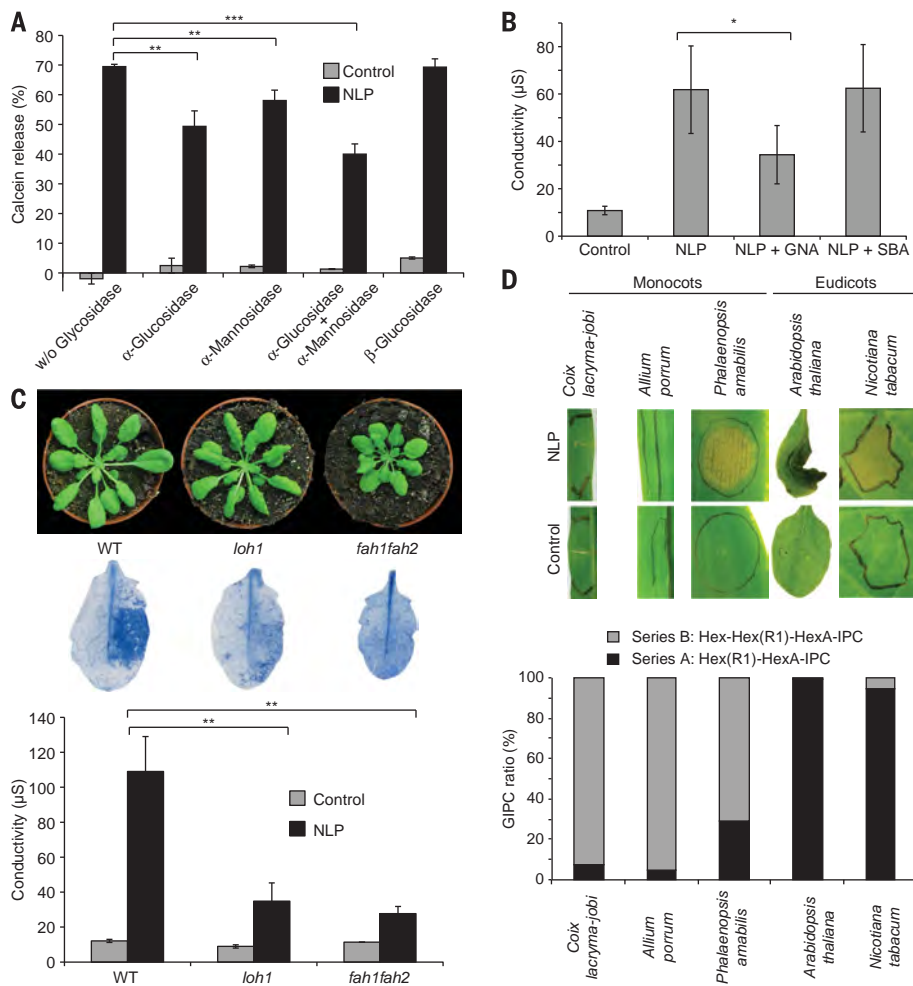


**Fig. 4. Series A GIPCs determine NLP cytotoxicity.** (A) Calcein-filled *Arabidopsis* plasma membrane vesicles pretreated (1 hour) with  $\alpha$ -glucosidase,  $\alpha$ -mannosidase, or  $\beta$ -glucosidase before addition of NLP<sub>Pyra</sub> or water (control). Values represent means  $\pm$  SD of three replicates. Student's *t* test analyses ( $^{*}P < 0.01$ ,  $^{***}P < 0.001$ ). (B) Cell death (quantified by means of ion leakage) in *Arabidopsis* Col-0 leaves treated for 6 hours with water (control) or NLP<sub>Pyra</sub> with and without mannose-specific GNA or galactose-specific SBA. Values are means  $\pm$  SD of three replicates. Student's *t* test analyses ( $^{*}P < 0.05$ ). (C) (Top) *Arabidopsis loh1* and *fah1fah2* plants. (Middle) Cell death (Trypan blue) staining of leaves after infiltration of NLP<sub>Pyra</sub> or water (control). (Bottom) Cell death (quantified by means of ion leakage) in *Arabidopsis* Col-0 leaves treated with NLP<sub>Pyra</sub> or water (control). Values are means  $\pm$  SD of three replicates. (D) NLP<sub>Pyra</sub> (1  $\mu$ M)-mediated plant leaf necrosis (top). Images were taken 48 hours after infiltration. GIPC quantification (bottom) is as in (17) and the supplementary materials. One of three experiments with similar results is shown.

asymmetric unit. Higher B-factors for the sugar atoms relative to the protein atoms suggest partial occupancy of the sugar, which is consistent with low-affinity binding to monomeric sugars (Fig. 3A, figs. S6A and S7, and table S1). The overall fit between structures was high [root mean square deviation values for apoprotein (apo)-NLP<sub>Pyra</sub> and GlcN-NLP<sub>Pyra</sub> or ManN-NLP<sub>Pyra</sub>-complexes are 0.56 and 0.55 Å, respectively], but we observed structural changes attributable to sugar binding (Fig. 3, B and C, and fig. S6, B and C). Hexose moieties bound to an elongated crevice between loops L2 and L3, adjacent to a bound Mg<sup>2+</sup>-ion crucial for NLP<sub>Pyra</sub> cytotoxicity (Fig. 3C and fig. S6C) (3). Sugar binding induces a conformational change in loop L3, causing widening of the L2-L3 crevice

and movement of Mg<sup>2+</sup> toward the center of the protein relative to its position in apo-NLP<sub>Pyra</sub> [Protein Data Bank (PDB) 3GNZ] (Fig. 3, B to E, and fig. S6, B and C) (3). L3 loops of sugar-free NLP<sub>Pyra</sub> chains within the same asymmetric unit exhibited conformations similar to that of apo-NLP<sub>Pyra</sub> (fig. S6D). Conformational rearrangements within hexose-bound NLP<sub>Pyra</sub> suggest that a portion of the GIPC head group is accommodated within the protein (Fig. 3, D and E, and fig. S6C). Residue W155 is placed at the bottom of loop L3 close to the hexose-binding site (Fig. 3, C to E). NLP<sub>Pyra</sub> W155A mutant protein exhibited neither binding to GIPCs (fig. S8) nor cytotoxic activity (Fig. 3, F and G and fig. S9), suggesting the involvement of this hydrophobic residue in inter-

action with the membrane. (Single-letter abbreviations for the amino acid residues are as follows: A, Ala; C, Cys; D, Asp; E, Glu; F, Phe; G, Gly; H, His; I, Ile; K, Lys; L, Leu; M, Met; N, Asn; P, Pro; Q, Gln; R, Arg; S, Ser; T, Thr; V, Val; W, Trp; and Y, Tyr. In the mutants, other amino acids were substituted at certain locations; for example, W155A indicates that tryptophan at position 155 was replaced by alanine.)

Translational movement of Mg<sup>2+</sup> affects its coordination. In apo-NLP<sub>Pyra</sub>, Mg<sup>2+</sup> is octahedrally coordinated by D93 and D104, and via four water molecules, with side chains of residues H101, E106, D158, and the main-chain carbonyl of H159 (fig. S10A and table S2) (3). Upon binding of either GlcN or ManN, Mg<sup>2+</sup> is shifted 2.9 Å closer to E106 and becomes directly coordinated by E106 and the H159 main-chain carbonyl, whereas D93, D104, D158 side chains, and the A127 carbonyl group coordinate Mg<sup>2+</sup> indirectly via four water molecules (fig. S10, B and C). The hexose is positioned between H101 and D158 side chains (Fig. 3C and fig. S6C), preventing interaction with Mg<sup>2+</sup>. Mutations in D93, H101, D104, and E106 impair NLP cytotoxicity and microbial infection (3), which can now be explained by our structural insights.

Replacement of charged D158 with A158 did not compromise NLP cytotoxic activity, but mutation to hydrophobic F158 and L158 or charged E158 and K158 residues reduced NLP cytotoxicity (Fig. 3, F and G, and fig. S9). Space constraints in the hexose-binding cavity of these NLP<sub>Pyra</sub> mutants probably hinder interaction with GIPC hexose head groups. Again, hexose-NLP<sub>Pyra</sub> structures suggest an interpretation for the loss of function because D93, D104, and E106 are involved in Mg<sup>2+</sup>-binding, whereas H101 and D158 are engaged in hexose binding (Fig. 3C; figs. S6C and S10, B and C; and table S2).

Unlike tobacco, *Arabidopsis* GIPC terminal sugars are mannose or glucose (8, 10). To corroborate the role of GIPC hexose head groups in NLP function, we pretreated calcein-loaded *Arabidopsis* plasma membrane vesicles with  $\alpha$ -glucosidase or  $\alpha$ -mannosidase before addition of NLP<sub>Pyra</sub>. NLP<sub>Pyra</sub> caused calcein release from mock-treated vesicles, whereas calcein release from enzyme-treated vesicles was reduced (Fig. 4A). Vesicle pretreatment with  $\beta$ -glucosidase did not impair NLP toxicity (Fig. 4A). Thus, plant surface-exposed sugar residues are important for NLP toxicity. *Galanthus nivalis* agglutinin (GNA), a mannose-specific lectin (11), partially blocked NLP-mediated membrane damage, whereas galactose-specific soybean agglutinin (SBA) did not (Fig. 4B). This suggests that a mannose-specific lectin and NLP<sub>Pyra</sub> compete for binding to the NLP receptor.

Plants with completely disabled GIPC biosynthesis pathways are either nonviable or display developmental defects (9, 10). Consequently, we used *Arabidopsis* mutants with reduced GIPC levels (fig. S11) to assess NLP sensitivity. NLP<sub>Pyra</sub> infiltration into leaves of ceramide synthase mutant *loh1* (LONGEVITY ASSURANCE 1 HOMOLOG1) (12) caused less cell death than in wild type (Fig. 4C), suggesting that lower GIPC levels promote increased toxin tolerance. GIPCs from *Arabidopsis*

*gonst1* mutants lacking mannosylation (13) were less efficient in vesicle protection assays (fig. S12), implying reduced NLP binding. *Arabidopsis* FATTY ACID HYDROXYLASE (FAH) mutant *fah1fah2* (14) has reduced GIPC content (fig. S11) and altered plasma membrane organization (fig. S13), as observed in rice (15). When treated with NLP<sub>PP</sub>, *fah1fah2* mutants exhibited enhanced NLP toxin tolerance (Fig. 4C), suggesting that intact GIPCs or ordered plasma membranes are required for NLP cytotoxicity.

Of the two major clades of angiosperms, monocots and eudicots, only eudicots are sensitive to NLPs (1, 2, 16). Monocot GIPCs often carry three hexose units linked to IPC (series B GIPC), whereas eudicot GIPCs carry only two (series A GIPC) (17). Monocot *Phalaenopsis* species represent an exception in producing both series A GIPCs and series B GIPCs (Fig. 4D) (17). Unlike other monocots tested, *P. amabilis* developed necrotic lesions upon NLP<sub>Pya</sub> treatment (Fig. 4D). Thus, it is series A GIPCs that determine plant clade-specific NLP toxin sensitivity.

NLP<sub>Pya</sub> and NLP<sub>PP</sub> bind to monocot and eudicot-derived GIPCs with similar affinities (Fig. 2B and fig. S14). This is conceivable because both GIPC types carry terminal hexose residues (17). In model lipid membranes, both GIPCs occupy similar surface areas, despite their different hexose chain lengths (fig. S15A). This is in agreement with computer simulations, suggesting a similar perpendicular arrangement of series A (8) and B GIPCs. Thus, the terminal hexose residue in series B GIPCs is located further away from the membrane surface than that in series A (fig. S15B).

Microbial toxins affecting vertebrate or insect hosts often bind to glycosylated lipid receptors

(18, 19). We show that this mode of toxin action extends to plant hosts and that conformational changes upon binding of NLPs to GIPC sugars facilitate cytotoxicity in a manner that differs from those of other cytotoxins (5). Although GIPC sphingolipids are abundant in plants (8, 10), only eudicot and not monocot plants are sensitive to NLP cytotoxins (1, 2, 16). We found the explanation to lie in the presence of series A GIPCs. Monocots that lack series A GIPCs are indeed insensitive to NLP cytotoxins, but exceptions that produce both series A and B GIPCs were sensitive. Series A- and B-type GIPCs carry terminal hexose residues, but in different numbers (8, 17). Binding of NLPs to series B GIPC trisaccharide terminal sugars would result in more distant positioning of the L3 loop relative to the plant membrane, impeding NLP insertion into the plasma membrane. Thus, the difference in plant sensitivity to NLP cytotoxins is explained by the length of GIPC head groups and the architecture of the NLP sugar-binding site, which also excludes the branched sugar head groups found in higher-series GIPCs (8, 20).

#### REFERENCES AND NOTES

- S. Oome, G. Van den Ackerveken, *Mol. Plant Microbe Interact.* **27**, 1081–1094 (2014).
- M. Gijzen, T. Nürnberger, *Phytochemistry* **67**, 1800–1807 (2006).
- C. Ottmann *et al.*, *Proc. Natl. Acad. Sci. U.S.A.* **106**, 10359–10364 (2009).
- D. Qutob *et al.*, *Plant Cell* **18**, 3721–3744 (2006).
- G. Anderluh, J. H. Lakey, *Trends Biochem. Sci.* **33**, 482–490 (2008).
- N. Rojko, M. Dalla Serra, P. Maček, G. Anderluh, *Biochim. Biophys. Acta* **1858**, 446–456 (2016).
- B. Bakrač *et al.*, *J. Biol. Chem.* **283**, 18665–18677 (2008).
- J. L. Cacas *et al.*, *Plant Physiol.* **170**, 367–384 (2016).
- J. E. Markham, D. V. Lynch, J. A. Napier, T. M. Dunn, E. B. Cahoon, *Curr. Opin. Plant Biol.* **16**, 350–357 (2013).
- L. Fang *et al.*, *Plant Cell* **28**, 2991–3004 (2016).
- E. J. M. Van Damme *et al.*, *Eur. J. Biochem.* **202**, 23–30 (1991).
- P. Ternes *et al.*, *New Phytol.* **192**, 841–854 (2011).
- J. C. Mortimer *et al.*, *Plant Cell* **25**, 1881–1894 (2013).
- S. König *et al.*, *New Phytol.* **196**, 1086–1097 (2012).
- M. Nagano *et al.*, *Plant Cell* **28**, 1966–1983 (2016).
- B. A. Bailey, *Phytopathology* **85**, 1250–1255 (1995).
- J. L. Cacas *et al.*, *Phytochemistry* **96**, 191–200 (2013).
- J. S. Griffiths *et al.*, *Science* **307**, 922–925 (2005).
- D. G. Pina, L. Johannes, *Toxicol.* **45**, 389–393 (2005).
- C. Buré, J. L. Cacas, S. Mongrand, J. M. Schmitter, *Anal. Bioanal. Chem.* **406**, 995–1010 (2014).

#### ACKNOWLEDGMENTS

Work was supported by Deutsche Forschungsgemeinschaft (Nu70/1-9, SFB1101, INST 186/1167-1), Slovenian Research Agency (P1-0391, J1-7515), Seventh Framework Program BioStructX N°283570, Japan Ministry for Science and Technology JP16K08259, L'Agence Nationale de la Recherche (11-INBS-0010), U.S. Department of Energy Joint BioEnergy Institute (DE-AC02-05CH11231), Fonds de la Recherche Scientifique (Projet de Recherche grant T.1003.14, IAP P7/44 iPros), Belgian Program on Interuniversity Attraction Poles (IAPP7/44iPros), University of Liège (FIELD), RIKEN Integrated Lipidology Program, RIKEN Center for Sustainable Resource Science Wako, Platform Métabolome-Fluxome-Lipidome Bordeaux, and Göttingen Metabolomics and Lipidomics Platform. We thank Š. P. Novak, C. Thurow, N. Li, B. Thomma, G. Felix, M. Gijzen, A. Gust, J. Parker, T. Romeis, synchrotron ELETTRA, and the Graduate School of Biomedicine, University of Ljubljana (T.L.) for support. This work is dedicated to late Prof. Hanns Ulrich Seitz. All authors agreed on the manuscript. Structures are deposited (PDB: 5NNW, 5NO9). Supplementary materials contain additional data.

#### SUPPLEMENTARY MATERIALS

www.sciencemag.org/content/358/6369/1431/suppl/DC1  
Materials and Methods  
Figs. S1 to S15  
Tables S1 and S2  
References (21–46)

18 May 2017; accepted 31 October 2017  
10.1126/science.aan6874

## Eudicot plant-specific sphingolipids determine host selectivity of microbial NLP cytolysins

Tea Lenarcic, Isabell Albert, Hannah Böhm, Vesna Hodnik, Katja Pirc, Apolonija B. Zavec, Marjetka Podobnik, David Pahovnik, Ema Zagar, Rory Pruitt, Peter Greimel, Akiko Yamaji-Hasegawa, Toshihide Kobayashi, Agnieszka Zienkiewicz, Jasmin Gömann, Jenny C. Mortimer, Lin Fang, Adiiilah Mamode-Cassim, Magali Deleu, Laurence Lins, Claudia Oecking, Ivo Feussner, Sébastien Mongrand, Gregor Anderluh and Thorsten Nürnberger

*Science* **358** (6369), 1431-1434.  
DOI: 10.1126/science.aan6874

### An extra sugar protects

Many microbial pathogens produce proteins that are toxic to the cells that they are targeting. Broad-leaved plants are susceptible to NLP (necrosis and ethylene-inducing peptide 1-like protein) toxins. Lenarcic *et al.* identified the receptors for NLP toxins to be GIPC (glycosylinositol phosphorylceramide) sphingolipids (see the Perspective by Van den Ackerveken). Their findings reveal why these toxins only attack broad-leaved plants (so-called eudicots): If the sphingolipid carries just two hexoses, as is the case for eudicots, the toxin binds and causes cell lysis. But in monocots with sphingolipids that have three hexoses, the toxin is ineffective.

*Science*, this issue p. 1431; see also p. 1383

#### ARTICLE TOOLS

<http://science.sciencemag.org/content/358/6369/1431>

#### SUPPLEMENTARY MATERIALS

<http://science.sciencemag.org/content/suppl/2017/12/13/358.6369.1431.DC1>

#### RELATED CONTENT

<http://science.sciencemag.org/content/sci/358/6369/1383.full>

#### REFERENCES

This article cites 44 articles, 9 of which you can access for free  
<http://science.sciencemag.org/content/358/6369/1431#BIBL>

#### PERMISSIONS

<http://www.sciencemag.org/help/reprints-and-permissions>

Use of this article is subject to the [Terms of Service](#)



## Supplementary Material for

### **Eudicot plant-specific sphingolipids determine host selectivity of microbial NLP cytolysins**

Tea Lenarčič, Isabell Albert, Hannah Böhm, Vesna Hodnik, Katja Pirc, Apolonija B. Zavec, Marjetka Podobnik, David Pahovnik, Ema Žagar, Rory Pruitt, Peter Greimel, Akiko Yamaji-Hasegawa, Toshihide Kobayashi, Agnieszka Zienkiewicz, Jasmin Gömann, Jenny C. Mortimer, Lin Fang, Adiilah Mamode-Cassim, Magali Deleu, Laurence Lins, Claudia Oecking, Ivo Feussner, Sébastien Mongrand, Gregor Anderluh,\* Thorsten Nürnberger\*

\*Corresponding author. Email: [gregor.anderluh@ki.si](mailto:gregor.anderluh@ki.si) (G.A.); [nuernberger@uni-tuebingen.de](mailto:nuernberger@uni-tuebingen.de) (T.N.)

Published 15 December 2017, *Science* **358**, 1431 (2017)  
DOI: 10.1126/science.aan6874

#### **This PDF file includes:**

Materials and Methods  
Figs. S1 to S15  
Tables S1 and S2  
References

## Materials and Methods

### Leaf infiltration assays and plant materials

Adult plant leaves [leek (*Allium porrum*), *Arabidopsis thaliana*, cauliflower (*Brassica oleracea*), *Coix lacryma-jobi*, tobacco (*Nicotiana tabacum*), *Phalaenopsis amabilis*] were infiltrated abaxially with NLP proteins or NLP<sub>Pya</sub> mutant proteins (100 µl) or water as control using a needleless syringe. Necrotic symptoms occurred within 1-2 h, and images were taken after 48 h to enhance visibility of the phenotype. *Arabidopsis thaliana* wild-type (Col-0), *loh1*, *fah1fah2* and *gost1* mutants were grown in growth chamber under long-day conditions with a 16 h light (120-150 µmol/m<sup>2</sup>s) and 8 h dark cycle at 22 °C and 60 % humidity. *Commelina communis* and tobacco plants were grown as in (3). Cauliflower, *Coix lacryma-jobi*, *Phalaenopsis amabilis* plants were grown as in (17).

### Production of recombinant NLP protein

NLP<sub>Pp</sub> was expressed as described (3). NLP<sub>Pya</sub> WT and NLP<sub>Pya</sub> mutant protein expression was conducted with minor modifications of the original protocol (3). Prior to overexpression of the protein in *E. coli* BL21(DE3) cells, NLP<sub>Pya</sub> cDNA was subcloned into the pET21c vector. Transformed cells were grown to an OD<sub>600</sub> of 1.0 in TB media, and protein expression was induced with 0.5 mM IPTG for 20 h at 20 °C (21). Site-directed mutagenesis was carried out as described (22).

### Protein crystallization

After purification, concentrated NLP<sub>Pya</sub> protein (32 mg/ml) was subjected to a set of optimized crystallization trials (3, 23) by employing a hanging-drop vapor diffusion method using a 0.5:1 ratio of the protein to precipitant over 1 ml of well solution. Crystallization was carried out at 21 °C. To slow crystal growth and thus improve their quality 10 % glycerol was added to 22-24 % PEG 4000, 0.3 M MgCl<sub>2</sub>, 0.1 M Tris, pH 9, and 5 % methanol mixture. The crystals were soaked for 10 min in their crystallization solution containing 10 mM glucosamine and 5 mM mannosamine, respectively, and frozen in liquid N<sub>2</sub>.

### Structure determination

X-ray diffraction data were collected at the ELETTRA Synchrotron XRD-1 beamline (Trieste, Italy), and processed using XDS (24). Structures were determined by molecular replacement program Phaser-MR using a 3GNZ NLP<sub>Pya</sub> search model to calculate initial phases, followed by automated tracing using PHENIX (25). The atomic models were rebuilt by iterative cycles of manual model building in COOT (26) and refined using PHENIX (25). At the final stages of refinement, glucosamine and mannosamine were taken into consideration after generating eLBOW (27) ligand restraints. Models were validated using MolProbity (28) and figures were generated using Pymol (29).

### Circular dichroism spectroscopy and thermofluor assay of NLP<sub>Pya</sub> and NLP<sub>Pp</sub> proteins

Far ultraviolet circular dichroism spectra of NLP<sub>Pya</sub> and NLP<sub>Pp</sub> (0.08 mg/ml) were recorded on a Chirascan spectrometer (Applied Photophysics) in a 0.1 cm path length quartz cuvette. Spectra were measured in a 200-260 nm wavelength range with a step size of 0.5 nm and integration time of 0.5 s. Each spectrum was the average of 10 scans. Spectra were processed, baseline corrected, smoothed and converted with the Chirascan software. Spectral units were expressed as the mean molar ellipticity per residue.

The stability of proteins was measured by differential scanning fluorimetry using a thermofluor assay at a protein concentration of 0.1 mg/ml supplemented with 2x SYPRO Orange dye (Thermo Fisher Scientific) in 20 mM MES, 150 mM NaCl, pH 5.8. Samples were subjected to temperature

denaturation from 25 °C to 95 °C at a gradient of 1 °C/min. Temperature melting profiles were acquired with LightCycler 480 (Roche). Melting temperatures  $T_m$  were determined by using Boltzmann function in Origin 8.1 (Origin Lab). Shown are averages of 6 repeats, measured in 3 independent experiments.

### GIPC preparations

Tobacco GIPCs were extracted as described (20, 30) Briefly, tobacco leaves were blended with cold 0.1 N aqueous acetic acid and filtered through miracloth. The slurry was extracted with hot 70 % ethanol/0.1 N HCl, filtered and washed with acidic 70 % ethanol followed by two re-extractions with acidic 70 % ethanol. The mixture was centrifuged (2,000 g), the GIPC-containing pellet washed with cold acetone and diethyl ether to yield a whitish precipitate. This pellet was dissolved in tetrahydrofuran (THF):methanol:water (4:4:1, v:v:v) containing 0.1 % formic acid and sonicated at 60 °C. The GIPC extract was then dried and submitted to a butan-1-ol:water (1:1, v:v) phase partition. The upper, GIPC-containing butanol phase was dried and the residue was dissolved in THF:methanol:water (4:4:1, v:v:v) containing 0.1 % formic acid. *Arabidopsis*, cauliflower, *Commelina communis* or leek GIPCs were prepared as described (10, 31). Total leaf GIPC contents were estimated by GC-MS (10, 31) on the basis of the amount of very long chain fatty acids. GIPC concentrations (n = 3) such as those shown in Fig. 4D were (in mg GIPC per gram leaf fresh weight):  $0.58 \pm 0.07$  (*Allium porrum*),  $0.47 \pm 0.34$  (*Arabidopsis thaliana*),  $0.65 \pm 0.03$  (*Coix lacryma-jobi*),  $0.69 \pm 0.17$  (*Nicotiana tabacum*),  $0.39 \pm 0.09$  (*Phalaenopsis amabilis*).

### Thin-layer chromatography (TLC) blotting

TLC was performed using HPTLC (high performance thin-layer chromatography) plates (Merck). Standard lipids monosialotetrahexosylganglioside 1 (GM1), glucosyl ceramide (Glc-Cer), bovine brain sphingomyelin (SM) and 1-palmitoyl-2-oleoyl-*sn*-glycero-3-phosphocholine (POPC) were from Avanti Polar Lipids (Alabaster, AL, USA). Approximately 8 µg of standard lipids (GM1 dissolved in chloroform:methanol (2:1, v:v) and Glc-Cer, SM and POPC dissolved in chloroform) and 180 µg of GIPCs dissolved in THF:methanol/water (4:4:1, v:v:v) containing 0.1 % formic acid were applied in thin lines to HPTLC plates. Lipids were separated using a chloroform:methanol:2 M ammonia (65:25:4, v:v:v) mixture and visualized under UV light after primuline staining.

For TLC blotting, plates were completely dried using a desiccator for 1 h, and lipids were heated and transferred to activated polyvinylidene difluoride (PVDF) membrane (32). After overnight incubation at 4 °C in PBS (137 mM NaCl, 2.7 mM KCl, 10 mM Na<sub>2</sub>HPO<sub>4</sub>, 1.8 mM KH<sub>2</sub>PO<sub>4</sub>, pH 7.4) containing 5 % bovine serum albumin (BSA), the PVDF membrane was transferred into PBS containing 5 % BSA and 10 µg/ml of NLP<sub>pya</sub> and incubated for 2 h at room temperature (RT). Unbound protein was washed off 3 times for 10 min in TBS (20 mM Tris, 150 mM NaCl, pH 7.4). The PVDF membrane was incubated in PBS, containing 5 % BSA, for 1 h at RT with the primary anti-4His antibody and, subsequently, with the secondary antibody tagged with horseradish peroxidase. Before addition of the secondary antibody filters were washed thrice with TBS. Bound protein was detected using a Pierce ECL Western Blotting Substrate (Thermo Scientific, USA).

### Mass spectrometric analysis

The NLP-reactive spot was extracted from silica gel adopting the single phase sphingolipid extraction protocol as described (33). In brief, the sample was extracted twice with a mixture of ethyl acetate (1.2 ml), isopropanol (0.6 ml) and water (0.2 ml), subjected to three cycles of 30 s sonic bath (AS One US-4R), each followed vigorous shaking (10 s). Solid material was pelleted by 15 min centrifugation (Hitachi himac CF-16RN) at 3,100 rpm at RT. Supernatants were

collected in a fresh glass vial and dried under a flow of N<sub>2</sub> gas. The resulting lipid film was dissolved in methanol, transferred to a screw vial with fixed insert, dried under a flow of N<sub>2</sub> gas and stored under vacuum until analysis. Prior to analysis, the lipid film was resuspended in running buffer (isopropanol:water:ammonium acetate, 2:1:4 mM) and the solution was kept at 4 °C until analysis. Electron spray ionization tandem mass (ESI-MS/MS) analysis was carried out on an Agilent 1100 Series HPLC system with an integrated AB SCIEX 4000 QTrap mass spectrometer. The mobile phase (isopropanol:water:ammonium acetate, 2:1:4 mM) was maintained at a flow rate of 20 µl/min. The mass spectrometer was operated in negative ion mode utilizing the same parameter set as described (31). Samples were analyzed utilizing either Q3 or product ion mode.

Nanoelectrospray ionization triple quadrupole tandem mass spectrometry (UPLC-nanoESI-MS/MS) of targeted molecular lipid species analysis was performed as described (34) and adapted to a 6500 QTRAP<sup>®</sup> tandem mass spectrometer (AB Sciex, <http://sciex.com/>). Lipid extraction was achieved by immersing 100 mg of the frozen leaf material in a pre-heated (60 °C) solvent mixture containing isopropanol:hexane:water (60:26:14, v:v:v) and performing a one-phase extraction as described (35).

### **Surface plasmon resonance**

Binding of NLPs to GIPC hybrid monolayers was monitored on Biacore X100 (GE Healthcare) by using sensor chip HPA and 20 mM MES, pH 5.8, 140 mM NaCl as running buffer. For analyzing NLP binding to GIPCs, small unilamellar vesicles produced by sonication in running buffer (30 min on ice, 20 s pulse on, 20 s pulse off, amplitude 25 %) were captured on the second flow cell (500 - 1000 response units) and both flow cells were washed with 100 mM NaOH and blocked with 0.1 mg/ml BSA. Serial dilutions of NLPs were applied and steady-state affinity calculation using Biacore X100 Evaluation Software was used to determine K<sub>D</sub> values.

Binding of *Arabidopsis* GIPCs to NLP<sub>Pya</sub> was monitored using Biacore T100 (GE Healthcare), Series S sensor chip CM5 and 20 mM MES, pH 5.8, 140 mM NaCl. NLP<sub>Pp</sub> was captured on flow cell 2 (5000 RU) and binding of GIPCs (0.005 mg/ml), POPC (0.25 mg/ml) or bovine brain SM (0.09 mg/ml) was determined.

Binding of sugars to NLP<sub>Pya</sub> was monitored using Biacore T100, SPR running buffer (20 mM MES, pH 5.8, 140 mM NaCl) and Series S sensor chip CM7. Following surface activation according to manufacturer's recommendations, NLP<sub>Pya</sub> diluted in 10 mM sodium acetate, pH 4.5, was injected three times for 180 s over the second flow cell. Both flow cells were blocked with 1 M ethanolamine (final immobilization level 10500 RU). Glucosamine and mannosamine were titrated in concentrations of 78.1 µM-5 mM.

### **Liposome sedimentation assay**

Multilamellar vesicles (MLVs) composed of POPC or POPC:GIPCs 1:1 (m:m) were prepared by hydrating lipid film with 20 mM MES, 150 mM NaCl, pH 5.8, and vortexing. MLVs (4.5 mg/ml) were incubated with NLP<sub>Pya</sub> (0.06 mg/ml) in 20 mM MES, 150 mM NaCl, pH 5.8, for 30 min and 600 rpm at RT. The mixture was centrifuged at 16,100 g for 20 min at RT. The liposomes were washed twice with the same buffer, centrifuged at 16,100 g for 20 min and subjected to SDS-PAGE followed by Coomassie Brilliant Blue staining.

### **Protoplast isolation, Cyanine3-labeling of NLP<sub>Pp</sub> and di-4-ANEPPDHQ staining**

Cells from 3-day-old *Arabidopsis thaliana* dark-grown cell culture were collected by centrifugation at 400 g for 5 min and the pellet was washed with buffer A (8 mM CaCl<sub>2</sub>, 0.4 M mannitol, pH 5.5). Subsequently, cells were incubated with buffer A including 1 % w/v cellulose, 0.25 % Macerozyme in the dark (RT, 50 rpm, 6 h). After sedimentation (5 min, 100 g, RT) and

washing with buffer A without enzymes and W5 solution (154 mM NaCl, 125 mM CaCl<sub>2</sub>, 5 mM KCl, 5 mM glucose), protoplasts were resuspended in W5 solution and incubated in the dark (20 min, 4 °C). Protoplasts were pelleted as before and resuspended in K3 solution (36) and kept in the dark at RT.

For Cyanine3-labeling, NLP<sub>pp</sub> (~10 mg/ml) was incubated with Cyanine3 mono-reactive NHS ester (ThermoFisher Scientific) according to the manufacturer instructions. Excess dye was removed by gel filtration (GE Healthcare HiLoad™ 16/60 Superdex 75, 20 mM Tris, pH 8.0, 150 mM KCl). Labeled protein was added to the protoplast solution (50 nM end concentration) and analyzed via fluorescence microscopy after 30 s for 10 min.

For di-4-ANEPPDHQ staining *Arabidopsis* mesophyll protoplasts were isolated according to (37) with some minor modifications. Mature leaves (numbers five to seven) from 4-week old plants (three plants per one experiment) were cut with razor blade and digested in 10 ml of enzyme solution (1.25 % cellulase R10, 0.3 % macerozyme R10, 0.4 M mannitol, 20 mM MES, pH 5.7, 20 mM KCl, 20 mM CaCl<sub>2</sub>) for 6 h at RT. Next steps, including protoplasts filtration and washing with W5 solution were carried out as described (37). For plasma membrane labeling fresh protoplasts were incubated with 10 μM di-4-ANEPPDHQ in DMSO (Molecular Probes) for 10 min at RT, washed briefly in W5 solution and analyzed under Zeiss LSM 510 Meta confocal laser scanning microscope (CLSM) (Carl Zeiss).

### **Confocal Laser Scanning Microscopic observation and generalized polarization (GP) calculation**

To analyze differences in membrane lipid order between *Arabidopsis* wild-type (Col-0) and *fah1fah2* mutants, di-4-ANEPPDHQ labeled *Arabidopsis* mesophyll protoplasts were used to estimate GP values according to (15, 38, 39). Protoplasts were excited at 488 nm and emitted fluorescence was detected in two channels: 500-580 nm (green) and 620-750 nm (red). A x63 oil immersion objective was used. CLSM settings were applied from the protocol described (38) including laser power or offset values. GP and HSB (Hue-Saturation-Brightness) images and GP values were generated by using ImageJ software (<http://rsbweb.nih.gov/ij>) with ImageJ macro (38). GP values were obtained by using the following equation:

$$GP = (I_{500-580} - GI_{620-750}) / (I_{500-580} + GI_{620-750}) \quad (1)$$

$I_{500-580}$ ,  $I_{620-750}$ : Fluorescence intensity detected by CLSM in channel 500-580 nm and 620-750 nm, G: calibration factor calculated by using equation 2 and 3.

In order to normalize GP values obtained from the two CLSM channels G factor was calculated according to (39) by using following equations:

$$GP_{mes} = (I_{500-580} - I_{620-750}) / (I_{500-580} + I_{620-750}) \quad (2)$$

$$GP = (GP_{ref} + GP_{ref} GP_{mes} - GP_{mes} \cdot 1) / (GP_{mes} + GP_{ref} GP_{mes} - GP_{ref} \cdot 1) \quad (3)$$

$GP_{mes}$ : mean pixel intensities of the undiluted di-4-ANEPPDHQ in DMSO measured in two CLSM channels,  $GP_{ref}$ : reference value of the di-4-ANEPPDHQ in DMSO of -0.85 (38). Histograms of GP values (n=3) and Gaussian fitted curves were created by using Origin 2016 (b9.3.2.303) software.

### **Calcein release assay and enzymatic treatment of plasma membrane vesicles**

Calcein-filled plasma membrane vesicles were prepared from 6 week-old *Arabidopsis thaliana* as described (3). Permeabilization of the vesicles (1 ng protein/μL) induced by 100 nM NLP (0.2 ng/μl) was assayed at RT in 20 mM MES, pH 5.8, 140 mM NaCl by measuring fluorescence (excitation 485 nm, emission 520 nm) in a microplate reader (Sirius HT Injector, MWG). The percentage of calcein release ( $R$ ) was calculated according to the equation

$$R = (F_{\text{meas}} - F_{\text{init}}) / (F_{\text{max}} - F_{\text{init}}) * 100 \quad (4),$$

where  $F_{\text{meas}}$ ,  $F_{\text{init}}$ , and  $F_{\text{max}}$  are the measured, initial, and maximal fluorescence, respectively.  $F_{\text{max}}$  was obtained by the addition of Triton X-100 to 0.5% (v:v) final concentration at the end of each measurement. To test interference of GIPCs with NLP cytolysin activity, 100 nM NLP<sub>pya</sub> was incubated with a 10 to 1000x molar excess of cauliflower or leek GIPCs for 15 min prior to the addition of vesicles. For digestion with proteases, plasma membrane vesicles (125 µg protein) were incubated with 1 µg Trypsin, 40 µg PronaseE or 5 µg Chymotrypsin (+ 10 mM CaCl<sub>2</sub>) for 2.5 h at RT and subsequently applied to gel filtration as described above to remove external calcein and proteases. Calcein release was analyzed by treatment with 20 nM NLP<sub>pp</sub>. Plasma membrane vesicles were pre-incubated with 125 µg/ml of the respective enzyme (Sigma-Aldrich: α-glucosidase G5003, β-glucosidase 49290, α-mannosidase M7257) for 1 h at RT prior to treatment with 10 nM NLP<sub>pya</sub>. Enzyme activities were tested prior to use with synthetic *p*-nitrophenyl-α-D-glucopyranoside, *p*-nitrophenyl-β-D-glucopyranoside or *p*-nitrophenyl-α-D-mannopyranoside substrate (Sigma-Aldrich) for activity according to the supplier's instruction.

### Ion leakage

Leaves of 4 to 6-week-old *Arabidopsis* Col-0, *loh1* or *fah1fah2* plants were infiltrated with 500 nM NLP<sub>pya</sub>. 4-week-old *Arabidopsis*, tobacco and cauliflower plants were used for infiltration with serial dilutions of NLP<sub>pya</sub> and its mutants for determination of EC<sub>50</sub> values or with NLP<sub>pp</sub>. For ion leakage experiments in the presence of *Galanthus nivalis* or soybean (*Glycine max*) lectin (Medicago, lot no. 05-0120-5 and 05-0117-10), 500 nM NLP<sub>pya</sub> was co-infiltrated with 10 µM of the respective lectin. After 10 min of incubation, leaf discs were punched out (Ø 7 mm) and transferred into a 24-well plate. Two leaf pieces per well were floated on 1 ml ddH<sub>2</sub>O and shaken at 50 rpm. After 30 min, leaf pieces were transferred to fresh ddH<sub>2</sub>O and conductivity was measured at the times indicated using conductometer QCond2200. EC<sub>50</sub> values correspond to protein concentrations required to trigger half-maximum ion leakage after 6 h (*Arabidopsis*, cauliflower) or 4 h (tobacco), respectively. Six replicates from three independent experiments were used to calculate EC<sub>50</sub> values.

### Trypan blue staining

Leaves of 5-week-old *Arabidopsis* Col-0, *loh1* and *fah1fah2* plants were infiltrated with 500 nM NLP<sub>pp</sub> and harvested after 4 h. Leaves were incubated for 1 min at 100 °C in trypan blue solution [1x lactophenol (equal amounts of lactic acid, glycerol, phenol and H<sub>2</sub>O), 2x EtOH, 2.5 mg/ml trypan blue] and de-stained in chloral hydrate solution (1 mg/ml) overnight.

### Langmuir Trough

To facilitate quantification of molecular areas occupied by series A- and B-type GIPCs, we studied the organization of GIPC polar heads in model membranes by Langmuir monolayer tensiometry. Cauliflower (series A) and leek GIPCs (series B) (32) were used in this study. GIPC solutions at 0.39 mM and at 0.31 mM in chloroform:methanol:water (30:60:8) were prepared for series A and series B GIPCs, respectively. The surface pressure-area (Π-A) isotherms were recorded by means of an automated Langmuir trough (KSV Minitrough [width, 75 mm; area, 24.225 mm<sup>2</sup>]; KSV Instruments) equipped with a platinum plate attached to a Wilhelmy-type balance. The GIPC sample was heated to 60 °C for 15 min for better solubilization. Pure solutions were spread (fixed volume of 30 µl) as tiny droplets to produce a uniform monolayer on a Tris-HCl (10 mM), pH 7, sub-phase. After evaporation of the solvent (15 min), monolayers were compressed at a rate of 5 mm/min and at a temperature of 22 °C ± 1 °C. Before each experiment, the cleanliness of the system was confirmed by checking the surface pressure over the surface compression of the pure subphase. The reproducibility of the Π-A isotherms was checked by repeated recordings, and the relative SD in surface pressure and area was found to be

3 % or less.

### **Molecular Modeling Approaches**

The conformation of major cauliflower series A GIPC: glucose ( $\alpha$ 1-4) glucuronic acid ( $\alpha$ 1-2) inositol phosphate-ceramide [t18:0/h24:0], and major leek series B GIPC: mannose ( $\alpha$ 1-4) *N*-acetylglucosamine ( $\alpha$ 1-4) glucuronic acid ( $\alpha$ 1-2) inositol phosphate-ceramide [t18:0/h24:0] was calculated using the structure tree procedure as described (40). The Hypermatrix docking procedure was used to study the monolayer formed by GIPC and to calculate the mean surface area as described (8, 41, 42). The insertion of GIPC A and B into an implicit bilayer was carried out using the IMPALA procedure as described (8, 43).

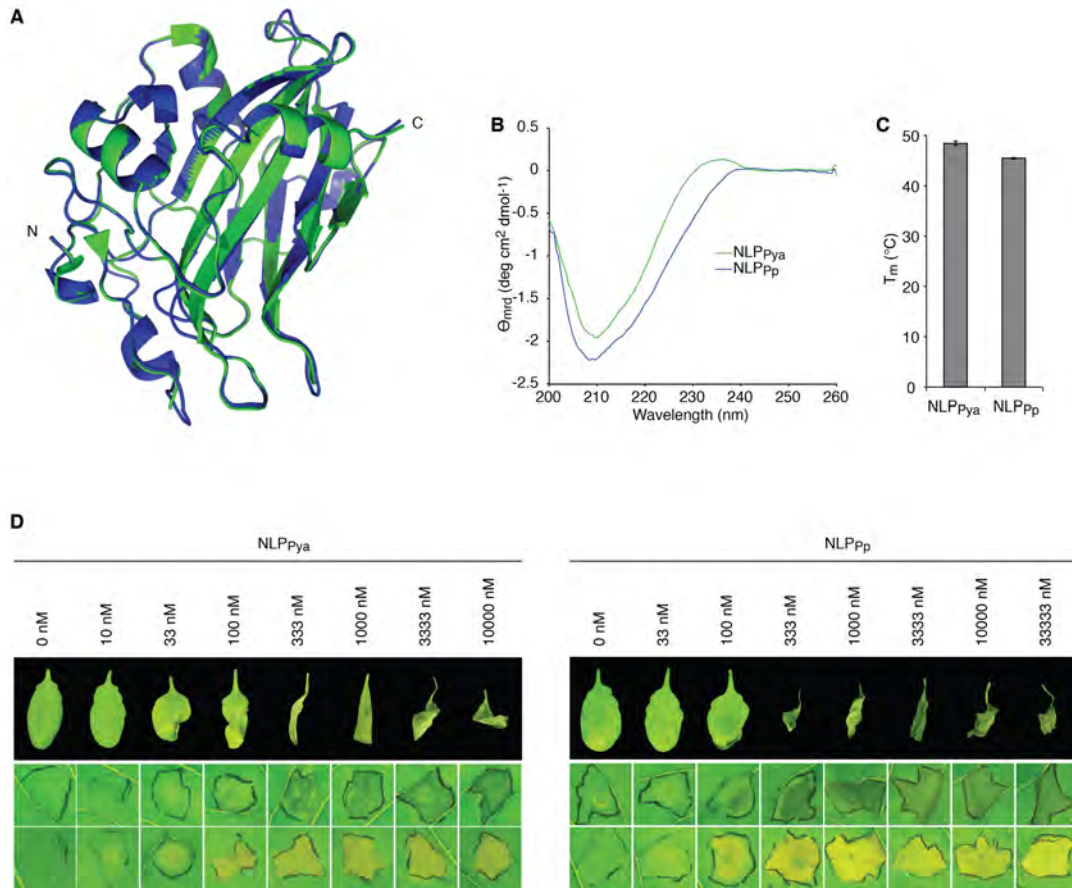


**Fig. S1 Comparative analysis of NLP<sub>Pya</sub> and NLP<sub>Pp</sub> proteins.**

(A) The NLP<sub>Pya</sub> fold (green) was used as template to model the 3-dimensional structure of NLP<sub>Pp</sub> (blue) (3) using Modeler (44). (B, C) Circular dichroism (B) and differential scanning fluorimetry (C) reveal comparable secondary structure properties and stability of both proteins. (D) Analysis of NLP<sub>Pya</sub> (left panel) and NLP<sub>Pp</sub> (right panel) necrotic activities in leaves of *Arabidopsis* (top row), cauliflower (middle row) and tobacco (bottom row). Experiments were repeated three times with similar results.

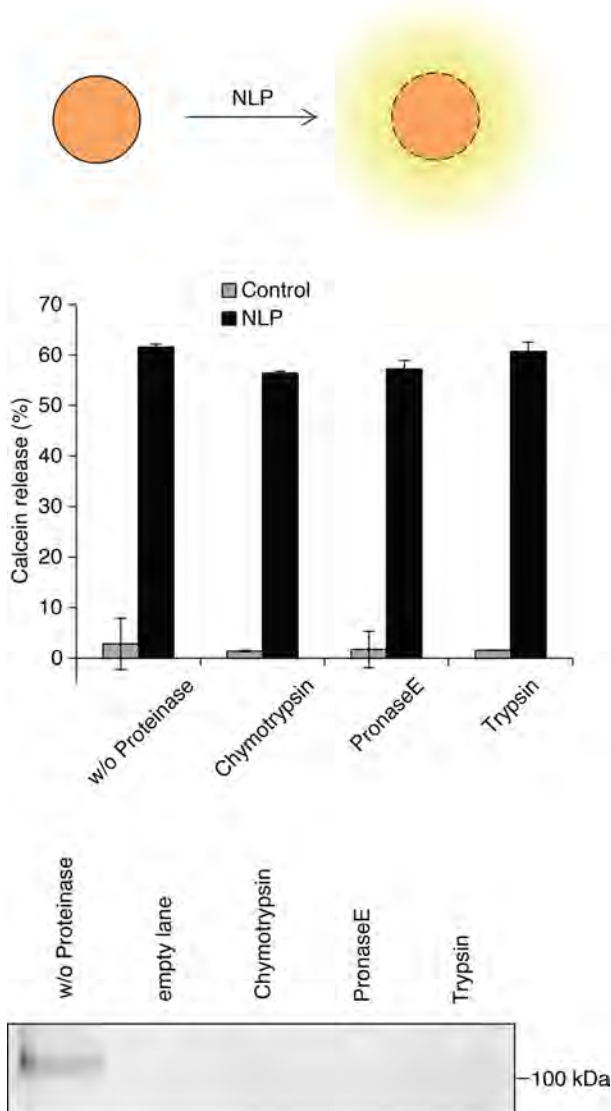


**Fig. S2 Analysis of NLP cytolitic activity using a vesicle-based assay.**

Intact fluorophor calcein-loaded *Arabidopsis* plasma membrane vesicles do not show fluorescence emission due to quenching. Disintegration of membranes due to cytolitic NLP results in calcein release and fluorescent light emission (top panel). Vesicles pretreated with proteases Pronase E, Chymotrypsin or Trypsin were supplemented with 20 nM NLP<sub>pp</sub> for 10 min. Water and NLP<sub>pp</sub> treatments served as controls. Values represent means  $\pm$  SD. Similar results were obtained in two independent experiments (middle panel). Immunoblot analysis of *Arabidopsis* plasma membrane vesicle protein before (w/o proteinase) or after protease treatment indicated proteolytic degradation of intrinsic plasma membrane protein (bottom panel). Immunoblotting was performed as described (45) using an antiserum recognizing plasma membrane H<sup>+</sup>-ATPase.

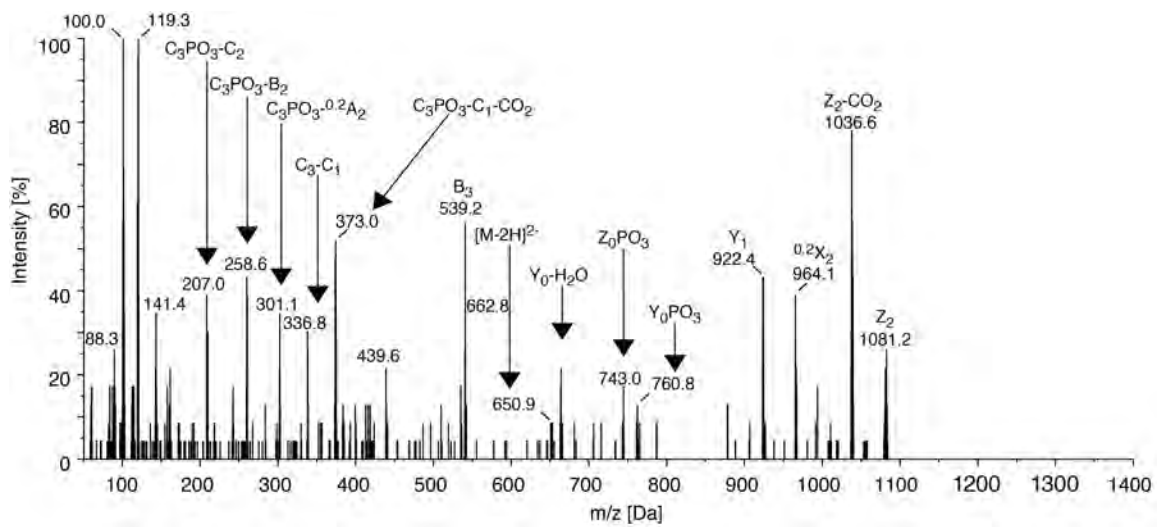


**Fig. S3** ESI-MS/MS fragmentation pattern of HexNAcGlcA-IPC isolated from the NLP reactive TLC spot (Fig. 1B).

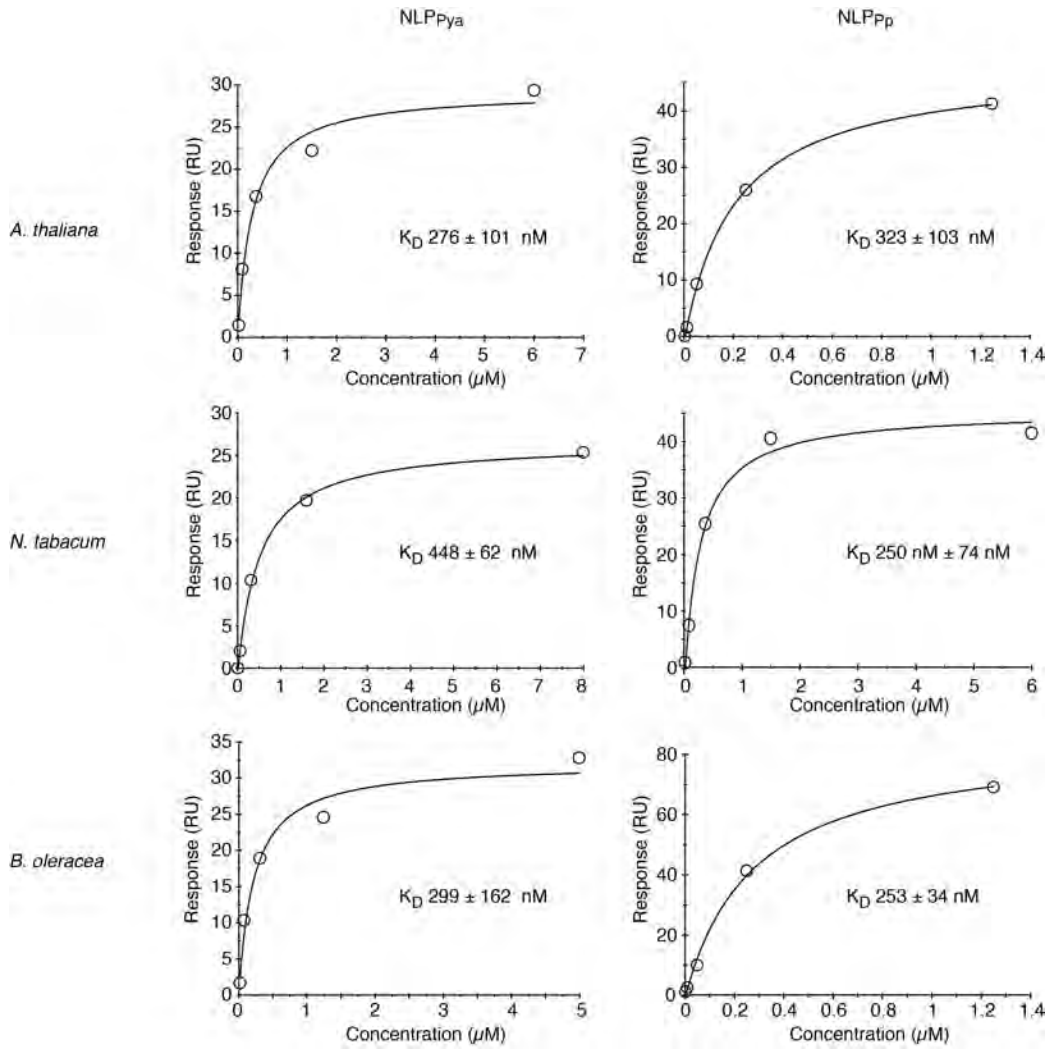


**Fig. S4 Surface plasmon resonance (SPR) analysis of NLP proteins.**

SPR analysis of chip-immobilized *Arabidopsis*, tobacco or cauliflower GIPCs and NLP<sub>pya</sub> (left column) or NLP<sub>pp</sub> (right column). Mean values of dissociation constants (K<sub>D</sub>) are given ± SD (n = 3).

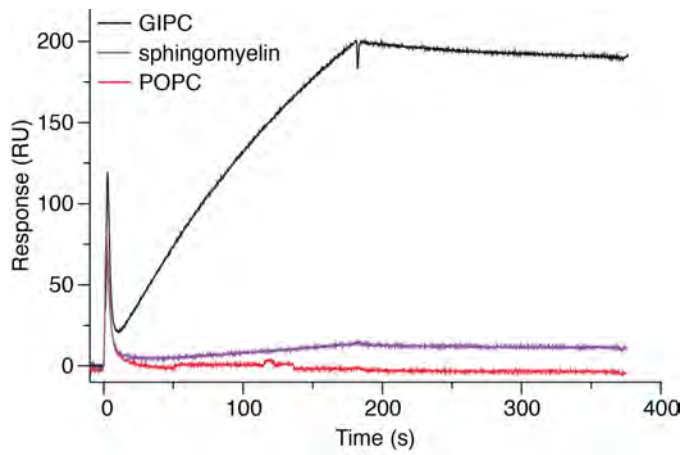


**Fig. S5 Binding of NLP<sub>PyA</sub> to plant GIPCs.**

Surface plasmon resonance analysis of binding of *Arabidopsis* GIPCs prepared as in (15), bovine brain SM or POPC to immobilized NLP<sub>PyA</sub>.

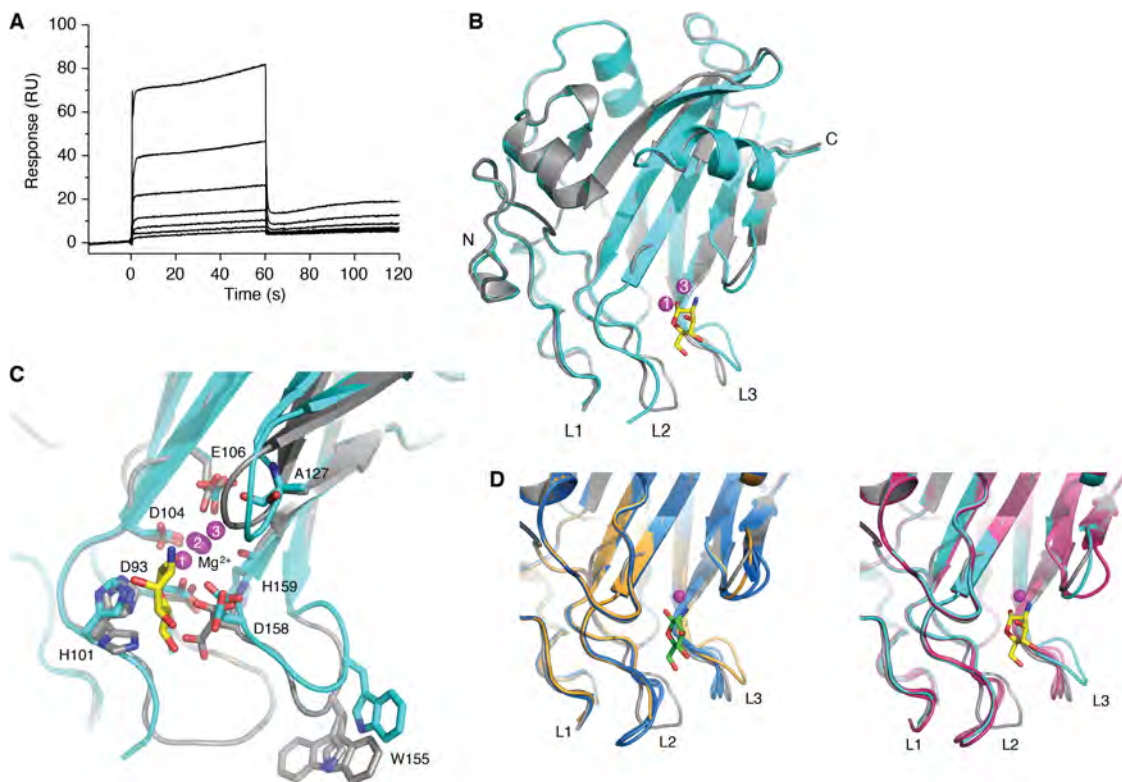


**Fig. S6 Interaction, structural and functional analysis of a ManN binding site in NLP<sub>Pya</sub>.**

(A) SPR analysis of ManN binding to NLP<sub>Pya</sub>. ManN was injected across chip-immobilized NLP<sub>Pya</sub> at concentrations of 5 mM-78.1  $\mu$ M (from top to bottom in two-fold dilutions). (B) Structural comparison of apo-NLP<sub>Pya</sub> (gray) (PDB-ID 3GNZ) and NLP<sub>Pya</sub> in complex with ManN (cyan). ManN is displayed in sticks (carbon: yellow; oxygen: red; nitrogen: blue). Numbers in spheres are as in (C). (C) Close-up view of ManN binding site. Amino acid residues involved in coordination of Mg<sup>2+</sup> and binding of ManN are highlighted and shown in sticks. ManN is displayed in yellow sticks. Residue W155, placed at the bottom of the loop L3, is shown in sticks as well. Mg<sup>2+</sup> ions are shown in magenta spheres: state 1 – a position in apo-NLP<sub>Pya</sub>; state 2 – positions of Mg<sup>2+</sup> ions in other three polypeptide chains from the asymmetric unit that did not bind hexose; state 3 – a position of Mg<sup>2+</sup> ion in complex with ManN. (D) Left panel: superposition of apo-NLP<sub>Pya</sub> (gray) (PDB-ID 3GNZ), NLP<sub>Pya</sub> polypeptide chains without bound hexose in the asymmetric unit (blue), and NLP<sub>Pya</sub> in complex with GlcN (orange). Mg<sup>2+</sup> is displayed in magenta sphere, GlcN is shown in green sticks. Right panel: Superposition of apo-NLP<sub>Pya</sub> (gray), NLP<sub>Pya</sub> polypeptide chains without bound hexose in the asymmetric unit (pink), and NLP<sub>Pya</sub> in complex with ManN (cyan). Mg<sup>2+</sup> is displayed in magenta sphere, ManN is shown in yellow sticks.

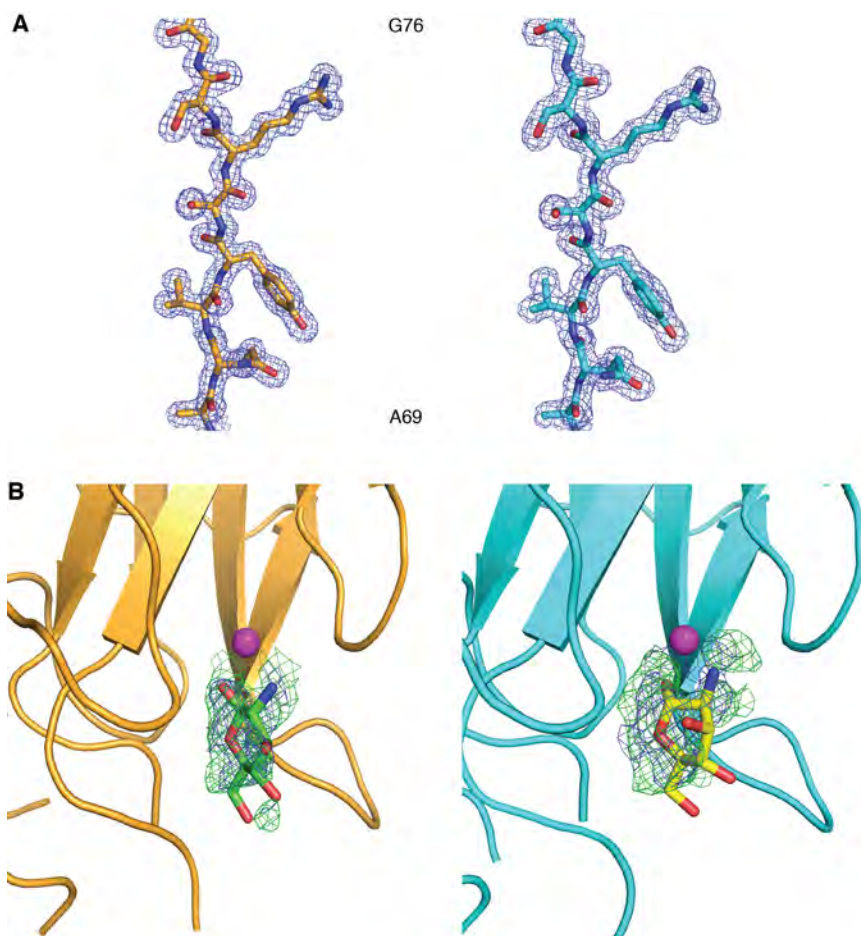


**Fig. S7 Representative sections of electron-density maps.**

(A) Polypeptide chains of NLP<sub>pya</sub> and sections of 2Fo-Fc electron-density map contoured at 1 $\sigma$  (blue) are shown: NLP<sub>pya</sub> in complex with GlcN (left panel); NLP<sub>pya</sub> in complex with ManN (right panel). In both cases, chains are depicted between residues A69 and G76. (B) 2 $\sigma$  Fo-Fc (before hexose placement) and 0.8 $\sigma$  2Fo-Fc (final refinement - hexose included) electron-density maps of GlcN (left panel) and ManN (right panel) are displayed in green and blue mesh, respectively. Sugars are shown as sticks, NLP<sub>pya</sub> polypeptide chains as ribbons. Mg<sup>2+</sup> ions are shown as magenta spheres. The incomplete electron density of the hexose ligand is reflected in substantially high B-factors compared to the protein (Table S1).

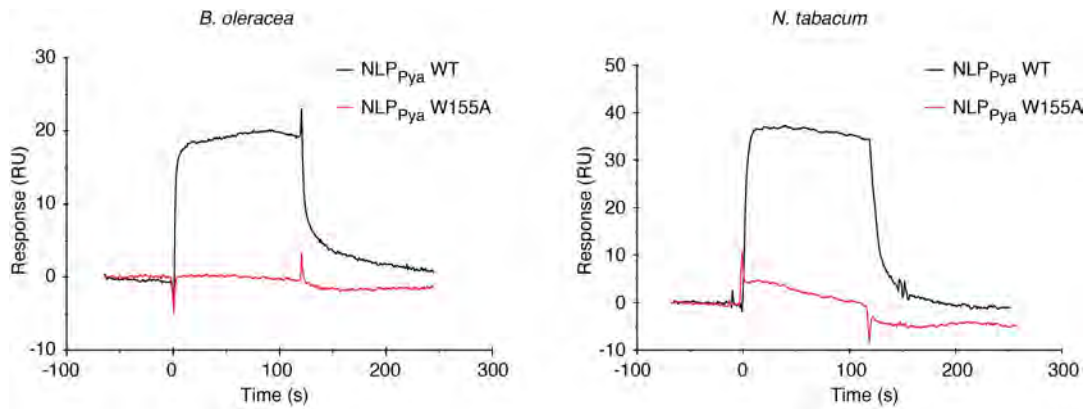


**Fig. S8 Surface plasmon resonance (SPR) analysis of NLP<sub>Pya</sub> W155A mutant protein.** SPR analysis of NLP<sub>Pya</sub> and mutant NLP<sub>Pya</sub> W155A with GIPCs from cauliflower (left graph) or tobacco (right graph). NLP concentrations used were 1.6  $\mu$ M.

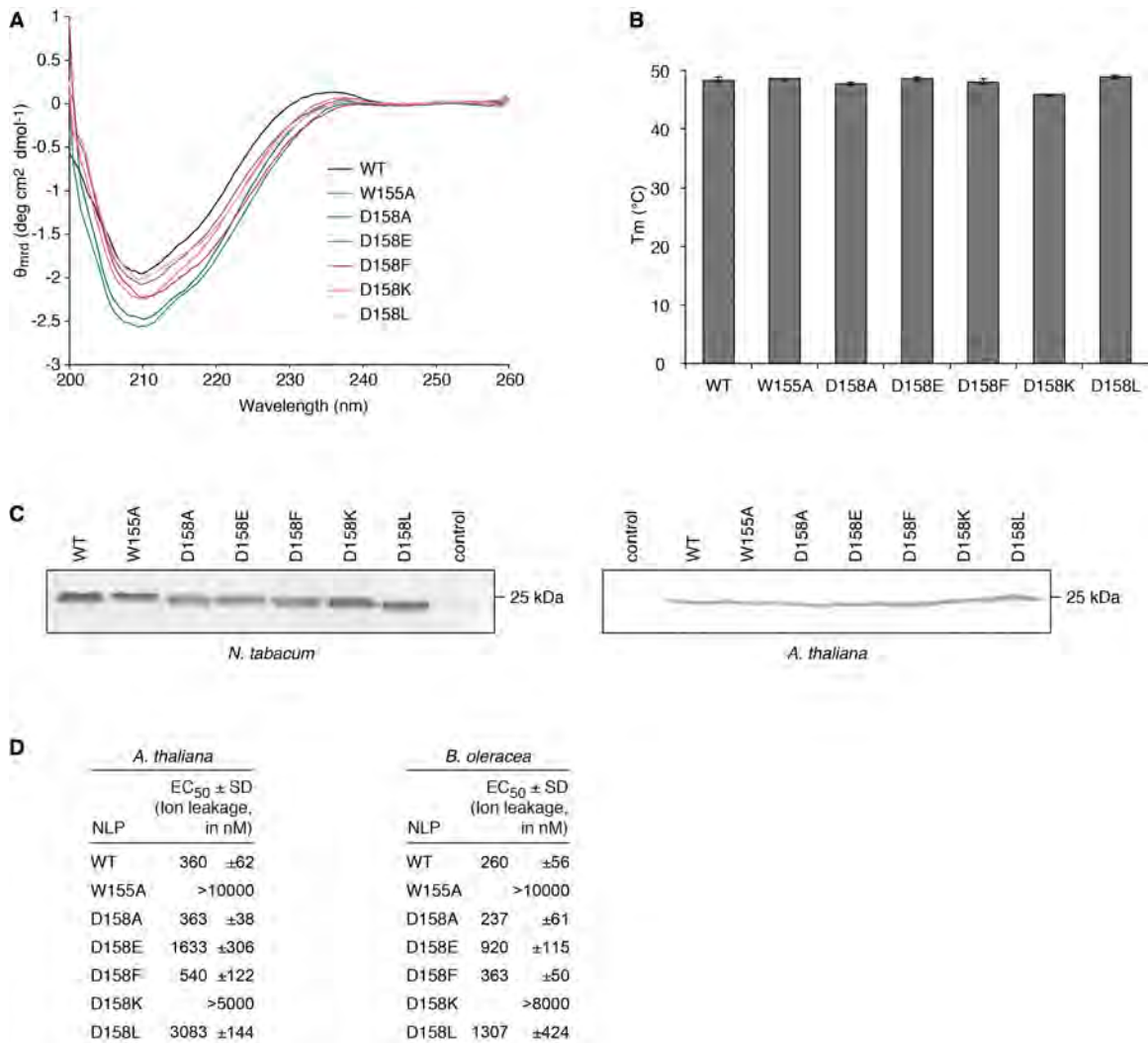


**Fig. S9 NLP<sub>Pya</sub> mutant protein analysis.**

(A) Circular dichroism analysis of NLP<sub>Pya</sub> mutant proteins. (B-C) NLP<sub>Pya</sub> protein stability as determined by differential scanning fluorimetry (B) or immunoblot analysis (C) in tobacco (left panel) or *Arabidopsis* (right panel) leaves. Leaves were harvested at onset of visible necrosis (1 h post inoculation of 1 μM protein as indicated). NLP<sub>Pya</sub>-specific antibodies (3) were used to detect proteins. (D) NLP<sub>Pya</sub>-mediated *Arabidopsis* (left column) and cauliflower (right column) leaf necrosis quantified by ion leakage measurements, water (control). Six replicates from three independent experiments were used to calculate EC<sub>50</sub> values.

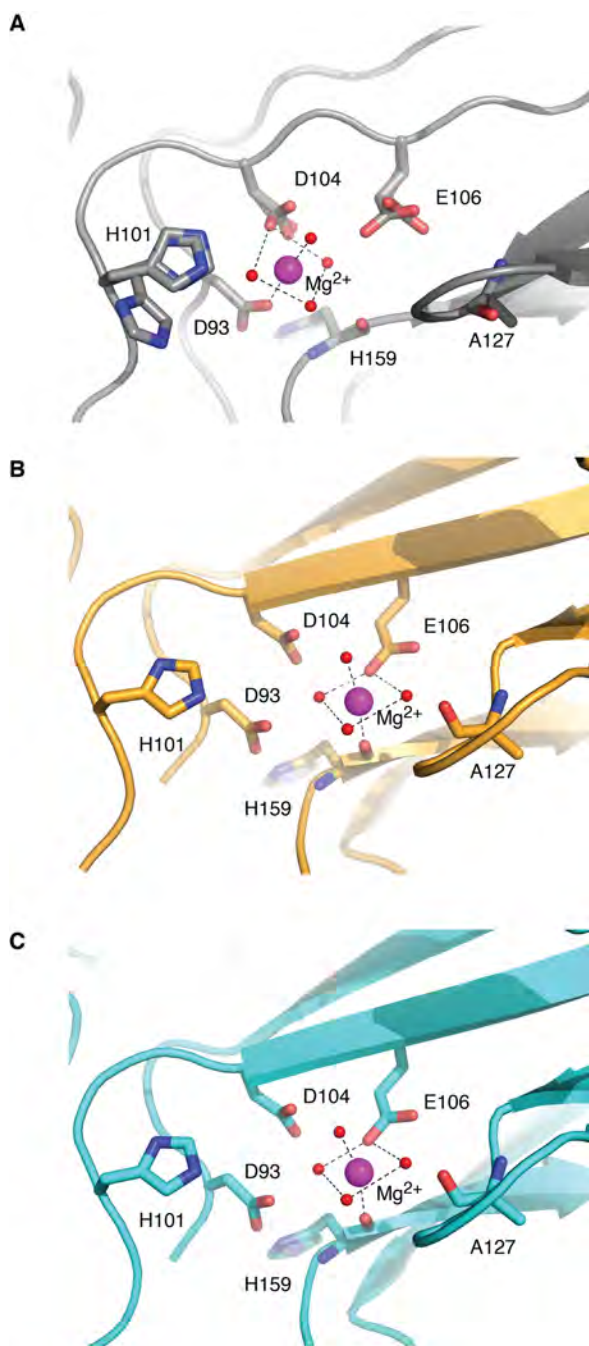


**Fig. S10  $Mg^{2+}$  coordination sites.**

(A)  $Mg^{2+}$  coordination sites in apo-NLP<sub>Pya</sub> (gray), PDB-ID 3GNZ. (B)  $Mg^{2+}$  coordination site in NLP<sub>Pya</sub> in complex with GlcN (orange). (C)  $Mg^{2+}$  coordination site in NLP<sub>Pya</sub> in complex with ManN (cyan). For better understanding of the coordination shift, sugars are not shown in panels (B) and (C). Coordinating waters are presented as red spheres, sticks indicate amino acid residues involved in coordination.  $Mg^{2+}$  ions are colored magenta. Black dashed lines represent octahedral coordination.

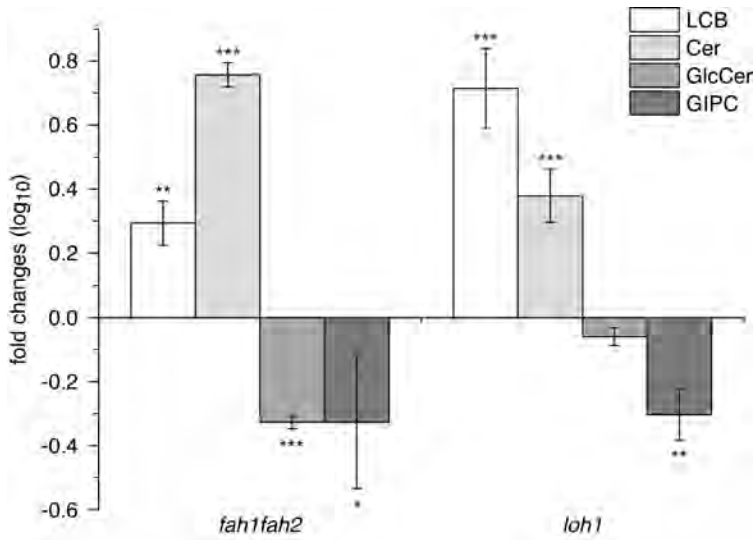


**Fig. S11 *Arabidopsis loh1* and *fah1fah2* mutants display reduced GIPC levels.**

Lipids were analyzed using UPLC-nanoESI-MS/MS. Fold changes of the sum of all detected molecular species are given in logarithmic scaling relative to the amounts detected in wild-type plants. LCB, long-chain bases, Cer, ceramides, GlcCer, glucosyl ceramides, GIPC, glycosylinositol phosphorylceramides. Each data point represents the mean value  $\pm$ SD of six biological replicates from two independent experiments. Data sets marked with asterisks indicate significant differences to the wild-type confirmed by Student's t-test assuming equal variances (\*,  $p < 0.05$ ; \*\*,  $p < 0.01$ ; \*\*\*,  $p < 0.001$ ).

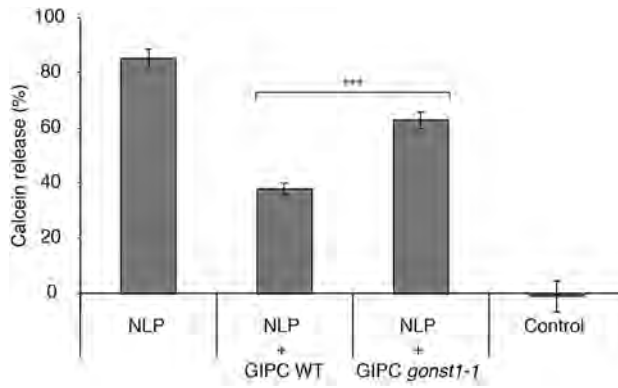


**Fig. S12 *Arabidopsis gonst1* mutants display reduced ability to protect plasma membrane vesicles from NLP cytotoxicity.**

GIPCs prepared from *Arabidopsis* wild-type (Col-0) and *gonst1* mutants inhibit NLP<sub>pp</sub>-induced (100 nM) calcein release from purified *Arabidopsis* plasma membrane vesicles. GIPCs:NLP<sub>pp</sub> molar ratios are given. Values represent means  $\pm$  SD of three replicates. Student-t-test analysis (\*\*\*,  $p < 0.001$ ). Water was used as control. Three experiments with similar results were conducted.

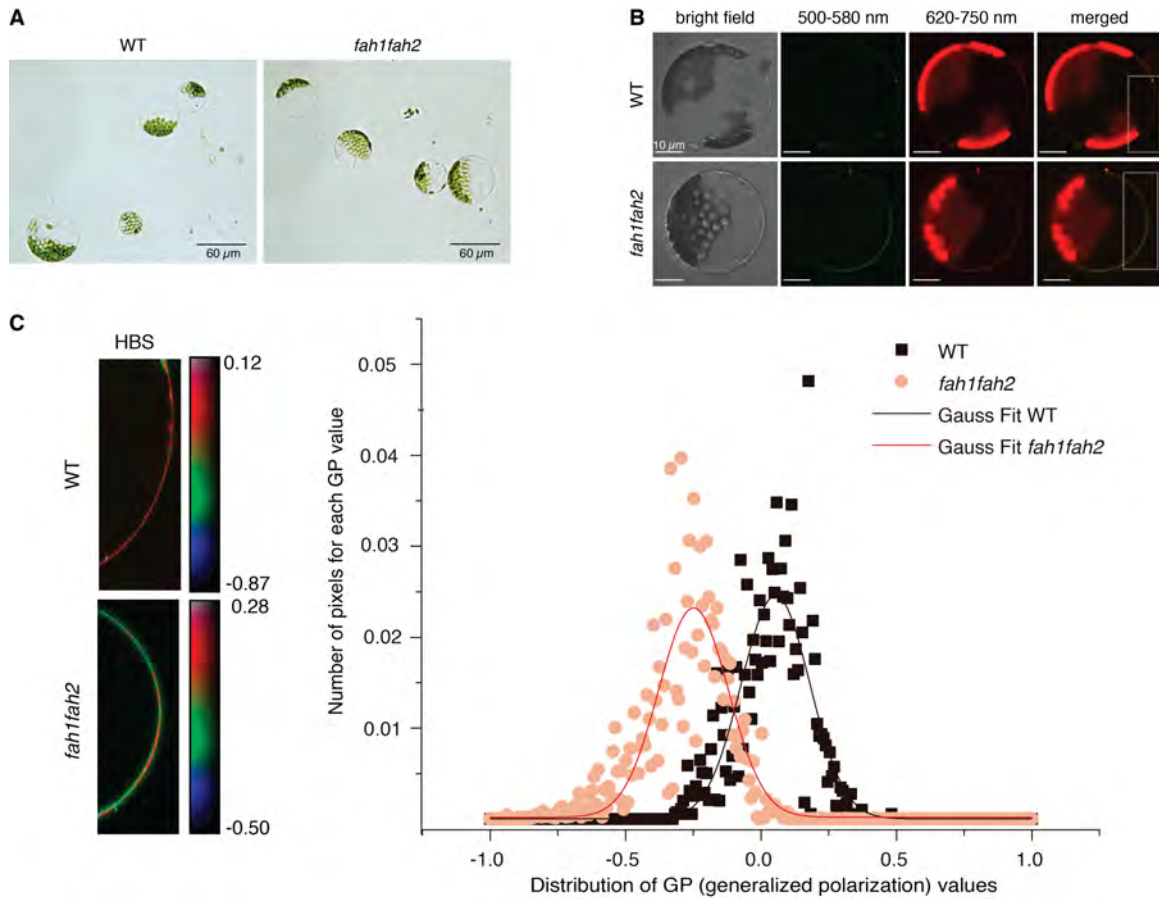


**Fig. S13 *Arabidopsis fah1fah2* mutants display lower levels of ordered plasma membranes in comparison to those observed in wild-type plants.**

(A) Mesophyll protoplasts isolated from mature leaves of *Arabidopsis* wild-type (Col-0) and *fah1fah2* mutant. (B) Representative CLSM images of Col-0 and *fah1fah2* mesophyll protoplasts labeled with di-4-ANEPPDHQ. To avoid saturated pixels in the area occupied by chloroplasts, acquisition of images was carried out at low photomultiplier tube gain according to (38). Thus, the remaining areas of the cell exhibited low levels of fluorescence and proportional increase of brightness and saturation was necessary to visualize properly the labeling in all images. (C) Quantitative comparison of plasma membrane order between the wild-type (Col-0) and *fah1fah2* double mutant. Pseudocolored HSB (Hue-Saturation-Brightness) images of ROI (region of interest) showing generalized polarization (GP) values of each pixel, where green represents low order of plasma membranes and red indicates highly ordered plasma membranes. The scatter plot shows the distribution of average GP values ( $n = 3$ ) between the plasma membrane of Col-0 (black) and *fah1fah2* double mutant (rose). GP values for Col-0 plasma membranes are shifted towards higher GP (higher membrane order), whereas for *fah1fah2* GP values move towards negative GP (disordered membrane). Solid line curves show fitted Gaussian curves from the relative distribution of respective GP values. Areas marked with dashed lines in (B) represent the ROI used for quantification of GP values here.

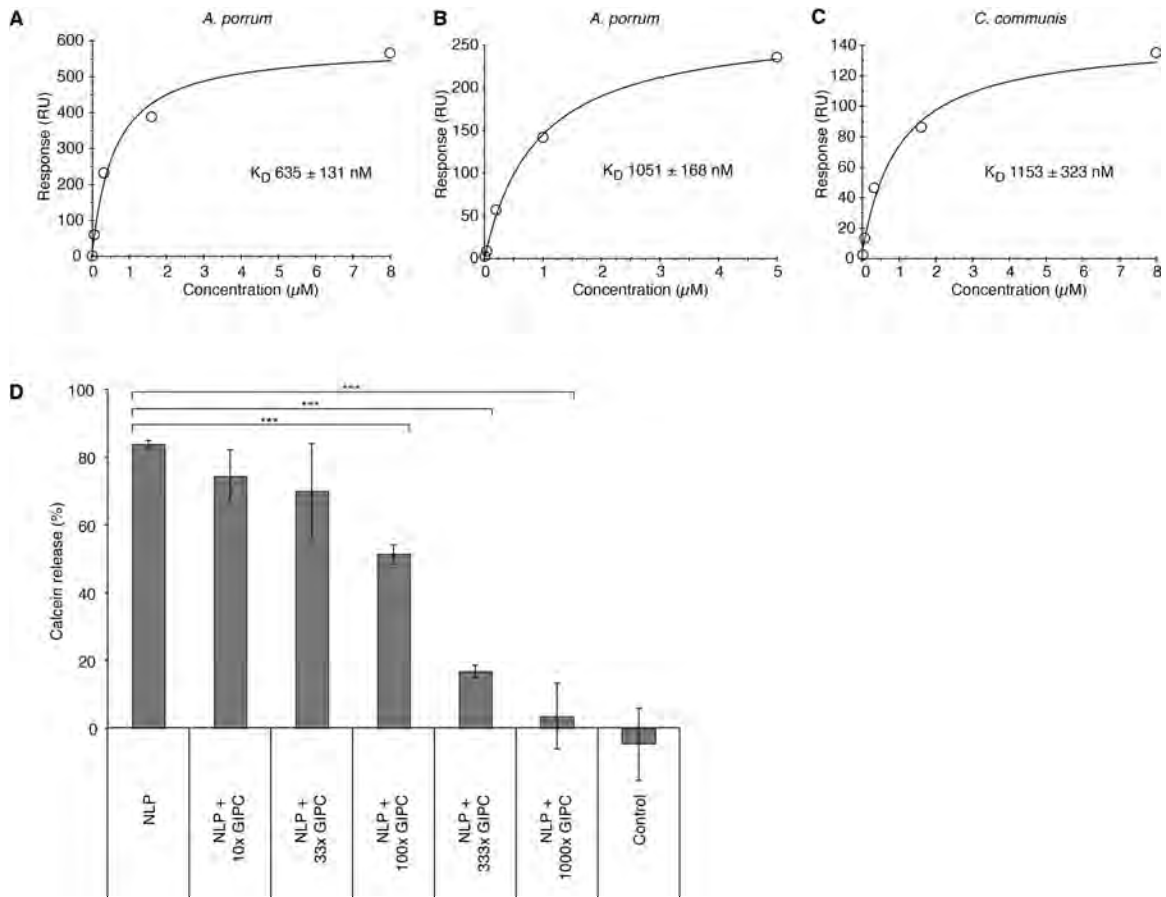


**Fig. S14 Monocot plant-derived GIPCs bind NLPs.**

(A-C) SPR analysis of chip-immobilized leek (*Allium porrum*) (A, B) and *Commelina communis* (C) GIPCs and NLP<sub>Pp</sub> (B) or NLP<sub>PyA</sub> (A, C). Mean values of dissociation constants ( $K_D$ ) are given  $\pm$ SD ( $n = 3$ ) (A-C). (D) Calcein-filled *Arabidopsis* plasma membrane vesicles treated with water (control), NLP<sub>Pp</sub> (500 nM) or NLP<sub>Pp</sub> (500 nM) in the presence of leek GIPCs. GIPCs:NLP<sub>Pp</sub> molar ratios are given. Values represent means  $\pm$  SD of three replicates. Student-t-test analyses (\*\*\*,  $p < 0.001$ ). Experiments were conducted three times with similar results.

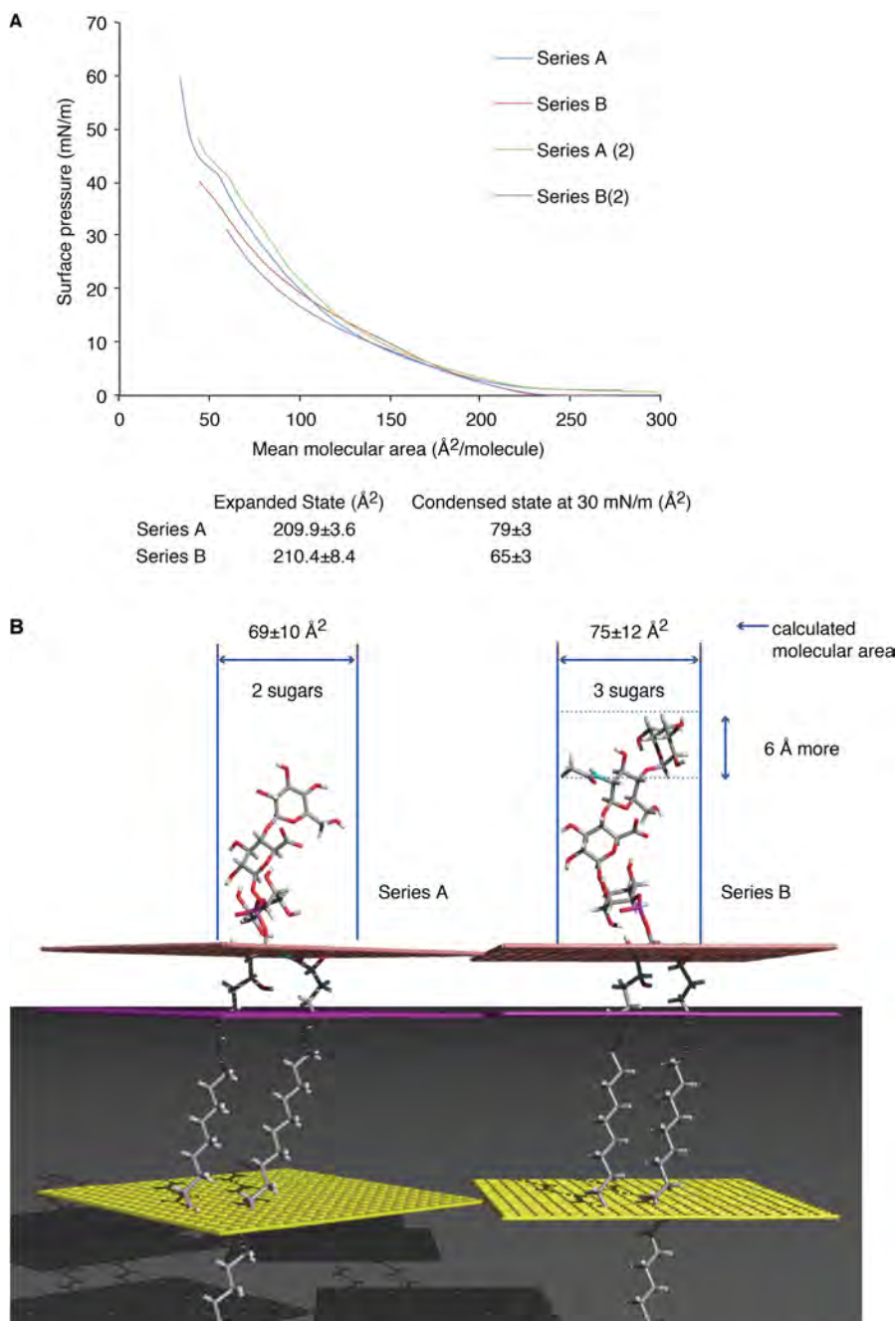


**Fig. S15 Monocot and eudicot GIPCs are arranged in a perpendicular manner in model membranes.**

(A) Surface pressure-area ( $\Pi$ -A) isotherms at the air-aqueous phase interface of cauliflower series A and leek series B GIPC monolayers. The isotherms were recorded at 22 °C with an aqueous sub-phase composed of 10 mM Tris-HCl buffer, pH 7. Duplicate experiments using independent preparations performed at an expanded or condensed state (8) yielded similar results. (B) Modeling approach. Most stable insertion of series A and series B GIPCs into an implicit bilayer. The yellow plane represents the center of the bilayer, the mauve plane represents the lipid polar head/acyl chain interface, and the pink plane represents the water/lipid polar head interface. The mean calculated interfacial molecular areas for GIPCs A and B are indicated.

**Table S1 Data collection and refinement statistics**

	Glucosamine complex PDB ID: 5NNW	Mannosamine complex PDB ID: 5NO9
<b>Data collection</b>		
Space group	C222 <sub>1</sub>	C222 <sub>1</sub>
Cell dimensions		
a, b, c (Å)	115.0, 122.3, 121.1	115.0, 122.3, 121.1
$\alpha$ , $\beta$ , $\gamma$ (°)	90.0, 90.0, 90.0	90.0, 90.0, 90.0
Resolution (Å)	49.09-1.54	43.03-1.75
R <sub>meas</sub> (%) <sup>a</sup>	6.5 (61.8)	11.7 (87.1)
R <sub>p.i.m.</sub> (%) <sup>a, b</sup>	2.5 (37.2)	4.5 (40.2)
I/ $\sigma$ I <sup>a</sup>	17.75 (2.26)	11.63 (2.19)
CC <sub>1/2</sub> (%) <sup>a</sup>	99.9 (79.4)	99.7 (80.9)
Completeness (%) <sup>a</sup>	98.2 (89.3)	99.5 (98.3)
Redundancy <sup>a</sup>	6.2 (4.4)	6.7 (6.7)
No. unique reflections	123,317	85,943
<b>Refinement</b>		
Resolution (Å)	36.62-1.54	36.59-1.75
No. reflections	123,279	85,885
R <sub>work</sub> /R <sub>free</sub> (%)	17.4/19.4 (28.4/32.7)	17.5/20.3 (26.9/28.3)
No. atoms		
Protein	6409	6422
Ligand (hexose)	12	12
Ions (Mg <sup>2+</sup> )	4	4
Water	721	806
B-factors		
Protein	20.1	23.3
Ligand (hexose)	54.1	70.5
Ions (Mg <sup>2+</sup> )	23.6	32.4
Water	27.5	30.2
R.m.s deviations		
Bond lengths (Å)	0.006	0.006
Bond angles (°)	0.830	0.810
Ramachandran plot		
Favoured (%)	98	98
Allowed (%)	2	2
Outliers (%)	0	0

<sup>a</sup>Values in parentheses are for the highest-resolution shell. <sup>b</sup>R<sub>p.i.m.</sub> is calculated by Aimless (46). For each complex one crystal was used to measure the data.

**Table S2 Overview on NLP<sub>PyA</sub> amino acid residues implicated in coordination of Mg<sup>2+</sup> in the absence (-) and presence (+) of GlcN/ManN.**

Residue	-	+
D93	Mg <sup>2+</sup> (direct)	Mg <sup>2+</sup> (via H <sub>2</sub> O)
H101	Mg <sup>2+</sup> (via H <sub>2</sub> O)	Hexose
D104	Mg <sup>2+</sup> (direct)	Mg <sup>2+</sup> (via H <sub>2</sub> O)
E106	Mg <sup>2+</sup> (via H <sub>2</sub> O)	Mg <sup>2+</sup> (direct)
A127 (carbonyl group)		Mg <sup>2+</sup> (via H <sub>2</sub> O)
D158	Mg <sup>2+</sup> (via H <sub>2</sub> O)	Hexose and Mg <sup>2+</sup> (via H <sub>2</sub> O)
H159 (carbonyl group)	Mg <sup>2+</sup> (via H <sub>2</sub> O)	Mg <sup>2+</sup> (direct)

## References and Notes

1. S. Oome, G. Van den Ackerveken, Comparative and functional analysis of the widely occurring family of Nep1-like proteins. *Mol. Plant Microbe Interact.* **27**, 1081–1094 (2014). [doi:10.1094/MPMI-04-14-0118-R](https://doi.org/10.1094/MPMI-04-14-0118-R) [Medline](#)
2. M. Gijzen, T. Nürnberger, Nep1-like proteins from plant pathogens: Recruitment and diversification of the NPP1 domain across taxa. *Phytochemistry* **67**, 1800–1807 (2006). [doi:10.1016/j.phytochem.2005.12.008](https://doi.org/10.1016/j.phytochem.2005.12.008) [Medline](#)
3. C. Ottmann, B. Luberaeki, I. Kűfner, W. Koch, F. Brunner, M. Weyand, L. Mattinen, M. Pirhonen, G. Anderluh, H. U. Seitz, T. Nürnberger, C. Oecking, A common toxin fold mediates microbial attack and plant defense. *Proc. Natl. Acad. Sci. U.S.A.* **106**, 10359–10364 (2009). [doi:10.1073/pnas.0902362106](https://doi.org/10.1073/pnas.0902362106) [Medline](#)
4. D. Qutob, B. Kemmerling, F. Brunner, I. Kűfner, S. Engelhardt, A. A. Gust, B. Luberaeki, H. U. Seitz, D. Stahl, T. Rauhut, E. Glawischnig, G. Schween, B. Lacombe, N. Watanabe, E. Lam, R. Schlichting, D. Scheel, K. Nau, G. Dodt, D. Hubert, M. Gijzen, T. Nürnberger, Phytotoxicity and innate immune responses induced by Nep1-like proteins. *Plant Cell* **18**, 3721–3744 (2006). [doi:10.1105/tpc.106.044180](https://doi.org/10.1105/tpc.106.044180) [Medline](#)
5. G. Anderluh, J. H. Lakey, Disparate proteins use similar architectures to damage membranes. *Trends Biochem. Sci.* **33**, 482–490 (2008). [doi:10.1016/j.tibs.2008.07.004](https://doi.org/10.1016/j.tibs.2008.07.004) [Medline](#)
6. N. Rojko, M. Dalla Serra, P. Maček, G. Anderluh, Pore formation by actinoporins, cytolysins from sea anemones. *Biochim. Biophys. Acta* **1858**, 446–456 (2016). [doi:10.1016/j.bbamem.2015.09.007](https://doi.org/10.1016/j.bbamem.2015.09.007) [Medline](#)
7. B. Bakrač, I. Gutiérrez-Aguirre, Z. Podlesek, A. F.-P. Sonnen, R. J. C. Gilbert, P. Maček, J. H. Lakey, G. Anderluh, Molecular determinants of sphingomyelin specificity of a eukaryotic pore-forming toxin. *J. Biol. Chem.* **283**, 18665–18677 (2008). [doi:10.1074/jbc.M708747200](https://doi.org/10.1074/jbc.M708747200) [Medline](#)
8. J. L. Cacas, C. Buré, K. Grosjean, P. Gerbeau-Pissot, J. Lherminier, Y. Rombouts, E. Maes, C. Bossard, J. Gronnier, F. Furt, L. Fouillen, V. Germain, E. Bayer, S. Cluzet, F. Robert, J.-M. Schmitter, M. Deleu, L. Lins, F. Simon-Plas, S. Mongrand, Revisiting plant plasma membrane lipids in tobacco: A focus on sphingolipids. *Plant Physiol.* **170**, 367–384 (2016). [doi:10.1104/pp.15.00564](https://doi.org/10.1104/pp.15.00564) [Medline](#)
9. J. E. Markham, D. V. Lynch, J. A. Napier, T. M. Dunn, E. B. Cahoon, Plant sphingolipids: Function follows form. *Curr. Opin. Plant Biol.* **16**, 350–357 (2013). [doi:10.1016/j.pbi.2013.02.009](https://doi.org/10.1016/j.pbi.2013.02.009) [Medline](#)
10. L. Fang, T. Ishikawa, E. A. Rennie, G. M. Murawska, J. Lao, J. Yan, A. Y.-L. Tsai, E. E. K. Baidoo, J. Xu, J. D. Keasling, T. Demura, M. Kawai-Yamada, H. V. Scheller, J. C. Mortimer, Loss of inositol phosphorylceramide sphingolipid mannosylation induces plant immune responses and reduces cellulose content in *Arabidopsis*. *Plant Cell* **28**, 2991–3004 (2016). [doi:10.1105/tpc.16.00186](https://doi.org/10.1105/tpc.16.00186) [Medline](#)
11. E. J. M. Van Damme, H. Kaku, F. Perini, I. J. Goldstein, B. Peeters, F. Yagi, B. Decock, W. J. Peumans, Biosynthesis, primary structure and molecular cloning of snowdrop

- (*Galanthus nivalis* L.) lectin. *Eur. J. Biochem.* **202**, 23–30 (1991). [doi:10.1111/j.1432-1033.1991.tb16339.x](https://doi.org/10.1111/j.1432-1033.1991.tb16339.x) [Medline](#)
12. P. Ternes, K. Feussner, S. Werner, J. Lerche, T. Iven, I. Heilmann, H. Riezman, I. Feussner, Disruption of the ceramide synthase LOH1 causes spontaneous cell death in *Arabidopsis thaliana*. *New Phytol.* **192**, 841–854 (2011). [doi:10.1111/j.1469-8137.2011.03852.x](https://doi.org/10.1111/j.1469-8137.2011.03852.x) [Medline](#)
  13. J. C. Mortimer, X. Yu, S. Albrecht, F. Sicilia, M. Huichalaf, D. Ampuero, L. V. Michaelson, A. M. Murphy, T. Matsunaga, S. Kurz, E. Stephens, T. C. Baldwin, T. Ishii, J. A. Napier, A. P. M. Weber, M. G. Handford, P. Dupree, Abnormal glycosphingolipid mannosylation triggers salicylic acid-mediated responses in *Arabidopsis*. *Plant Cell* **25**, 1881–1894 (2013). [doi:10.1105/tpc.113.111500](https://doi.org/10.1105/tpc.113.111500) [Medline](#)
  14. S. König, K. Feussner, M. Schwarz, A. Kaefer, T. Iven, M. Landesfeind, P. Ternes, P. Karlovsky, V. Lipka, I. Feussner, *Arabidopsis* mutants of sphingolipid fatty acid  $\alpha$ -hydroxylases accumulate ceramides and salicylates. *New Phytol.* **196**, 1086–1097 (2012). [doi:10.1111/j.1469-8137.2012.04351.x](https://doi.org/10.1111/j.1469-8137.2012.04351.x) [Medline](#)
  15. M. Nagano, T. Ishikawa, M. Fujiwara, Y. Fukao, Y. Kawano, M. Kawai-Yamada, K. Shimamoto, Plasma membrane microdomains are essential for Rac1-RbohB/H-mediated immunity in rice. *Plant Cell* **28**, 1966–1983 (2016). [doi:10.1105/tpc.16.00201](https://doi.org/10.1105/tpc.16.00201) [Medline](#)
  16. B. A. Bailey, Purification of a protein from culture filtrates of *Fusarium oxysporum* that induces ethylene and necrosis in leaves of *Erythroxylum coca*. *Phytopathology* **85**, 1250–1255 (1995). [doi:10.1094/Phyto-85-1250](https://doi.org/10.1094/Phyto-85-1250)
  17. J. L. Cacas, C. Buré, F. Furt, J.-P. Maalouf, A. Badoc, S. Cluzet, J.-M. Schmitter, E. Antajan, S. Mongrand, Biochemical survey of the polar head of plant glycosylinositolphosphoceramides unravels broad diversity. *Phytochemistry* **96**, 191–200 (2013). [doi:10.1016/j.phytochem.2013.08.002](https://doi.org/10.1016/j.phytochem.2013.08.002) [Medline](#)
  18. J. S. Griffiths, S. M. Haslam, T. Yang, S. F. Garczynski, B. Mulloy, H. Morris, P. S. Cremer, A. Dell, M. J. Adang, R. V. Aroian, Glycolipids as receptors for *Bacillus thuringiensis* crystal toxin. *Science* **307**, 922–925 (2005). [doi:10.1126/science.1104444](https://doi.org/10.1126/science.1104444) [Medline](#)
  19. D. G. Pina, L. Johannes, Cholera and Shiga toxin B-subunits: Thermodynamic and structural considerations for function and biomedical applications. *Toxicon* **45**, 389–393 (2005). [doi:10.1016/j.toxicon.2004.12.014](https://doi.org/10.1016/j.toxicon.2004.12.014) [Medline](#)
  20. C. Buré, J. L. Cacas, S. Mongrand, J. M. Schmitter, Characterization of glycosyl inositol phosphoryl ceramides from plants and fungi by mass spectrometry. *Anal. Bioanal. Chem.* **406**, 995–1010 (2014). [doi:10.1007/s00216-013-7130-8](https://doi.org/10.1007/s00216-013-7130-8) [Medline](#)
  21. S. E. Kubis, K. S. Lilley, P. Jarvis, Isolation and preparation of chloroplasts from *Arabidopsis thaliana* plants. *Methods Mol. Biol.* **425**, 171–186 (2008). [doi:10.1007/978-1-60327-210-0\\_16](https://doi.org/10.1007/978-1-60327-210-0_16) [Medline](#)
  22. A. R. Shenoy, S. S. Visweswariah, Site-directed mutagenesis using a single mutagenic oligonucleotide and DpnI digestion of template DNA. *Anal. Biochem.* **319**, 335–336 (2003). [doi:10.1016/S0003-2697\(03\)00286-0](https://doi.org/10.1016/S0003-2697(03)00286-0) [Medline](#)

23. B. Luberaeki, M. Weyand, U. Seitz, W. Koch, C. Oecking, C. Ottmann, Purification, crystallization and preliminary X-ray diffraction analysis of an oomycete-derived Nep1-like protein. *Acta Crystallogr. Sect. F Struct. Biol. Cryst. Commun.* **64**, 1178–1180 (2008). [doi:10.1107/S1744309108037640](https://doi.org/10.1107/S1744309108037640) [Medline](#)
24. W. Kabsch, Integration, scaling, space-group assignment and post-refinement. *Acta Crystallogr. D Biol. Crystallogr.* **66**, 133–144 (2010). [doi:10.1107/S0907444909047374](https://doi.org/10.1107/S0907444909047374) [Medline](#)
25. P. D. Adams, P. V. Afonine, G. Bunkóczi, V. B. Chen, I. W. Davis, N. Echols, J. J. Headd, L.-W. Hung, G. J. Kapral, R. W. Grosse-Kunstleve, A. J. McCoy, N. W. Moriarty, R. Oeffner, R. J. Read, D. C. Richardson, J. S. Richardson, T. C. Terwilliger, P. H. Zwart, *PHENIX: A comprehensive Python-based system for macromolecular structure solution.* *Acta Crystallogr. D Biol. Crystallogr.* **66**, 213–221 (2010). [doi:10.1107/S0907444909052925](https://doi.org/10.1107/S0907444909052925) [Medline](#)
26. P. Emsley, K. Cowtan, *Coot: Model-building tools for molecular graphics.* *Acta Crystallogr. D Biol. Crystallogr.* **60**, 2126–2132 (2004). [doi:10.1107/S0907444904019158](https://doi.org/10.1107/S0907444904019158) [Medline](#)
27. N. W. Moriarty, R. W. Grosse-Kunstleve, P. D. Adams, *electronic Ligand Builder and Optimization Workbench (eLBOW): A tool for ligand coordinate and restraint generation.* *Acta Crystallogr. D Biol. Crystallogr.* **65**, 1074–1080 (2009). [doi:10.1107/S0907444909029436](https://doi.org/10.1107/S0907444909029436) [Medline](#)
28. V. B. Chen, W. B. Arendall 3rd, J. J. Headd, D. A. Keedy, R. M. Immormino, G. J. Kapral, L. W. Murray, J. S. Richardson, D. C. Richardson, *MolProbity: All-atom structure validation for macromolecular crystallography.* *Acta Crystallogr. D Biol. Crystallogr.* **66**, 12–21 (2010). [doi:10.1107/S0907444909042073](https://doi.org/10.1107/S0907444909042073) [Medline](#)
29. *The PYMOL Molecular Graphics System, Version 1.3r1* (Schrodinger, 2010).
30. H. E. Carter, J. L. Koob, Sphingolipids in bean leaves (*Phaseolus vulgaris*). *J. Lipid Res.* **10**, 363–369 (1969). [Medline](#)
31. C. Buré, J.-L. Cacas, F. Wang, K. Gaudin, F. Domergue, S. Mongrand, J.-M. Schmitter, Fast screening of highly glycosylated plant sphingolipids by tandem mass spectrometry. *Rapid Commun. Mass Spectrom.* **25**, 3131–3145 (2011). [doi:10.1002/rcm.5206](https://doi.org/10.1002/rcm.5206) [Medline](#)
32. T. Taki, S. Handa, D. Ishikawa, Blotting of glycolipids and phospholipids from a high-performance thin-layer chromatogram to a polyvinylidene difluoride membrane. *Anal. Biochem.* **221**, 312–316 (1994). [doi:10.1006/abio.1994.1418](https://doi.org/10.1006/abio.1994.1418) [Medline](#)
33. J. Bielawski, Z. M. Szulc, Y. A. Hannun, A. Bielawska, Simultaneous quantitative analysis of bioactive sphingolipids by high-performance liquid chromatography-tandem mass spectrometry. *Methods* **39**, 82–91 (2006). [doi:10.1016/j.ymeth.2006.05.004](https://doi.org/10.1016/j.ymeth.2006.05.004) [Medline](#)
34. P. Tarazona, K. Feussner, I. Feussner, An enhanced plant lipidomics method based on multiplexed liquid chromatography-mass spectrometry reveals additional insights into cold- and drought-induced membrane remodeling. *Plant J.* **84**, 621–633 (2015). [doi:10.1111/tpj.13013](https://doi.org/10.1111/tpj.13013) [Medline](#)
35. K. Grillitsch, P. Tarazona, L. Klug, T. Wriessnegger, G. Zellnig, E. Leitner, I. Feussner, G. Daum, Isolation and characterization of the plasma membrane from the yeast *Pichia*

- pastoris*. *Biochim. Biophys. Acta* **1838**, 1889–1897 (2014).  
[doi:10.1016/j.bbamem.2014.03.012](https://doi.org/10.1016/j.bbamem.2014.03.012) [Medline](#)
36. J. Nagy, P. Maliga, Callus induction and plant regeneration from mesophyll protoplasts of *Nicotiana sylvestris*. *Z. Pflanzenphysiol.* **78**, 453–455 (1976). [doi:10.1016/S0044-328X\(76\)80093-1](https://doi.org/10.1016/S0044-328X(76)80093-1)
37. S. D. Yoo, Y. H. Cho, J. Sheen, *Arabidopsis* mesophyll protoplasts: A versatile cell system for transient gene expression analysis. *Nat. Protoc.* **2**, 1565–1572 (2007).  
[doi:10.1038/nprot.2007.199](https://doi.org/10.1038/nprot.2007.199) [Medline](#)
38. D. M. Owen, C. Rentero, A. Magenau, A. Abu-Siniyeh, K. Gaus, Quantitative imaging of membrane lipid order in cells and organisms. *Nat. Protoc.* **7**, 24–35 (2011).  
[doi:10.1038/nprot.2011.419](https://doi.org/10.1038/nprot.2011.419) [Medline](#)
39. P. Gerbeau-Pissot, C. Der, M. Grebe, T. Stanislas, Ratiometric fluorescence live imaging analysis of membrane lipid order in *Arabidopsis* mitotic cells using a lipid order-sensitive probe. *Methods Mol. Biol.* **1370**, 227–239 (2016). [doi:10.1007/978-1-4939-3142-2\\_17](https://doi.org/10.1007/978-1-4939-3142-2_17) [Medline](#)
40. L. Lins, R. Brasseur, W. J. Malaisse, M. Biesemans, P. Verheyden, R. Willem, Importance of the hydrophobic energy: Structural determination of a hypoglycemic drug of the meglitinide family by nuclear magnetic resonance and molecular modeling. *Biochem. Pharmacol.* **52**, 1155–1168 (1996). [doi:10.1016/0006-2952\(96\)00424-8](https://doi.org/10.1016/0006-2952(96)00424-8) [Medline](#)
41. L. Lins, A. Thomas-Soumarmon, T. Pillot, J. Vandekerckhove, M. Rosseneu, R. Brasseur, Molecular determinants of the interaction between the C-terminal domain of Alzheimer's  $\beta$ -amyloid peptide and apolipoprotein E  $\alpha$ -helices. *J. Neurochem.* **73**, 758–769 (1999).  
[doi:10.1046/j.1471-4159.1999.0730758.x](https://doi.org/10.1046/j.1471-4159.1999.0730758.x) [Medline](#)
42. M. Deleu, J. M. Crowet, M. N. Nasir, L. Lins, Complementary biophysical tools to investigate lipid specificity in the interaction between bioactive molecules and the plasma membrane: A review. *Biochim. Biophys. Acta* **1838**, 3171–3190 (2014).  
[doi:10.1016/j.bbamem.2014.08.023](https://doi.org/10.1016/j.bbamem.2014.08.023) [Medline](#)
43. P. Ducarme, M. Rahman, R. Brasseur, IMPALA: A simple restraint field to simulate the biological membrane in molecular structure studies. *Proteins* **30**, 357–371 (1998).  
[doi:10.1002/\(SICI\)1097-0134\(19980301\)30:4<357::AID-PROT3>3.0.CO;2-G](https://doi.org/10.1002/(SICI)1097-0134(19980301)30:4<357::AID-PROT3>3.0.CO;2-G) [Medline](#)
44. N. Eswar *et al.*, *Curr Protoc Bioinformatics* chap. 5, unit 5-6 (2006).
45. J. Keicher, N. Jaspert, K. Weckermann, C. Möller, C. Throm, A. Kintzi, C. Oecking, *Arabidopsis* 14-3-3  $\epsilon$  members contribute to polarity of PIN auxin carrier and auxin transport-related development. *eLife* **6**, e24336 (2017). [doi:10.7554/eLife.24336](https://doi.org/10.7554/eLife.24336) [Medline](#)
46. P. R. Evans, G. N. Murshudov, How good are my data and what is the resolution? *Acta Crystallogr. D Biol. Crystallogr.* **69**, 1204–1214 (2013).  
[doi:10.1107/S0907444913000061](https://doi.org/10.1107/S0907444913000061) [Medline](#)

## Discussion and Perspectives

The mode of action of NLP family remains to be deciphered. After binding to GIPC, NLPs likely oligomerized in the PM and form a pore leading to the lysis of the cell. A number of questions need to be addressed about the biological activities of NLP: At what extend NLPs are functionally conserved proteins in phytopathogenic organism? How the necrosis induced by NLPs contributes to infection? What is the mechanism leading to necrosis and defence activities? What is the tertiary/quaternary structure of NLP in the membrane? What is the role of lipids of the PM and particularly sterols involved in domain formation with GIPC, (see Chapter 1)? To answer these questions, molecular modelling, biochemical and genetic tools will be used. (Ottmann et al., 2009) showed that the tertiary structure of NLPs is highly conserved and that the proteins of the family might be functionally homologous. The structure of NLP consists of a beta-sandwich flanked by alpha-helices. The promotion of virulence and cytolysis by NLPs is based on structural requirements. They also showed that NLP structure bear resemblance to the animal cytolitic toxin, actinoporins (Anderluh & Maček, 2002). Actinoporins are cytolitic proteins in sea anemones that disrupt the PM upon binding to sphingomyelin (SM) through pore formation (Črnigoj Kristan, Viero, Dalla Serra, Maček, & Anderluh, 2009; Rojko, Dalla Serra, Maček, & Anderluh, 2016). While NLPs are structurally similar to actinoporins, GIPCs are quite similar to SM even if the later has a different polar head, indeed both are found in the outer leaflet of the PM and form microdomains. The animal structural homologue of GIPC is gangliosides. Cholera toxin subunit B (CT-B) interacts specifically with nanodomain-residing ganglioside  $G_{M1}$ , forming pore in the PM. As such, fluorescently-labelled CT-B may be used as a lipid probe for membrane domains (Skocaj et al., 2013). Do NLPs have the same cytolitic mechanism when bound to GIPC as actinoporins or CT-B in  $G_{M1}$ ? How does the mechanism occur? The answer might rely in their structures. A recent study of our collaborators in *Plas Pathogens*, showed that the conformation of the toxin is key for its cytotoxicity (Lenarčič et al., 2019). They used two members of the NLP type 1 family: non-toxic NLP (HaNLP3) and toxic NLP<sub>pya</sub> to study the structural differences and how they impacted on the function of the protein. They did surface plasmon resonance (SPR) on supported bilayers containing GIPC and found that NLP binding to GIPC was concentration-dependent but non-toxic HaNLP3 did not bind to GIPC. Moreover, the conservative loops L1-L3 were present in HaNLP3 as well as the crevice located between loops L2 and L3 where GIPC sugar residue binds in the NLP. Upon binding with the hexose residue of GIPC, there is a dislocation of the L3 loop of NLP<sub>pya</sub> (Lenarčič et al., 2017b).

There is an opening of the crevice between loop L2 and L3 such that the magnesium ion is displaced, crucial for the binding of GIPC. In HaNLP3, all amino acids involved in the movement of  $Mg^{2+}$  are conserved except for Asp158 which is replaced by Asn184. Asp158 is important for glucosamine binding in NLPPya. HaNLP3 lacks a metal ion in its structure. The  $Mg^{2+}$  ion of NLPPya in the crevice between L2 and L3, is indirectly involved in GIPC binding. In the presence of divalent ions  $Mg^{2+}$  and  $Ca^{2+}$ , HaNLP3 did not promote toxin activity. HaNLP3 has the particularity of having a second disulphide bond responsible for the rigidity of HaNLP3 upon interacting with membrane GIPC. These particular features of HaNLP3 could explain the importance of particular structure in conducting specific role in the toxicity of NLP. By mutation of particular amino acid of NLP<sub>Pya</sub>, unique structural motifs were important for the toxin activity. The introduction of amino acid residues in the plastic region of the L2/L3 loop of HaNLP3, resulted in generating HaNLP3 variants which were able to bind with GIPC. The toxicity of these HaNLP3 variants was at a lesser extent compared to that of NLP<sub>Pya</sub>.

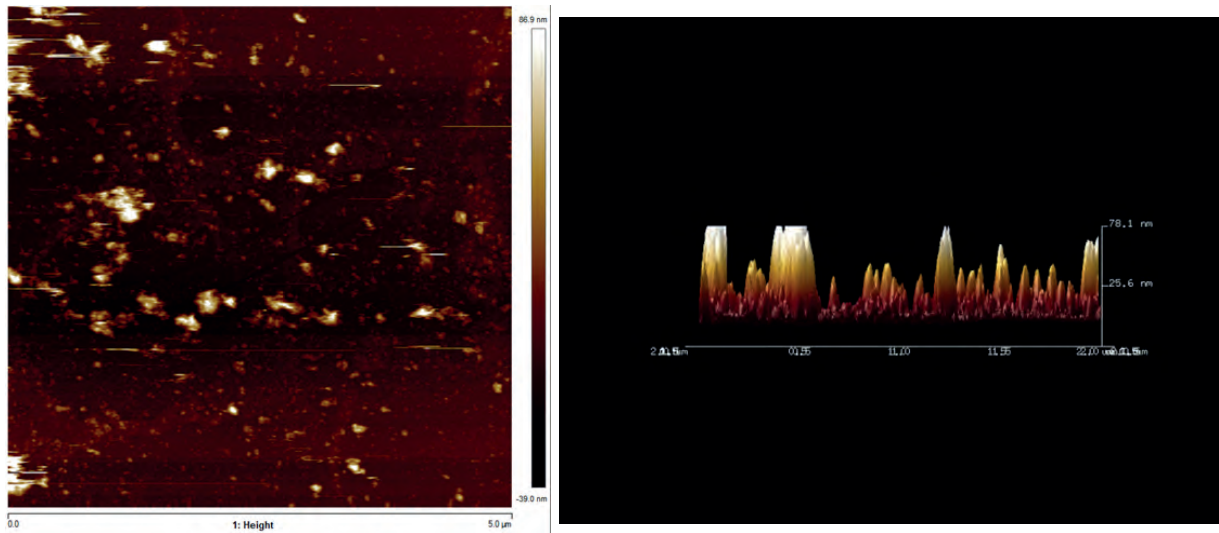
These results reveal the functional importance of loops L2 and L3 and the loops content for GIPC head group binding and cytolytic activity of the toxin. The study highlighted how minute changes of the primary structure affect functional features of NLP<sub>Pya</sub> to the extent of suppressing its toxicity. The amino acids of the loops around the binding cavity are essential at two different levels of the toxin activity. They affect the conformational plasticity of the loops, hence the binding cavity, as well as the interaction with the membrane. Membrane anchoring seems to rely on residue Trp155 and its surrounding as well as distal amino acids Pro41, Asp44, Asn48. The mutations of these amino acids can lead to generate a NLP protein, able to bind on GIPC and anchor on the PM without inducing necrosis. For instance a GIPC fused HaNLP3 mutated to unable GIPC binding, could be used as GIPC sensor, in the same way as CT-B are used as gangliosides-enriched domain sensors (Skocaj et al., 2013). Such probe will give tremendous information on the organisation of GIPCs in the outer leaflet of the PM. By using inside out (ISO) and right-side out (RSO) PM fractions, we will be able to confirm the hypothesis of an asymmetrical distribution of GIPC favouring the outer membrane at 90% (Cacas et al., 2016a).

The question to tackle in the near future is the mechanisms mediated by NLPs in pore formation upon binding to GIPCs. It seemed to be a complex process where distinct parts of the toxin are involved differently in the stages leading to pore formation and subsequently plant cell death. The review of (Yilmaz & Kobayashi, 2016) was a useful resource for information on analysing pore-forming toxins by atomic force microscopy. Pore-forming toxins are monomers soluble in aqueous medium, but on self-assembling, they form defined oligomers on the PM. These structures can be visualized by high-resolution AFM imaging which require appropriate

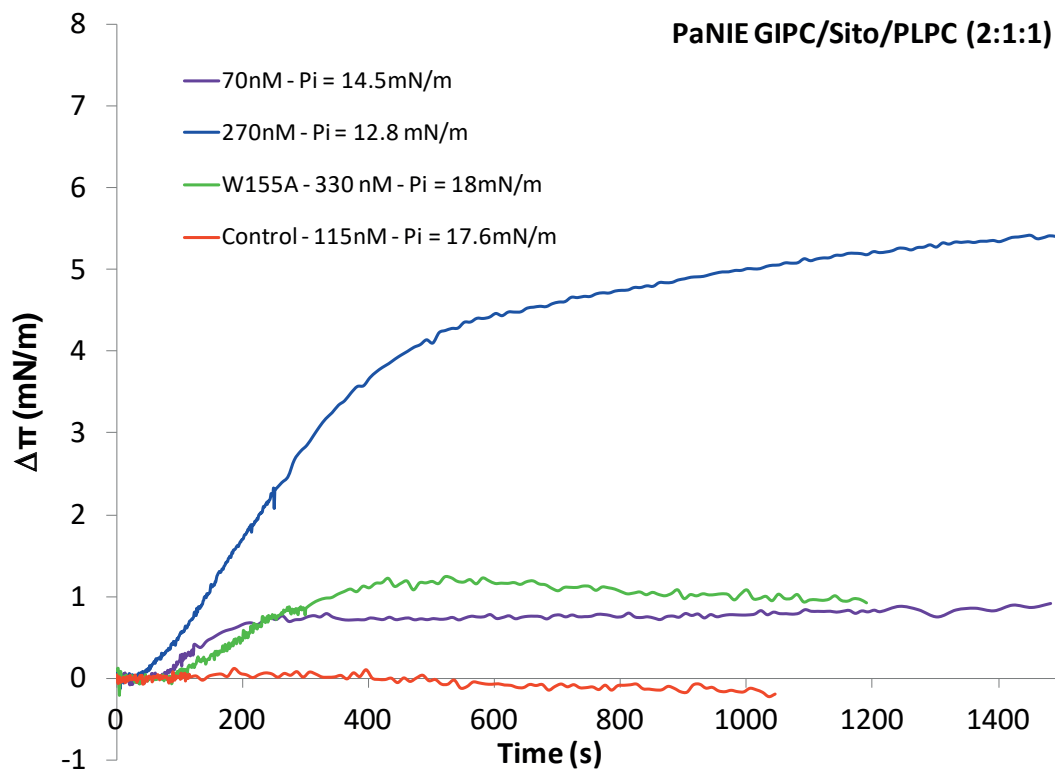
adjustments of conditions in order to obtain electrostatic balanced interaction between the tip and the protein surface in contact mode (Müller, Fotiadis, Scheuring, Müller, & Engel, 1999). However to avoid damaging the fragile and weakly attached structures by friction forces, tapping mode is more suitable for AFM analysis of pore-formation toxin oligomers. For AFM imaging, supported lipid bilayers (SLBs) are used as membrane models (Sackmann, 1996). Langmuir–Blodgett (LB) technique and liposome fusion can be employed to prepare SLBs (El Kirat, Morandat, & Dufrêne, 2010). For the LB technique, a solid support is lowered into the trough containing an aqueous subphase. The appropriate lipid mix dissolved in solvent is deposited on the surface on the subphase at the air/water interface, such as to form a lipid monolayer. The solvent used has to be evaporated such that the surface pressure is stabilised, before starting the transfer of the monolayer onto the support. Using automated movable barriers, the monolayer is compressed. At a constant surface pressure, the substrate support is withdrawn vertically from the subphase causing the deposition of the lipid monolayer onto the support with the hydrophilic head group on the support and lipid tails exposed to the air. The trough is cleaned and another lipid layer deposited. The support is once more, dipped into the subphase at constant surface pressure or is lowered horizontally onto the Langmuir film to form the bilayer. These are known as the Langmuir-Blodgett and Langmuir–Schaeffer techniques, respectively. (Yilmaz & Kobayashi, 2016) listed pore-formation toxins assemblies whose structure was solved by AFM, among which CT-B. We decided to investigate pore-formation properties of NLPs on SLB containing GIPCs using AFM. The first step was to make SLB with GIPCs. With the help of our collaborators L. Lins from the LBMI, Université de Liège Gembloux, and E Lesniewska from Université de Bourgogne Franche-Comté, I went to Gembloux to perform Langmuir-Blodgett experiments and AFM analysis. We made asymmetric bilayer mimicking plant PM lipid model. The inner lipid layer in contact with the mica substrate consists of PLPC/sitosterol (80:20, mol ratio) and the outer layer consists of GIPC/sitosterol (60:40, mol ratio) (Additional Data A). The buffer for the subphase was MES 20mM NaCl 140mM, pH 5.8 at 22°C, based on the condition necessary for NLP binding used in surface plasmon resonance assay of (Lenarčič et al., 2017b). The presence of salts in the SLB made AFM imaging challenging. The signal was blurry and in spite of changing the tip several times, we were unable to obtain a clearer image as shown in Additional Data A. The topography of the bilayer was also very irregular, with the formation of patches from 1nm to 70nm high reminiscent to what we observed in monolayer, see chapter 1. The SLB was hence unsuitable to be used for further experiments. Too large height variations could undermine the detection of the anchoring of the NLP protein, suggesting a wrong fixation of the protein. We are currently still looking for a solution to make asymmetrical SLB. While symmetrical SLB can be obtained by fusion of lipid vesicle, asymmetrical ones are

A

Assymmetric bilayer of GIPC/sitosterol (60:40) outer layer and PLPC/sitosterol (80:20)



B



Additional data : A. AFM imaging of assymmetric SLB. Inner lipid layer in contact with mica, PLPC/sitosterol (80:20, mol ratio) and outer lipid layer, GIPC/sitosterol (60:40, mol ratio). Subphase, MES NaCl pH 5,8. B. Langmuir monolayer technique. Adsorption kinetic of NLP PaNIE (novel protein elicitor from *Pythium aphanidermatum*, Viet et al., 2001) in a mix monolayer of GIPC/Sitosterol/PLPC (2:1:1, mol ratio). The surface pressure (mN/m) was measured after injection of PaNIE in the subphase, in its native form at 70nM, 270nM., in his mutated form at 330nM. The subphase is MES NaCl pH 5.8, at a temperature of 22°C.

more challenging. The challenge is to find the right approach in modelling a membrane system where the formation of complex protein structures, is as close as possible at what happens *in vivo*. On SLBs, the curvature, protein content and membrane potential are not taken into account and can produce significant bias in the way NLPs might organized themselves.

To further our investigation on the binding properties of GIPCs, we also tested the affinity of different variants of NLP, among which Novel Protein Elicitor (PaNIE) from *Pythium aphanidermatum* and inactive mutant NLP W155 provided by our collaborator Isabel Albert from the Nürnberger team, University of Tübingen, Germany. NLPs were produced, extracted and purified from *Pichia pastoris* in Tübingen and sent to Gembloux where I performed the experiments. Preliminary results showed that as expected, novel protein elicitor NLP PANie binds to GIPC in a concentration-dependent manner and that the elicitor that worked best was NLPPya PaNIE (Veit, Wörle, Nürnberger, Koch, & Seitz, 2001). In good agreement, the mutant W155 was unable to bind the GIPC monolayer – see Additional Data B. These preliminary results pave the way to tackle the role of lipids such as sterols that make domains with GIPC, in the anchoring mechanism and pore forming of NLPs.

Our aim now, is still to find new approach to further increase our understanding in the pore-formation mechanism of NLPs upon binding to GIPC. The best approach seems to be multidisciplinary, combining biophysics, biochemistry, molecular dynamic modelling and molecular biology. NLP structure has been mostly studied by crystallography, which is not the proper method to study protein/membrane interaction because of the very nature of the protein crystal structure not allowing lipid/membrane/protein interactions. Solid state-NMR (ssNMR) is clearly the appropriate approach to study protein-lipid interactions both in model membrane and in cells (Kaplan et al., 2016; Medeiros-Silva et al., 2018). ssNMR has been successfully used at LBM in collaboration with the team of Birgit Habenstein, IECB Pessac, to decipher the molecular mechanism of REMORIN anchoring -a plant protein REMORIN- in inner leaflet nanodomain of the PM (Gronnier et al., 2017). New methods are developed, such as the use of nanodiscs, for the study of the organisation of lipids and protein-lipid interactions in nanodomains, that can pave the way in understanding pre-pore and pore-formation in membrane models closer to plant PM reality or in cell PM (Gronnier et al., 2017; Martinez et al., 2017; Meca et al., 2019). For instance, NLP<sub>Pya</sub>, the most virulent

NLP (Lenarčič et al., 2017b, 2019), could be marked with C13 and N15 (to be detectable in ssNMR), and its binding to tobacco (BY-2) cultured cell or rice cultured cell would be studied and compared. Tobacco will be used as the eudicot (enriched in GIPC series A, refer to chapter 1) sensitive to NLP while rice being a monocot (enriched in GIPC series B, refer to chapter 1) is resistant to NLP-induced necrosis. By <sup>13</sup>C-ssNMR, we should be able to analyse the anchoring of <sup>13</sup>C marked NLP onto eudicot and monocot cells. The analysis will give information on whether NLP agglomerates at specific regions upon its interaction with the PM. To see the specific interactions with the PM, we shall purify PM from tobacco and rice cell, by phase partitioning or make GIPC containing-liposomes (GUVs), before marked <sup>13</sup>C- and <sup>15</sup>C-NLP treatment for NMR analysis. We will obtain information on the chemical shift of the marked <sup>13</sup>C-NLP and <sup>15</sup>C-NLP which will be complementary to the crystallography structure data published in (Lenarčič et al., 2017b). By comparing ss-NMR data between the two conditions (tobacco PM and rice PM), we shall see the change of conformation of the toxin upon anchoring to the PM. To conclude this top-down approach, we can construct liposomes with GIPCs of different series, so as to analyse the effect of different sugar residues of the headgroup on the conformation of NLP upon binding. With all those data, we might be able to characterize the anchoring steps of NLP, just like that of REM (Gronnier et al., 2017).

Understanding the mechanism of NLP toxin family will help us prevent crop loss infected by bacterial, fungal and oomycete phytopathogens. The consequences of NLP-induced necrosis have dramatic economical and agricultural impacts. In our era, *Phytophthora infestans*, an NLP-secreting phytopathogen, was responsible for the dissemination of potatoes leading to the Great Irish Famine. With the threat of global warming, immigration and the emerging number of organisms secreting pore-formation toxins, such studies might lead to finding proper solution to secure food security.

# Chapter 4

## Miscellaneous

I participated in the redaction of a News & Views with Sébastien Mongrand on a paper published in *Nature plants* on the development of a FRET biosensors of Phosphatidic Acid (PA) in plants, called PAleon.

**Mamode Cassim, A., Mongrand, S.** *Lipids light up in plant membranes. Nat. Plants* 5, 913–914 (2019) doi:10.1038/s41477-019-0494-9

## LIPID BIOSENSOR

## Lipids light up in plant membranes

Phosphatidic acid (PA) is a simple phospholipid of crucial importance in cell biology. Now, a new ratiometric, PA-specific, optogenetic biosensor has been developed to track PA concentration and dynamics at the plant plasma membrane. Using this tool, scientists have revealed a remarkable stress-specific temporal complexity of PA accumulation.

Adilah Mamode Cassim and Sébastien Mongrand

Phosphatidic acid (PA) represents around 1% of all lipids. It predominantly accumulates at the plasma membrane (PM), but a significant pool is also located in the endoplasmic reticulum (ER) and in plastids. It is the precursor of most phospholipid and triglyceride synthesis, and also a key signalling lipid. PA signalling is at the crossroad of plant responses to a large variety of stimuli, ranging from hormones and biotic and abiotic stresses, to many other developmental and environmental cues. This involves abscisic acid (ABA)-mediated guard cell regulation and response against pathogens<sup>1</sup>. PA also plays a role in vesicular trafficking, secretion and endocytosis. It modulates the activity of effector proteins, such as kinases, phosphatases, phospholipases, transcription factors, NADPH oxidases and microtubule-associated proteins<sup>2</sup>. PA can be generated via different routes: through its main metabolic pathway by the sequential acylation of glycerol-3-phosphate and lyso-PA; through the hydrolytic cleavage mediated by a plethora of plant phospholipase D (PLD) isoforms<sup>3</sup>; through the sequential phosphorylation of diacylglycerol; and finally, through the dephosphorylation of diacylglycerolpyrophosphate.

Intriguingly, PA production can be triggered by opposite stimuli, such as cold and heat or ABA and salicylic acid (hormones that are considered as having antagonistic effects). This property highlights very paradoxical features of PA molecular species, questioning the specificity of the responses controlled by PA. It was proposed that PA regulatory messages are perceived as complex signatures that take into account the site of production, the availability of target proteins and cellular environments<sup>2</sup>. Until now, the study of the role of PA has been strongly impaired by the lack of biosensors efficiently localizing and quantifying the production of PA after stimuli. In a recent paper published

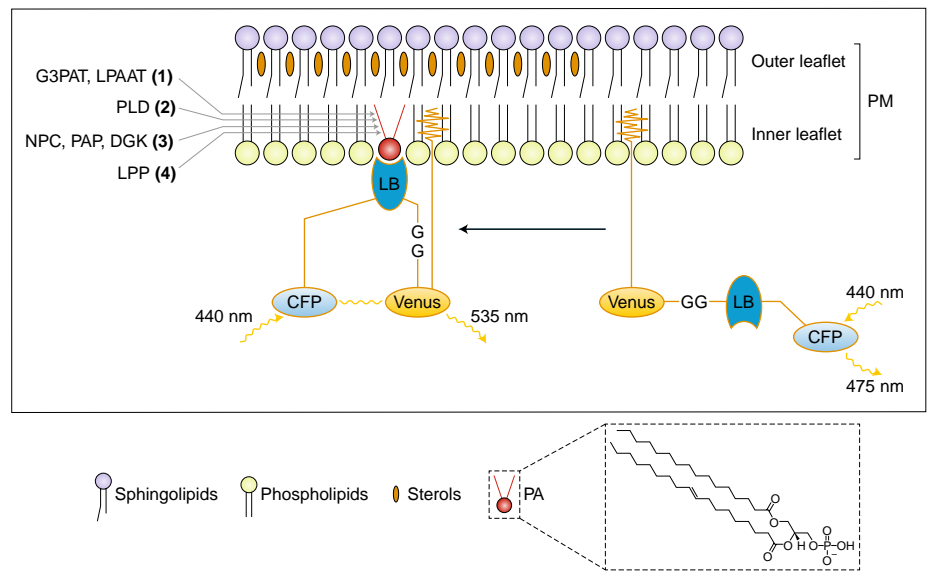


**Fig. 1 | Building a PA-binding biosensor to measure pools of PA in the plant PM.** Simplified PM (constituted of lipids) is shown, with sphingolipid and sterols mostly in the outer leaflet and phospholipids in the inner leaflet. PA is indicated in red. The four pathways leading to PA synthesis are represented on the left sides: (1) glycerol-3-phosphate acyltransferase (G3PAT) and lyso-PA acyltransferase (LPAAT); (2) PLD; (3) non-specific phospholipase (NPC), PA phosphatase (PAP) and diacylglycerol kinase (DGK); and (4) lipid phosphate phosphatase (LPP) of diacylglycerolpyrophosphate.

in *Nature Plants*, Li et al.<sup>4</sup> developed a ratiometric, PA-specific, optogenetic biosensor (named PAleon) that reports PA concentration and dynamics at the PM.

PAleon is based on the translational fusion of five domains: cyan fluorescent protein (CFP) bound to a PA lipid-binding domain (LB) of the NADPH oxidase, named respiratory burst oxidase homologue protein D; a flexible linker containing two glycines; a yellow fluorescent protein, named VENUS; and a C-terminal farnesylation signal of the protein K-Ras4B, which targets the whole chimaeric protein to the PM (Fig. 1). The authors generated a mutated PAleon (mPAleon), in which the four PA-binding arginine residues were replaced

by alanines, to function as a negative control. After PA binding, PAleon undergoes a conformational change resulting in a Förster resonance energy transfer (FRET) between CFP and VENUS. PAleon was shown to be sensitive in vivo to physiological concentrations of PA, thereby enabling the visualization of PA dynamics at subcellular resolution in *Arabidopsis*.

To test the validity of PAleon, the authors first exogenously supplied PA to the system and recorded a dramatic increase of FRET after 500 s of exposure, while no other phospholipids induced FRET. In a more physiological system, the authors applied ABA to plants and observed PA changes in the guard cells. PA accumulation was

increased within 200 s after ABA exposure and reached saturation at 300 s, moments preceding stomatal closure. Salt stress also induces specific patterns of PA accumulation at the same rate in three different root tissues: the root tip, differentiation zone and maturation zone. Treatment with an inhibitor of PLD efficiently hindered PA accumulation in all three zones to near basal levels. Consistently, PA accumulation was impaired in *plda1* mutants. By comparing PA changes under salt stress and osmotic stress, the authors revealed that the remarkable temporal complexity of PA accumulation is highly stress-specific. Finally, authors rationalized that changes in intracellular pH would modulate the protonation of PA polar head, the free phosphate group. Consequently, PA may function as a pH sensor during salt tolerance management in plants.

PAleon is a biosensor that was developed to study the role of lipids in planta among other biosensors, such as

the ones detecting phosphoinositides<sup>5</sup> and diacylglycerol<sup>6</sup>. Besides the PM, PAleon will also pave the way for the study of PA by changing the C-terminal farnesylation domain to target other organelles, such as mitochondria or plastids. In this latter case, PA is a fine regulator of the plastidial lipids as it allosterically regulates the monogalactosyldiacylglycerol synthase responsible for the synthesis of galactolipids in the plastid envelope. The direct quantification of the pool of plastidial PA in vivo would be essential to better understand the regulation of these metabolic pathways<sup>7</sup>. PAleon could also find its use in the study of the nuclear membrane or vesicular pathways. In addition, this new tool will probably help to gain insight into the paradoxical effect of PA raised in the beginning of this article. How can PA be synthesized both by cold and heat stress, but trigger opposite physiological responses? PAleon could help solve this enigma by precisely localizing

and quantifying PA after exposure to specific stimuli. □

**Adiilah Mamode Cassim and Sébastien Mongrand\***

*Laboratoire de Biogénèse Membranaire, UMR 5200, CNRS, University of Bordeaux, Bordeaux, France.*

\*e-mail: [sebastien.mongrand@u-bordeaux.fr](mailto:sebastien.mongrand@u-bordeaux.fr)

Published online: 26 August 2019

<https://doi.org/10.1038/s41477-019-0494-9>

#### References

1. Testerink, C. & Munnik, T. *Trends Plant Sci.* **10**, 368–375 (2005).
2. Pokotylo, I., Kravets, V., Martinec, J. & Ruelland, E. *Prog. Lipid Res.* **71**, 43–53 (2018).
3. Wang, G., Ryu, S. & Wang, X. in *Lipases and Phospholipases: Methods in Molecular Biology* Vol. 861 (ed. Sandoval, G.) 123–137 (Humana Press, 2012).
4. Li, W. et al. *Nat. Plants* <https://doi.org/10.1038/s41477-019-0497-6> (2019).
5. Simon, M. L. et al. *Plant J.* **77**, 322–337 (2014).
6. Vermeer, J. E. M. et al. *Plant Cell Physiol.* **58**, 1196–1207 (2017).
7. Dubots, E. et al. *Biochimie* **94**, 86–93 (2012).

#### Competing interests

The authors declare no competing interests.

# General Conclusions and Perspectives

The plant plasma membrane (PM) is a bilayer barrier between the cell interior and its environment. It is essential for cellular survival and is a signalling control tower. Among its components are sphingolipids, more precisely GIPCs. GIPCs are the most abundant sphingolipid in the plant kingdom and modelled to be localised almost exclusively in the PM outer leaflet (Cacas et al., 2016a). The combined features of GIPC's VLCFA, trihydroxylated LCB and large polar head group, made it an interesting molecule to investigate, suggesting fundamental roles in plant PM as important as those of SM and gangliosides in animal PM.

The aim of this thesis has been to understand GIPC, so as to establish foundation through multipolar approaches, on its role in plant PM leaflet asymmetry regarding its interaction with other lipid components. Throughout our findings, we yield new hypothesis for enquiry about how the whole PM membrane system might function. We have developed tools and methods such as a GIPC purification protocol, sphingolipidomics by LC-MS, and *At fah* mutants expressing PM markers. This will be useful for the plant PM and sphingolipid community to investigate more hypotheses and test models about the organisation of GIPC in PM leaflets and its physiological impact in the plant overall.

Still much has to be done to contemplate the overall organisation and structuring of the plant PM. Understanding the identity and organisation of PM lipids in the leaflets remain a mystery. So far only models of PM asymmetry have been proposed with no or little experimental proves (Cacas et al., 2016a; Tjellstrom et al., 2010) (Takeda & Kasamo, 2002). So many questions remain such as the molecular coupling between the two leaflets believed to have different compositions and physical properties. The molecular mechanisms involved in coordinating the two leaflets such as interdigitation and registration (Fujimoto & Parmryd, 2017). There is also the lateral segregation of specific lipids and protein into sub-compartmentalization of the PM into nano- and micro-domains exhibiting different biophysical characteristics. The dynamic of the molecules in those domains remains also unsolved (discussed in chapter 2). The fact that the PM, an essential part of the cell physiology is still largely undeciphered, testifies of its complexity as a biological subject of study. In the recent years, essential methodologies and tools have been developed, combining traditional molecular biology with advance biophysics and molecular modelling

experiments such as a complementary way to tackle complex questions. This thesis is a testimony of an original way using multiple approaches to characterize and highlight the role of a very important component of plant PM, GIPC that has been largely forgotten for 50 years. I believe that my thesis paves the way to investigate the ambiguity of the PM leaflet organisation in a comprehensive way. The combined results of experimental and modelling approaches seem to be a good approach to shed some clues in order to move forward on this non-negligible issue.

### **Purification and identification of GIPC**

We managed to obtain GIPC-enriched fractions from eudicots (cauliflower and tobacco BY-2 cell culture) and monocots (leek and rice cell culture) at an average purity of 85%. There is still much to be done to obtain a 100% pure GIPC fractions. The challenge lays in the identification of the contaminants that pollute our GIPC fractions. Indeed, arabinogalactans (AGs) can be a major problem to solve, together with a unknown phosphorous-containing contaminants detected in solid-state  $^{31}\text{P}$ -NMR. It seems that GIPCs are intricately woven in the cell wall lattice at some extent (Voxeur & Fry, 2014b). Butan-1-ol/water phase extraction at the end of the purification column might get rid of any soluble sugar moieties of the cell wall. A solid phase extraction is also a potential option although the yield might be negatively affected. The right balance between yield and purity remains a challenge without using kilos of fresh weigh and litres of solvents as was the case in old publication of Lester (Hsieh et al., 1981)(Kaul & Lester, 1978). Our goal is to obtain pure enough GIPCs of a particular series in order to decipher its structure by liquid-state NMR as described for fungi GIPC in (Gutierrez et al., 2007). The development of sphingolipidomics by LC-MS/MS is a key part in succeeding to obtain combined structure of the identity of the polar head group and the ceramide moiety (see chapter 2). So far, we are able to do so for GIPC series A and GIPC series B. The method has to be further developed to accommodate the study of polyglycosylated GIPC.

This will be the starting point for further studies on the role of GIPC in structuring and organising the plant PM. It is interesting to note that the lipidome of plant PM is missing. The starting step will allow the investigation of the content of lipids in each

leaflets of Arabidopsis, the reference model in plant biology, using a combination of lipidomics studies. By studying the exact lipid species content of At PM of the three main lipid classes: phospholipid, sphingolipid and sterols, we will be able to challenge a model for plant PM similar to what has been described by (Ingólfsson et al., 2014) for animal PM, using molecular dynamics simulations with 63 different lipid species and thousands of lipids ! The advance in sphingolipidomics is a key part for identifying different species of the sphingolipid class. GIPCs can account for a few hundreds of molecules with different permutations and combinations considering the vast possibilities of VLCFA, LCB and sugar head group moieties (branched or linear). There is also the issue of missing standards for GIPC. So far in all sphingolipidomics used to identify GIPC,  $G_{M1}$  is used. Our collaborator, Jenny Mortimer's team of the Joint BioEnergy Institute (JBEI), in Berkley, works on  $^{13}C$ -labelled Arabidopsis plants. The plants during growth are fed with  $^{13}CO_2$  such that 80-90% of xylan molecules are labelled. I hence purified  $^{13}C$ -enriched GIPC using the same method as described in chapter 1. Although theoretically, for a GIPC series A t18:1/h24, the molecule is only 80% labelled by  $^{13}C$ , it could still worth using it more accurately as an internal standard instead of  $G_{M1}$  for LC-MS analysis of plant GIPC species.

### **GIPC and its interactants in the PM organisation *in vivo***

Described as mysterious, the lateral heterogeneity of PM and the relationships between the dynamics of membrane organization and cell signalling are key features being investigated in cell biology (Levental & Veatch, 2016)(Sezgin, Levental, Mayor, & Eggeling, 2017)(Grosjean et al., 2015a) showed that plant lipids in model membranes generate a biophysical heterogeneity with different order levels. The liquid ordered (lo) regions are domains that can be of the nano- or micro-scale level, depending on the type and spatial distribution of specific PM lipids and proteins in plants (Gerbeau-Pissot et al., 2014b; Gronnier et al., 2018; Raffaele et al., 2009).

Previous studies have demonstrated the link between plant/pathogen responses and the segregation of lipids and proteins, relocalization in PM regions modifying its order and fluidity to promote PM domains as signalling platforms (Gronnier et al., 2018)(T. Ott, 2017). Distinct PM nanodomains can be considered as signalling

platforms involved where plant immune responses and growth receptors are localized (Bücherl et al., 2017). What could GIPC role be in nanodomain formation *in vivo*? What impact does the structure of GIPC have in constituting lo domains in the outer leaflet and its potential repercussion on the plant phenotype and response to environmental stress?

A large part of the puzzle remains unsolved. Although we have shown that GIPC interacts preferentially with sterols, more precisely sitosterol to form domain-like structures on supported bilayer (refer to Chapter 1), we are missing essential pieces of information on the general composition and organization of plant nanodomains. The *in silico* through molecular modelling and biophysics experiments on model membranes are reliable data, but it is difficult to gauge at what extent it reflects the reality of plant PM. We usually use two or three lipids to model a membrane, be it supported bilayers or vesicles, which in no case account for the complexity of the composition of the plant PM. The use of membrane models, is a step forward into understanding this complexity and should not substitute *in vivo* experiments into asserting realities that do not exist.

The solution is to use arrays of complementary expertise on membrane biochemistry, lipid analysis, and modelling to develop an interdisciplinary approach to address the issue of comprehending the role of GIPC in plant PM asymmetry. The first step will be to make a vast repertoire of the different possible lipid interactants of GIPC in the plant PM using biophysics and modelling. By characterizing the lipid composition and *in vivo* biophysical characteristics (lateral segregation, degree of order...) of each leaflet of plant PM, we can tackle the question of plant PM asymmetry. This can be done using purified PM from tobacco BY-2 cells or *Arabidopsis* plantlets as described in Chapter 2. Use of RSO and ISO PM fractions treated by non-permeable lipases (phospholipases A1, A2, or sphingolipases) or labelled with lipid-specific antibodies and dyes can be the key on validating the plant PM model proposed by (Cacas et al., 2016a; Tjellstrom et al., 2010). Understanding the components of each leaflet will yield information on potential interactions between the two leaflets through interdigitation (Raghupathy et al., 2015). The information is still crucially lacking in plant membrane biology.

We showed in Chapter 2 that decreasing the acyl chain length of PM lipids containing VLCFA, affects outer leaflet marker (GPI-GFP) mobility. In the conclusion that was drawn, we considered the membrane protein mobility between the leaflets and the interactions of proteins associated to each leaflet as well as their respective composition and physical properties. These factors contribute to PM protein localization and regulation through processes largely unidentified. One important potential interaction that we aim to identify is the potential interaction of GIPC in the outer leaflet with PS in the inner leaflet. Both having VLCFA, we hypothesised that they can interdigitate as reported in (Raghupathy et al., 2015) making a link between extracellular matrix and actin for example. The team of Yvon Jaillais showed that PA and PS sensors accumulate in the PM cytosolic leaflet in Arabidopsis root epidermis, together with PI4P (Platre et al., 2018). This accumulation might confer the electrostatic characteristics of plant PM inner leaflet while we showed that GIPC confer strong electronegativity to the PM when inserted in model membrane. The precise localization of each molecular species of GIPCs in PM remain elusive. One solution could be to develop GIPC tags by using non-necrolytic NLP as described in Chapter 3. A “desactivated” NLP tag with GFP used as powerful biosensor that can bind to GIPC can be a solution to detect GIPC *in vivo*. By using RSO and ISO PM fractions, we will be able at least to detect the percentage of enrichment of GIPC in each leaflet.

The detection of the other components of the PM that can influence interdigitation is unknown. Since we used only lipid sensors targeting PI4P and PS *in vivo*, we do not have any indication about the localization of the different molecular species of free sterols and on the fatty acid associated with lipids.

### **GIPC-sterol interaction and GIPC role in membrane phase transition**

We used the Langmuir film balance methodology in compression mode to determine the molecular area of GIPC and each sterol (free or conjugated) and the cooperativity behaviour of the lipid components within one leaflet as already applied characterizing the specific interaction between GIPC and sitosterol, stigmasterol, SG or ASG (refer to Chapter 1). To understand more about the different interactions in the PM, we can do the same compression isotherms experiments with all the lipid binary combinations based on the lipidomic analysis performed on plant PM.

Within a mixed monolayer, if the two components are immiscible (or ideally miscible), the area occupied by the mixed film will be the sum of the areas of the separate components (obeying the additivity rule as described in (Maget-Dana, 1999)). Any deviation from the additivity rule can be attributed to a specific interaction between the two components (K. Fang, Zou, & He, 2003; Maget-Dana, 1999). The calculation of the excess free energy of mixing will give information about the repulsive or attractive nature of the interaction. In addition, the free energy of mixing will be calculated in order to evaluate the thermodynamic stability of the system and compare with data of theoretical docking using HyperMatrix or Big Monolayer molecular modelling. This will pave the way to molecular dynamic studies of the asymmetrical model of plan PM.

IR and NMR spectroscopies on model membrane (refer to Chapter 1, Additional Data) will be useful not only to identify aspect of the lipid-lipid interactions but also to characterize the lipid chain dynamics in the monolayer. For instance, we showed that solid-state NMR ( $^2\text{H}$ -NMR on liposomes) is quite useful to determine the order properties of the lipid system. This experiment was not conclusive due to quantitative issues of lipids. Other sterols can be tested by both IR and NMR experiments, performed over a range of temperatures so as to determine the phase transition temperature of the different PM lipids and the influence of each other. The data generated will be useful for modelling parametrization. We can also determine the transition temperature of GIPC using differential scanning calorimetry (DSC). The transition temperature of GIPC is important as we tend to heat till  $60^\circ\text{C}$  when purifying and solubilizing GIPC in solvents. The importance of GIPC in membrane phase transition closer to a plant PM model can be done by modifying the carbon terminal of the GIPC acyl chain with a  $^{13}\text{C}$  and perform solid-state  $^{13}\text{C}$ -NMR.

*In vivo*, environment-sensitive probes specific to each leaflet coupled with fluorescence spectroscopy can be a powerful approach for imaging membrane biophysical properties and organization (Oncul et al., 2010). Hence we can use PM of tobacco and Arabidopsis cells to investigate the overall order level of both leaflets and correlate with lipidomic analysis of each leaflet to have a better understanding of how *in vivo* lipid may influence the physical state of each leaflet of plant PM.

Characterizing all the lipid dynamics of the membrane is quite challenging. The use of super-resolution microscopy and single-particle tracking as suggested in Chapter 2 to track particular lipid species can give valuable information on the diffusion, confinement and segregation of particular lipid in PM (Levental & Veatch, 2016) (Platre et al., 2019a). In order to map all PM lipids, it is best to consider the combined use of super-resolution imaging and molecular modelling. Recently, the work of (Gronnier et al., 2017) provided unique insight on how the control of spatial segregation is critical to support biological function related to plant immunity. They showed that this segregation was specific to the PM inner leaflet and was directly related to the lipid composition, in particular sterols.

### **Quid of the polar head group of GIPC?**

The identification and characterization of the polar head group of GIPC remain an imperative. In the structuring of the plant PM, GIPC have all the necessary qualities to be involved in the umbrella effect. The umbrella model states that the shift between the small polar head of cholesterol and its large apolar body determines its preferential association with some adjacent molecules of the membrane (Huang, 2002). In this model, cholesterol is covered by the polar heads of neighbouring phospholipids to limit the unfavourable free energy due to the exposure of the apolar portion of cholesterol to water molecules. The polar head group of GIPC seems to be an ideal candidate to shelter the apolar portion of sterols in plant PM. Could the polar head size of GIPC be determinant in favouring GIPC/sterol interactions in plant PM? (Cacas et al., 2016a) showed that polyglycosylated GIPC were mainly in the DRMs. The combination of simulation and compression isotherms experiments appears to be a good approach to determine the importance of polar head group of GIPC in domain formation, phase transition through its interaction with sterols.

The polar head group of GIPC is also involved in cell wall - PM continuum, more precisely GIPC is linked to rhamnogalacturonan II (RGII) through a boron bridge. Yotam Navon, one of our collaborators in my PhD project, works on cellulose nanocrystals (CNC). He showed the preferential interaction of GIPC with CNCs in presence of calcium ions (data not published). This opens doors on investigating more

about the role of GIPC in cell wall-PM continuum. There are also hypotheses that polyglycosylated GIPC could be a scaffold providing sugar moieties for the cell wall construction.

In plant host/pathogen interactions, the sugar head group of GIPC proved to be decisive in determining the host sensitivity to necrotoxin NLP (Lenarčič et al., 2017b). It will be interesting to decipher the mechanism of NLP anchoring and pore formation upon binding to GIPC as discussed in Chapter 3. Unexpectedly, a few experiments that I performed during the beginning of my PhD project showed the importance of the polar head group of GIPC in interacting with surfactin (collaboration with Marc Ongena, Gembloux Agro-Bio Tech, and Magali Deleu, LBMI). The data are not yet published but it seems that gluCER rather than mutated GIPC, bind preferentially to surfactin. This study evidences that all sugar-containing lipids may serve as receptor to plant elicitors and toxins.

### **Molecular modelling and molecular dynamics simulation of plant PM components**

The use of modelling approaches will be inevitable in order to provide a comprehensive model of the plant PM bilayer. With data generated by biophysics experiments (Langmuir trough, NMR or IR) to fuel the topologies of lipids, molecular dynamic simulation studies seem to be the best option to provide a dynamic model of a realistic plant PM just like (Ingólfsson et al., 2014) for animal PM model.

In this project, we experimentally observed thermodynamically stable interaction between cauliflower GIPC and the plant specific sterol, sitosterol. This was further confirmed by the use of a theoretical docking method indicating a good steric fit between the two molecules. This interaction was however reversed in the case of GIPC and stigmasterol (Chapter1). In (Cacas et al., 2016a) simulations were done to compare the behaviour of GIPCs with t18:0/h24:0 and the one of gluCER with d18:2/ h16:0 regarding their insertion in a simplified bilayer. The results indicated that the size of the polar heads and the positioning of acyl chains are strikingly different and that the saturated VLCFA of GIPCs runs out of the middle of the bilayer and interdigitates by at least six to seven carbon atoms within the inner leaflet.

In our project, the same docking methodology also suggests that the interaction of a GIPC molecule with sitosterol and stigmasterol are different, notably by the positioning of the  $\alpha$  face of the sterols. Surface pressure measurements have confirmed that GIPC/Sitosterol interactions are cooperative while GIPC/stigmasterol are not (Chapter 1). This docking approach known as HyperMatrix (HM) enables the study specific lipid-lipid interactions. HM can be used as a screening approach to match interesting binary lipid interactions before MD simulation which is more time-consuming and intensive. These two approaches are complementary to successfully describe PM lipid-lipid interactions. MD simulations can also yield order parameters of acyl chain of the lipids in the bilayer, which can be compared to NMR and IR data.

Once the asymmetric plant PM is obtained by MD simulation, we can use the data to build MD topologies to understand the binding and pore formation process of phytotoxins such as NLP upon binding to the plant PM. A realistic plant PM model will be an essential tool to understand molecular details of the membrane activity especially in plant immune signalling.

In order to understand the ability of plant cells to face different biotic and abiotic stresses, it is undoubtedly necessary to decipher the basis of PM organization at the molecular level. The crucial aspect of PM organisation to study is PM asymmetry to confirm that GIPC is evidently representing 90% of the sphingolipid of PM outer leaflet. With a combination of approaches, the future aim should be to develop a single model of a more accurate perspective of plant PM. The deciphering of a plant model PM organisation from molecular to cellular scale is long due. In an era where climate change is a scientific, political and social reality, it is of utmost importance to anticipate plant responses to ever changing environmental fluctuations. This goes through the better understanding of the molecular mechanisms of the PM, whose global organisation play a role in setting up plant responses.

# Annexes



## *Formation Universitaire*

**2017-2018 – Thèse en biologie végétale.** Titre du sujet de thèse : Les Glycosyl-Inositol Phosphoryl Céràmides (GIPCs), sphingolipides majeurs des plantes, rôle dans la structuration membranaire et dans les relations hôte-pathogènes chez les **plantes (boursier MRENT, classé 3<sup>ème</sup> au concours de l'ED)**

2014-2016 – **Master 2 Recherche Biologie et Biotechnologie des Plantes et Espèces Fongiques**, Université de Bordeaux, mention **TB (1/17)**

2014 – **Diplôme de Licence Science De la Vie Biologie, Santé** (Spécialité Biologie Moléculaire Cellulaire & Physiologie) Université de Bordeaux, mention AB

## *Expériences et Compétences acquises*

- Participation au congrès **FEBS Special Meeting in Sphingolipid Biology 2019** et participation à un flash présentation
- Participation au congrès **Gordon Research Conference 2019 Plant Lipids: Structure, Metabolism and Function**: présentation de poster
- Participation au congrès GEM XIX: Congrès international du Groupe d'Etude des Membranes
- Conférence **Tsukuba Global Science Week TGSW 2016**, Japon – Présentation orale au symposium international sur la formation en Bio-Entreprenariat
- Formations complémentaires en :
  - Enseignement par l'Enseignement,**
  - Communication et Gestion des conflits,**
  - Expression écrite, fondamentaux écrits professionnels,**
  - Affirmation de soi**
  - Introduction à la mesure de la mobilité des protéines par FRAP, FCS et SPT,**
- **96h de mission d'enseignement TP** Licence 2 et Licence 3 Biologie Végétale - (2017-2019)
- Stage à **Rothamsted Research** avec Dr. Michealson sur l'analyses lipidomiques de sphingolipides de plantes, au **Laboratoire de Biophysique Moléculaire et des Interfaces, Gembloux, Belgique** avec Dr. Deleu sur la biophysique des membranes, au **Laboratoire de Biogenèse membranaire, Bordeaux** avec Dr. Mongrand sur la biochimie des lipides de plantes – Janvier à Juin 2015 (Master 2) sur l'optimisation et caractérisation en biophysique des GIPCs
- **Informatique**: C2i ; Outil bioinformatique tel que 'R' ; ImageJ **Linguistique** : Français DALF C1 ; Anglais Niveau C2

## *Publications scientifiques*

**Eudicot plant-specific sphingolipids determine host selectivity of microbial NLP cytolysins.** Lenarčič et al., *Science* 358, 1431-1434 (2017), 18<sup>ème</sup>/25 auteur

**Progress in Lipid Research : "Plant lipids: key players of plasma membrane organization and function",** 1<sup>er</sup> auteur

**News and Views: Lipids light up in plant membranes.** Mamode Cassim, A., Mongrand, S., *Nat. Plants* 5, 913–914 (2019)

# References

- Alessandrini, A., & Facci, P. (2005, June 1). AFM: A versatile tool in biophysics. *Measurement Science and Technology*, Vol. 16. <https://doi.org/10.1088/0957-0233/16/6/R01>
- Ali, U., Li, H., Wang, X., & Guo, L. (2018, October 15). Emerging Roles of Sphingolipid Signaling in Plant Response to Biotic and Abiotic Stresses. *Molecular Plant*, Vol. 11, pp. 1328–1343. <https://doi.org/10.1016/j.molp.2018.10.001>
- Anderluh, G., & Maček, P. (2002). Cytolytic peptide and protein toxins from sea anemones (Anthozoa: Actiniaria). *Toxicon*, Vol. 40, pp. 111–124. [https://doi.org/10.1016/S0041-0101\(01\)00191-X](https://doi.org/10.1016/S0041-0101(01)00191-X)
- Bach, L., & Faure, J.-D. (2010). Role of very-long-chain fatty acids in plant development, when chain length does matter. *C. R. Biologies*, 333, 361–370. <https://doi.org/10.1016/j.crv.2010.01.014>
- Baumgart, T., Hunt, G., Farkas, E. R., Webb, W. W., & Feigenson, G. W. (2007). Fluorescence probe partitioning between Lo/Ld phases in lipid membranes. *Biochimica et Biophysica Acta - Biomembranes*, 1768(9), 2182–2194. <https://doi.org/10.1016/j.bbmem.2007.05.012>
- Beck, J. G., Mathieu, D., Loudet, C., Buchoux, S., & Dufourc, E. J. (2007a). Plant sterols in “rafts”: a better way to regulate membrane thermal shocks. *The FASEB Journal*, 21(8), 1714–1723. <https://doi.org/10.1096/fj.06-7809com>
- Beck, J. G., Mathieu, D., Loudet, C., Buchoux, S., & Dufourc, E. J. (2007b). Plant sterols in “rafts”: A better way to regulate membrane thermal shocks. *FASEB Journal*, 21(8), 1714–1723. <https://doi.org/10.1096/fj.06-7809com>
- Blaas, N., & Humpf, H. U. (2013). Structural profiling and quantitation of glycosyl inositol phosphoceramides in plants with fourier transform mass spectrometry. *Journal of Agricultural and Food Chemistry*. <https://doi.org/10.1021/jf4001499>
- Bücherl, C. A., Jarsch, I. K., Schudoma, C., Segonzac, C., Mbengue, M., Robatze, S., ... Zipfe, C. (2017). Plant immune and growth receptors share common signalling components but localise to distinct plasma membrane nanodomains. *ELife*, 6. <https://doi.org/10.7554/eLife.25114>
- Buré, C., Cacas, J. L., Badoc, A., Mongrand, S., & Schmitter, J. M. (2016). Branched glycosylated inositolphosphosphingolipid structures in plants revealed by MS3analysis. *Journal of Mass Spectrometry*. <https://doi.org/10.1002/jms.3758>
- Buré, C., Cacas, J. L., Mongrand, S., & Schmitter, J. M. (2014). Characterization of glycosyl inositol phosphoryl ceramides from plants and fungi by mass spectrometry. *Analytical and Bioanalytical Chemistry*, Vol. 406, pp. 995–1010. <https://doi.org/10.1007/s00216-013-7130-8>
- Buré, C., Cacas, J. L., Wang, F., Gaudin, K., Domergue, F., Mongrand, S., & Schmitter, J. M. (2011). Fast screening of highly glycosylated plant sphingolipids by tandem mass spectrometry. *Rapid Communications in Mass Spectrometry*. <https://doi.org/10.1002/rcm.5206>
- Cacas, J. L., Buré, C., Furt, F., Maalouf, J. P., Badoc, A., Cluzet, S., ... Mongrand, S. (2013). Biochemical survey of the polar head of plant glycosylinositolphosphoceramides unravels broad diversity. *Phytochemistry*. <https://doi.org/10.1016/j.phytochem.2013.08.002>
- Cacas, J. L., Buré, C., Grosjean, K., Gerbeau-Pissot, P., Lherminier, J., Rombouts, Y., ... Mongrand, S. (2016a). Revisiting plant plasma membrane lipids in tobacco: A focus on sphingolipids. *Plant Physiology*, 170(1), 367–384. <https://doi.org/10.1104/pp.15.00564>

- Cacas, J. L., Buré, C., Grosjean, K., Gerbeau-Pissot, P., Lherminier, J., Rombouts, Y., ... Mongrand, S. (2016b). Revisiting plant plasma membrane lipids in tobacco: A focus on sphingolipids. *Plant Physiology*, *170*(1), 367–384. <https://doi.org/10.1104/pp.15.00564>
- CARTER, H. E., GIGG, R. H., LAW, J. H., NAKAYAMA, T., & WEBER, E. (1958). Biochemistry of the sphingolipides. XI. Structure of phytoglycolipide. *The Journal of Biological Chemistry*, *233*(6), 1309–1314. Retrieved from <http://www.jbc.org/>
- Carter, H. E., Strobach, D. R., & Hawthorne, J. N. (1969). Biochemistry of the Sphingolipids. XVIII. Complete Structure of Tetrasaccharide Phytoglycolipid. *Biochemistry*, *8*(1), 383–388. <https://doi.org/10.1021/bi00829a053>
- Carter, H E, & Koob, J. L. (1969). Sphingolipids in bean leaves (*Phaseolus vulgaris*). *Journal of Lipid Research*, *10*(4), 363–369.
- Carter, Herbert E, Brooks, S., Gigg, R. H., Strobach, D. R., & Suami~, T. (1964). Biochemistry of the Sphingolipids XVI. STRUCTURE OF PHYTOGLYCOLIPID\*. *THE JOURNAL OF BIOLOGICAL CHEMISTRY*, *239*(3).
- Chen, M., Han, G., Dietrich, C. R., Dunn, T. M., & Cahoon, E. B. (2006). The Essential Nature of Sphingolipids in Plants as Revealed by the Functional Identification and Characterization of the Arabidopsis LCB1 Subunit of Serine Palmitoyltransferase. *THE PLANT CELL ONLINE*. <https://doi.org/10.1105/tpc.105.040774>
- Chen, Ming, Markham, J. E., & Cahoon, E. B. (2012). Sphingolipid  $\Delta 8$  unsaturation is important for glucosylceramide biosynthesis and low-temperature performance in Arabidopsis. *Plant Journal*, *69*(5), 769–781. <https://doi.org/10.1111/j.1365-313X.2011.04829.x>
- Contreras, F. X., Villar, A. V., Alonso, A., Kolesnick, R. N., & Goñi, F. M. (2003). Sphingomyelinase activity causes transbilayer lipid translocation in model and cell membranes. *Journal of Biological Chemistry*, *278*(39), 37169–37174. <https://doi.org/10.1074/jbc.M303206200>
- Courtney, K., Pezeshkian, W., Raghupathy, R., Zhang, G., Darbyson, A., Ipsen, J., ... Zha, X. (2017). C24 sphingolipids play a surprising and central role in governing cholesterol and lateral organization of the live cell plasma membrane. 212142. <https://doi.org/10.1101/212142>
- Črnigoj Kristan, K., Viero, G., Dalla Serra, M., Maček, P., & Anderluh, G. (2009). Molecular mechanism of pore formation by actinoporins. *Toxicon*, *54*(8), 1125–1134. <https://doi.org/10.1016/j.toxicon.2009.02.026>
- Daen, J. (1966). Insoluble monolayers at liquid-gas interfaces. *Journal of Colloid and Interface Science*, *22*(3), 309. [https://doi.org/10.1016/0021-9797\(66\)90041-5](https://doi.org/10.1016/0021-9797(66)90041-5)
- Deleu, M., Crowet, J. M., Nasir, M. N., & Lins, L. (2014). Complementary biophysical tools to investigate lipid specificity in the interaction between bioactive molecules and the plasma membrane: A review. *Biochimica et Biophysica Acta - Biomembranes*, *1838*(12), 3171–3190. <https://doi.org/10.1016/j.bbamem.2014.08.023>
- Dietrich, C., Yang, B., Fujiwara, T., Kusumi, A., & Jacobson, K. (2002). Relationship of lipid rafts to transient confinement zones detected by single particle tracking. *Biophysical Journal*, *82*(1), 274–284. [https://doi.org/10.1016/S0006-3495\(02\)75393-9](https://doi.org/10.1016/S0006-3495(02)75393-9)
- Dinic, J., Biverståhl, H., Mäler, L., & Parmryd, I. (2011). Laurdan and di-4-ANEPPDHQ do not respond to membrane-inserted peptides and are good probes for lipid packing. *Biochimica et Biophysica*

- Acta - Biomembranes*, 1808(1), 298–306. <https://doi.org/10.1016/j.bbamem.2010.10.002>
- Dynarowicz-Łątka, P., Dhanabalan, A., & Oliveira, O. N. (2001). Modern physicochemical research on Langmuir monolayers. *Advances in Colloid and Interface Science*, Vol. 91, pp. 221–293. [https://doi.org/10.1016/S0001-8686\(99\)00034-2](https://doi.org/10.1016/S0001-8686(99)00034-2)
- Eeman, M., & Deleu, M. (2010). From biological membranes to biomimetic model membranes. *Biotechnology, Agronomy and Society and Environment*, 14(4), 719–736.
- Eggeling, C., Ringemann, C., Medda, R., Schwarzmann, G., Sandhoff, K., Polyakova, S., ... Hell, S. W. (2009). Direct observation of the nanoscale dynamics of membrane lipids in a living cell. *Nature*, 457(7233), 1159–1162. <https://doi.org/10.1038/nature07596>
- El Kirat, K., Morandat, S., & Dufrêne, Y. F. (2010, April). Nanoscale analysis of supported lipid bilayers using atomic force microscopy. *Biochimica et Biophysica Acta - Biomembranes*, Vol. 1798, pp. 750–765. <https://doi.org/10.1016/j.bbamem.2009.07.026>
- Engel, A., Gaub, H. E., & Müller, D. J. (1999). Atomic force microscopy: A forceful way with single molecules. *Current Biology*, Vol. 9. [https://doi.org/10.1016/S0960-9822\(99\)80081-5](https://doi.org/10.1016/S0960-9822(99)80081-5)
- Engelman, D. M. (2005). Membranes are more mosaic than fluid. *Nature*, 438(7068), 578–580. <https://doi.org/10.1038/nature04394>
- Fang, K., Zou, G., & He, P. (2003). Dynamic viscoelastic properties of spread monostearin monolayer in the presence of glycine. *Journal of Colloid and Interface Science*, 266(2), 407–414. [https://doi.org/10.1016/S0021-9797\(03\)00505-8](https://doi.org/10.1016/S0021-9797(03)00505-8)
- Fang, L., Ishikawa, T., Rennie, E. A., Murawska, G. M., Lao, J., Yan, J., ... Mortimer, J. C. (2016). Loss of Inositol Phosphorylceramide Sphingolipid Mannosylation Induces Plant Immune Responses and Reduces Cellulose Content in Arabidopsis. *The Plant Cell*. <https://doi.org/10.1105/tpc.16.00186>
- Florine, K. I., & Feigenson, G. W. (1987). Protein Redistribution in Model Membranes: Clearing of M13 Coat Protein from Calcium-Induced Gel-Phase Regions in Phosphatidylserine/Phosphatidyletholine Multilamellar Vesicles. *Biochemistry*, 26(11), 2978–2983. <https://doi.org/10.1021/bi00385a004>
- Fujimoto, T., & Parmryd, I. (2017, January 10). Interleaflet coupling, pinning, and leaflet asymmetry—major players in plasma membrane nanodomain formation. *Frontiers in Cell and Developmental Biology*, Vol. 4. <https://doi.org/10.3389/fcell.2016.00155>
- Furt, F., Lefebvre, B., Cullimore, J., Bessoule, J. J., & Mongrand, S. (2007). Plant lipid rafts: Fluctuat nec mergitur. *Plant Signaling and Behavior*, 2(6), 508–511. <https://doi.org/10.4161/psb.2.6.4636>
- Furt, F., Simon-Plas, F., & Mongrand, S. (2010). Lipids of the plant plasma membrane. *Plant Cell Monographs*, 19, 3–30. [https://doi.org/10.1007/978-3-642-13431-9\\_1](https://doi.org/10.1007/978-3-642-13431-9_1)
- Geldner, N., Déneraud-Tendon, V., Hyman, D. L., Mayer, U., Stierhof, Y. D., & Chory, J. (2009). Rapid, combinatorial analysis of membrane compartments in intact plants with a multicolor marker set. *Plant Journal*, 59(1), 169–178. <https://doi.org/10.1111/j.1365-313X.2009.03851.x>
- Gerbeau-Pissot, P., Der, C., Grebe, M., & Stanislas, T. (2016). Ratiometric fluorescence live imaging analysis of membrane lipid order in arabidopsis mitotic cells using a lipid order-sensitive probe. In *Methods in Molecular Biology* (Vol. 1370, pp. 227–239). <https://doi.org/10.1007/978-1-4939->

- Gerbeau-Pissot, P., Der, C., Thomas, D., Anca, I.-A., Grosjean, K., Roche, Y., ... Simon-Plas, F. (2014a). Modification of Plasma Membrane Organization in Tobacco Cells Elicited by Cryptogein. *PLANT PHYSIOLOGY*, *164*(1), 273–286. <https://doi.org/10.1104/pp.113.225755>
- Gerbeau-Pissot, P., Der, C., Thomas, D., Anca, I. A., Grosjean, K., Roche, Y., ... Simon-Plas, F. (2014b). Modification of plasma membrane organization in tobacco cells elicited by cryptogein. *Plant Physiology*, *164*(1), 273–286. <https://doi.org/10.1104/pp.113.225755>
- Giner-Casares, J. J., Brezesinski, G., & Möhwald, H. (2014). Langmuir monolayers as unique physical models. *Current Opinion in Colloid and Interface Science*, Vol. 19, pp. 176–182. <https://doi.org/10.1016/j.cocis.2013.07.006>
- Giocondi, M. C., Yamamoto, D., Lesniewska, E., Milhiet, P. E., Ando, T., & Le Grimellec, C. (2010). Surface topography of membrane domains. *Biochimica et Biophysica Acta - Biomembranes*, *1798*(4), 703–718. <https://doi.org/10.1016/j.bbamem.2009.09.015>
- Goldenberg, N. M., & Steinberg, B. E. (2010, February 15). Surface charge: A key determinant of protein localization and function. *Cancer Research*, Vol. 70, pp. 1277–1280. <https://doi.org/10.1158/0008-5472.CAN-09-2905>
- Goñi, F. M. (2014). The basic structure and dynamics of cell membranes: an update of the Singer-Nicolson model. *Biochimica et Biophysica Acta*, *1838*(6), 1467–1476. <https://doi.org/10.1016/j.bbamem.2014.01.006>
- Green, W. (1991). Surface Charges And Ion Channel Function. *Annual Review of Physiology*, *53*(1), 341–359. <https://doi.org/10.1146/annurev.physiol.53.1.341>
- Grelard, A., Couvreur, A., Loudet, C., & Dufourc, E. J. (2009). Solution and solid-state NMR of lipids. *Methods in Molecular Biology (Clifton, N.J.)*, *462*, 111–133. [https://doi.org/10.1007/978-1-60327-115-8\\_7](https://doi.org/10.1007/978-1-60327-115-8_7)
- Griebel, T., & Zeier, J. (2010). A role for  $\beta$ -sitosterol to stigmasterol conversion in plant-pathogen interactions. *Plant Journal*, *63*(2), 254–268. <https://doi.org/10.1111/j.1365-313X.2010.04235.x>
- Grisson, M. S., Brocard, L., Fouillen, L., Nicolas, W., Wewer, V., Dörmann, P., ... Bayer, E. M. (2015). Specific membrane lipid composition is important for plasmodesmata function in arabidopsis. *Plant Cell*, *27*(4), 1228–1250. <https://doi.org/10.1105/tpc.114.135731>
- Gronnier, J., Crowet, J. M., Habenstein, B., Nasir, M. N., Bayle, V., Hosy, E., ... Mongrand, S. (2017). Structural basis for plant plasma membrane protein dynamics and organization into functional nanodomains. *ELife*, *6*. <https://doi.org/10.7554/eLife.26404>
- Gronnier, J., Gerbeau-Pissot, P., Germain, V., Mongrand, S., & Simon-Plas, F. (2018, October 1). Divide and Rule: Plant Plasma Membrane Organization. *Trends in Plant Science*, Vol. 23, pp. 899–917. <https://doi.org/10.1016/j.tplants.2018.07.007>
- Gronnier, J., Germain, V., Gouguet, P., Cacas, J. L., & Mongrand, S. (2016). GIPC: Glycosyl inositol phospho ceramides, the major sphingolipids on earth. *Plant Signaling and Behavior*. <https://doi.org/10.1080/15592324.2016.1152438>
- Gronnier, J., Legrand, A., Loquet, A., Habenstein, B., Germain, V., & Mongrand, S. (2019). Mechanisms governing subcompartmentalization of biological membranes. *Current Opinion in*

- Grosjean, K., Der, C., Robert, F., Thomas, D., Mongrand, S., Simon-Plas, F., & Gerbeau-Pissot, P. (2018). Interactions between lipids and proteins are critical for organization of plasma membrane-ordered domains in tobacco BY-2 cells. *Journal of Experimental Botany*, 69(15), 3545–3557. <https://doi.org/10.1093/jxb/ery152>
- Grosjean, K., Mongrand, S., Beney, L., Simon-Plas, F., & Gerbeau-Pissot, P. (2015a). Differential effect of plant lipids on membrane organization specificities of phytosphingolipids and phytosterols. *Journal of Biological Chemistry*, 290(9), 5810–5825. <https://doi.org/10.1074/jbc.M114.598805>
- Grosjean, K., Mongrand, S., Beney, L., Simon-Plas, F., & Gerbeau-Pissot, P. (2015b). Differential effect of plant lipids on membrane organization specificities of phytosphingolipids and phytosterols. *Journal of Biological Chemistry*, 290(9), 5810–5825. <https://doi.org/10.1074/jbc.M114.598805>
- Gutierrez, A. L. S., Farage, L., Melo, M. N., Mohana-Borges, R. S., Guerardel, Y., Coddeville, B., ... Guerardel, Y. (2007). Characterization of glycoinositolphosphoryl ceramide structure mutant strains of *Cryptococcus neoformans*. *Glycobiology*. <https://doi.org/10.1093/glycob/cwm030>
- Haslam, T. M., & Kunst, L. (2013, September). Extending The Story Of Very-Long-Chain Fatty Acid Elongation. *Plant Science*, Vol. 210, pp. 93–107. <https://doi.org/10.1016/j.plantsci.2013.05.008>
- Heerklotz, H., & Seelig, J. (2000). Titration calorimetry of surfactant-membrane partitioning and membrane solubilization. *Biochimica et Biophysica Acta - Biomembranes*, Vol. 1508, pp. 69–85. [https://doi.org/10.1016/S0304-4157\(00\)00009-5](https://doi.org/10.1016/S0304-4157(00)00009-5)
- Heilmann, I. (2016). Phosphoinositide signaling in plant development. *Development (Cambridge)*, 143(12), 2044–2055. <https://doi.org/10.1242/dev.136432>
- Hilbi, H., Weber, S., & Finsel, I. (2011). Anchors for effectors: Subversion of phosphoinositide lipids by *Legionella*. *Frontiers in Microbiology*, 2(APR). <https://doi.org/10.3389/fmicb.2011.00091>
- Hirano, T., Stecker, K., Munnik, T., Xu, H., & Sato, M. H. (2017). Visualization of Phosphatidylinositol 3,5-Bisphosphate Dynamics by a Tandem ML1N-Based Fluorescent Protein Probe in *Arabidopsis*. *Plant and Cell Physiology*, 58(7), 1185–1195. <https://doi.org/10.1093/pcp/pcx011>
- Hou, Q., Ufer, G., & Bartels, D. (2016). Lipid signalling in plant responses to abiotic stress. *Plant, Cell & Environment*, 39(5), 1029–1048. <https://doi.org/10.1111/pce.12666>
- Hruz, T., Laule, O., Szabo, G., Wessendorp, F., Bleuler, S., Oertle, L., ... Zimmermann, P. (2008). Genevestigator V3: A Reference Expression Database for the Meta-Analysis of Transcriptomes. *Advances in Bioinformatics*, 2008, 1–5. <https://doi.org/10.1155/2008/420747>
- Hsieh, T. C., Lester, R. L., & Laine, R. A. (1981). Glycophosphoceramides from plants. Purification and characterization of a novel tetrasaccharide derived from tobacco leaf glycolipids. *Journal of Biological Chemistry*.
- Huang, J. (2002). Exploration of molecular interactions in cholesterol superlattices: Effect of multibody interactions. *Biophysical Journal*, 83(2), 1014–1025. [https://doi.org/10.1016/S0006-3495\(02\)75227-2](https://doi.org/10.1016/S0006-3495(02)75227-2)
- Ingólfsson, H. I., Melo, M. N., Van Eerden, F. J., Arnarez, C., Lopez, C. A., Wassenaar, T. A., ... Marrink, S. J. (2014). Lipid organization of the plasma membrane. *Journal of the American Chemical Society*, 136(41), 14554–14559. <https://doi.org/10.1021/ja507832e>

- Ishikawa, T., Fang, L., Rennie, E. A., Sechet, J., Yan, J., Jing, B., ... Mortimer, J. C. (2018). GLUCOSAMINE INOSITOLPHOSPHORYLCERAMIDTRANSFERASE1 (GINT1) is a GlcNAc-containing glycosylinositol phosphorylceramide glycosyltransferase. *Plant Physiology*, *177*(3), 938–952. <https://doi.org/10.1104/pp.18.00396>
- Ismail, A., Takeda, S., & Nick, P. (2014). Life and death under salt stress: Same players, different timing? *Journal of Experimental Botany*, Vol. 65, pp. 2963–2979. <https://doi.org/10.1093/jxb/eru159>
- Jelesarov, I., & Bosshard, H. R. (1999). Isothermal titration calorimetry and differential scanning calorimetry as complementary tools to investigate the energetics of biomolecular recognition. *Journal of Molecular Recognition*, Vol. 12, pp. 3–18. [https://doi.org/10.1002/\(SICI\)1099-1352\(199901/02\)12:1<3::AID-JMR441>3.0.CO;2-6](https://doi.org/10.1002/(SICI)1099-1352(199901/02)12:1<3::AID-JMR441>3.0.CO;2-6)
- Jiang, Z., Zhou, X., Tao, M., Yuan, F., Liu, L., Wu, F., ... Pei, Z.-M. (2019). Plant cell-surface GIPC sphingolipids sense salt to trigger Ca<sup>2+</sup> influx. *Nature*. <https://doi.org/10.1038/s41586-019-1449-z>
- Jin, L., Millard, A. C., Wuskell, J. P., Clark, H. A., & Loew, L. M. (2005). Cholesterol-enriched lipid domains can be visualized by di-4-ANEPPDHQ with linear and nonlinear optics. *Biophysical Journal*, *89*(1). <https://doi.org/10.1529/biophysj.105.064816>
- Jin, L., Millard, A. C., Wuskell, J. P., Dong, X., Wu, D., Clark, H. A., & Loew, L. M. (2006). Characterization and application of a new optical probe for membrane lipid domains. *Biophysical Journal*, *90*(7), 2563–2575. <https://doi.org/10.1529/biophysj.105.072884>
- Joubès, J., Raffaele, S., Bourdenx, B., Garcia, C., Laroche-Traineau, J., Moreau, P., ... Lessire, R. (2008). The VLCFA elongase gene family in *Arabidopsis thaliana*: Phylogenetic analysis, 3D modelling and expression profiling. *Plant Molecular Biology*, *67*(5), 547–566. <https://doi.org/10.1007/s11103-008-9339-z>
- Kaplan, M., Narasimhan, S., de Heus, C., Mance, D., van Doorn, S., Houben, K., ... Baldus, M. (2016). EGFR Dynamics Change during Activation in Native Membranes as Revealed by NMR. *Cell*, *167*(5), 1241–1251.e11. <https://doi.org/10.1016/j.cell.2016.10.038>
- Kaul, K., & Lester, R. L. (1975). Characterization of Inositol-containing Phosphosphingolipids from Tobacco Leaves. *Plant Physiology*, *55*(1), 120–129. <https://doi.org/10.1104/pp.55.1.120>
- Kaul, K., & Lester, R. L. (1978). Isolation of Six Novel Phosphoinositol-Containing Sphingolipids from Tobacco Leaves. *Biochemistry*, *17*(17), 3569–3575. <https://doi.org/10.1021/bi00610a023>
- Kawaguchi, M., Imai, H., Naoe, M., Yasui, Y., & Ohnishi, M. (2000). Cerebrosides in grapevine leaves: Distinct composition of sphingoid bases among the grapevine species having different tolerances to freezing temperature. *Bioscience, Biotechnology and Biochemistry*, *64*(6), 1271–1273. <https://doi.org/10.1271/bbb.64.1271>
- Kim, J., Jung, J. H., Lee, S. B., Go, Y. S., Kim, H. J., Cahoon, R., ... Suh, M. C. (2013). Arabidopsis 3-ketoacyl-coenzyme a synthase9 is involved in the synthesis of tetracosanoic acids as precursors of cuticular waxes, suberins, sphingolipids, and phospholipids. *Plant Physiology*, *162*(2), 567–580. <https://doi.org/10.1104/pp.112.210450>
- Kitazawa, K., Tryfona, T., Yoshimi, Y., Hayashi, Y., Kawauchi, S., Antonov, L., ... Kotake, T. (2013).  $\beta$ -Galactosyl Yariv Reagent Binds to the  $\beta$ -1,3-Galactan of Arabinogalactan Proteins. *Plant*

*Physiology*, 161(3), 1117–1126. <https://doi.org/10.1104/pp.112.211722>

- Kubsch, B., Robinson, T., Steinkühler, J., & Dimova, R. (2017). Phase behavior of charged vesicles under symmetric and asymmetric solution conditions monitored with fluorescence microscopy. *Journal of Visualized Experiments*, 2017(128). <https://doi.org/10.3791/56034>
- Kusumi, A., Ike, H., Nakada, C., Murase, K., & Fujiwara, T. (2005). Single-molecule tracking of membrane molecules: Plasma membrane compartmentalization and dynamic assembly of raft-philic signaling molecules. *Seminars in Immunology*, 17(1), 3–21. <https://doi.org/10.1016/j.smim.2004.09.004>
- Ledeer, R. W., & Wu, G. (2015, July 1). The multi-tasked life of GM1 ganglioside, a true factotum of nature. *Trends in Biochemical Sciences*, Vol. 40, pp. 407–418. <https://doi.org/10.1016/j.tibs.2015.04.005>
- Lee, S.-B., Jung, S.-J., Go, Y.-S., Kim, H.-U., Kim, J.-K., Cho, H.-J., ... Suh, M.-C. (2009). Two Arabidopsis 3-ketoacyl CoA synthase genes, *KCS20* and *KCS2 / DAISY*, are functionally redundant in cuticular wax and root suberin biosynthesis, but differentially controlled by osmotic stress. *The Plant Journal*, 60(3), 462–475. <https://doi.org/10.1111/j.1365-3113X.2009.03973.x>
- Lefebvre, B., Furt, F., Hartmann, M.-A., Michaelson, L. V., Carde, J.-P., Sargueil-Boiron, F., ... Mongrand, S. (2007). Characterization of Lipid Rafts from Medicago truncatula Root Plasma Membranes: A Proteomic Study Reveals the Presence of a Raft-Associated Redox System. *PLANT PHYSIOLOGY*, 144(1), 402–418. <https://doi.org/10.1104/pp.106.094102>
- Lenarčič, T., Albert, I., Böhm, H., Hodnik, V., Pirc, K., Zavec, A. B., ... Nürnberger, T. (2017a). Eudicot plant-specific sphingolipids determine host selectivity of microbial NLP cytolysins. *Science*, 358(6369), 1431–1434. <https://doi.org/10.1126/science.aan6874>
- Lenarčič, T., Albert, I., Böhm, H., Hodnik, V., Pirc, K., Zavec, A. B., ... Nürnberger, T. (2017b). Eudicot plant-specific sphingolipids determine host selectivity of microbial NLP cytolysins. *Science*. <https://doi.org/10.1126/science.aan6874>
- Lenarčič, T., Pirc, K., Hodnik, V., Albert, I., Borišek, J., Magistrato, A., ... Anderluh, G. (2019). Molecular basis for functional diversity among microbial Nep1-like proteins. *PLOS Pathogens*, 15(9), e1007951. <https://doi.org/10.1371/journal.ppat.1007951>
- Levental, I., & Veatch, S. L. (2016, December 4). The Continuing Mystery of Lipid Rafts. *Journal of Molecular Biology*, Vol. 428, pp. 4749–4764. <https://doi.org/10.1016/j.jmb.2016.08.022>
- Lingwood, D., & Simons, K. (2010, January 1). Lipid rafts as a membrane-organizing principle. *Science*, Vol. 327, pp. 46–50. <https://doi.org/10.1126/science.1174621>
- London, E., & Brown, D. A. (2000). Insolubility of lipids in Triton X-100: physical origin and relationship to sphingolipid/cholesterol membrane domains (rafts). *Biochimica et Biophysica Acta (BBA) - Biomembranes*, 1508(1–2), 182–195. [https://doi.org/10.1016/S0304-4157\(00\)00007-1](https://doi.org/10.1016/S0304-4157(00)00007-1)
- Los, D. A., & Murata, N. (2004, November 3). Membrane fluidity and its roles in the perception of environmental signals. *Biochimica et Biophysica Acta - Biomembranes*, Vol. 1666, pp. 142–157. <https://doi.org/10.1016/j.bbamem.2004.08.002>
- Luttgeharm, K. D., Chen, M., Mehra, A., Cahoon, R. E., Markham, J. E., & Cahoon, E. B. (2015). Overexpression of Arabidopsis Ceramide Synthases Differentially Affects Growth, Sphingolipid

- Metabolism, Programmed Cell Death, and Mycotoxin Resistance. *Plant Physiology*.  
<https://doi.org/10.1104/pp.15.00987>
- Luttgeharm, K. D., Kimberlin, A. N., Cahoon, R. E., Cerny, R. L., Napier, J. A., Markham, J. E., & Cahoon, E. B. (2015). Sphingolipid metabolism is strikingly different between pollen and leaf in *Arabidopsis* as revealed by compositional and gene expression profiling. *Phytochemistry*, *115*(1), 121–129. <https://doi.org/10.1016/j.phytochem.2015.02.019>
- Lynch, D. V., & Steponkus, P. L. (1987). Plasma Membrane Lipid Alterations Associated with Cold Acclimation of Winter Rye Seedlings ( *Secale cereale* L. cv Puma). *Plant Physiology*, *83*(4), 761–767. <https://doi.org/10.1104/pp.83.4.761>
- Maget-Dana, R. (1999). The monolayer technique: A potent tool for studying the interfacial properties of antimicrobial and membrane-lytic peptides and their interactions with lipid membranes. In *Biochimica et Biophysica Acta - Biomembranes* (Vol. 1462).  
[https://doi.org/10.1016/S0005-2736\(99\)00203-5](https://doi.org/10.1016/S0005-2736(99)00203-5)
- Malekar, V. C., Morton, J. D., Hider, R. N., Cruickshank, R. H., Hodge, S., & Metcalf, V. J. (2018). Effect of elevated temperature on membrane lipid saturation in Antarctic notothenioid fish. *PeerJ*, *2018*(5), 1–25. <https://doi.org/10.7717/peerj.4765>
- Mamode Cassim, A., Gouguet, P., Gronnier, J., Laurent, N., Germain, V., Grison, M., ... Mongrand, S. (2019). Plant lipids: Key players of plasma membrane organization and function. *Progress in Lipid Research*, *73*(November 2018), 1–27. <https://doi.org/10.1016/j.plipres.2018.11.002>
- Maneta-Peyret, L., Lai, Y. S., Stefano, G., Fouillen, L., Brandizzi, F., & Moreau, P. (2014). Phospholipid biosynthesis increases in RHD3-defective mutants. *Plant Signaling and Behavior*, *9*(9), 1–7. <https://doi.org/10.4161/psb.29657>
- Manna, M., Javanainen, M., Monne, H. M. S., Gabius, H. J., Rog, T., & Vattulainen, I. (2017). Long-chain GM1 gangliosides alter transmembrane domain registration through interdigitation. *Biochimica et Biophysica Acta - Biomembranes*, *1859*(5), 870–878. <https://doi.org/10.1016/j.bbamem.2017.01.033>
- Mannock, D. A., Lewis, R. N. A. H., McMullen, T. P. W., & McElhaney, R. N. (2010, June). The effect of variations in phospholipid and sterol structure on the nature of lipid-sterol interactions in lipid bilayer model membranes. *Chemistry and Physics of Lipids*, Vol. 163, pp. 403–448. <https://doi.org/10.1016/j.chemphyslip.2010.03.011>
- Markham, J. E., & Jaworski, J. G. (2007). Rapid measurement of sphingolipids from *Arabidopsis thaliana* by reversed-phase high-performance liquid chromatography coupled to electrospray ionization tandem mass spectrometry. *Rapid Communications in Mass Spectrometry*. <https://doi.org/10.1002/rcm.2962>
- Markham, J. E., Li, J., Cahoon, E. B., & Jaworski, J. G. (2006). Separation and identification of major plant sphingolipid classes from leaves. *Journal of Biological Chemistry*. <https://doi.org/10.1074/jbc.M604050200>
- Markham, J. E., Molino, D., Gissot, L., Bellec, Y., Hématy, K., Marion, J., ... Faure, J.-D. (2011). Sphingolipids Containing Very-Long-Chain Fatty Acids Define a Secretory Pathway for Specific Polar Plasma Membrane Protein Targeting in *Arabidopsis*. *The Plant Cell*. <https://doi.org/10.1105/tpc.110.080473>

- Marques, E. F. (2000). Size and stability of cationic vesicles: effects of formation path, sonication, and aging. *Langmuir*, *16*(11), 4798–4807. <https://doi.org/10.1021/la9908135>
- Martin, C. E., Oh, C. S., & Jiang, Y. (2007, March). Regulation of long chain unsaturated fatty acid synthesis in yeast. *Biochimica et Biophysica Acta - Molecular and Cell Biology of Lipids*, Vol. 1771, pp. 271–285. <https://doi.org/10.1016/j.bbalip.2006.06.010>
- Martinez, D., Decossas, M., Kowal, J., Frey, L., Stahlberg, H., Dufourc, E. J., ... Loquet, A. (2017). Lipid Internal Dynamics Probed in Nanodiscs. *ChemPhysChem*, *18*(19), 2651–2657. <https://doi.org/10.1002/cphc.201700450>
- Martiniere, A., Lavagi, I., Nageswaran, G., Rolfe, D. J., Maneta-Peyret, L., Luu, D.-T., ... Runions, J. (2012). Cell wall constrains lateral diffusion of plant plasma-membrane proteins. *Proceedings of the National Academy of Sciences*, *109*(31), 12805–12810. <https://doi.org/10.1073/pnas.1202040109>
- Martinière, A., Lavagi, I., Nageswaran, G., Rolfe, D. J., Maneta-Peyret, L., Luu, D. T., ... Runions, J. (2012). Cell wall constrains lateral diffusion of plant plasma-membrane proteins. *Proceedings of the National Academy of Sciences of the United States of America*, *109*(31), 12805–12810. <https://doi.org/10.1073/pnas.1202040109>
- Martinière, A., Shvedunova, M., Thomson, A. J. W., Evans, N. H., Penfield, S., Runions, J., & Mcwatters, H. G. (2011). Homeostasis of plasma membrane viscosity in fluctuating temperatures. *New Phytologist*, *192*(2), 328–337. <https://doi.org/10.1111/j.1469-8137.2011.03821.x>
- Mason, J. T. (1998). Investigation of phase transitions in bilayer membranes. *Methods in Enzymology*, *295*, 468–494. [https://doi.org/10.1016/S0076-6879\(98\)95054-6](https://doi.org/10.1016/S0076-6879(98)95054-6)
- Meca, J., Massoni-Laporte, A., Martinez, D., Sartorel, E., Loquet, A., Habenstein, B., & McCusker, D. (2019). Avidity-driven polarity establishment via multivalent lipid–GTPase module interactions. *The EMBO Journal*, *38*(3). <https://doi.org/10.15252/embj.201899652>
- Medeiros-Silva, J., Jekhmane, S., Paioni, A. L., Gawarecka, K., Baldus, M., Swiezewska, E., ... Weingarth, M. (2018). High-resolution NMR studies of antibiotics in cellular membranes. *Nature Communications*, *9*(1). <https://doi.org/10.1038/s41467-018-06314-x>
- Michaelson, L. V., Napier, J. A., Molino, D., & Faure, J. D. (2016). Plant sphingolipids: Their importance in cellular organization and adaptation. *Biochimica et Biophysica Acta - Molecular and Cell Biology of Lipids*, *1861*(9), 1329–1335. <https://doi.org/10.1016/j.bbalip.2016.04.003>
- Molino, D., Van Der Giessen, E., Gissot, L., Hématy, K., Marion, J., Barthelemy, J., ... Faure, J. D. (2014). Inhibition of very long acyl chain sphingolipid synthesis modifies membrane dynamics during plant cytokinesis. *Biochimica et Biophysica Acta - Molecular and Cell Biology of Lipids*, *1841*(10), 1422–1430. <https://doi.org/10.1016/j.bbalip.2014.06.014>
- Mongrand, S., Morel, J., Laroche, J., Claverol, S., Carde, J. P., Hartmann, M. A., ... Bessoule, J. J. (2004). Lipid rafts in higher plant cells: Purification and characterization of triton X-100-insoluble microdomains from tobacco plasma membrane. *Journal of Biological Chemistry*, *279*(35), 36277–36286. <https://doi.org/10.1074/jbc.M403440200>
- Moreau, R. A., Nyström, L., Whitaker, B. D., Winkler-Moser, J. K., Baer, D. J., Gebauer, S. K., & Hicks, K. B. (2018, April 1). Phytosterols and their derivatives: Structural diversity, distribution,

- metabolism, analysis, and health-promoting uses. *Progress in Lipid Research*, Vol. 70, pp. 35–61. <https://doi.org/10.1016/j.plipres.2018.04.001>
- Morel, J., Clavero, S., Mongrand, S., Furt, F., Fromentin, J., Bessoule, J. J., ... Simon, F. (2006). Proteomics of plant detergent-resistant membranes. *Molecular and Cellular Proteomics*, 5(8), 1396–1411. <https://doi.org/10.1074/mcp.M600044-MCP200>
- Morikawa, T., Mizutani, M., Aoki, N., Watanabe, B., Saga, H., Saito, S., ... Ohta, D. (2006). Cytochrome P450 CYP710A encodes the sterol C-22 desaturase in Arabidopsis and tomato. *Plant Cell*, 18(4), 1008–1022. <https://doi.org/10.1105/tpc.105.036012>
- Morré, D. M., & Morre, D. J. (2000). Aqueous two-phase partition applied to the isolation of plasma membranes and Golgi apparatus from cultured mammalian cells. *Journal of Chromatography B: Biomedical Sciences and Applications*, 743(1–2), 377–387. [https://doi.org/10.1016/S0378-4347\(00\)00058-X](https://doi.org/10.1016/S0378-4347(00)00058-X)
- Mortimer, J. C., Yu, X., Albrecht, S., Sicilia, F., Huichalaf, M., Ampuero, D., ... Dupree, P. (2013). Abnormal glycosphingolipid mannosylation triggers salicylic acid-mediated responses in Arabidopsis. *Plant Cell*, 25(5), 1881–1894. <https://doi.org/10.1105/tpc.113.111500>
- Müller, D. J., & Dufrêne, Y. F. (2009). Atomic force microscopy as a multifunctional molecular toolbox in nanobiotechnology. In *Nanoscience and Technology: A Collection of Reviews from Nature Journals* (pp. 269–277). [https://doi.org/10.1142/9789814287005\\_0028](https://doi.org/10.1142/9789814287005_0028)
- Müller, D. J., Fotiadis, D., Scheuring, S., Müller, S. A., & Engel, A. (1999). Electrostatically balanced subnanometer imaging of biological specimens by atomic force microscope. *Biophysical Journal*, 76(2), 1101–1111. [https://doi.org/10.1016/S0006-3495\(99\)77275-9](https://doi.org/10.1016/S0006-3495(99)77275-9)
- Munns, R., & Tester, M. (2008). Mechanisms of Salinity Tolerance. *Annual Review of Plant Biology*, 59(1), 651–681. <https://doi.org/10.1146/annurev.arplant.59.032607.092911>
- Nagano, M., Takahara, K., Fujimoto, M., Tsutsumi, N., Uchimiya, H., & Kawai-Yamada, M. (2012). Arabidopsis sphingolipid fatty acid 2-hydroxylases (AtFAH1 and AtFAH2) are functionally differentiated in fatty acid 2-hydroxylation and stress responses. *Plant Physiology*, 159(3), 1138–1148. <https://doi.org/10.1104/pp.112.199547>
- Nievola, C. C., Carvalho, C. P., Carvalho, V., & Rodrigues, E. (2017). Rapid responses of plants to temperature changes. *Temperature*, 4(4), 371–405. <https://doi.org/10.1080/23328940.2017.1377812>
- Oncul, S., Klymchenko, A. S., Kucherak, O. A., Demchenko, A. P., Martin, S., Dontenwill, M., ... Mély, Y. (2010). Liquid ordered phase in cell membranes evidenced by a hydration-sensitive probe: Effects of cholesterol depletion and apoptosis. *Biochimica et Biophysica Acta - Biomembranes*, 1798(7), 1436–1443. <https://doi.org/10.1016/j.bbamem.2010.01.013>
- Ott, F., Cousin, F., & Menelle, A. (2004). Surfaces and interfaces characterization by neutron reflectometry. *Journal of Alloys and Compounds*, 382(1–2), 29–38. <https://doi.org/10.1016/j.jallcom.2004.05.046>
- Ott, T. (2017, December 1). Membrane nanodomains and microdomains in plant–microbe interactions. *Current Opinion in Plant Biology*, Vol. 40, pp. 82–88. <https://doi.org/10.1016/j.pbi.2017.08.008>
- Ottmann, C., Luberacki, B., Küfner, I., Koch, W., Brunner, F., Weyand, M., ... Oecking, C. (2009). A

- common toxin fold mediates microbial attack and plant defense. *Proceedings of the National Academy of Sciences of the United States of America*, 106(25), 10359–10364. <https://doi.org/10.1073/pnas.0902362106>
- Owen, D. M., Williamson, D. J., Magenau, A., & Gaus, K. (2012). Sub-resolution lipid domains exist in the plasma membrane and regulate protein diffusion and distribution. *Nature Communications*, 3. <https://doi.org/10.1038/ncomms2273>
- Pata, M. O., Hannun, Y. A., & Ng, C. K. Y. (2010). Plant sphingolipids: Decoding the enigma of the Sphinx. *New Phytologist*, Vol. 185, pp. 611–630. <https://doi.org/10.1111/j.1469-8137.2009.03123.x>
- Pinto, S. N., Silva, L. C., De Almeida, R. F. M., & Prieto, M. (2008). Membrane domain formation, interdigitation, and morphological alterations induced by the very long chain asymmetric C24:1 ceramide. *Biophysical Journal*, 95(6), 2867–2879. <https://doi.org/10.1529/biophysj.108.129858>
- Platre, M. P., Bayle, V., Armengot, L., Bareille, J., del Mar Marquès-Bueno, M., Creff, A., ... Jaillais, Y. (2019a). Developmental control of plant Rho GTPase nano-organization by the lipid phosphatidylserine. *Science*, 364(6435), 57–62. <https://doi.org/10.1126/science.aav9959>
- Platre, M. P., Bayle, V., Armengot, L., Bareille, J., del Mar Marquès-Bueno, M., Creff, A., ... Jaillais, Y. (2019b). Developmental control of plant Rho GTPase nano-organization by the lipid phosphatidylserine. *Science*, 364(6435), 57–62. <https://doi.org/10.1126/science.aav9959>
- Platre, M. P., Noack, L. C., Doumane, M., Bayle, V., Simon, M. L. A., Maneta-Peyret, L., ... Jaillais, Y. (2018). A Combinatorial Lipid Code Shapes the Electrostatic Landscape of Plant Endomembranes. *Developmental Cell*, 45(4), 465-480.e11. <https://doi.org/10.1016/j.devcel.2018.04.011>
- Raffaele, S., Bayer, E., Lafarge, D., Cluzet, S., Retana, S. G., Boubekur, T., ... Mongrand, S. (2009). Remorin, a solanaceae protein resident in membrane rafts and plasmodesmata, impairs potato virus X movement. *Plant Cell*, 21(5), 1541–1555. <https://doi.org/10.1105/tpc.108.064279>
- Raffaele, S., Vailleau, F., Léger, A., Joubès, J., Miersch, O., Huard, C., ... Roby, D. (2008). A MYB transcription factor regulates very-long-chain fatty acid biosynthesis for activation of the hypersensitive cell death response in Arabidopsis. *Plant Cell*, 20(3), 752–767. <https://doi.org/10.1105/tpc.107.054858>
- Raghupathy, R., Anilkumar, A. A., Polley, A., Singh, P. P., Yadav, M., Johnson, C., ... Mayor, S. (2015). Transbilayer lipid interactions mediate nanoclustering of lipid-anchored proteins. *Cell*, 161(3), 581–594. <https://doi.org/10.1016/j.cell.2015.03.048>
- Rennie, E. A., Ebert, B., Miles, G. P., Cahoon, R. E., Christiansen, K. M., Stonebloom, S., ... Scheller, H. V. (2014). Identification of a sphingolipid  $\alpha$ -glucuronosyltransferase that is essential for pollen function in Arabidopsis. *Plant Cell*, 26(8), 3314–3325. <https://doi.org/10.1105/tpc.114.129171>
- Róg, T., Orłowski, A., Llorente, A., Skotland, T., Sylvänne, T., Kauhanen, D., ... Vattulainen, I. (2016). Interdigitation of long-chain sphingomyelin induces coupling of membrane leaflets in a cholesterol dependent manner. *Biochimica et Biophysica Acta - Biomembranes*, 1858(2), 281–288. <https://doi.org/10.1016/j.bbamem.2015.12.003>
- Rojko, N., Dalla Serra, M., Maček, P., & Anderluh, G. (2016, March 1). Pore formation by actinoporins, cytolyticins from sea anemones. *Biochimica et Biophysica Acta - Biomembranes*, Vol. 1858, pp.

446–456. <https://doi.org/10.1016/j.bbamem.2015.09.007>

- Rubenstein, J. L., Smith, B. A., & McConnell, H. M. (1979). Lateral diffusion in binary mixtures of cholesterol and phosphatidylcholines. *Proceedings of the National Academy of Sciences of the United States of America*, 76(1), 15–18. <https://doi.org/10.1073/pnas.76.1.15>
- Ruocco, M. J., & Shipley, G. G. (1984). Interaction of cholesterol with galactocerebroside and galactocerebroside-phosphatidylcholine bilayer membranes. *Biophysical Journal*, 46(6), 695–707. [https://doi.org/10.1016/S0006-3495\(84\)84068-0](https://doi.org/10.1016/S0006-3495(84)84068-0)
- Sackmann, E. (1996). Supported membranes: Scientific and practical applications. *Science*, 271(5245), 43–48. <https://doi.org/10.1126/science.271.5245.43>
- Saita, E., Albanesi, D., & De Mendoza, D. (2016). Sensing membrane thickness: Lessons learned from cold stress. *Biochimica et Biophysica Acta - Molecular and Cell Biology of Lipids*, Vol. 1861, pp. 837–846. <https://doi.org/10.1016/j.bbali.2016.01.003>
- Sampaio, J. L., Levental, I., Lingwood, D., Simons, K., Rajendran, L., Kalvodova, L., & Kaiser, H.-J. (2009). Order of lipid phases in model and plasma membranes. *Proceedings of the National Academy of Sciences*, 106(39), 16645–16650. <https://doi.org/10.1073/pnas.0908987106>
- Seelig, J. (2004, November 3). Thermodynamics of lipid-peptide interactions. *Biochimica et Biophysica Acta - Biomembranes*, Vol. 1666, pp. 40–50. <https://doi.org/10.1016/j.bbamem.2004.08.004>
- Sewelam, N., Oshima, Y., Mitsuda, N., & Ohme-Takagi, M. (2014). A step towards understanding plant responses to multiple environmental stresses: A genome-wide study. *Plant, Cell and Environment*, 37(9), 2024–2035. <https://doi.org/10.1111/pce.12274>
- Sezgin, E., Levental, I., Mayor, S., & Eggeling, C. (2017, June 1). The mystery of membrane organization: Composition, regulation and roles of lipid rafts. *Nature Reviews Molecular Cell Biology*, Vol. 18, pp. 361–374. <https://doi.org/10.1038/nrm.2017.16>
- Sibille, E., Berdeaux, O., Martine, L., Bron, A. M., Creuzot-Garcher, C. P., He, Z., ... Masson, E. A. Y. (2016). Ganglioside profiling of the human retina: Comparison with other ocular structures, brain and plasma reveals tissue specificities. *PLoS ONE*. <https://doi.org/10.1371/journal.pone.0168794>
- Siebers, M., Brands, M., Wewer, V., Duan, Y., Hölzl, G., & Dörmann, P. (2016). Lipids in plant–microbe interactions. *Biochimica et Biophysica Acta - Molecular and Cell Biology of Lipids*, 1861(9), 1379–1395. <https://doi.org/10.1016/j.bbali.2016.02.021>
- Simenel, C., Coddeville, B., Delepierre, M., Latgé, J. P., & Fontaine, T. (2008). Glycosylinositolphosphoceramides in *Aspergillus Fumigatus*. *Glycobiology*. <https://doi.org/10.1093/glycob/cwm122>
- Simon, M. L. A., Platre, M. P., Assil, S., Van Wijk, R., Chen, W. Y., Chory, J., ... Jaillais, Y. (2014). A multi-colour/multi-affinity marker set to visualize phosphoinositide dynamics in *Arabidopsis*. *Plant Journal*, 77(2), 322–337. <https://doi.org/10.1111/tpj.12358>
- Simons, K., & Gerl, M. J. (2010). Revitalizing membrane rafts: New tools and insights. *Nature Reviews Molecular Cell Biology*, Vol. 11, pp. 688–699. <https://doi.org/10.1038/nrm2977>
- Simons, K., & Ikonen, E. (1997, June 5). Functional rafts in cell membranes. *Nature*, Vol. 387, pp. 569–

572. <https://doi.org/10.1038/42408>

- Simons, K., & Vaz, W. L. C. (2004). Model systems, lipid rafts, and cell membranes. *Annual Review of Biophysics and Biomolecular Structure*, Vol. 33, pp. 269–295. <https://doi.org/10.1146/annurev.biophys.32.110601.141803>
- Singer, S. J., & Nicolson, G. L. (1972). The fluid mosaic model of the structure of cell membranes. *Science*, 175(4023), 720–731. <https://doi.org/10.1126/science.175.4023.720>
- Skocaj, M., Bakrac, B., Krizaj, I., Macek, P., Anderluh, G., & Sepcic, K. (2013). The Sensing of Membrane Microdomains Based on Pore-Forming Toxins. *Current Medicinal Chemistry*, 20(4), 491–501. <https://doi.org/10.2174/0929867311320040002>
- Sonnino, S., & Prinetti, A. (2010). Gangliosides as regulators of cell membrane organization and functions. *Advances in Experimental Medicine and Biology*, 688, 165–184. [https://doi.org/10.1007/978-1-4419-6741-1\\_12](https://doi.org/10.1007/978-1-4419-6741-1_12)
- Spassieva, S. D., Markham, J. E., & Hille, J. (2002). The plant disease resistance gene Asc-1 prevents disruption of sphingolipid metabolism during AAL-toxin-induced programmed cell death. *Plant Journal*, 32(4), 561–572. <https://doi.org/10.1046/j.1365-313X.2002.01444.x>
- Sperling, P., & Heinz, E. (2003). Plant sphingolipids: Structural diversity, biosynthesis, first genes and functions. *Biochimica et Biophysica Acta - Molecular and Cell Biology of Lipids*. [https://doi.org/10.1016/S1388-1981\(03\)00033-7](https://doi.org/10.1016/S1388-1981(03)00033-7)
- Stefaniu, C., Brezesinski, G., & Möhwald, H. (2014). Langmuir monolayers as models to study processes at membrane surfaces. *Advances in Colloid and Interface Science*, Vol. 208, pp. 197–213. <https://doi.org/10.1016/j.cis.2014.02.013>
- Swamy, M. J., Ciani, L., Ge, M., Smith, A. K., Holowka, D., Baird, B., & Freed, J. H. (2006). Coexisting domains in the plasma membranes of live cells characterized by spin-label ESR spectroscopy. *Biophysical Journal*, 90(12), 4452–4465. <https://doi.org/10.1529/biophysj.105.070839>
- Takeda, Y., & Kasamo, K. (2001). Transmembrane topography of plasma membrane constituents in mung bean (*Vigna radiata* L.) hypocotyl cells: I. Transmembrane distribution of phospholipids. *Biochimica et Biophysica Acta - Biomembranes*, 1513(1), 38–48. [https://doi.org/10.1016/S0005-2736\(01\)00342-X](https://doi.org/10.1016/S0005-2736(01)00342-X)
- Takeda, Y., & Kasamo, K. (2002). Transmembrane topography of plasma membrane constituents in mung bean (*Vigna radiata* L.) hypocotyl cells. II. The large scale asymmetry of surface peptides. *Biochimica et Biophysica Acta - Biomembranes*, 1558(1), 14–25. [https://doi.org/10.1016/S0005-2736\(01\)00404-7](https://doi.org/10.1016/S0005-2736(01)00404-7)
- Tarazona, P., Feussner, K., & Feussner, I. (2015). An enhanced plant lipidomics method based on multiplexed liquid chromatography-mass spectrometry reveals additional insights into cold- and drought-induced membrane remodeling. *Plant Journal*, 84(3), 621–633. <https://doi.org/10.1111/tpj.13013>
- Tejos, R., Sauer, M., Vanneste, S., Palacios-Gomez, M., Li, H., Heilmann, M., ... Friml, J. (2014). Bipolar plasma membrane distribution of phosphoinositides and their requirement for auxin-mediated cell polarity and patterning in Arabidopsis. *Plant Cell*, 26(5), 2114–2128. <https://doi.org/10.1105/tpc.114.126185>
- Tellier, F., Maia-Grondard, A., Schmitz-Afonso, I., & Faure, J. D. (2014). Comparative plant

- sphingolipidomic reveals specific lipids in seeds and oil. *Phytochemistry*.  
<https://doi.org/10.1016/j.phytochem.2014.03.023>
- Tiku, P. E., Gracey, A. Y., Macartney, A. I., Beynon, R. J., & Cossins, A. R. (1996). Cold-induced expression of  $\Delta 9$ -desaturase in carp by transcriptional and posttranslational mechanisms. *Science*, *271*(5250), 815–818. <https://doi.org/10.1126/science.271.5250.815>
- Tjellstrom, H., Hellgren, L. I., Wieslander, A., & Sandelius, A. S. (2010). Lipid asymmetry in plant plasma membranes: phosphate deficiency-induced phospholipid replacement is restricted to the cytosolic leaflet. *The FASEB Journal*. <https://doi.org/10.1096/fj.09-139410>
- Tresch, S., Heilmann, M., Christiansen, N., Looser, R., & Grossmann, K. (2012). Inhibition of saturated very-long-chain fatty acid biosynthesis by mefluidide and perfluidone, selective inhibitors of 3-ketoacyl-CoA synthases. *Phytochemistry*, *76*, 162–171.  
<https://doi.org/10.1016/j.phytochem.2011.12.023>
- Uemura, M., Joseph, R. A., & Steponkus, P. L. (1995). Cold acclimation of *Arabidopsis thaliana*: Effect on plasma membrane lipid composition and freeze-induced lesions. *Plant Physiology*, *109*(1), 15–30. <https://doi.org/10.1104/pp.109.1.15>
- Vacklin, H. P., Tiberg, F., Fragneto, G., & Thomas, R. K. (2005). Composition of supported model membranes determined by neutron reflection. *Langmuir*, *21*(7), 2827–2837.  
<https://doi.org/10.1021/la047389e>
- Van Leeuwen, W., Vermeer, J. E. M., Gadella, T. W. J., & Munnik, T. (2007). Visualization of phosphatidylinositol 4,5-bisphosphate in the plasma membrane of suspension-cultured tobacco BY-2 cells and whole *Arabidopsis* seedlings. *Plant Journal*, *52*(6), 1014–1026.  
<https://doi.org/10.1111/j.1365-313X.2007.03292.x>
- Veit, S., Wörle, J. M., Nürnberger, T., Koch, W., & Seitz, H. U. (2001). A novel protein elicitor (PaNie) from *Pythium aphanidermatum* induces multiple defense responses in carrot, *Arabidopsis*, and tobacco. *Plant Physiology*, *127*(3), 832–841. <https://doi.org/10.1104/pp.010350>
- Vermeer, J. E. M., & Munnik, T. (2013). *Using Genetically Encoded Fluorescent Reporters to Image Lipid Signalling in Living Plants*. [https://doi.org/10.1007/978-1-62703-401-2\\_26](https://doi.org/10.1007/978-1-62703-401-2_26)
- Voxeur, A., André, A., Breton, C., & Lerouge, P. (2012). Identification of Putative Rhamnogalacturonan-II Specific Glycosyltransferases in *Arabidopsis* Using a Combination of Bioinformatics Approaches. *PLoS ONE*, *7*(12). <https://doi.org/10.1371/journal.pone.0051129>
- Voxeur, A., & Fry, S. C. (2014a). Glycosylinositol phosphorylceramides from *Rosa* cell cultures are boron-bridged in the plasma membrane and form complexes with rhamnogalacturonan II. *Plant Journal*, *79*(1), 139–149. <https://doi.org/10.1111/tpj.12547>
- Voxeur, A., & Fry, S. C. (2014b). Glycosylinositol phosphorylceramides from *Rosa* cell cultures are boron-bridged in the plasma membrane and form complexes with rhamnogalacturonan II. *Plant Journal*. <https://doi.org/10.1111/tpj.12547>
- Wang, W., Yang, X., Tangchaiburana, S., Ndeh, R., Markham, J. E., Tsegaye, Y., ... Xiao, S. (2008). An inositolphosphorylceramide synthase is involved in regulation of plant programmed cell death associated with defense in *arabidopsis*. *Plant Cell*, *20*(11), 3163–3179.  
<https://doi.org/10.1105/tpc.108.060053>
- Wattelet-Boyer, V., Brocard, L., Jonsson, K., Esnay, N., Joubès, J., Domergue, F., ... Boutté, Y. (2016).

- Enrichment of hydroxylated C24-and C26-acyl-chain sphingolipids mediates PIN2 apical sorting at trans-Golgi network subdomains. *Nature Communications*, 7. <https://doi.org/10.1038/ncomms12788>
- White, S. H. (2007, May). Membrane protein insertion: The biology-physics nexus. *Journal of General Physiology*, Vol. 129, pp. 363–369. <https://doi.org/10.1085/jgp.200709741>
- Xie, L. J., Chen, Q. F., Chen, M. X., Yu, L. J., Huang, L., Chen, L., ... Xiao, S. (2015). Unsaturation of Very-Long-Chain Ceramides Protects Plant from Hypoxia-Induced Damages by Modulating Ethylene Signaling in Arabidopsis. *PLoS Genetics*, 11(3), e1005143. <https://doi.org/10.1371/journal.pgen.1005143>
- YAMAMOTO, T. (1963). On the thickness of the unit membrane. *The Journal of Cell Biology*, 17, 413–421. <https://doi.org/10.1083/jcb.17.2.413>
- Yamaoka, Y., Yu, Y., Mizoi, J., Fujiki, Y., Saito, K., Nishijima, M., ... Nishida, I. (2011). PHOSPHATIDYLSERINE SYNTHASE1 is required for microspore development in Arabidopsis thaliana. *Plant Journal*, 67(4), 648–661. <https://doi.org/10.1111/j.1365-313X.2011.04624.x>
- Yang, Y., & Guo, Y. (2018). Elucidating the molecular mechanisms mediating plant salt-stress responses. *New Phytologist*, 217(2), 523–539. <https://doi.org/10.1111/nph.14920>
- Yetukuri, L., Ekroos, K., Vidal-Puig, A., & Orešič, M. (2008). Informatics and computational strategies for the study of lipids. *Mol. BioSyst.*, 4(2), 121–127. <https://doi.org/10.1039/B715468B>
- Yilmaz, N., & Kobayashi, T. (2016). Assemblies of pore-forming toxins visualized by atomic force microscopy. *Biochimica et Biophysica Acta - Biomembranes*. <https://doi.org/10.1016/j.bbamem.2015.11.005>
- Yoshida, S., Washio, K., ... J. K.-P. and cell, & 1988, U. (1988). Thermotropic Properties of Lipids Extracted from Plasma Membrane and Tonoplast Isolated from Chilling-Sensitive Mung Bean (*Vigna radiata* [L.] Wilczek). *Plant and Cell Physiology*. <https://doi.org/10.1093/oxfordjournals.pcp.a077654>
- Yuan, F., Yang, H., Xue, Y., Kong, D., Ye, R., Li, C., ... Pei, Z.-M. (2014). OSCA1 mediates osmotic-stress-evoked Ca<sup>2+</sup> increases vital for osmosensing in Arabidopsis. *Nature*, 514(7522), 367–371. <https://doi.org/10.1038/nature13593>
- Zachowski, A. (1993). Phospholipids in animal eukaryotic membranes: Transverse asymmetry and movement. *Biochemical Journal*, 294(1), 1–14. <https://doi.org/10.1042/bj2940001>